AN ABSTRACT OF THE THESIS OF

GEORGE RANDY PRIEST for the degree of DOCTOR OF PHILOSOPHY

in GEOLOGY presented on May 29, 1979

Title: GEOLOGY AND GEOCHEMISTRY OF THE LITTLE WALKER VOLCANIC CENTER, MONO COUNTY, CALIFORNIA

Redacted for Privacy

Abstract approved: Edward M. Taylor

Detailed mapping and geochemical analysis of Oligocene to early Pliocene volcanic rocks in the Little Walker volcanic center, Mono County, California have revealed a complex eruptive history. After eruption of widespread rhyolitic ash flows of the Valley Springs Formation in the Oligocene, Miocene to early Pliocene volcanism of the western Great Basin and northern Sierra Nevada was dominated by eruption of calc-alkalic, andesitic lavas bearing abundant hydrous mafic phenocrysts, and, thus, high H_2O contents. These kinds of calc-alkaline magmas are associated with most of the major epithermal Au-Ag districts of the western Great Basin.

A highly potassic latitic pulse of volcanism occurred at the Little Walker volcanic center about 9.5 m.y. ago during the ongoing calc-alkalic activity. The latitic series is unusually enriched in K and other incompatible elements, as well as Fe compared to the surrounding calc-alkaline rocks. The latites have mineralogic evidence of

much lower H_2O content than the calc-alkaline lavas; yet early latitic magmas were rich enough in volatiles to produce very large, welded ash-flow sheets (e.g., the Eureka Valley Tuff). Rapid evacuation of the magma reservoir beneath the Little Walker center during the ash-flow activity resulted in formation of the Little Walker caldera. Intracaldera volcanism culminated with extrusion of viscous, phenocryst-rich plug domes and coulees of transitionally calc-alkaline, low-K latite lava of the Lavas of Mahogany Ridge. The low-K latite series is severely depleted in all incompatible elements relative to early latitic rocks and has mineralogic, geologic, and trace element evidence of higher H_2O content relative to early latites. Significant phenocrystic hornblende, association with hydrothermal alteration, and high Eu^{+3}/Eu^{+2} all suggest significant H_2O concentration in the low-K latite magmas. These rocks probably come from a source region intermediate between that of the calc-alkaline and latite series.

Trace and major element data favor generation of latitic magmas from a primitive mantle diapir. The diapir rose into a subduction zone that was actively generating widespread calc-alkalic lavas throughout the region from hydrous mantle and, possibly, lower crustal sources. The latite magmas were drier and hotter than the calc-alkaline magmas, but were also enriched in volatiles, particularly CO_2, and incompatible elements from their undepleted mantle source. Rising latitic magmas may have gained additional

incompatible elements by wall rock reaction and zone refining of upper mantle and lower crustal rocks. Extensive qualitative trace element evidence of crystal fractionation shows that incompatible elements may have been further concentrated by variable amounts of crystal settling. High-pressure (plagioclase-poor, pyroxene-rich) fractionation of the early, dry latitic series produced low-Ca-Mg latites with high Fe/Mg and Al_2O_3 but low SiO_2. Low-pressure (plagioclase rich) differentiation of the early latitic magmas produced quartz latite ash flows with high SiO_2 and moderate Fe/Mg, while low-pressure differentiation of hydrous low-K latite magmas yielded silicic low-K latite and quartz latite lavas with low Fe/Mg. More extensive separation of olivine relative to pyroxenes at low pressures and increased stability of subsilicic hydrous crystals and Fe-Ti oxides in the hydrous magmas account for changes in differentiation trends caused by P_{total} and P_{H_2O} variations.

Lack of giant welded ash-flow sheets in the hydrous calc-alkaline series and common eruption of such ash flows from volcanic centers with rather anhydrous magmas led to the conclusion that H_2O/CO_2 as well as total volatile content are critical controls on the likelihood of large scale, hot ash-flow eruptions. Giant, hot ash-flow sheets and associated calderas are favored in magmas with low H_2O/CO_2 and high total volatile content. Basaltic and latitic volcanism in areas of thick sialic crust, where crystal fractionation is extensive are,

therefore, the best sources of giant ash-flow sheets.

H_2O/CO_2 and total volatile content were also critical controls of the probability of hydrothermal ore deposition. Magmas with high H_2O/CO_2 and moderate total volatile contents are most favored for ore deposition, because such magmas tend to form mesozonal or epizonal plutons rather than volcanic rocks. Plutonic crystallization of hydrous magma will yield a fluid phase capable of transferring incompatible metals and geothermal heat to ground water. If permeable structures and rocks are present, as in a caldera, widespread mineralization will be favored, but there may be no genetic relation between ore-forming magmas and magmas which produce calderas.

Geology and Geochemistry of the Little Walker Volcanic Center, Mono County, California

by

George R. Priest

A THESIS

submitted to

Oregon State University

in partial fulfillment of
the requirements for the
degree of

Doctor of Philosophy

Completed May 1979

Commencement June 1980

APPROVED:

Redacted for Privacy

Professor of Geology

in charge of major

Redacted for Privacy

Chairman of Department of Geology

Redacted for Privacy

Dean of Graduate School

Date thesis is presented May 29, 1979

Typed by Clover Redfern for George Randy Priest

ACKNOWLEDGMENTS

This study was partially supported by Geological Society of America Research Grants 2243-77, 2072-76, and 2243-77. Grants for many hours of spectrometer and reactor time from Dr. C.H. Wang, Director of the Oregon State University Radiation Center, were crucial to investigation of the trace element geochemistry. Thanks must also go to the Geology departments of Oregon State University and the University of Oregon for making available their analytical facilities for major element analysis. Data reduction was greatly facilitated by generous awards of computer time from Oregon State University and the University of Oregon. Dr. Gordon G. Goles of the University of Oregon Department of Geology has been especially helpful in allowing me access to the considerable computer program library of the University of Oregon.

Special thanks must go to Dr. Maw-Suen Ma, Dr. Roman A. Schmitt, and Vernon N. Smith for their encouragement and unselfish help during the long period of neutron activation analysis. Dr. Schmitt and Dr. Edward M. Taylor have contributed greatly to the quality of this dissertation by their critical review. Dr. Taylor has also given valuable guidance on the field geology of the study area.

Barbara Portwood, Gretchen Jones, and Virginia Pfaff worked long and arduous hours during their free time to type the preliminary

draft of the paper. Their help in a time of critical deadlines is greatly appreciated.

My wife, Barbara, has given me unflagging encouragement and support throughout this long investigation; she also drafted all of the figures and maps. The cartography and illustrations of the paper are a credit to her considerable skill.

Finally, I must thank Dr. Donald C. Noble who initially interested me in the study of the Little Walker area. Dr. Noble has provided valuable advice as the investigation progressed.

TABLE OF CONTENTS

LIST OF FIGURES

LIST OF TABLES

GEOLOGY AND GEOCHEMISTRY OF THE LITTLE WALKER VOLCANIC CENTER, MONO COUNTY, CALIFORNIA

INTRODUCTION

The Little Walker volcanic center is the source for much of the highly potassic, latitic lavas and tuffs of the late Miocene (8.6-10 m.y.) Stanislaus Group. The center is located about ten miles west-northwest of Bridgeport, California on the eastern slopes of the Sierra Nevada mountains (Figures 1, 2). It is one of a series of late Tertiary potassic volcanic centers which are spread in an E-W band across the southern Great Basin (Figure 1, Noble, and others, 1974).

This paper will summarize an investigation of this important volcanic center begun by Donald C. Noble and William R. Dickinson in 1969 and continued by the writer during 1973 to 1979. Detailed field mapping as well as considerable petrographic and chemical analysis have been utilized in an effort to understand the evolution of the Little Walker center.

Detailed mapping and sampling of about 90 square miles and reconnaissance mapping of another 45 square miles of the Fales Hot Springs quadrangle are the basis for structural and stratigraphic interpretations. Whole rocks and mineral separate samples have been analyzed for major and trace element composition utilizing X-ray fluorescence, instrumental neutron activation, and atomic absorption

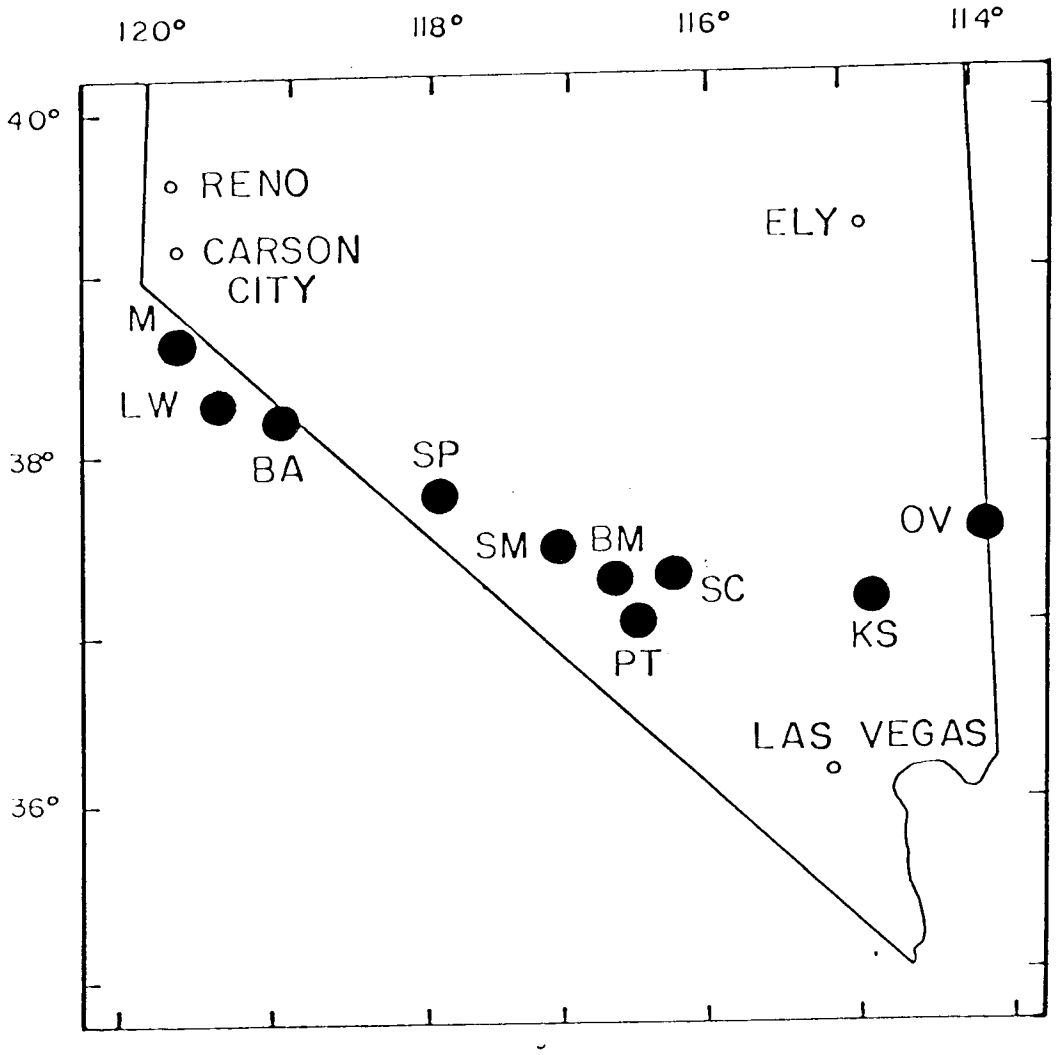

Figure 1. Index map of potassic volcanic centers of the southern Great Basin. Taken from Noble and others (1974).

M - Markleeville, 10 m.y. (M.L. Silberman, unpub. data)
LW - Little Walker, 10 to 8.6 m.y. (Noble and others, 1974; M.L. Silberman, unpub. data)
BA - Bodie-Aurora, 9 m.y. (Chesterman, 1968; Silberman and others, 1972)
SP - Silver Peak, 6 m.y. (Robinson, 1972)
SM - Stonwall Mountain (Cornwall, 1972; Ashley, 1974)
BM - Black Mountain, 7 m.y. (Noble and Christiansen, 1974)
PT - Paintbrush and Timber Mountain, 13.5-10 m.y. (Lipman and others, 1966; Noble and Hedge, 1969; Byers and others, 1968)
SC - Silent Canyon, 14 m.y. (Noble and others, 1968)
KS - Kane Springs Wash, 13 m.y. (Noble, 1968)
OV - Ox Valley (inferred location), approx. 14 m.y. (Noble and McKee, 1972)

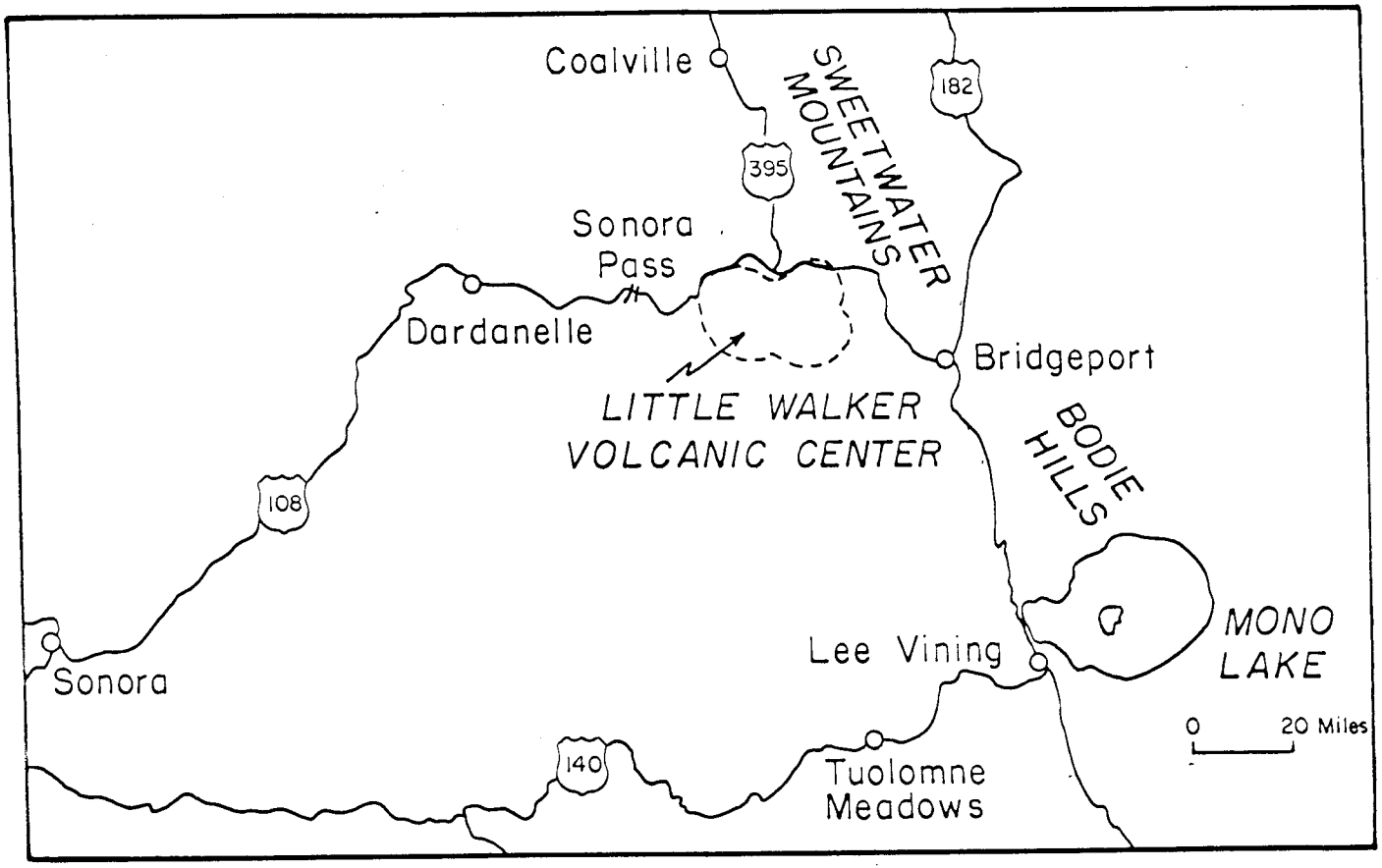

Figure 2. Geography of the Sonora Pass area and Little Walker volcanic center.

spectrophotometry (see Appendices). The chemical data have been used to test various models for generation of the magmas of the center and as correlation tools. Three K-Ar dates have been provided by Miles Silberman (1974, unpublished data) of the U.S. Geological Survey.

It will be shown that much of the Stanislaus Group has, in fact, erupted from the Little Walker center and that a great deal of evidence supports the formation of a volcano-tectonic depression after eruptions of the voluminous quartz latite ash flows of the Eureka Valley Tuff. Rare earth element (REE) models will be presented which place constraints on source assemblages which may have been partially melted to produce low-silica latite magma. High level differentiation will be modeled utilizing both major and trace element data, especially distribution coefficients (D's) from mineral separates.

While the chief thrust of this paper is to describe the genesis of the latitic series, a subsidiary investigation of Mio-Pliocene (7.3 m.y.) calc-alkaline lavas (the Lavas of Rickey Peak) erupted within and far outside of the center will be presented. It will be shown that these hornblende-biotite, andesitic-to-dacitic lavas were erupted from a source (upper mantle?) very different from that of the latites when Basin and Range tectonism began along the Sierra Nevada Front.

PREVIOUS WORK AND STRATIGRAPHIC NOMENCLATURE

Recent changes of the stratigraphic nomenclature of the rocks of the Stanislaus Group make it appropriate to summarize the development of geologic literature on the subject (Figure 3). Rocks now included in the Eureka Valley Tuff were first described by Ransome (1898) as "biotite-augite-latite" flows. This unit overlies an augite-latite lava flow which Ransome named the Table Mountain flow and underlies a sequence of augite-latite flows named by Ransome the Dardanelles flow. This was the first use of the term latite for a rock which stands chemically between andesite and trachyte, being distinguished by much higher alkalis, especially potassium, than andesite but with much higher calcium and magnesium than trachyte. In 1948 D.B. Slemmons (1953) recognized the "biotite-augite-latite" of Ransome as a welded tuff; R.L. Smith (Ross and Smith, 1961) also recognized this unit as a welded tuff at about the same time. Slemmons (1953) found the biotite-augite-latite to extend from the Sierran foothills across the Sonoran Crest, and Johnson (1951), Halsey (1953), Gilbert and others (1968), and Al-Rawi (1969) located outcrops of the unit as far east as the Bodie Hills (Figure 4). Slemmons (1966) formally named the units described by Ransome the Stanislaus Formation, consisting from bottom to top of the Table Mountain Latite, Eureka Valley, and Dardanelles Members.

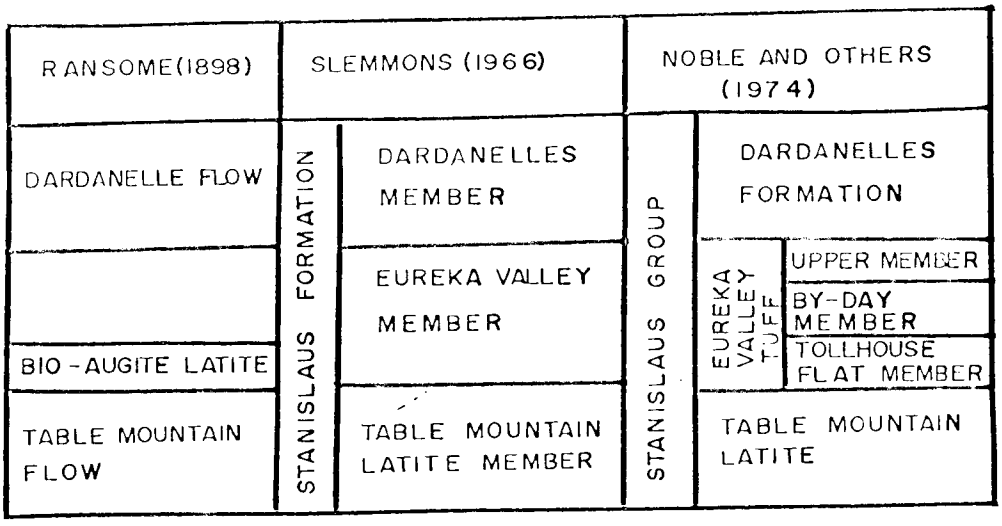

Figure 3. Evolution of stratigraphic nomenclature of the Stanislaus Group.

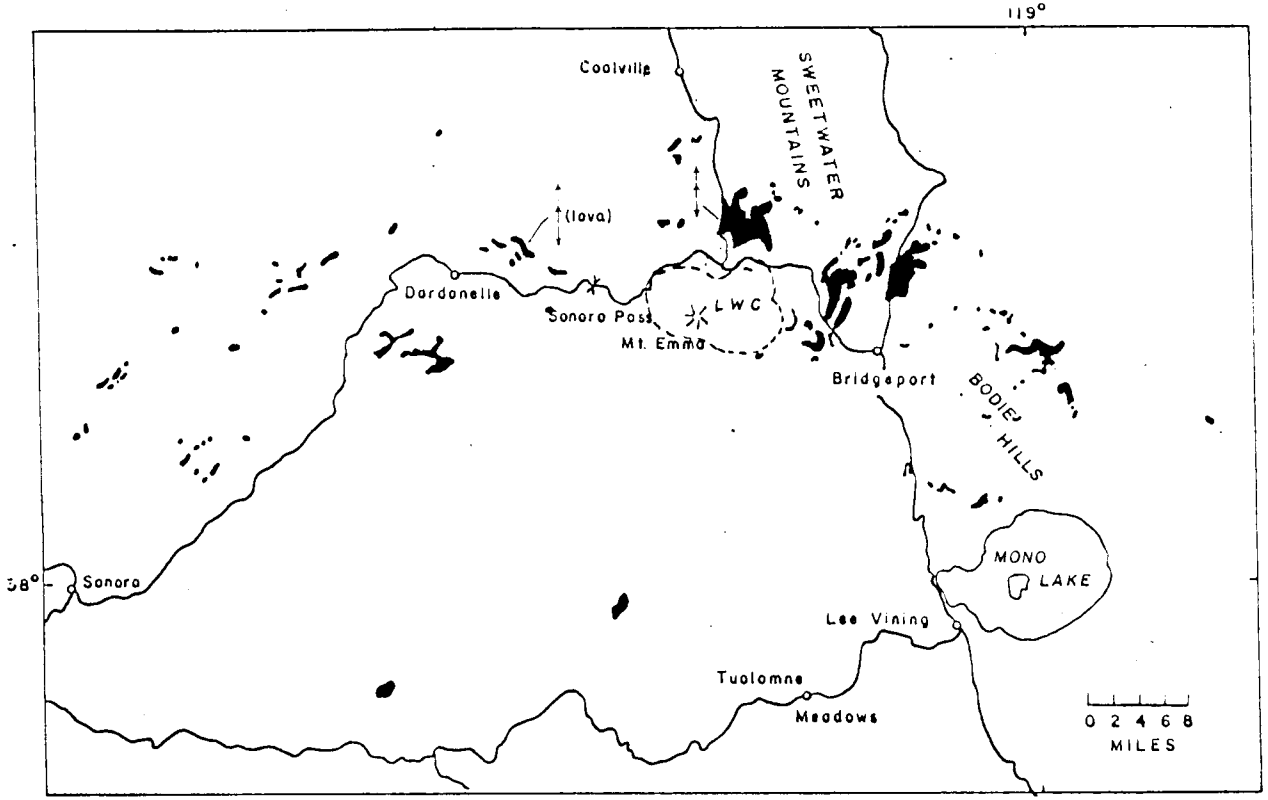

Figure 4. This map shows the regional distribution of the Eureka Valley Tuff (in black). The map is taken from Noble and others (1974). Arrows indicate direction of remnant magnetic poles. LWC stands for the Little Walker caldera. Dashed lines are the maximum extent of the caldera.

Noble and others (1974) recognized that the Eureka Valley Member contains two major ash-flow sheets; they raised the member to formational status, renaming it the Eureka Valley Tuff. The Stanislaus Formation was raised to group rank and the Table Mountain Latite and Dardanelles Members to formations. From bottom to top the Eureka Valley Tuff consists of a biotite-bearing quartz latite ash-flow sheet, the Tollhouse Flat Member, equivalent to the "biotite-augite-latite" of Ransome; a biotite-free latite ash-flow sheet, the By-Day Member; and a small overlying unit of ash-flow tuff informally named the Upper Member (Noble and others, 1974). In mapping the regional distribution of the Eureka Valley Tuff (Figure 4) Noble and others (1969, 1974) recognized the Little Walker caldera which marks the vent area for the Eureka Valley Tuff.

PERIODICITY OF VOLCANISM IN THE CENTRAL SIERRA NEVADA

Volcanism in and around the Little Walker center has occurred episodically throughout the last 33 m.y. (since early Oligocene, according to the Cenozoic time scale of Berggren, 1972). The relative extent and timing of volcanism in the central Sierra Nevada are summarized in Figures 5a and 5b. In sheer volume and areal extent, the two large hornblende andesite eruptions of the middle Miocene Relief Peak Formation and Mio-Pliocene Disaster Peak dominate the Tertiary volcanic history of the Sierras. The two regional calc-alkaline eruptions occurred from numerous vents along the eastern Sierran axis and were preceded by widespread, but now highly eroded, late Oligocene to early Miocene rhyolitic ash flows of the Valley Springs Formation (Slemmons, 1966). This paper, however, will focus on the smaller volume, highly potassic (latitic) volcanism of the Little Walker volcanic center which is represented by the latite flows and quartz latite ash flows of the Stanislaus Group in the time interval between the two major calc-alkaline eruptions.

There is evidence that minor volumes of basaltic lavas have periodically erupted during the hiatus after the Valley Springs activity, possibly during and after the Relief Peak eruptions and during the Disaster Peak volcanism. Slemmons (1966) points out that small-volume bimodal basalt-rhyolite volcanism was frequent during

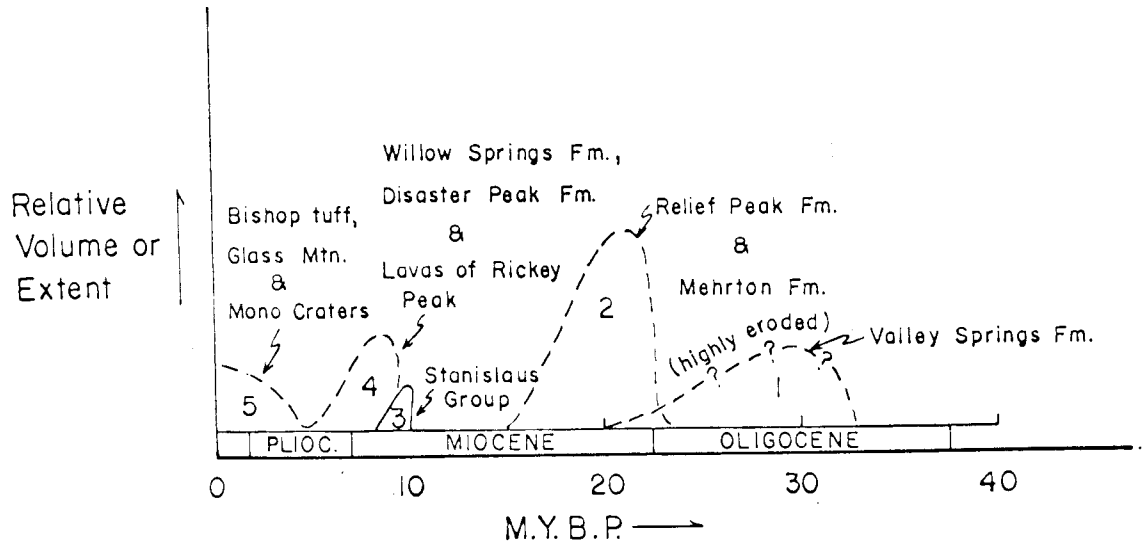

Figure 5a. Periodicity of volcanism in the east-central Sierra Nevada. Eruptions 2 and 4 may be part of a continuous regional calc-alkaline series in the northern Sierras and Great Basin.

AGE	SIERRA NEVADA	LITTLE WALKER AREA	MONO BASIN
1,500 - 10,000 y.			Mono Craters
700,000 y.			Bishop Tuff
900,000 y.			Glass Mtn. obsidian
2.5 m.y.			Cedar Hill - Trench Canyon andesites
3.2 - 3.8 m.y.			Alkali-rich andesite + olivine basalt of Anchorite Hills
1.6 - 3.6 m.y.			Rhyolite + basalt of Mt. Hicks and Beauty Peak
2.6 - 4.5 m.y.			Olivine basalt of east Mono Basin
7.3 - 8.9 m.y.	Disaster Peak Fm.	Lavas of Rickey Peak	Andesites of Bodie Mtn.
	Dardanelles Fm.	Lavas of Mahogany Ridge	Mount Biedemen rhyolite + andesite breccia
8.3 - 9.5 m.y.	EUREKA VALLEY TUFF Tollhouse Flat Member	EUREKA VALLEY TUFF Upper Member By-Day Member Tollhouse Flat Member	EUREKA VALLEY TUFF TollHouse Flat Member
	Table Mountain Latite	Table Mountain Latite	Latite welded tuff of Anchorite Hills
12.5 - 22 m.y.	Relief Peak Fm.	Relief Peak Fm.	Relief Peak Fm.
22 - 33 m.y.	Valley Springs Fm.	Valley Springs Fm.	Valley Springs Fm.
Jurassic	Sierra Nevada Batholithic rocks	Sierra Nevada Batholithic rocks	Sierra Nevada Batholithic rocks

Figure 5b. Volcanic stratigraphy of the Sierra Nevada-Mono Basin area (Gilbert and others, 1968; Noble and others, 1974).

the Pliocene and Quaternary in the eastern Sierra Nevada at the time of most active Basin and Range faulting (e. g., at Mono Lake and Owens Valley; Figure 5b).

Christiansen and Lipman (1972), Noble (1972), and Elston, and others (1976) have noted the coincidence of bimodal basalt-rhyolite volcanism coincident with the beginning of the Basin and Range faulting in the Great Basin about 15-17 m. y. ago. It appears that Basin and Range tectonism along the stable eastern Sierran block lagged behind the rest of the Great Basin, beginning about 7. 3 m. y. ago (K-Ar data, this paper) with most movement on normal faults during the last 3. 2 m. y. in the Mono Lake-Little Walker area (Slemmons, 1966; Gilbert and others, 1968). It is significant that the greatest volumes of bimodal assemblage have been erupted along the Sierran front during the last 3. 2 m. y. (Slemmons, 1966; Gilbert and others, 1968; Figure 5b).

ERUPTIVE HISTORY OF THE LITTLE WALKER CENTER

Middle Oligocene to early Miocene (32.2 to 20.5 m.y.) sanidine rhyolite ash flows of the Valley Springs Formation (Slemmons, 1966; Gilbert and others, 1968) swept across the Little Walker area, probably from vents several miles to the northwest. Evidence for a northwesterly source include thickening of the Valley Springs Formation in that direction and change in the character of the ash flows from poorly welded crystal-vitric tuffs at the Little Walker center to welded, lithic-rich ash flows containing block-size fragments of comagmatic, highly welded ash-flow tuff near Lost Cannon Peak to the northwest (Figure 2).

Structurally complex exposures of small flows of olivine basalt and aphyric basaltic andesite in the eastern half of the Little Walker center indicate eruption of these mafic rocks after the Valley Springs event but before the Relief Peak eruptions. These units are definitely below rocks similar to the Relief Peak rocks, at the eastern margin of the Little Walker center, but similar basaltic rocks in ambiguous exposures on the northern margin may lie on rocks correlative with the Relief Peak Formation. Aphyric basaltic andesitic units at Devils Gate appear to lie on Valley Springs rocks (Plate 1). Additional detailed mapping must be done to unravel correctly, the eruptive history of these discontinuous, poorly exposed units.

Between 22 and 12.5 m.y. ago (Gilbert and others, 1968) extremely large volumes of hornblende-pyroxene andesite flows, autobreccias, and mudflows erupted from vents several miles west of the Little Walker center at Relief Peak and from numerous areas throughout the northern Sierras (Slemmons, 1966; Figure 2). Slemmons (1966) also contends that a vent area for these andesites existed at Mount Emma in the Little Walker center, but no compelling evidence for this was found in the present study.

Thinning of the Relief Peak lavas from a thickness of about 3,000 feet at Mount Emma and Relief Peak to 300 feet in the western Sierran foothills led Slemmons (1966) to argue that both Relief Peak and Mount Emma were proabable sources of the Relief Peak Formation. He cited the occurrence of andesite dikes and plugs at Relief Peak and Mount Emma as further evidence that these were eruptive centers for the Relief Peak Formation. While these arguments may apply to Relief Peak, they are inconsistent with relationships at Mount Emma.

Intrusive rocks at Mount Emma are actually part of the Stainslaus Group rather than the Relief Peak Formation. The dikes and plugs are pyroxene monzodiorite and high-K andesite, lacking hornblende, which is the most characteristic phenocryst of the Relief Peak rocks. These intrusives cut biotite quartz latite ash flows of the Stanislaus Group (Tuffs of Poore Lake, Plate 1) which establishes the

low-Mg latite and pyroxene latite flows in the Little Walker center (Figure 6). This first phase of activity produced a sequence of increasingly more evolved (Ca-Mg-poor) latitic flows which finally culminated in eruption of the voluminous welded quartz latite ash flows of the Eureka Valley Tuff (the Tollhouse Flat and By-Day Members) from the Little Walker center about 9.5 m.y. ago (Noble and others, 1974; Figures 4 and 6). Sharp increase in the amount and size of poorly vesiculated pumice lumps and lithic fragments in the Eureka Valley Tuff toward the Little Walker center (Noble and others, 1969) and occurrence of lag-fall deposits of By-Day tuff on the eastern margin of the center north of Rickey Peak indicate that the Little Walker center is definitely the source of the Eureka Valley Tuff.

Several lines of evidence favor cauldron subsidence after eruption of the Tollhouse Flat and By-Day Members. Occurrence of blocks of welded Eureka Valley Tuff up to five meters in diameter within lacustrine tuffs northwest of the By-Day lag-fall outcrops suggests the presence of a caldera rim which developed landslide and talus in an intracaldera lake (see location of "Tmeb blocks" Plate 1; Figure 8). These lacustrine tuffs and other Stanislaus units younger than the By-Day Member are confined to a roughly circular area (Figure 6; Plate 1). The younger units lie unconformably above an erosional surface which cuts all pre-By-Day rocks. This unconformity appears to define an elliptical depression which may well

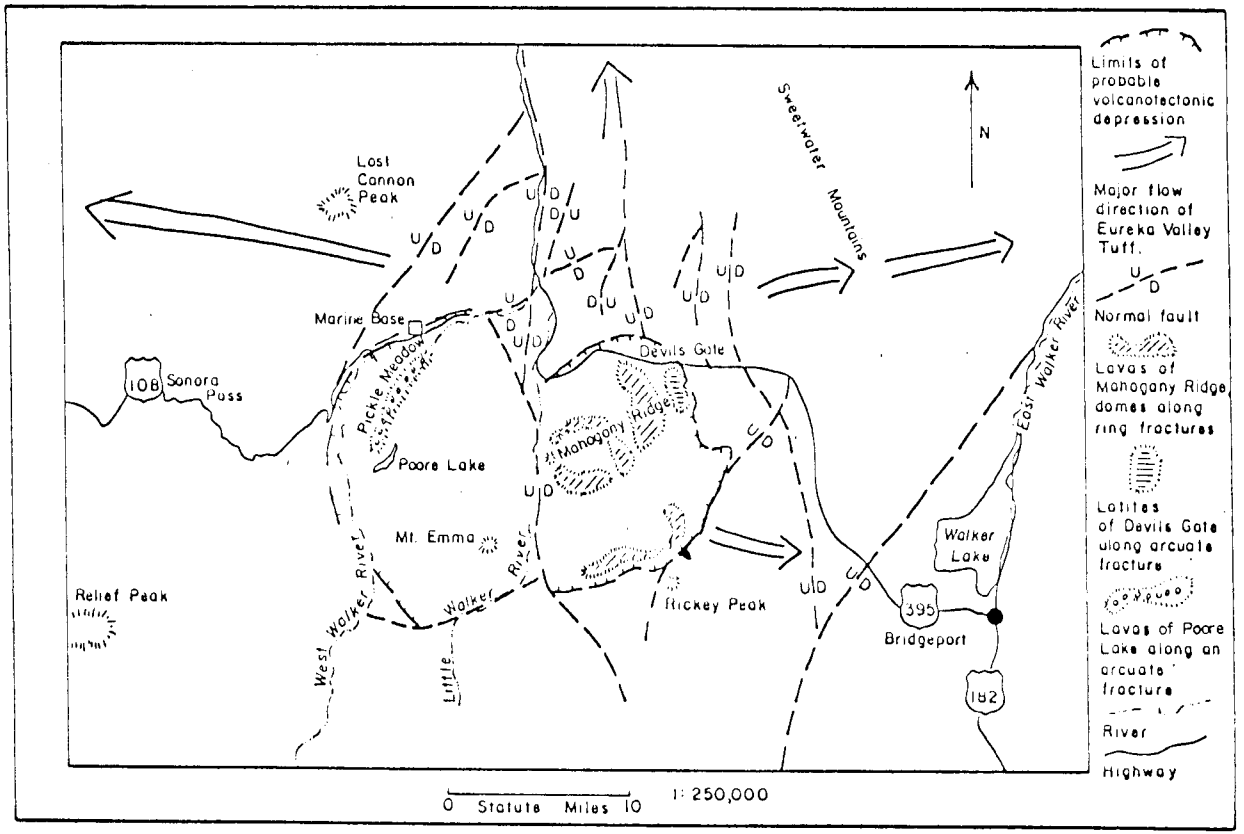

Figure 6. Tectonic map of the Little Walker volcanic center.

Figure 7. Welded lag-fall deposits of By-Day tuff on the north side of Rickey Peak. Note large unvesiculated blocks of magmas on the right and upper left.

Figure 8. Large blocks of By-Day welded tuff in lacustrine tuffs of the Upper Member of the Erueka Valley Tuff. These are probable caldera margin landslide blocks.

represent an erosionally widened caldera.

Extrusion of intracaldera lava domes along arcuate fractures is frequently the final eruptive event in caldera-forming, ash-flow eruptions (Smith and Bailey, 1968). Smith and Bailey (1968) also proposed that the final stage of intracaldera volcanism would be associated with extensive hydrothermal alteration as geothermal waters circulated in permeable intracaldera fill. Viscous plug domes in the eastern half of the proposed caldera follow well-defined arcuate and ring fractures which cut the intracaldera lacustrine tuffs (Lavas of Mahogany Ridge, Plate 1; Figure 6). Subvolcanic equivalents of these lavas in the western half of the caldera have pervasively altered intracaldera ash-flow tuffs (Tuffs of Poore Lake, Plate 1). The intracaldera plug domes and associated alteration, then, represent typical final episodes in the eruptive cycle at Little Walker and other major ash-flow centers.

These aregument and detailed data to be presented in the next section are compelling evidence that a caldera formed in the Little Walker area about 9.5 million years ago. It is probable that caldera margins were reshaped by mass wasting and that the caldera passed through a stage of intracaldera volcanism which began with ash-flow eruptions (Upper Member of the Eureka Valley Tuff, Plate 1) and culminated with intrusion of latitic plug domes along circular and ring fractures (Lavas of Mahogany Ridge, Plate 1). Widespread geothermal water circulation altered permeable units at subvolcanic levels

to close the eruptive cycle.

Maximum limits of this erosionally widened caldera are indicated by bold, hachured lines on Figure 6 and Plate 1. These boundaries define the precise limits of the Little Walker volcanic center in succeeding descriptions.

Noble and others (1974) give a preferred age of 9.5 m.y. to the Eureka Valley Tuff. It is probable that the ash-flow eruptions were approximately coincident with cauldron subsidence, so this date should be a good estimate of the age of the Little Walker caldera. The range of all age dates thus far compiled for Stanislaus rocks is from 10.7 m.y. to about 8.3 m.y. (Noble and others, 1974; unpublished K-Ar data of M. Silberman, 1974), but there is little correlation between these ages and stratigraphic position of the units dated. The radiometric data is apparently not able to resolve age differences of less than one to two million years in these samples. Because this amount of error approaches the probable magnitude of the life span of the Little Walker center, no reliable estimate of the total time of activity can be made.

Immediately after the end of the Little Walker activity, a series of viscous hornblende-biotite andesite to dacite lavas began to erupt throughout the southern Sweetwater Mountains and the Bodie Hills (Halsey, 1953; Chesterman, 1968; Silberman and McKee, 1974). Biotite from one of the dacite domes in the Little Walker center (Lavas

of Rickey Peak, Plate 1) provided a K-Ar age of 7.3 ± 0.2 m.y. (unpublished data of Miles Silberman, 1974). This age is close to ages of similar rocks of the Potato Peak Formation (7.8 m.y. ± 0.2 m.y. to 8.9 ± 0.2 m.y. of Chesterman, 1968) and Willow Springs Formation (Chesterman, 1968; Gilbert and others, 1968). This activity is also roughly coincident with the extensive gold-silver mineralization of the Bodie District (7 m.y. from K-Ar ages of Silberman and others, 1972). Rocks of similar age and lithology have been mapped as the Disaster Peak Formation in the western Sierras and as the upper Mehrton Formation in the northern Sierras (Slemmons, 1966). The eruptive style of these lavas in the northern and western Sierras, however, differs from that of the southern Sweetwater Mountains and Bodie Hills. In the latter areas and at the Little Walker center the flows occur as short coulees and endogenous lava domes following N-S-trending lineaments parallel to recent Basin and Range faults. In the western and northern Sierras these rocks are widespread intracanyon flows and mudflows very similar to the underlying Relief Peak Formation (Slemmons, 1966). It is possible that the lavas erupted at the Little Walker center and along the eastern Sierran Front were controlled by embryonic Basin and Range structures. If so, then the first Basin and Range faults may have begun to affect the eastern Sierras as early as 7 to 8 m.y. ago. Gilbert and others (1968), however, have shown that most movement on present

dip-slip faults has occurred in the last 4 million years in the Mono Basin to the south.

Extensive movement of these dip-slip faults in the Little Walker area has cut the volcanic center into two major westerly tilted blocks. The Little Walker River flows through the middle of the center along the boundary fault between these two major blocks (Figure 6; Plate 1). The vertical throw on that fault is probably at least 4,000 feet, although both major blocks are broken into so many smaller pieces by other normal faults of unknown displacement that estimates of total displacement are very tentative at best.

DETAILED VOLCANIC STRATIGRAPHY

Valley Springs Formation

The Valley Springs Formation is widespread in the northern Sierras, and Noble (1972) has recognized similar rhyolitic tuffs near the base of the Tertiary section throughout the Great Basin. In the northern Sierras the formation has yielded radiometric ages of 33.4 to 20.5 m.y. which is middle to late Oligocene (Cenozoic time scale of Berggren, 1972; Gilbert and others, 1968). Gilbert and others (1968) obtained K-Ar dates of 28 to 22 m.y. from outcrops twenty miles southeast of the Little Walker volcanic center.

At the Little Walker volcanic center the Valley Springs Formation crops out only near Lost Cannon Peak and south of Devils Gate (Plate 1). In both localities it lies beneath the Relief Peak Formation and rests on granitic basement rocks. South of Devils Gate the Valley Springs Formation consists of poorly indurated sanidine rhyolite ash-flow tuff with lesser amounts of moderately welded tuff in basal part. Near Lost Cannon Peak it is a much thicker sequence of poorly welded, much more lithic-rich ash-flow tuff. Lithic fragments in the latter area are chiefly dark andesitic rocks of lapilli-size, but blocks of welded sanidine rhyolite tuff are also abundant in the basal part of the section. The greater thickness of the ash flows near Lost Cannon Peak and greater abundance of lithics compared to the Devils Gate

locality argue that the former area is nearer a vent for the tuffs. Block-size fragments would suggest that the enclosing ash flow near Lost Cannon Peak was very near its vent.

Basalts and Basaltic Andesites

Gilbert and others (1968) have recognized small-volume olivine basalt flows intercalated in andesites of the Relief Peak Formation in the Mono Basin area. Similar olivine basalts and heterogeneous basaltic andesitic units have been found below and intercalated within hornblende andesites of the Relief Peak Formation in the Little Walker area. South of Devils Gate, these mafic rocks are above the Valley Springs Formation. No outcrops of these basaltic lavas have been found at Sonora Pass or Lost Cannon Peak west of the Little Walker area. This evidence suggests that at least one volcanic center was active east of the andesitic center at Relief Peak during much of the Relief Peak activity.

It is probable that the volcano-tectonic regime at the Relief Peak center was distinctly different from the regime of the basaltic volcanic center to the east. Christiansen and Lipman (1972) and Noble (1972) have noted the beginning of fundamentally basaltic volcanism with initiation of Basin and Range tectonism in the Great Basin about 20 to 16 m.y. ago. This time interval overlaps the 22 to 12.5 m.y. interval of Relief-Peak volcanism. The basaltic lavas may

be the product of the spreading Basin and Range tectonics to the east of the Little Walker center.

The lithology of the basalts and basaltic andesitic units is quite variable and not completely known, but some generalization can still be made. Basaltic andesitic rocks consit of 80 to 100 percent dark, pilotaxitic groundmass with or without olivine and augite phenocrysts and minor quartzite xenoliths. The olivine basalts have 17 to 19 percent olivine and 1 to 3 percent augite phenocrysts set in a dark felty or hyalopilitic groundmass. Iddingsitization affects the olivine in some samples. In outcrop both rock types are tough, black units which, nevertheless, do not crop out well. They are mapped as often from their characteristic red-brown soil as from outcrop. They probably form gentle slopes because of numerous fractures which penetrate them.

Relief Peak Formation

Outside of the Little Walker area, autobreccias and mudflows of the Relief Peak Formation blanket much of the northern Sierras (Slemmons, 1966), and correlative rocks along the eastern Sierran Front have been dated by K-Ar methods at 12.5 to 22 m.y. (Gilbert and others, 1968). Together with Mio-Pliocene andesites of the overlying Disaster Peak Formation, the Relief Peak Formation defines a major part of a Mio-Pliocene calc-alkalic volcanic event which

affected much of the northern Sierras (Gilbert and others, 1968; Noble, 1972). Viewed in this perspective, the Stanislaus eruptions represent a small, localized potassic anomaly in regional calc-alkalic volcanism of the northern Sierras.

Field relationships of the Relief Peak Formation in and adjacent to the Little Walker volcanic center are of considerable interest, because these rocks provided one of the few reliable stratigraphic markers in area. All hornblende-bearing pre-Stanislaus rocks were tentatively correlated to the Relief Peak Formation. These rocks are up to 1,000 feet thick near Mount Emma on the southwestern margin of the Little Walker center where they are propylitically altered and locally silicified. They thin rapidly or are absent along the eastern margin of the center where they are exposed by westward-tilted fault blocks. The formation also thins to a few tens of feet thick one-half of a mile west of Poore Lake where erosion during Stanislaus volcanism reduced its thickness (Plate 1). This erosional event is supported by the occurrence of an erosional surface of unconformity bearing Table Mountain Latite, Tollhouse Flat and By-Day Member lithics which separates post-By-Day-Member, Stanislaus rocks from the Relief Peak Formation at the Poore Lake locality and elsewhere in the center (Plate 1). At least 1,000 feet of Relief Peak rocks may have been removed at Poore Lake prior to

eruption of the tuffs and lavas of Poore Lake (Plate 1). The complex relationships in the Kirman Lake-Poore Lake area will be discussed in more detail in the section on the tuffs and lavas of Poore Lake.

Field relationships in and around the Little Walker center suggest that such of the local Relief Peak Formation may have erupted from vents in and around Relief Peak to the west. Slemmons (1966) found about 3,000 feet of the Relief Peak Formation exposed at Relief Peak, where dikes and plugs of the same rocks also occur. He argued that Relief Peak was a major source of the formation in this part of the Sierras. He, however, correlated dikes and pyroclastic rocks of the Stanislaus Group at Mount Emma with the Relief Peak Formation and mistakenly concluded that this was also a major vent for the Relief Peak Formation. Thinning of Relief Peak lavas and breccias from about 3,000 feet at Relief Peak to 1,000 feet near Mount Emma, and, finally to thin, discontinuous outcrops in the Rickey Peak-Devils Gate area on the eastern margin of the center argue that the major source was at Relief Peak (Plate 1). The formation thins much less rapidly from Relief Peak toward the west and is much thicker and more continuous in the western Sierras than along the eastern margin of the Little Walker center. It is proposed that flows and lahars spread out from Relief Peak in all directions but that flow was inhibited toward the east by discontinuous topographic barriers located along the eastern margin of the Little Walker area.

The lithology of the Relief Peak Formation at the Little Walker center is highly variable, but the unit may be distinguished unambiguously from most Stanislaus units by characteristically abundant hornblende in most Relief Peak specimens. Hornblende-bearing andesite mudflows and autobreccias are the dominant rock types in the formation, but considerable amounts of solid lava commonly also are present. North of Pickle Meadow, the lavas and breccias are interbedded with extensive lithic volcanic sandstones. Distinctive flows at Sonora Pass and Poison Creek have 10 percent large (1-2 cm) clumps of glomeroporphyritic hornblende with only 3 percent augite and minor plagioclase (An 79) set in a hyalopilitic groundmass. More typical flows on the north side of the Little Walker area have 17 to 42 percent, 1 to 2 mm plagioclase (An 58) phenocrysts with 1 to 5 percent augite, 2 percent hypersthene and 2 to 6 percent hornblende of about the same size set in a felsitic groundmass. Minor apatite and iron-titanium oxides are ubiquitous accessories. In outcrop the clastic units form hoodoos and appear dark gray to light bluish gray. Solid lavas tend to form cliffs or steep slopes and are of darker color than clastic units.

Stanislaus Group

The stratigraphy of the Stanislaus Group outside of the Little Walker center is relatively well known (e.g., Slemmons, 1966; Noble

and others, 1974) but the relationship of this sequence to intracaldera units of the center is not completely clear. Outside of the center, the Stanislaus Group consists of, from bottom to top, the Table Mountain Latite, Eureka Valley Tuff, and Dardanelles Formation (Noble and others, 1974). The Eureka Valley Tuff has been subdivided into the Tollhouse Flat, By-Day, and Upper members (Noble and others, 1974). Presumably, cauldron subsidence accompanied the eruption of the Eureka Valley Tuff, especially eruption of the giant welded ash-flow sheets of the Tollhouse Flat and By-Day members. The Dardanelles Formation may, then, have erupted while intracaldera volcanism continued at the Little Walker center, although intracaldera lavas chemically or mineralogically equivalent to pyroxene latites of the Dardanelles Formation have not been recognized in this study (Figure 3).

Stratigraphic relationships within the Little Walker center are far more complex than those outside of the center. The intracaldera sequence is dominated by ash-flow tuffs, plug domes, and dikes. Limited distribution of lavas and dikes makes correlation very difficult. Correlation has, in many cases, been accomplished by means of chemical-petrologic similarities when field relationships were obscure. Beginning with the oldest unit, the intracaldera sequence includes the Fales Hot Springs Quartz Latite, the Upper Member of the Eureka Valley Tuff and syngenetic tuffs and lavas of Poore Lake,

the Latite of Devils Gate and Lavas of Mahogany Ridge. The Lavas of Mahogany Ridge and pyroclastic units account for the vast majority of intracaldera fill. The Upper Member of the Eureka Valley Tuff is the only intracaldera unit which has locally escaped the Little Walker caldera.

Conflicting K-Ar ages for rocks of the Stanislaus Group, especially where ages have been determined in different laboratories, make estimation of the life span of the Little Walker center very uncertain. The Table Mountain Latite has yielded a K-Ar date of about 9.0 m.y. ± 0.2 m.y., although the age of the overlying Eureka Valley Tuff is estimated at 9.5 m.y. (Noble and others, 1974). Biotite from cogenetic lithic fragments of the intracaldera Tuffs of Poore Lake has given K-Ar ages of 8.3 and 8.5 m.y. ± 0.3 m.y. (unpublished data of M. Silberman, 1974), but lithologically and stratigraphically equivalent units of the Upper Member of the Eureka Valley Tuff have yielded K-Ar ages of 9.9 ± 0.4 m.y. and 10.0 ± 0.3 m.y. on biotite (Noble and others, 1974). Errors of at least one million years are thus indicated by differences between ages for the Table Mountain Latite and overlying Upper Member of the Eureka Valley Tuff. This data suggests that the total active life of the center is not long enough to be resolved by K-Ar dating.

Timing of Cauldron Subsidence

Distribution of Stanislaus rocks at the Little Walker center suggests the formation of a caldera shortly after the eruption of the two largest welded ash-flow sheets of the Eureka Valley Tuff. The welded quartz latite ash-flow sheet of the Tollhouse Flat Member of the Eureka Valley Tuff is nearly twice as large as the overlying welded quartz latite ash-flow sheet of the By-Day Member (Noble and others, 1974). According to Noble and others (1974) these two ash-flow sheets are much larger than the overlying Upper Member of the Eureka Valley Tuff. It follows that most cauldron subsidence should have occurred contemporaneously or after the two early ash-flow eruptions. Outcrops of the By-Day and Tollhouse Flat members are rare and very thin along the caldera rim and floor. Rim outcrops consist of extremely lithic-rich welded lag-fall deposits and thin ash flows. No outcrop of welded tuff has been found along an uplifted block of the proposed caldera floor in the Mount Emma-Kirman Lake area, however. Only lithic fragments of the welded tuffs on an erosional surface of unconformity cut in Relief Peak Formation suggest their former presence on the caldera floor. The relief on this unconformity is probably as much as a thousand feet in the Mount Emma-Poore Lake area (Plate 1), where it is completely submerged by up to 3,000 feet of poorly welded, lithic-rich, ash-flow tuff, here

called the Tuff of Poore Lake. This tuff appears to be lithologically and stratigraphically correlative with the Upper Member of the Eureka Valley Tuff and represents a significant addition to the total volume of the Upper Member. Considerable erosion of a caldera floor with high relief must have locally stripped the welded tuffs from the interior of the caldera, although later Upper Member ash flows filled in the depression and locally escaped along outward-flowing drainages. It is possible that cauldron subsidence could have continued during the Upper Member eruptions, which may account for the change from erosion in the Mount Emma-Kirman Lake area to accumulation and ponding of the ash flows. The presence of probable landslide blocks of By-Day Member welded tuff in lacustrine tuffs of the Upper Member northwest of Rickey Peak (Plate 1) suggests that a rapidly eroding caldera rim was certainly present on the southeast caldera margin after eruption of the Upper Member.

It is improbable that all cauldron subsidence coincided with the Upper Member eruptions. Not only would this discount the probably important role of the voluminous welded tuffs of the Tollhouse Flat and By-Day Members, but it fails to explain the distribution of the Fales Hot Springs Quartz Latite (FQL). At Fales Hot Springs welded and unwelded ash flows of the Upper Member bury a thick pile of FQL plug domes and flows. The presence of feeder dikes and associated endogenous domes of the FQL at Fales Hot Springs proves that this is

a major vent area for the formation. The FQL was evidently capable of flowing five miles to the south, because a thin flow of FQL crops out on the southeast margin of New Range beneath lacustrine tuffs of the Upper Member (Plate 1). Only a few hundred feet north of the vent at Fales Hot Springs, only pre-Eureka Valley Tuff lavas crop out. This data suggests that a steep caldera margin existed on the north side of Fales Hot Springs and ponded both the Upper Member and underlying FQL. This pre-Upper Member caldera must have been the result of voluminous eruptions of the Tollhouse-Flat and By-Day ash flows.

Resurgent Fracturing

Ring fracturing and faulting may not have ceased with the last pyroclastic eruptions. All intracaldera lavas and dikes have vent areas located in arcuate and ring patterns which may represent resurgent fractures and faults at depth. Perhaps most suggestive of this is location of a series of endogenous, low-K latite plug domes of the Lavas of Mahogany Ridge in a nearly perfect circle in the center of the caldera at Mahogany Ridge (Plate 1; Figure 6). Unfortunately, no indisputable proof of resurgent doming was found.

Table Mountain Latite

The Table Mountain Latite is the oldest and most widespread formation of the Stanislaus Group. It consists of dark colored augite-olivine-bearing latites in its lower part which is the bulk of the formation. Upper flows are less voluminous and more highly differentiated than the underlying mafic latite flows. The higher SiO_2 and Al_2O_3 of the upper latites caused them to be more viscous than the lower flows and, together with their small volume, restricted them to areas near their vents.

Lower flows of Table Mountain Latite probably erupted from vents at Sonora Pass and possibly the Little Walker center, but the upper flows must have come largely from the Little Walker volcanic center. Thick sections of pyroxene-olivine latite lavas with cogenetic dikes in the Sonora Pass area make it certain that this was a major vent area for much of the formation (Slemmons, 1966). The lower mafic flows reached as far west as Sonora in the western foothills of the Sierras, but are recognized no farther east than the eastern margin of the southern Sweetwater Mountains. The silicic upper flows are restricted to areas within several miles around the Little Walker volcanic center and are thickest and most lithologically variable at the center. Much of the lower part of the Table Mountain Latite may have flowed from the Sonora Pass area west of the Little

Walker center, but by the time of eruption of the upper part of the formation the center of magmatism had shifted to the Little Walker area. This shift was accompanied by a compositional shift toward more highly evolved lavas which climaxed with the eruption of overlying quartz latite ash flows of the Eureka Valley Tuff.

The Table Mountain Latite has been subdivided into several informal units within the Little Walker center to aid in detailed structural analysis of the caldera margin. From bottom to top the Table Mountain Latite consists of the Lower Member, Large-plagioclase Member, Two-pyroxene Member and Upper Member. The Lower Member consists of augite-olivine-bearing lavas which are similar to those at Sonora Pass. The overlying members are much less voluminous and mafic than the Lower Member. The Large-plagioclase Member is the only upper unit which occurs more than a few miles outside of the Little Walker center.

Lower Member-Table Mountain Latite

The basal unit of the Table Mountain Latite is here informally called the Lower Member. It is about 700 to 800 feet thick at Flat Iron Ridge where it consists of several flows of augite-olivine-bearing latite lava and subordinate autobreccia (Figure 9; Plate 1). The Lower Member is thicker than this at Sonora Pass to the east (Slemmons, 1966) which may be the source of much of the unit. Flows

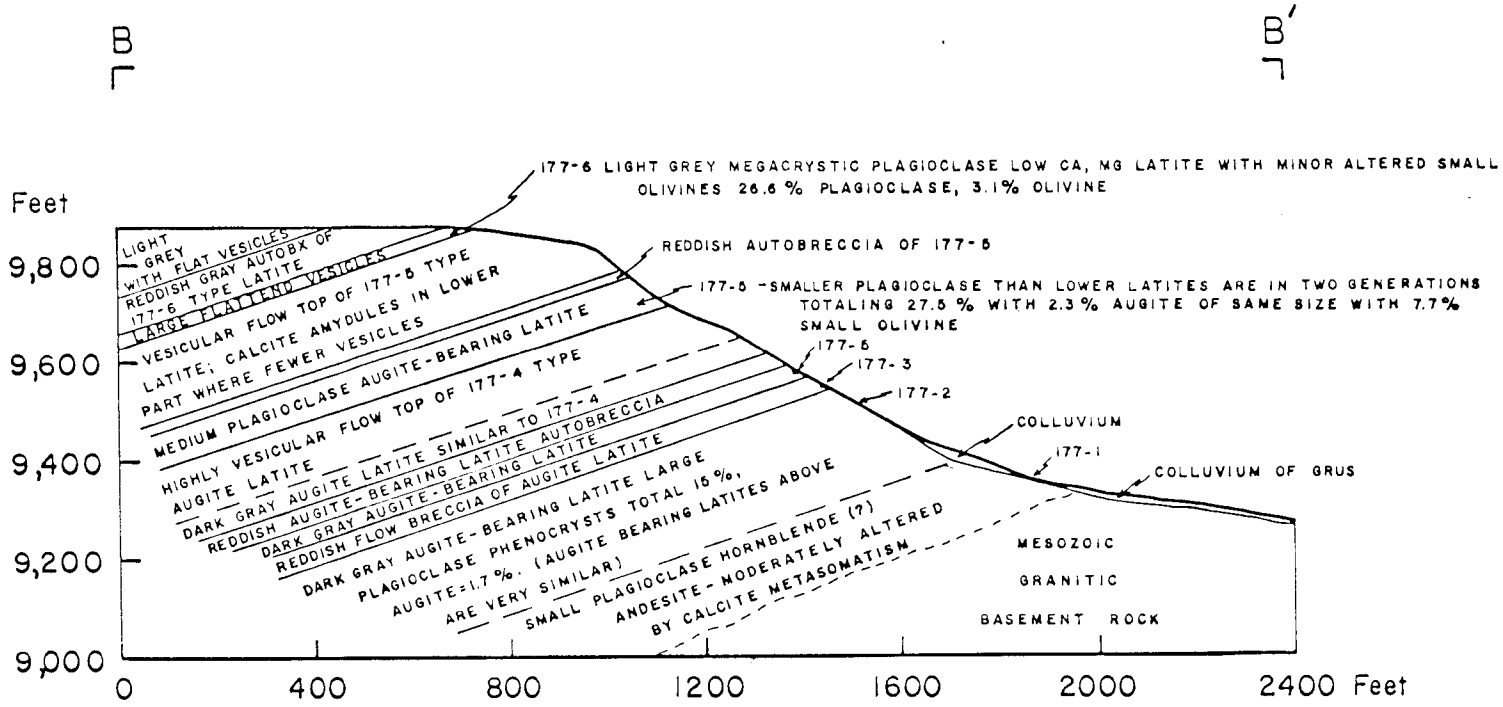

Figure 9. Measured section of Table Mountain Latite at Flat Iron Ridge. (See C-C', Plate 1).

correlative to the Lower Member thin both east and west of Sonora Pass, but are most extensive toward the west. The western exposures appear to be intracanyon flows which roughly follow a river valley nearly coincident with the present Stanislaus River. The Lower Member has been recognized as far west as Knights Ferry near Sonora in the western Sierran foothills but appears restricted on the east to the southern Sweetwater Mountains and Little Walker Volcanic center.

The age of the Lower Member is not known with certainty, but it is older than overlying Eureka Valley Tuff which has been radiometrically dated at 9.5 m.y. (Noble and others, 1974). Dalrymple (1964) obtained a K-Ar data of 9.0 m.y. ± 0.2 m.y. on a Lower Member lava flow, but this age is probably too young. The Lower Member may be so similar in age to the Eureka Valley Tuff that the difference in age is not resolvable by K-Ar dating.

The Lower Member is lithologically variable at the Little Walker center, but may normally be distinguished from all other lavas by the presence of olivine and augite phenocrysts without significant orthopyroxene or hornblende. The lower part of the Lower Member is most easily recognized because of distinctive large (3 to 5 mm) plagioclase and augite phenocrysts. In thin section lower flows of the Lower Member have anhedral to subhedral labradorite (An 58, 15 percent) phenocrysts with much less subhedral to euhedral augite (2 percent) and anhedral, 0.8 mm olivine (4.6 percent) phenocrysts

often altered to iddingsite or serpentine. The groundmass is a pilotaxitic mixture of plagioclase microlites with subordinate augite, olivine, and accessories. Sparse apatite and Fe-Ti oxides are the chief accessory minerals.

The lower flows of the Lower Member are overlain at Flat Iron Ridge (Figure 9) and elsewhere in the southeastern part of the Little Walker center by a flow of similar augite-olivine latite which has somewhat smaller augite and olivine phenocrysts than the lower flows and a second generation of plagioclase microphenocrysts. In hand-sample this flow is very difficult to distinguish from the Lavas of Mahogany Ridge, but careful inspection will reveal the second generation of plagioclase phenocrysts, lack of orthopyroxene, and somewhat fewer large phenocrysts than is characteristic of the Lavas of Mahogany Ridge. In thin section the two generations of plagioclase phenocrysts (An 54, 2.5 mm and 1 mm) are more abundant (27.5 percent) than plagioclase in the lower flows and are accompanied by subhedral to euhedral augite (2.3 percent, 2 mm) and smaller, anhedral olivine (7.7 percent, 0.8 mm) phenocrysts. Phenocrysts are set in a groundmass of subaligned microlites of plagioclase with subordinate augite, olivine and Fe-Ti oxides. Apatite and Fe-Ti oxides are ubiquitous accessory phases.

Outcrops of the Lower Member, like much of the Table Mountain Latite, appear less fresh than intracaldera lavas and tend

to form cliffs or steep slopes. Reddish brown autobreccias and vesicular flow tops however, tend to form gentle slopes (see Figure 9). Hand samples are generally medium gray to reddish brown and have numerous small scale fractures in some cases. Samples from flow tops are generally vesicular and locally have abundant amygdules of calcite or chalcedony. No plug domes or coulees of the Lower Member have been found; instead, all outcrops appear to be simple, relatively thin flows, similar to basaltic flows. This is in marked contrast to similarly mafic lavas of the intracaldera Lavas of Mahogany Ridge rocks which substantilly increase the viscosity of the original magmas. In any case, this difference in occurrence together with lack of amygdaloidal flow tops or reddish autobrecciated units in the Lavas of Mahogany Ridge help to distinguish them from the Lower Member.

Large-Plagioclase Member-Table Mountain Latite

The Large-plagioclase Member of the Table Mountain Latite is probably one of the most easily recognized units at the Little Walker center. It may be unambiguously recognized by its large (1 to 2 cm) labradorite (An 55) phenocrysts which are normally the only large crystals in the rock. Lack of significant large mafic crystals and predominance of plagioclase reveal a radical compositional change in these rocks compared to the underlying Lower Member and overlying

Two-pyroxene Member. The Large-plagioclase Member is a very aluminous, low-Ca-Mg latite compared to normal mafic latites of the Lower Member.

Both the source and relative volume of the Large-plagioclase Member may be estimated by its distribution. All known outcrops of these rocks occur within a few miles of the Little Walker volcanic center, and in most areas remote from the southeast margin of the Little Walker caldera, the Large-plagioclase Member is directly overlain by the Eureka Valley Tuff. The Little Walker center is, thus, the most likely source of the Large-plagioclase Member. Persistence of the Large-plagioclase Member beyond areas where the overlying Two-pyroxene Member and Upper Member of the Table Mountain Latite crop out suggests that it is of much larger volume than those lavas. The Large-plagioclase Member is much more restricted in areal distribution and therefore of smaller volume than widespread flows of the Lower Member of the Table Mountain Latite.

The Large-plagioclase Member undoubtedly consists of two or more flows, because the percentage of plagioclase phenocrysts ranges from about 30 percent to 3 or 4 percent in various outcrops. The most extensive flow contains 26.6 percent anhedral labradorite (5 mm to 15 mm, An 55) phenocrysts and heavily iddingsitized, anhedral microphenocrysts of olivine (0.8 mm) set in a pilotaxitic groundmass of the same minerals. Traces of Fe-Ti oxides and apatite are

common to all specimens. Where this extensive flow crops out at Flat Iron Ridge (Figure 9), it grades from a solid, highly fractured gray lava in its interior to highly vesicular light gray rock at the top. The vesicles are highly flattened parallel to the flow surface and are coated with a powdery yellow-colored substance. Flow tops tend to form very gentle slopes, whereas lower parts of flows tend to underlie moderate slopes. The lower parts do not usually form steep slopes because of their highly fractured nature.

Two-Pyroxene Member-Table Mountain Latite

The Two-pyroxene Member is a series of two-pyroxene, low-K latite lavas and autobreccias which crop out about one mile northwest of Rickey Peak and below the Eureka Valley Tuff in By-Day Canyon. Limitation of the thickest sequence of Two-pyroxene Member to the southeast margin of the Little Walker volcanic center and thinning of the lavas toward the only other known outcrops at By-Day Canyon strongly suggest that the Two-pyroxene Member erupted from a vent at the Little Walker center.

The Two-pyroxene Member is chemically and mineralogically distinct from the rest of the Table Mountain Latite. It is much less potassic than other Table Mountain Latite members and contains orthopyroxene which is very rare in the Table Mountain Latite. The Two-pyroxene Member actually resembles the Lavas of Mahogany

Ridge much more closely than it does most of the Table Mountain Latite. Outcrops of the Two-pyroxene Member at the south end of Huntoon Creek could be interpreted as intracanyon flows of nearby Lavas of Mahogany Ridge which may have flowed around high-standing ridges of Eureka Valley Tuff. Identical outcrops in steep slopes on the north side of By-Day Canyon appear, however, to be unequivocally below the Eureka Valley Tuff. The Two-pyroxene Member appears to represent a real chemical anomaly within the pre-caldera Stanislaus Group. Later petrologic arguments will suggest that the Two-pyroxene Member may have been partially melted from a source which was more closely related to the source of the Lavas of Mahogany Ridge than the source of most of the Table Mountain Latite.

Three features of the Two-pyroxene Member distinguish it from the Lavas of Mahogany Ridge. A thick section of these lavas consists of reddish brown autobreccias on the east side of the upper end of Huntoon Creek (Plate 1). Such autobreccias are rare in the Lavas of Mahogany Ridge and, where present, are light gray to tan, not reddish brown. Plagioclase and hypersthene phenocrysts are highly corroded by reaction with the liquid in the Two-pyroxene Member, but most phenocrysts of the Lavas of Mahogany Ridge are much less corroded and more euhedral. The Two-pyroxene Member also has distinctive, highly colored purplish apatite prisms which are lacking in the Lavas of Mahogany Ridge.

In thin section the Two-pyroxene Member has 19.7 percent heavily embayed, anhedral to subhedral plagioclase (3.0 mm, An 47) phenocrysts with 10.8 percent euhedral augite (2.5 mm), frequently in clusters, and 4.7 percent anhedral, resorbed hypersthene (2.0 mm) phenocrysts showing abundant opaque inclusions along cleavages. The phenocrysts are set in a pilotaxitic groundmass of pyroxene and plagioclase. Accessories include 1.4 percent Fe-Ti oxides and minor, but conspicuous purplish apatite prisms. In outcrop the rock is usually dark gray and compact but autobrecciated parts are reddish brown and friable. Solid lava forms steep slopes and autobrecciated phases frequently form hoodoos.

Upper Member-Table Mountain Latite

Numerous small lava flows which overlie the Two-pyroxene Member on the southeast margin of the Little Walker center are here called the Upper Member of the Table Mountain Latite. The heterogeneous nature of this unit makes it difficult to describe and even more difficult to correlate between widely separated outcrops. Most lavas lumped under this name have few mafic phenocrysts except for one flow at Flat Iron Ridge which has 8 percent pyroxene. The lack of mafic phases reflects the rather highly differentiated nature of most lavas of the Upper Member. These rocks seem to be part of a general chemical change in the character of the Table Mountain Latite as it

erupted from vents in the Little Walker Volcanic center. Lavas of the Upper Member are generally very low in MgO, CaO, and FeO but high in Al_2O_3, similar to the Large-plagioclase Member. In fact, many outcrops of Upper Member cannot be readily distinguished from phenocryst-poor lavas of the Large-plagioclase Member unless field relationships with the Two-pyroxene Member are clear.

In most flows of Upper Member the only phenocryst is plagioclase which typically accounts for 2 to 3 percent of the rock, although some lavas have 28 percent plagioclase, and aphyric units also crop out locally. Hand samples are usually gray with many closely spaced fractures which may disaggregate the rock into thin plates, especially in aphyric and nearly aphyric rocks. Completely rehealed, autobrecciated texture is typical of nearly all of the rocks of this unit and appears to be one of the few characteristics which is useful in correlation. Such texture, however, is not unknown in the Large-plagioclase Member.

Tollhouse Flat Member-Eureka Valley Tuff

The Tollhouse Flat Member of the Eureka Valley Tuff is the most voluminous and widespread pyroclastic unit of the Stanislaus Group. It is as thick as 300 feet near the Little Walker volcanic center and generally thins away from the center (Noble and others, 1974). It extends at least 50 miles west of the Little Walker center and

35 miles to the east. The ash-flow sheet is generally contained within an east-west drainage system which limited its distribution to within 10 or eleven miles north and south of the center. Coincidence of most outcrops of the Tollhouse Flat Member with underlying Table Mountain Latite suggests that both units followed similar topographic lows.

Increasing abundance of lithic fragments and large, partially vesiculated magma lumps (Figure 10) in the ash-flows toward the Little Walker volcanic center, suggest that the Little Walker center was the source of the Tollhouse Flat Member. This is supported by general thickening of the ash-flow sheet toward the margin of the Little Walker caldera. However, outcrops of the Tollhouse Flat Member at the rim of the caldera are thin and discontinuous. These variations in thickness may be explained by efficient flow of much of the ash-flow sheet off of a topographically high area at the Little Walker center. This high may have been the result of tumescence of the area from magmatic pressure, but pre-eruptive topographic highs may also have been present.

The Tollhouse Flat Member may be distinguished from the overlying By-Day Member by presence of phenocrystic biotite in pumice lumps. It is much more difficult to distinguish the Tollhouse Flat Member from welded units of the Upper Member of the Eureka Valley Tuff. Noble and others (1974) noted fewer slightly

vesiculated pumice blocks in the Upper Member, reversed magnetic polarity in the Tollhouse Flat Member versus normal polarity in the Upper Member, and more "spongy plagioclase phenocrysts" in the Upper Member relative to the Tollhouse Flat Member.

Figure 10. Near-vent facies of Tollhouse Flat tuff with large, moderately flattened magma lumps.

Abundant collapsed pumice which may exceed one foot in diameter gives the gray to red brown Tollhouse Flat Member striking eutaxitic texture in densely to moderately welded sections (Figure 10). Most of the ash-flow sheet is welded except for thin upper and lower glassy zones which are only a few inches in thickness. Five or more

partings can be present within the cooling unit, and the upper 5 to 20 feet of the sheet generally have ash flows with fewer and smaller pumice fragments, phenocrysts, and lithic fragments than lower ash flows (Noble and others, 1974). Lithic fragments of intermediate lavas and granitic rocks make up about 15 to 20 percent of most Tollhouse Flat ash flows.

Pumice lumps have somewhat variable amounts of phenocrysts, but most have oscillatory zoned plagioclase (An 45) with smaller quantities of biotite, augite, magnetite and apatite. Rare hornblende laths have been observed in some thin sections (Noble and others, 1974). A typical pumice lump sampled from the northeast margin of the Little Walker caldera contains 12 percent subhedral plagioclase (An 45, 2 mm), 2 percent subhedral biotite (2 mm), 1 percent euhedral augite (0.5 mm) and minor Fe-Ti-oxide phenocrysts set in a glassy groundmass. Apatite is commonly included within other phenocrysts. Phenocrysts occur as widely spaced glomeroporphyritic aggregates in pumice lumps but are broken and much more abundant in the ash matrix, indicating winnowing of fine ash from crystals.

Intercalated Lavas-Eureka Valley Tuff

Thin latite lava flows have been found between the Tollhouse Flat Member and overlying By-Day Member of Eureka Valley Tuff at By-Day Canyon, Tollhouse Flat and on the lower north slope of

Rickey Peak (Tmel on Plate 1). Only the flow at Rickey Peak has been sampled in this study, but if it is typical of these units, then these lavas represent a sharp departure from the composition of the ash flows. The low concentration of K_2O and presence of two pyroxenes in this low-K latite lava are anomalous when compared to the highly potassic Eureka Valley Tuff and underlying Table Mountain Latite, both of which lack significant orthopyroxene. Petrologic considerations in a later section will suggest that this lava, together with the Lavas of Mahogany Ridge, represent magmas derived from a fundamentally different source than the latites and quartz latites of the Stanislaus Group. This source dominated volcanism in the closing phase of activity at the Little Walker center when extensive two-pyroxene, low-K latite flows and plug domes of the Lavas of Mahogany Ridge filled in most of the western interior of the Little Walker caldera.

About 60 to 100 feet of the two-pyroxene lava crop out north of Rickey Peak (Plate 1), where it is a dark gray, vesicular rock with scattered, round vesicles. Phenocrysts consist of 20 percent subhedral plagioclase (An 54), 8 percent subhedral augite, and minor, corroded orthopyroxene set in a felsitic groundmass. All phenocrysts are about 2 to 3 mm in diameter. Fe-Ti oxides and apatite are minor accessories, and much of the Fe-Ti oxide is concentrated within and around hypersthene phenocrysts. The lava typically underlies gentle

to moderate slopes, and generally does not crop out well.

By-Day Member-Eureka Valley Tuff

The By-Day Member of the Eureka Valley Tuff was the second major welded ash-flow sheet to erupt from the Little Walker volcanic center. It probably has less than half of the volume and areal extent of the underlying Tollhouse Flat Member (Noble and others, 1974). In most localities the By-Day Member lies directly on the Tollhouse Flat Member with only a few inches of poorly welded tuff to suggest a cooling break between the two ash-flow sheets. At Tollhouse Flat and other areas the two members locally are separated by latite lava or cross-bedded volcanic sandstones.

Outcrops of Tollhouse Flat and By-Day tuff look very similar but the By-Day Member is normally of darker color and lacks phenocrystic biotite in pumice. A second generation of plagioclase microphenocrysts in the By-Day Member is also distinctive, and the first generation of phenocrysts is somewhat smaller than those of the Tollhouse Flat Member. The By-Day Member is also somewhat less silicic than the Tollhouse Flat Member. The upper, poorly welded zone of the By-Day Member, where preserved, is much thicker than that of the Tollhouse Flat Member. The poorly welded zone is up to 10 or 20 feet thick in some areas. These features are sufficient to distinguish By-Day Member outcrops from those of the Tollhouse Flat

or Upper Member, regardless of the quality of the outcrop.

Areal variations in lithology and thickness of the By-Day Member provide compelling evidence that the Little Walker volcanic center was the vent area for these ash flows. The By-Day Member thickens from distal areas toward the Little Walker center to a maximum of 200 feet near the rim of the Little Walker caldera (Noble and others, 1974). Outcrops on the rim of the Little Walker caldera, however, are thin and discontinuous, but abruptly thicken outward to the maximal thicknesses around the margins of the caldera. The selvages of By-Day on the caldera rim have extremely abundant lithic fragments and locally contain unvesiculated magma blocks of up to 2 feet in diameter (Figure 7). These outcrops appear to be dense fractions which lagged behind the more mobile part of the ash-pumice emulsion. Similar deposits have elsewhere (e.g., Wright and Walker, 1977) been called lag-fall deposits. Because all of these outcrops have densely welded ash matrices, they are called welded lag-fall deposits. It is evident that such rocks must have been deposited at or very near their vent. This is considered the best evidence that the By-Day Member erupted from the Little Walker center. Concentration of welded lag-fall deposits only on the southeast margin of the Little Walker caldera indicate that this was a specific vent for the By-Day Member. It is possible that the same ring fault which bounds

the caldera on its southeast margin served also as the conduit for the By-Day ash flows.

There is very good evidence that cauldron subsidence occurred shortly after the By-Day eruption. Large blocks of By-Day Member are found in lacustrine tuffs of the Upper Member of the Eureka Valley Tuff on the southeast interior margin of the proposed caldera (Figure 8). The Upper Member is underlain at this same location by lavas of the Fales Hot Spring Quartz Latite. Because it is unlikely that eruption of the Fales Hot Springs Quartz Latite could have caused collapse, limitation of its lavas to the margins of the proposed caldera implies that a caldera was caused by previous ash-flow activity. The only previous ash-flow activity was eruption of the By-Day and Tollhouse Flat members of the Eureka Valley Tuff. The best explanation for these observations is that some collapse occurred during or after eruption of the By-Day and Tollhouse Flat tuffs and that a caldera lake formed and gradually filled with landslide and talus debris from the caldera rim as intracaldera volcanism continued.

In outcrop the By-Day Member is black to dark gray in densely welded parts but is medium gray in the poorly welded upper part of the ash-flow sheet. Noble and others (1974) recognized at least three partings within the cooling unit but concluded that many more are probably present. Most of the By-Day Member consists of

spectacularly eutaxitic pumice-rich welded tuff, but where the welded lag-fall facies is present, it may be mistaken for an autobreccia or lahar. Abundant welded ash and pumice in the matrix between the large blocks of cogenetic lava and smaller lithic fragments will, upon close inspection, reveal the pyroclastic nature of the lag-fall rocks. The densely welded zone underlies steep slopes or cliffs, while the poorly welded zone forms gentle slopes.

The composition of the By-Day Member in hand sample and thin section is distinctive. Pumice has 3 percent oscillatory-zoned plagioclase phenocrysts in two generations (2 mm and 0.5 mm) with 0.5 percent euhedral augite (0.5 mm) phenocyrsts. All phenocrysts tend to be euhedral. The first generation of plagioclase crystals is quite calcic (An 60) compared to plagioclase of the rest of the Eureka Valley Tuff. Minor Fe-Ti oxides and apatite are ubiquitous minor accessories. The ash matrix is more abundant (65-70 percent) than lithic fragments and pumice in most of the ash-flow sheet, and is enriched in crystals relative to pumice from winnowing of the ash component. Dark andesitic lithics account for 10 to 20 percent of the rock in most outcrops but become much more abundant (50 percent) in exposures along the rim of the Little Walker caldera. Where lithic fragments are abundant, they locally are accompanied by unvesiculated magma blocks as large as 2 feet in diameter. In such outcrops, the rock is best called a welded lag-fall deposit.

Fales Hot Springs Quartz Latite

Approximately 500 feet of biotite-bearing quartz latite lavas crop out beneath the Upper Member of the Eureka Valley Tuff at Fales Hot Springs (Plate 1). This unit is here formally called the Fales Hot Springs Quartz Latite (FQL) for exposures at the type section south of Fales Hot Springs (latitude 38° 28' 49" N, longitude 110° 24' 50" W; Plate 1). The FQL is also well exposed at a reference section on the east side of Sawmill Creek, one-half mile southeast of the type section (latitude 38° 20' 27" N, longitude 119° 23' 16" W; Plate 1). Isolated outcrops of these lavas are found less frequently south of the Fales Hot Springs-Bush Mountain area and none are known in the western part of the Little Walker caldera. No FQL has been recognized outside of the Little Walker caldera. The FQL is definitely older than the Upper Member of the Eureka Valley Tuff and appears to be younger than the By-Day Member. Although the FQL is overlain by Upper Member tuff south of Fales Hot Springs, the lower contact is frequently obscured by younger dikes or sediments. In a poor exposure on the southeast margin of the caldera the FQL appears to lie on an erosional surface of unconformity cut in the Large-plagioclase Member of the Table Mountain Latite. Loose boulders and cobbles of By-Day Member are strewn over the erosion surface around this outcrop of FQL. Although these boulders and cobbles are

colluvium, they may represent loosely consolidated lithic fragments from this basal unconformity. If this is the case, then the FQL is definitely younger than the By-Day Member. In any case, limitation of the FQL to the proposed eastern margin of the Little Walker caldera suggests that it is younger than the caldera.

Fales Hot Springs is probably a major vent for the FQL. Steeply dipping flow foliation with concentric to random strike suggest that the FQL exposures at the type section are part of an endogenous dome. A slightly altered dike of FQL crops out at the edge of Fales Hot Springs, below this dome, and may represent a major feeder conduit. These relations together with general thinning of the FQL toward the south and its absence north of Fales Hot Springs suggest that much of the formation welled up along a steep caldera rim at Fales Hot Springs and spread out toward the south along the eastern interior of the caldera.

The lithology of the FQL varies very little except in terms of degree of alteration and crystallinity. At Fales Hot Springs and the reference section, it consists of biotite-bearing, perlitic vitrophyre. Exposures to the south locally are heavily zeolitized and some flows on the southwest side of Bush Mountain have more groundmass microlites than the FQL at the type section. In thin section the FQL has 17.4 percent anhedral to subhedral, glomeroporphyritic plagioclase (1.5 mm, An 30) and subhedral biotite phenocrysts set in

a hypohyaline groundmass containing aligned feldspar and biotite microlites. Fe-Ti oxides and apatite are ubiquitous accessories. In perlitic specimens plagioclase microlites have slender extensions growing from the corners of the laths, parallel to their length. Such "swallowtail" textures are typical of crystals grown in very viscous, supercooled liquids (Lofgren, 1971). Lack of swallowtail texture in the microlite-rich lavas on the southwest side of Bush Mountain suggests that these lavas cooled less quickly than was typical for most of the FQL. The Bush Mountain lavas also lack perlitic texture.

Color varies with crystallinity and alteration. Perlitic, glass-rich FQL is light gray while nearly holocrystalline lavas are reddish tan. Zeolitic alteration affects the FQL at Little Long Valley (Plate 1) where outcrops are nearly white.

Flow foliation cleavage and resistance to weathering also vary according to the degree of alteration. Non-zeolitized units underlie moderate to steep slopes, whereas altered rocks crop out poorly in gentle slopes. Unaltered units display excellent flow-foliation cleavage.

Upper Member-Eureka Valley Tuff

The Upper Member of the Eureka Valley Tuff represents the dying stages of pyroclastic activity in the Little Walker caldera. Poorly welded and non-welded ash-flows dominated in these final

eruptions, although some densely welded units are interbedded in many sections. Within the caldera the Upper Member is interbedded with volcanic sandstones and lacustrine tuffs, but in exposures outside of the caldera, detrital units are much less common.

One thousand feet of Upper member at Yaney Canyon, immediately beyond the caldera rim, shows distinctive textures which may reveal the mode of eruption. The tuff at Yaney Canyon varies from typical non-welded ash-flow tuff to crudely bedded, poorly sorted tuff (Figure 11). The crude beds resemble beds in tuff cones and may be the result of effusion of water-saturated ash slurries. Such eruptions may have accompanied repeated ejection of the caldera lake. Outcrops farther removed from the rim are dominated by non-bedded ash flows. It may be that only the hot, dry ignimbrites were mobile enough to travel more than a few miles from the rim where ash slurries or phreatic blasts of ash were dominant.

The Upper Member was probably ponded within the Little Walker caldera. Estimation of stratigraphic thickness within the eastern half of the caldera is complicated by extensive disruption of the Upper Member by younger intracaldera dikes and plug domes. Up to 500 feet of the tuff is locally exposed in the eastern part of the caldera, but it may be much thicker at depth. Up to 3,000 feet of correlative tuffs at Poore Lake (Tuff of Poore Lake, Plate 1) on the west side of the caldera may represent the true thickness of intracaldera tuffs in

local topographic lows.

Figure 11. Crudely bedded and non-bedded outcrops of the Upper Member of the Eureka Valley Tuff on the south side of Yaney Canyon.

Some of the intracaldera fill was derived from erosion of the rim. On the southeast margin of the caldera northwest of Rickey Peak (Plate 1), lacustrine tuffs of the caldera lake contain large blocks of the By-Day Member of the Eureka Valley Tuff. Such blocks were probably derived from landslides off the nearby caldera rim. Deltaic sandstones within the Upper Member on the north side of Bush Mountain contain penecontemporaneous deformation which indicates rolling of hydroplastic sand layers down a steep depositional slope. This slope was oriented west, toward the interior of the caldera. It may be that enormous quantities of sand from drainages along the rim

fed this delta, causing oversteepened, unstable depositional slopes. The combination of rapid stream deposition and mass movement probably accounted for a large amount of the total fill along the caldera margin.

K-Ar ages of welded ash flows within the Upper Member of the Eureka Valley Tuff are anomalously high. Noble and others (1974) determined K-Ar ages of 10 ± 0.3 m.y. and 9.9 ± 0.4 m.y. from biotites in welded Upper Member ash flows at Fales Hot Springs and Tollhouse Flat, respectively. These dates are higher than values of 9.5 m.y. which are typical for underlying members of the Eureka Valley Tuff (Noble and others, 1974).

Welded units of the Upper Member are very difficult to distinguish from the Tollhouse Flat Member of the Eureka Valley Tuff. Both are biotite-bearing quartz latite tuffs, but they differ in several respects. Noble and others (1974) noted that the Upper Member has normal polarity and no large, slightly vesiculated pumice blocks as found in the Tollhouse Flat Member. In thin section the Upper Member has highly resorbed, spongy plagioclase. Interbedding of welded units with abundant non-welded ash flows is also distinctive of the Upper Member.

Outcrops of the bulk of the Upper Member are usually easily recognized. Most exposures are dominated by cream to white, hoodoo-forming non-welded tuff bearing abundant dark andesite or

light gray, biotite quartz latite lithic fragments. In the lower part of the Yaney Canyon exposure, local four to five foot lenses of nearly 100 percent, angular rock fragments occur. Such lenses may represent a vent-clearing explosion or settling of dense fractions during ash flow. Poorly welded and non-welded tuffs form low slopes, while black, densely welded ash flows form cliffs and steep slopes.

Hand samples of the Upper Member have highly variable compositions but some generalizations can be made. The tuffs are predominantly, perhaps entirely, biotite-bearing quartz latite. Thin sections of collapsed pumice in a welded ash flow of the Upper Member near Fales Hot Springs contain 4 percent subhedral plagioclase (5 mm, An 43), 1 percent subhedral biotite (2 mm), 0.5 percent subhedral to euhedral augite (1 mm) and 0.5 percent brown hornblende (1 mm) phenocrysts set in a glassy groundmass. This welded ash flow is strikingly eutaxitic with abundant (30 percent) collapsed lapilli and lithic fragments (10 percent). The poorly welded tuffs appear to have similar compositions, although the amount of various constituents may vary from ash flow to ash flow. Some poorly welded ash flows have abundant biotite-quartz latite rock fragments which may be cogenetic with the enclosing ash, but dark andesitic fragments of older lavas are generally the most common lithic fragments.

Lavas and Tuffs of Poore Lake-Eureka Valley Tuff

Preliminary mapping of the western part of the Little Walker caldera has revealed extensive outcrops of biotite-bearing quartz latite ash-flow tuff. This tuff is predominantly non-welded or poorly welded and very rich in lithic fragments. At Poore Lake at least 2,400 feet and perhaps as much as 3,000 feet of these rocks are exposed (Plate 1). Because only a few days of field work were available for reconnaissance of these units in the Pickle Meadow-Poore Lake area, the stratigraphic relations of the tuffs and associated lavas in this area are not well known.

The Tuff of Poore Lake resembles the Upper Member of the Eureka Valley Tuff in most respects and is here tentatively correlated with the Upper Member. This correlation is supported by the presence of lithic fragments of By-Day-like and Tollhouse Flat-like tuffs on an erosional surface of unconformity below the Tuffs and Lavas of Poore Lake north of Kirman Lake (Plate 1). The Tuff of Poore Lake is also cut by cogenetic biotite-quartz latite dikes on the west side of Pickle Meadow, and these dikes are, in turn, cut by plug domes of the Lavas of Mahogany Ridge at the same locality (Plate 1). The Tuffs and Lavas of Poore Lake are therefore older than the Lavas of Mahogany Ridge and younger than the By-Day Member of the Eureka Valley Tuff.

K-Ar ages of 8.9 ± 0.2 m.y. and 8.6 ± 0.2 m.y. (unpublished K-Ar data of M. Silberman, 1974) from biotites in cogenetic lithic fragments of the Tuff of Poore Lake also suggest that the tuffs are younger than the 9.5 million-year-old Tollhouse Flat Member and By-Day Member (Noble and others, 1974). Unfortunately, these dates are younger than ages determined for the Upper Member at Tollhouse Flat and Fales Hot Springs (9.9 to 10.0 m.y. according to Noble and others, 1974). The latter ages are considered too high by Noble and others (1974) who argue that the preferred age of the entire Eureka Valley Tuff is 9.5 m.y. These arguments indicate that correlation by K-Ar data is rather equivocal, but that the Tuffs of Poore Lake may be, in part, younger than the rest of the Eureka Valley Tuff.

Use of chemical and mineralogical composition to correlate the Tuffs of Poore Lake is limited by widespread hydrothermal alteration which affects most outcrops in the western part of the caldera. The poorly welded tuffs are pervasively propylitized and locally silicified and sericitized by hypabyssal, intracaldera plutons which cut the tuffs at and north of Mount Emma (Plate 1). These monzodiorite plutons are compositionally correlative to the Lavas of Mahogany Ridge (Plate 1). Except in heavily altered areas, sparse biotite can usually be recognized in most outcrops and greater amounts of subhedral plagioclase are always present as phenocrysts. Lapilli-size pumice

generally make up 25 to 30 percent of the rock and lapilli- to block-size lithic fragments locally make up 10 to 25 percent. Some lithic blocks in the Tuff of Poore Lake are up to several feet in length in the Poore Lake-Poison Creek area and can be mistaken for short dikes in poorly exposed areas (Plate 1).

Because of incomplete mapping in the westernmost part of the caldera, no attempt has been made to subdivide various lavas associated with the Tuff of Poore Lake, thus only a general description of their mineralogy is appropriate at this time. All of the lavas and dikes thus far examined have abundant biotite and plagioclase and most have silica contents high enough to be called quartz latite. The similarity of phenocrysts in the tuffs to those of the Lavas of Poore Lake suggests that the tuffs and lavas are cogenetic. The lavas may be easily recognized by their light gray to cream color and abundant, conspicuous biotite. They appear to be the most biotite-rich members of the Stanislaus Group. The only Stanislaus rocks known to contain as much biotite as these lavas are biotite-rich lithic fragments in the Upper Member at Yaney Canyon. In outcrop the Lavas of Poore Lake underlie steep slopes.

Field relationships among the Lavas and Tuffs of Poore Lake indicate that the lavas erupted before and after pyroclastic activity. The lavas have been found below the tuffs and as lithic fragments within the tuffs, whereas similar magma appears to have cut the Tuffs

of Poore Lake in long arcuate dikes on the east side of Pickle Meadow (Plate 1). These dikes appear to follow arcuate fractures or faults parallel to the projected caldera margin (Plate 1). One altered biotite latite flow caps the Tuffs of Poore Lake west of Mount Emma (Tmpu, Plate 1). This flow may have been fed by the nearby dikes.

Both the Lavas and Tuffs of Poore Lake probably erupted from vents within the western part of the caldera. The large quantity and size of lithic fragments in the tuff between Poore Lake and Poison Creek suggest that this area may be at or very close to a vent for the tuffs. The extreme thickness of the ash flows in the same area (e.g., up to 3,000 feet at Poore Lake) is also evidence that a vent was nearby. Arcuate dikes of the Lavas of Poore Lake on the western margin of the caldera is proof that the lavas erupted there from arcuate fracture or fault zones. It is likely that magma for both the lavas and tuffs was conducted to the surface along caldera-margin faults in the Pickle Meadow and Poore Lake areas.

Variations in the thickness of the Tuffs of Poore Lake and underlying Relief Peak Formation may be explained by irregular topography along the unconformity separating the two units. The tuffs at Poore Lake, Secrete Lake, and Pickle Meadow are up to 3,000 feet and lie close to granitic basement (Plate 1). The Mount Emma-Kirman Lake section includes up to 1,000 feet of Relief Peak Formation between the granitic basement and overlying tuffs (Plate 1).

Thickening of the tuffs thus correlates with thinning of the underlying Relief Peak Formation and vice versa. Such a situation arises when overlying rocks are deposited on a surface with significant relief. In this case a north-south-trending valley must have cut through the Relief Peak Formation in the western part of the Little Walker area. If the valley was drained by a river, the old river would have followed a channel near the modern West Walker River through Pickle Meadow (Plate 1).

Distribution of the Tuffs of Poore Lake and variation in thickness of underlying Relief Peak Formation support the conclusion that the ancestral West Walker River drained to the south. A thick sequence of the Tuffs of Poore Lake appears to reach out of the Little Walker area toward the south, beyond the limits of the map area (Plate 1). Thick exposures of Relief Peak Formation on the north end of this river valley at the Marine Cold Weather Station and north of Kirman Lake are free of overlying tuff. The extension of the tuffs to the south, where they lie close to granitic basement, and absence of the tuffs on the north, where Relief Peak rocks are thick, may be explained if the ancestral West Walker River had headwaters on the north side of Pickle Meadow and flowed south.

The age of the ancestral West Walker River valley may be inferred from units that it cuts and from lithic fragments left in sands along its bottom. The valley is definitely older than overlying Tuffs

of Poore Lake and younger than the underlying Relief Peak Formation. Angular blocks of Tollhouse Flat and By-Day Member tuff in thin, poorly indurated sandstones on the old valley floor north of Kirman Lake show that the valley was present shortly after eruption of the By-Day Member of the Eureka Valley Tuff, and that it began to receive coarse, angular sediments from nearby highlands shortly before the Tuffs of Poore Lake filled it up. If the ancestral West Walker River valley were well developed prior to eruption of the Table Mountain Latite and giant welded tuff sheets of the Eureka Valley Tuff, it is strange that no thick sections of these units have been found on its surface. It seems more likely that the valley was not present when the By-Day Member erupted from nearby vents. This leads to the conclusion that most of the erosion which cut the ancestral West Walker River valley occurred after the major period of cauldron subsidence associated with eruption of the By-Day and Tollhouse Flat ash-flow sheets.

If the above arguments are valid, then the ancestral West Walker River coexisted with the Little Walker caldera. If the river were outside of the caldera, then it must have cut its valley around the western rim of the caldera. If the river were within the western part of the caldera, then it would have had its northern headwall near the north end of Pickle Meadow at the caldera rim. The river would then have been guided south along the western wall of the caldera to issue

out through a break in the wall on the southwest side of the rim.

It seems improbable that a river would flow around the outside of a caldera rim. It is much more likely that it was guided by the caldera wall and associated faults. Structural control of this river valley is supported by evidence of arcuate faults or fractures along the deepest part of the valley parallel to the valley axis and the projected western margin of the Little Walker caldera. The best evidence for these faults are the arcuate dikes of the Lavas of Poore Lake which follow the deepest part of the ancestral West Walker River valley. Considerable offset on caldera faults in the bottom of this valley is suggested by downward displacement of the contact of the Relief Peak Formation and underlying basement rocks across the old valley area. Exposures of this contact in high cliffs above the west side of the modern West Walker River at Pickle Meadow are structurally higher than outcrops of the contact at Mount Emma to the east. This apparent offset is, however, complicated by Basin and Range faults with the same sense of movement which may extend through the same area from Lost Cannon Peak (Plate 1). In any case, the weight of evidence seems to favor interpretation of the ancestral West Walker River as an intracaldera stream which left the caldera where an earlier caldera lake overflowed and cut the rim on the southwest side. Extensive escape of the ash flows correlative with the Tuff of Poore Lake on the north and east side of the caldera is evidence that such

erosional breaks in the rim were quite common (see the Upper Member of the Eureka Valley Tuff, Plate 1).

A final, very speculative paleogeographic picture emerges from the above arguments. The Little Walker caldera may have had a valley along its western rim which was 1,000 feet deeper than the adjacent caldera floor and pierced the rim on its southwest side. This valley and several others which cut the north and east walls of the caldera allowed large ash flows and base-surge deposits of the Upper Member of the Eureka Valley Tuff and Tuffs of Poore Lake to escape the caldera. Nearly 3,000 feet of these ash flows exposed at Poore Lake is evidence that the ancestral West Walker River valley was completely buried by intracaldera ash flows which lapped onto the floor of the caldera to the east. The pre-erosion volume of these ash-flows is difficult to estimate, but if the section at Poore Lake is any indication, then a tremendous amount of poorly welded tuff may have once been present in the caldera and surrounding areas. It would not be surprising if these eruptions were also associated with cauldron subsidence. Such subsidence might explain how the tuffs became ponded to such great depths in the Poore Lake area.

Latites of Devils Gate

Small dikes and glassy plug domes of low-Ca-Mg latite and high-silica latite cut intracaldera tuffs of the Upper Member of the

Eureka Valley Tuff near Devils Gate and along the north side of Long Valley Creek near its junction with Huntoon Creek (Plate 1). These diverse rocks are informally called the Latities of Devils Gate, for prominent exposures on the south side of Devils Gate. Because these dikes and domes are apparently overlain and cut by flows and plug domes of the Lavas of Mahogany Ridge at Bush Mountain (Plate 1), the Latites of Devils Gate are inferred to be older than the Lavas of Mahogany Ridge but younger than the Upper Member of the Eureka Valley Tuff.

The total volume of these rather highly evolved magmas was quite small compared to all other volcanic units at the Little Walker center. A few small dikes and domes of the Latites of Devils Gate along the eastern margin of caldera are the only known exposures. Petrologic arguments to be presented later suggest that the Latites of Devils Gate may be small-volume differentiates of rising masses of low-K latite similar in composition to the younger Lavas of Mahogany Ridge.

The largest dike of the Latites of Devils Gate follows an arcuate lineament along a probable caldera fault adjacent to the south side of Devils Gate (Plate 1). This rock has 25.3 percent subhedral plagioclase (An 62; 3 mm), 1.5 percent anhedral augite (1 mm), and 0.9 percent anhedral hypersthene (0.5 mm) phenocrysts set in a felty groundmass of plagioclase and pyroxene microlites. Minor Fe-Ti oxides and apatite are distributed throughout the rocks. Outcrops are

medium gray with prominent, nearly horizontal columnar jointing.

Most of the other small intrusions of the Latites of Devils Gate are somewhat less mafic than the large dike at Devils Gate. This difference in composition is reflected in the mineralogy of the other intrusions. Small glassy plug domes of high-silica latite at Bush Mountain have more hypersthene than clinopyroxene and some contain minor biotite. The plagioclase in these rocks is also more sodic (An 40) than plagioclase phenocrysts in the dike at Devils Gate. Small dikes of the Latites of Devils Gate on the north side of Long Valley Creek commonly lack mafic phenocrysts altogether.

Lavas of Mahogany Ridge

Large, coalescing two-pyroxene, low-K latite coulees and endogenous domes completely dominate outcrops in the eastern interior of the Little Walker caldera (Figure 6; Plate 1). These lavas are informally named for distinctive outcrops at Mahogany Ridge where a series of endogenous domes of low-silica, low-K latite to high-silica, low-K latite crop out in a nearly perfect circle one mile in diameter. Subvolcanic dikes and stocks of low-K latite and monzodiorite at Mount Emma and low-K latite endogenous domes at Pickle Meadow are chemically and mineralogically correlative to the Lavas of Mahogany Ridge to the east. Extensive hydrothermal alteration is associated with the monzodiorite stocks at Mount Emma and Poison Creek to the

north. Minor patches of similar alteration affects some outcrops on the south side of Mahogany Ridge as well.

The Lavas of Mahogany Ridge are the youngest rocks of the Stanislaus Group at the Little Walker volcanic center. They appear to have erupted from ring and arcuate fracture systems which cut earlier units in the caldera floor. The lavas cut and overlie the Latites of Devils Gate at Bush Mountain but are overlain by short flows of the Lavas of Rickey Peak at the junction of Huntoon Creek and Long Valley Creek. The Lavas of Mahogany Ridge may have erupted at about the same time as the Dardanelles Formation which overlies the Eureka Valley Tuff and underlies the Disaster Peak Formation to the west (Slemmons, 1966).

It is possible that the close of volcanism at the Little Walker caldera was associated with extensive resurgent fracturing as the Lavas of Mahogany Ridge welled up from the central and eastern part of the cauldron. Occurrence of all known outcrops along arcuate and ring lineaments is certainly suggestive of this, but older caldera fractures and faults may also have served as conduits for the magma.

Two-pyroxene low-K latite is by far the most voluminous rock type in the Lavas of Mahogany Ridge, but three other lithologies occur locally. At Mahogany Ridge a low-silica olivine latite and high-silica, biotite-hornblende-bearing latite crop out (Plate 1). The most highly evolved members of the formation are biotite-pyroxene-bearing

quartz latites which occur in small outcrops at Buck Springs near New Range (Plate 1). Some of the quartz latites may have erupted before the main part of the Lavas of Mahogany Ridge, but outcrops at Buck Springs are not well enough exposed to confirm or deny this interpretation.

Except where heavily weathered, the two-pyroxene low-K latites may be distinguished from most older Stanislaus lavas. They generally appear much less altered and weathered than older units and have a much greater abundance of phenocrysts than any older unit, except the Two-pyroxene Member and upper flow of the Lower Member of the Table Mountain Latite. Thin section study may be required to distinguish the Two-pyroxene Member and upper flow of the Lower Member of the Table Mountain Latite. The upper flow of the Lower Member of the Table Mountain Latite lacks orthopyroxene and has a second generation of plagioclase microphenocrysts. Hypersthene and plagioclase of the Two-pyroxene Member is much more corroded than that of the Lavas of Mahogany Ridge.

Two pyroxenes occur in every flow of the Lavas of Mahogany Ridge, regardless of variations in chemical composition, but pyroxenes are most abundant in the low-K latites which probably account for 90 percent of the formation. The two-pyroxene low-K latites usually contain 30 to 35 percent euhedral plagioclase (An 54, 3mm), 7 to 10 percent euhedral augite (2 mm) and 2 to 5 percent subhedral

hypersthene (1 to 2 mm) phenocrysts set in a groundmass of dark brown glass or felsitic material. Minor anhedral microphenocrysts of olivine (0.1 mm to 0.5 mm) are commonly present but may be wholly or partly altered to iddingsite or serpentine. Apatite and Fe-Ti oxides are ubiquitous in all units. Orthopyroxene is sometimes rimmed in augite and microphenocrysts of olivine are commonly gathered around these augite rims. This sequence of crystallization may occur as basic magma rises from depths where orthopyroxene is the dominant mafic phase to shallow levels where olivine and clinopyroxene are most stable (Green and Ringwood, 1968). Hornblende-bearing members of the formation contain the usual two-pyroxenes but pyroxenes are in reaction to hornblende. The biotite-bearing quartz latites also contain two-pyroxenes but biotite is more abundant and has relict amphibole cleavage lines. Outcrops of all units are dark gray, and weather to reddish gray. The lavas generally form steep slopes and cliffs.

Lavas of Rickey Peak

The youngest volcanic units in the Little Walker volcanic center are hornblende-biotite dacites and high-silica, andesites which crop out extensively in the eastern half of the area (Plate 1). In keeping with previous nomenclature of Halsey (1953) these rocks are informally named the Lavas of Rickey Peak for a prominent plug dome

which forms the top of Rickey Peak. Coulees of these viscous lavas overlie the Lavas of Mahogany Ridge at the junction of Long Valley Creek and Huntoon Creek. A K-Ar age of 7.3 ± 0.2 m.y. on biotite from a dacite dome at New Range confirms their post-Stanislaus age (unpublished K-Ar data of M. Silberman, 1974). This age is similar to ages obtained on hornblende andesites and dacites of the Disaster Peak Formation to the west and the Willow Springs Formation and Bodie andesite to the east (Slemmons, 1966; Gilbert and others, 1968). The andesites and dacites of all of these formations are representative of the dying phases of general calc-alkalic volcanism in the northern Sierras and western Great Basin during the early Pliocene.

The Lavas of Rickey Peak appear to erupt exclusively as plug domes which merge upward into endogenous domes and short coulees. Because virtually every outcrop is at or very near a vent, the distribution of outcrops is also the distribution of vent areas. In most cases the vents appear to lie along north-south lineaments parallel to Basin and Range faults. Many of these vents follow presently active normal faults. It is possible that Basin and Range tectonism began to affect the Little Walker area as early as 7.3 m.y. ago when these fractures or faults channeled the Lavas of Rickey Peak to the surface.

The Lavas of Rickey Peak are the most easily mapped units in the area. Their occurrence in steep-sided flow-foliated flows and

plug domes together with their light color and abundant hornblende and biotite phenocrysts are distinctive (Figure 12). The only rocks which might be mistaken for the Lavas of Rickey Peak are the Relief Peak Formation and hornblende-biotite-bearing members of the Lavas of Mahogany Ridge. Absence of phenocrystic pyroxene in the Lavas of Rickey Peak, their intrusive character, and less potassic composition compared to the Relief Peak and Mahogany Ridge rocks will unambiguously distinguish them.

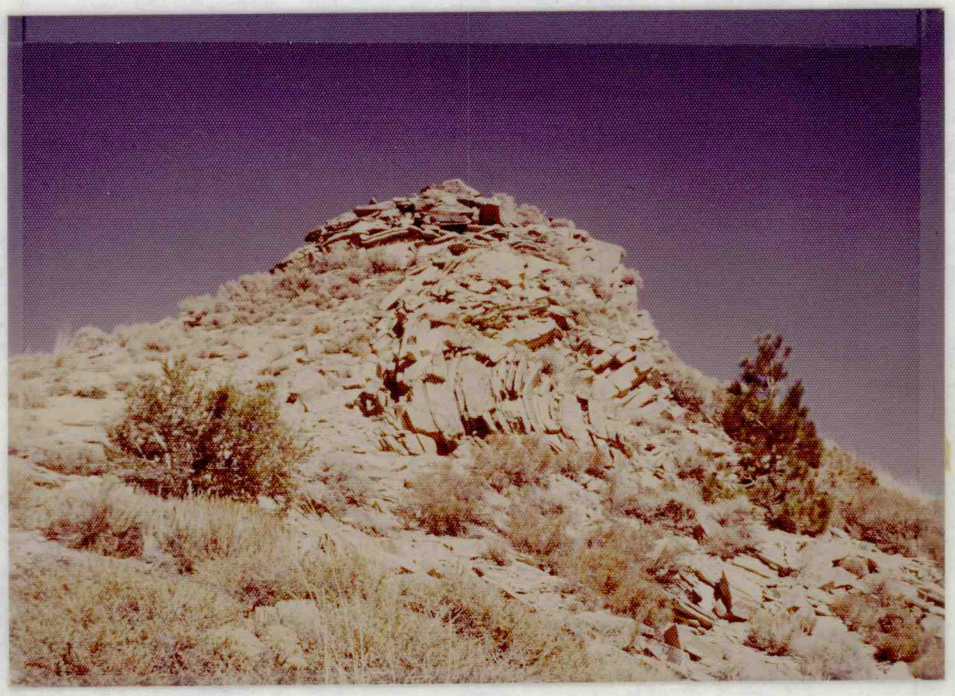

Figure 12. Endogenous dome of biotite-dacite of the Lavas of Rickey Peak on the north side of Long Valley Creek. Note the excellent flow foliation cleavage and light color which characterizes the Rickey Peak rocks.

Prominent white to light gray ridges and isolated buttes all over the eastern part of the map area and much of the eastern Sweetwater Mountains are composed of the Lavas of Rickey Peak. The outcrops usually show prominent flow foliation cleavage which forms talus cones of thin cleavage plates at the base of steep slopes. These cleavage plates may be a valuable source of decorative building stone. Hand specimens normally appear fresh and unaltered with conspicuous phenocrysts of hornblende or biotite or both. Large glomero-porphyritic clumps of plagioclase are present in most specimens and may be accompanied by unmelted xenoliths of granitic rocks. In thin section the Lavas of Rickey Peak have 5 to 10 percent euhedral to subhedral hornblende (1 to 3 mm) and 5 to 25 percent euhedral to subhedral plagioclase (An 50 to An 68) phenocrysts set in a felsitic to glassy groundmass. Plagioclase phenocrysts are either in one generation averaging 1.0 to 1.5 mm or in two generations averaging 1.0 mm and 4 mm. The early 4 mm crystals are heavily embayed while the later phenocrysts appear to be in equilibrium with the melt. The ratio of hornblende to biotite phenocrysts is a function of the silica content such that mafic end members may have only hornblende while silicic dacites have biotite as the sole mafic phase. Apatite and Fe-Ti oxides are common to all samples, but minor zircon is limited to the dacites.

CHEMICAL CHARACTER OF MAJOR VOLCANIC UNITS

Introduction

The chemical character of volcanic units at the Little Walker center may be evaluated in terms of chemical trends and absolute abundance of major and trace elements. One of the most useful diagrams for this purpose is the MgO variation plot. MgO may be expected to decrease during either calc-alkaline or tholeiitic (e.g., Skaergaord-type) differentiation, so that the MgO content is an excellent differentiation index. However, some scatter is introduced in these diagrams as a result of analytical error when MgO is low in highly evolved units. MgO variation diagrams for all major elements are presented in Figures 13 through 17.

AFM, Harker, chondrite-normalized rare earth element (REE) plots, and other diagrams will also be used where appropriate. The distinction between "calc-alkaline" and "tholeiitic" differentiation will be based on the variation of Fe/Mg with SiO_2, utilizing Miyashiro's (1974) compositional fields, and on the standard Peacock Index.

Where sufficient data are available, petrogenetic processes will be examined which might account for the chemical trends. In later sections this qualitative treatment will be critically evaluated in the light of quantitative fractionation and melting models.

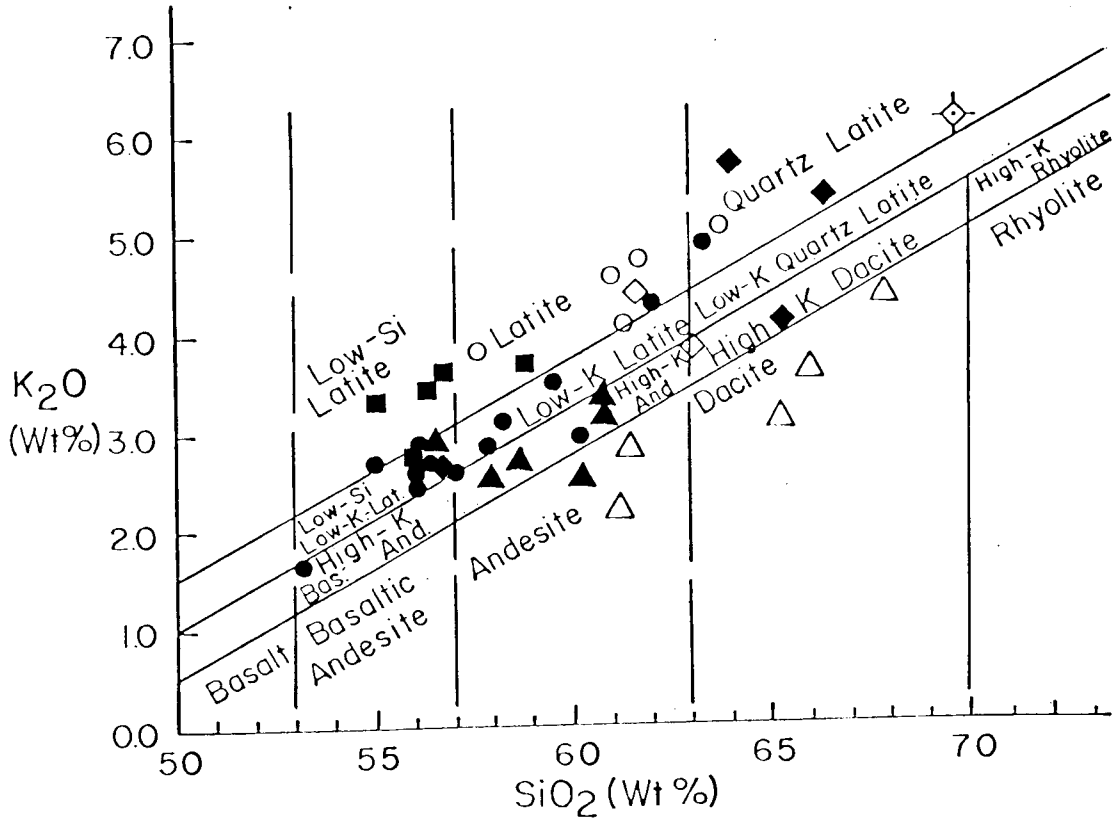

△ Relief Peak Formation

● Lavas of Mahogany Ridge

○ Latites of Devils Gate

◇ Lavas of Poore Lake

◆ Eureka Valley Tuff

⊹ Fales Hot Springs Quartz Latite

□ Low-Ca-Mg latites of the Table Mountain Latite

■ Lower Member of the Table Mountain Latite

▲ Lavas of Rickey Peak

Figure 13. Classification of volcanic rocks.

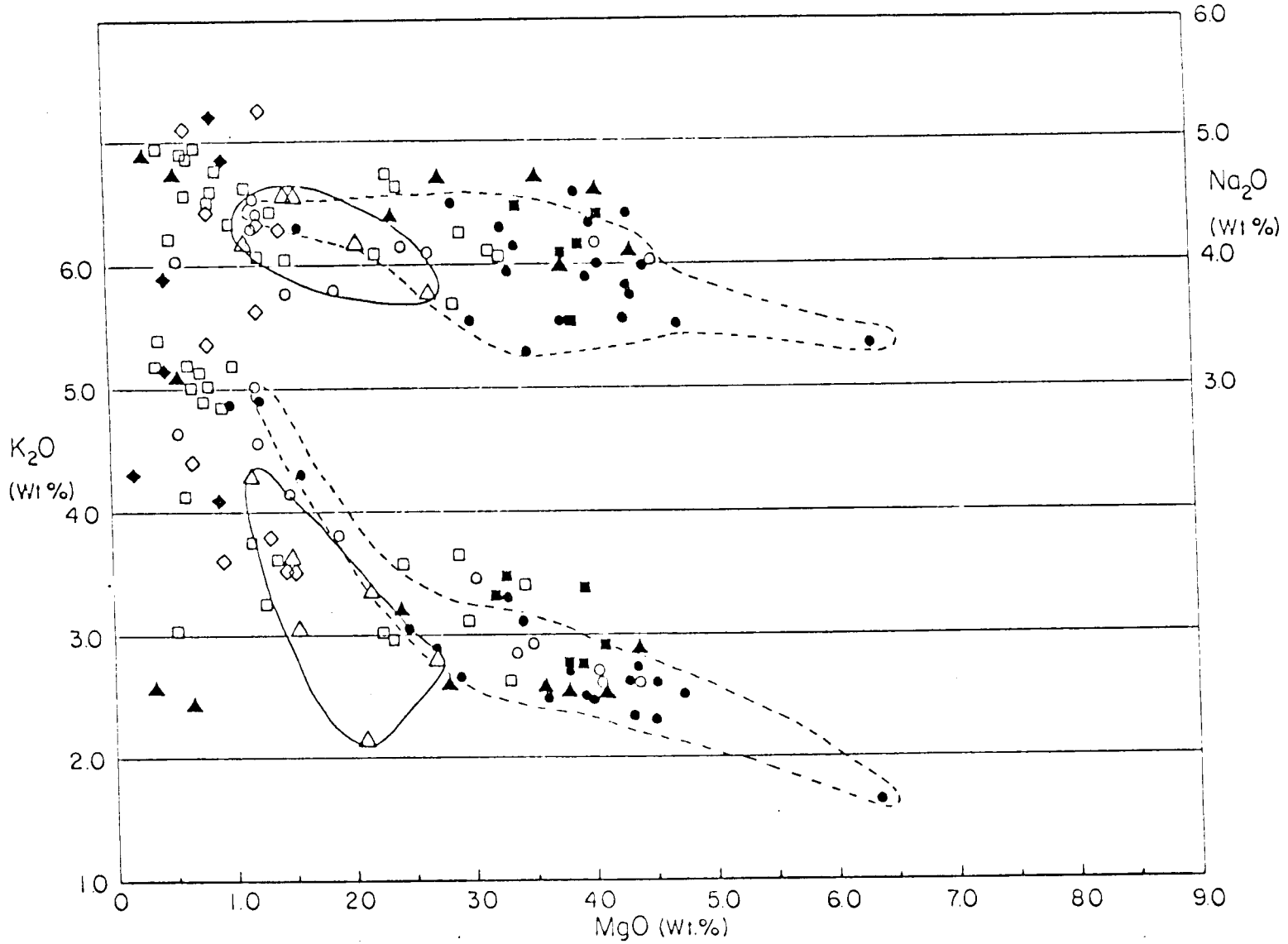

Figure 14. Variation of alkalis with MgO. Symbols as before.

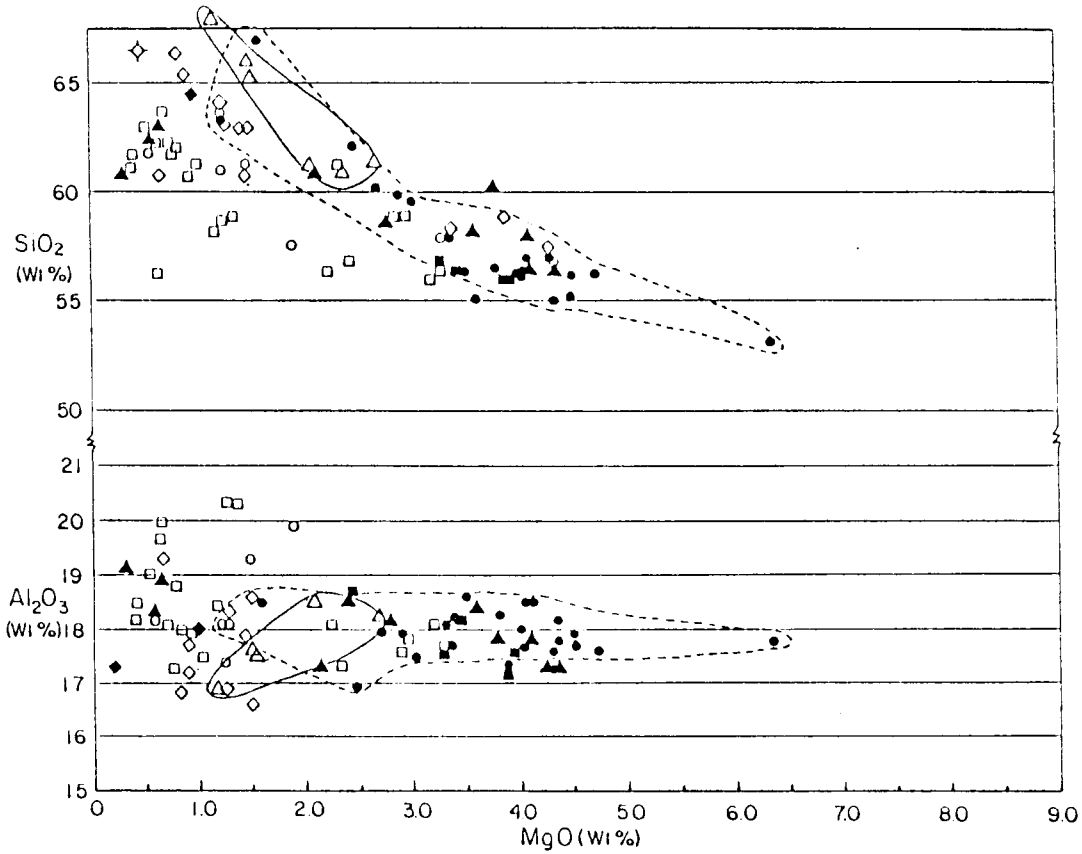

Figure 15. SiO_2 and Al_2O_3 versus MgO. Symbols as before.

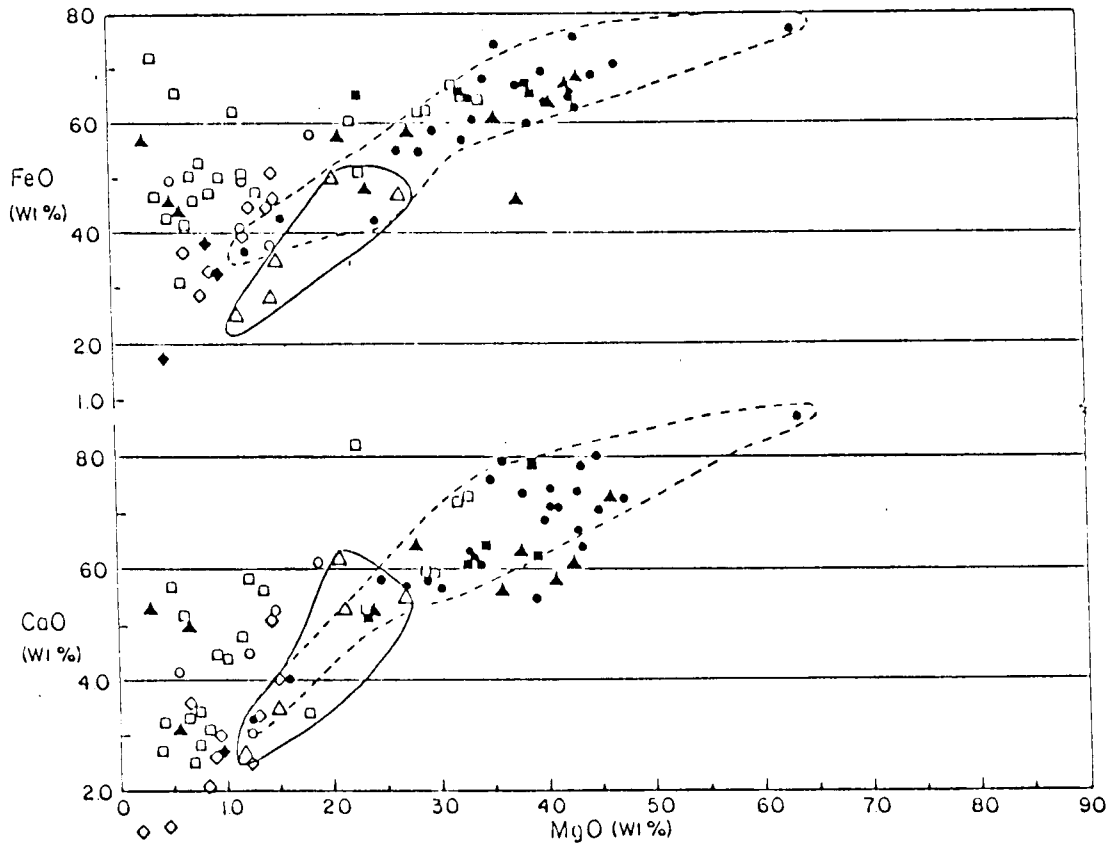

Figure 16. FeO and CaO versus MgO. Symbols as before.

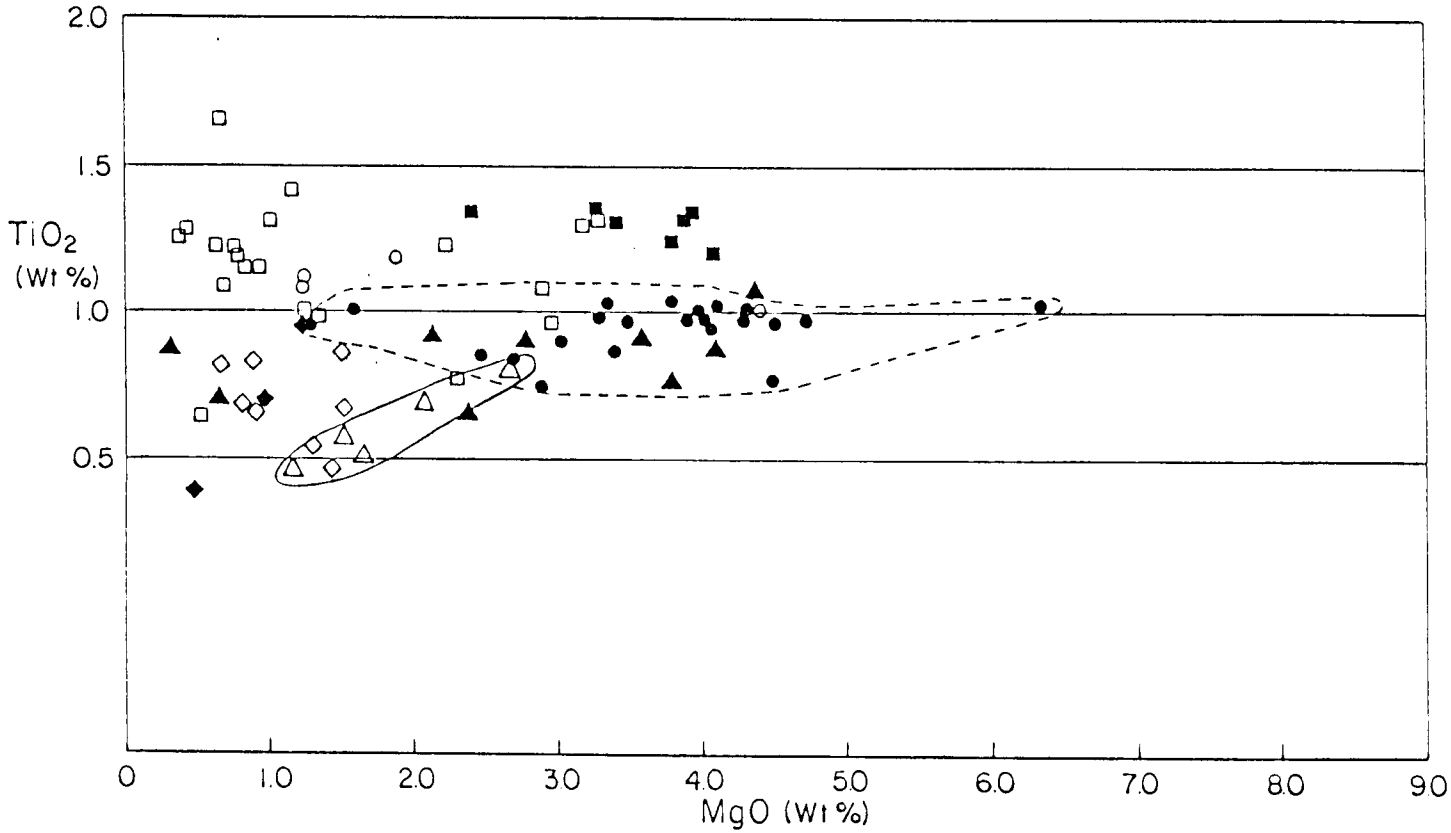

Figure 17. TiO_2 versus MgO. Symbols as before.

Rock Classification

Rock names have been assigned on the basis of the variation of K_2O and silica (Figure 13) adapted from Priest (in press) and Noble and others (1976). As can be seen from the diagram, the Table Mountain Latite and Latites of Devils Gate are chiefly latites, while the younger Lavas of Mahogany Ridge are chiefly low-K, low-Si latites. Some highly evolved end members of the Lavas of Mahogany Ridge, the Fales Hot Springs Quartz Latite, and the Eureka Valley Tuff are quartz latites. K_2O of the Lavas of Poore Lake is highly variable, probably from mild hydrothermal alteration, but at least one sample is latitic, and all are quite silicic.

The typically calc-alkaline Relief Peak and Rickey Peak lavas are much less potassic than the Stanislaus rocks (Figure 13). The Relief Peak andesites are, however, more potassic and less silicic than the younger Rickey Peak lavas. The Rickey Peak rocks are mostly dacites, whereas the Relief Peak lavas are chiefly high-K andesites.

Relief Peak Formation

The Relief Peak Formation is less silicic than the younger Rickey Peak lavas and less iron-enriched than the latitic series (Figure 18). The data for the Relief Peak Formation show considerable

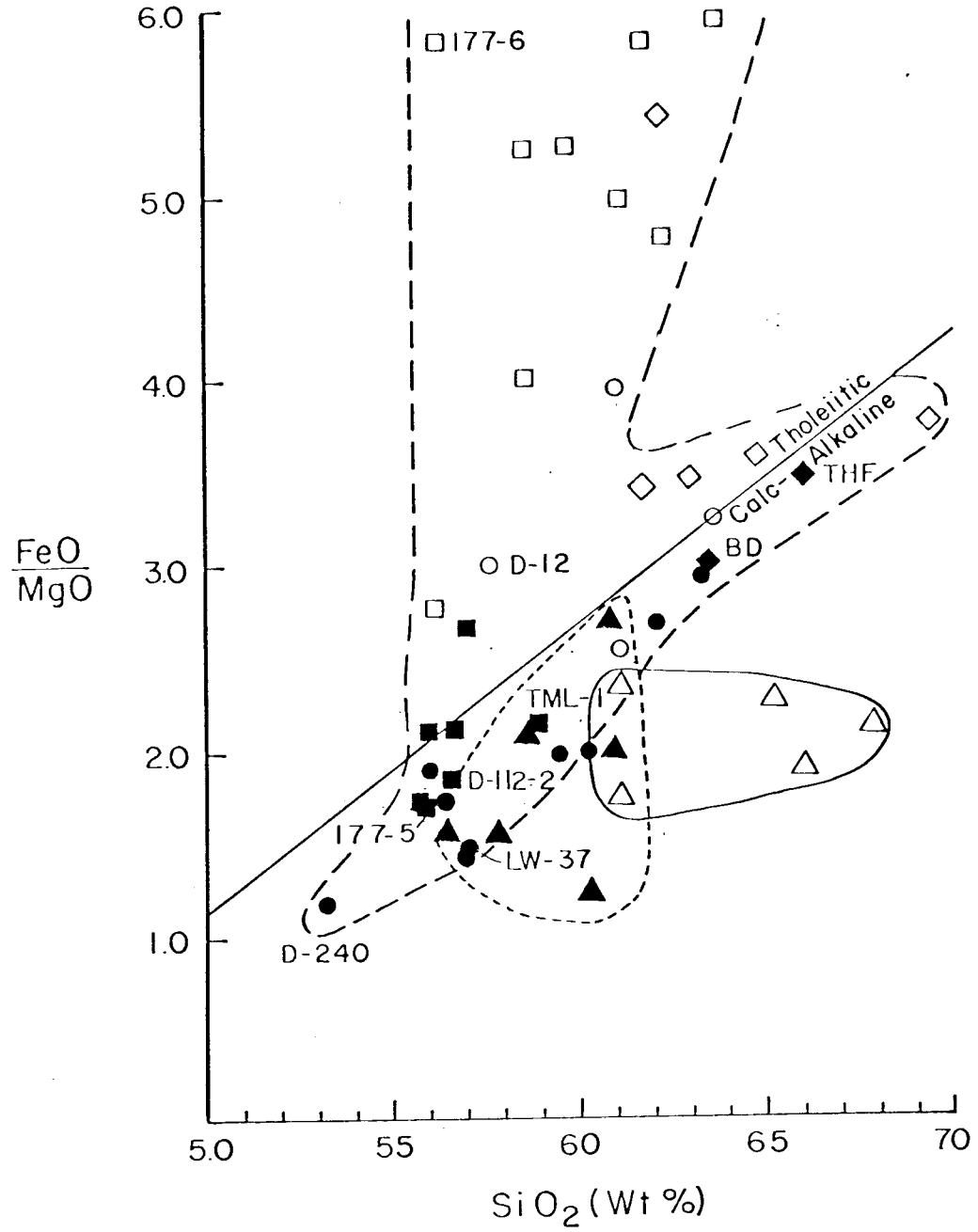

Figure 18. FeO/MgO versus SiO_2. Symbols as in Figure 13. Line between the tholeiitic and calc-alkaline series is from Miyashiro (1974).

scatter, indicating that samples may be from flow units of widely divergent evolution, possibly from widely separated volcanic centers. Because of this scatter, a meaningful Peacock Index cannot be calculated, but close approach of total alkalis to total CaO at silica contents of 55 percent to 60 percent suggests calc-alkaline character (Appendix Table II. 1).

It is significant that all samples of Relief Peak Formation have total alkalis greater than CaO even at low (55. 5 percent) SiO_2. They appear to be somewhat more alkaline than the Lavas of Rickey Peak (Peacock Index = 61); this is also reflected in the MgO variation diagrams of Figures 13, 14, and 19 which show that absolute alkalis and incompatible elements of the Relief Peak Formation are higher than the Lavas of Rickey Peak at similar MgO.

The Relief Peak Formation is much less potassic than the Stanislaus Group and has lower TiO_2 than the Table Mountain Latite at similar MgO (Figure 17). Incompatible elements are also lower in the Relief Peak than all Stanislaus rocks (Figure 20).

Table Mountain Latite

The mineralogical variability of the upper part of the Table Mountain Latite is reflected in the scatter in the variation diagrams (e. g., Figures 13-19). The formation is distinctive, however, in containing the greatest enrichment in large-ion-lithophile (LIL) and

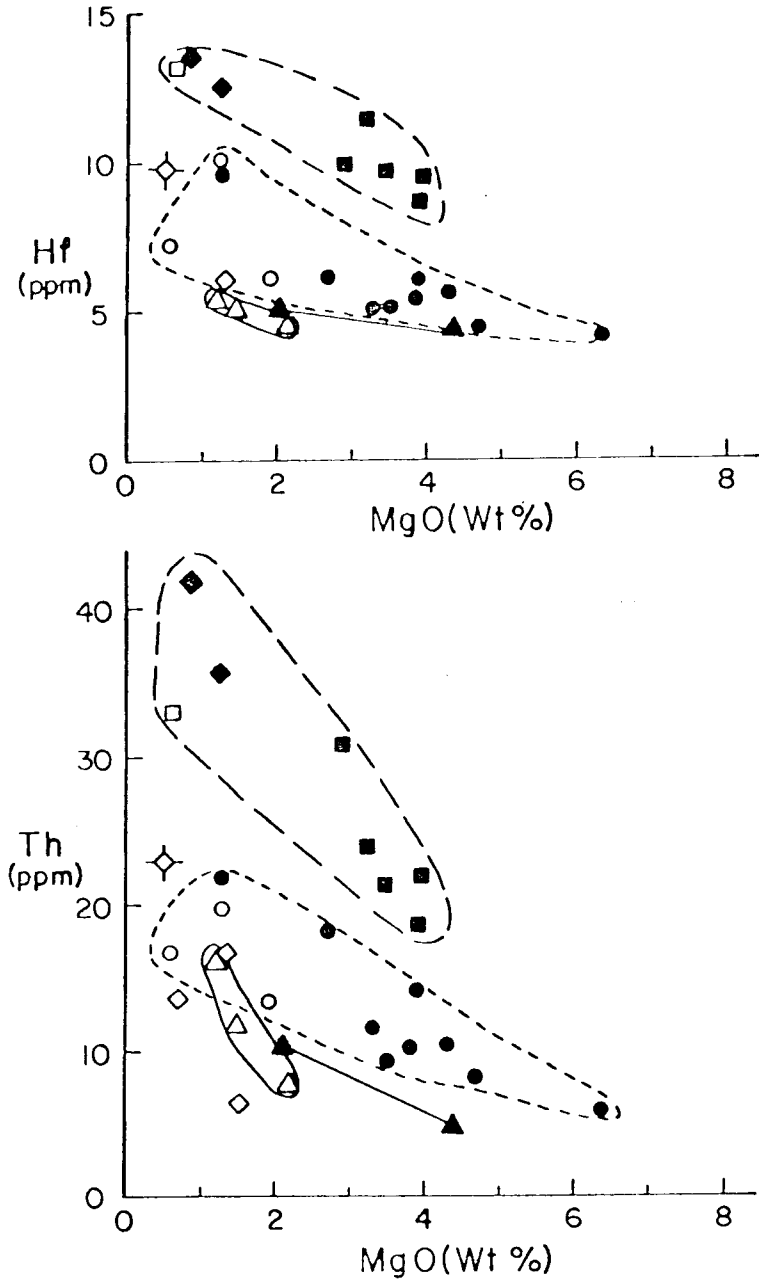

Figure 19. Variation of incompatible elements with MgO. Symbols as before.

incompatible elements of any unit exposed at the Little Walker center. It appears that this initial, voluminous outpouring of latitic magma tapped a source far richer in these elements than that available for subsequent eruptions.

Although the Eureka Valley Tuff has higher absolute abundances of LIL elements, it will be shown by quantitative modeling that any logical parental magma for the tuffs would be less enriched than the bulk of the Table Mountain Latite at equivalent degrees of differentiation. Stanislaus rocks younger than the Table Mountain Latite are successively less enriched in large-cation elements, until by the time of eruption of the youngest unit (the Lavas of Mahogany Ridge), the character of volcanic activity may be characterized as only marginally potassic (latitic) tending toward normal calc-alkaline magmatism (Figures 13, 14, and 18).

The series of differentiates from the voluminous Lower Member of the Table Mountain Latite (rich in pyroxene + olivine) tend to be aluminous, low-Ca-Mg latites of trachytic character with quite high Fe/Mg from Mg-depletion rather than Fe-enrichment. Nevertheless this series of evolved magmas has a distinctly noncalc-alkaline character compared to trends of normal calc-alkaline series such as the Lavas of Rickey Peak (Figure 18). An accurate Peacock Index cannot be calculated owing to lack of silica-enrichment in the evolved rocks, but the Lower Member sample, 177-2 (Appendix Table I. 1), has total

alkalis subequal to CaO at 56.0 percent SiO_2. One of the most highly differentiated units is the Large-plagioclase Member which has Hf and Th contents equivalent to the Eureka Valley Tuff (Appendix Table II.1). The SiO_2 of this unit (56.3 percent) is, however, much lower than that of the tuffs (64.5 percent to 66.4 percent SiO_2), whereas the Al_2O_3 of the Large-plagioclase Member (18.6 percent) is much higher than the tuffs (16.8 percent to 16.9 percent). If the tuffs had Low-silica latite parents, similar to the parent of the Large-plagioclase Member, then it may be possible that the total pattern of variation of Stanislaus samples on Figure 18 represents two divergent series from parents similar to the Lower Member of the Table Mountain Latite. These divergent paths may be produced by differences in the ratio of plagioclase + magnetite to pyroxene in fractionating assemblages. Clearly, high degrees of magnetite and plagioclase separation would limit enrichment in Fe and Al, as well as producing silica enrichment. Petrologic mixing models presented in a later section confirm this possibility. Similar arguments apply to evolution of the aluminous low-Ca-Mg latites of Devils Gate and the siliceous members of the Lavas of Mahogany Ridge. It may be that small differences in the oxygen fugacity and depth of crystallization-differentiation may account for the two divergent paths.

Chondrite-normalized rare earth (RE) abundance plots of the Lower Member of the Table Mountain Latite are distinctive for their

steep negative slopes (high La/Sm and Tb/Lu) and large negative europium anomalies (Figure 20). The absolute abundance of REE in the Table Mountain Latite is much greater than that of younger rocks and subequal to the highly evolved Eureka Valley Tuff (Figure 20). The larger europium anomalies may be from significant plagioclase involvement in the evolution of the Lower Member at relatively low oxygen fugacity (high Eu^{+2}/Eu^{+3}). It will be shown that the steep negative slope of the RE curves is not the product of high level fractionation. This leads to the conclusion that the steep slopes are an attribute of the original partial melts imposed by equilibration with a mantle source.

Eureka Valley Tuff

The Eureka Valley Tuff is distinctive for its high (64.0 to 66.4 percent) SiO_2 and very high LIL and incompatible element content (Figures 13, 14, 15, and 19). Using SiO_2 and K_2O limits of Noble and others (1976), the tuffs are quartz latites (Figure 13). The chemistry of the Upper Member of the Eureka Valley Tuff will not be discussed, because lack of analyses of non-hydrated glass from this unit preclude comparison with non-hydrated glass analyses of the rest of the Eureka Valley Tuff.

The Fe/Mg Harker diagram of Figure 18 shows the Eureka Valley Tuff as only marginally calc-alkaline, being very near the field

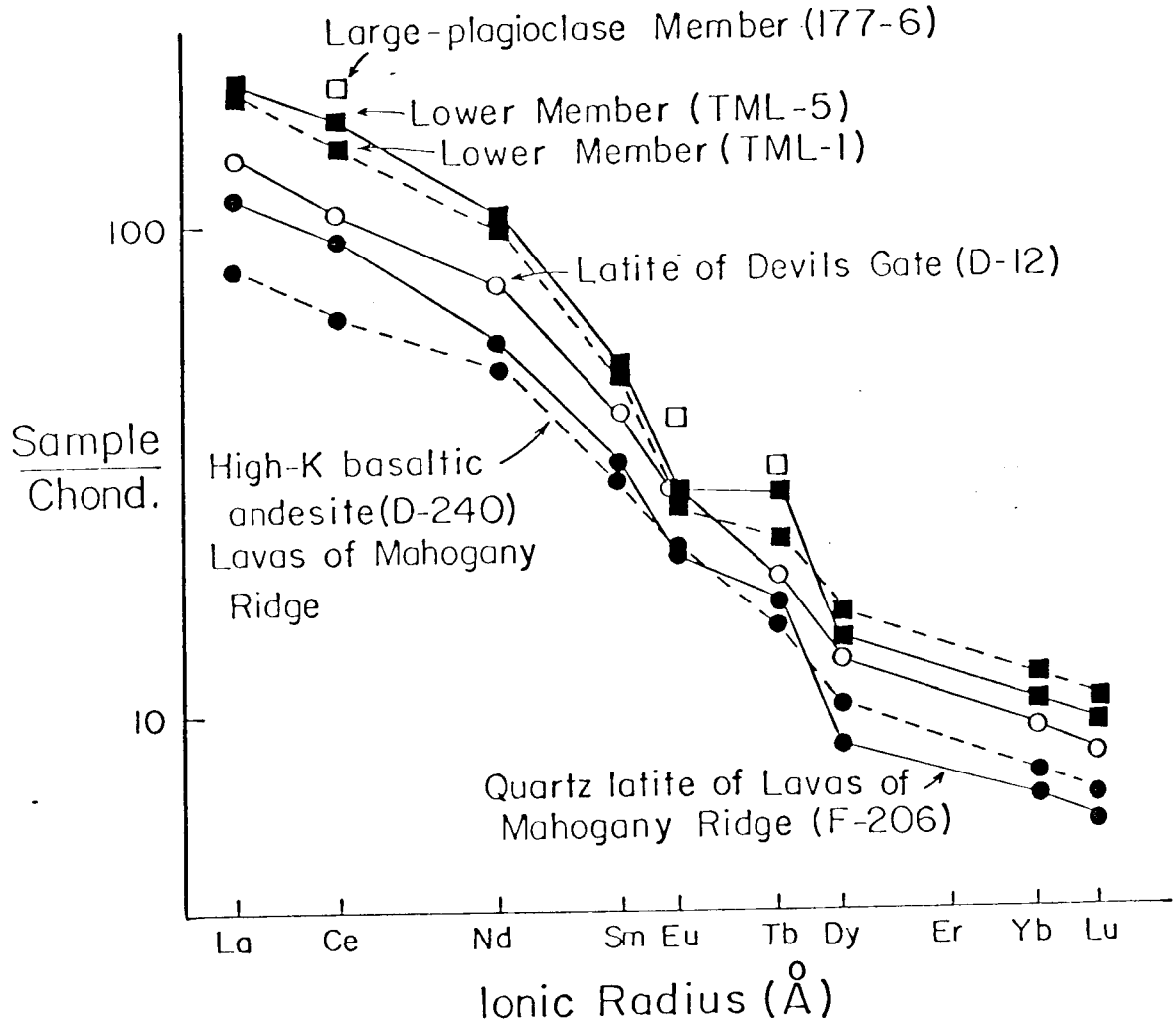

Figure 20. Chondrite-normalized RE curves for the Stanislaus Group. Eureka Valley Tuff plots in coincidence with the Lower Member of the Table Mountain Latite. Absolute chondrite abundances were taken from R. A. Schmitt and coworkers, Oregon State University, Radiation Center (personal communication, R. A. Schmitt, 1979).

of tholeiitic rocks. The ash flows are, however, much less iron-enriched than the aluminous low-Ca-Mg latitic lavas in the upper part of the Table Mountain Latite.

Chondrite-normalized RE curves of the Eureka Valley Tuff are nearly identical in relative and absolute abundances with those of the Lower Member of the Table Mountain Latite (Figure 20). This may disallow derivation of the tuffs from the more mafic Lower Member by fractionation, since REE would be expected to rise during differentiation, unless significant apatite separates. Quantitative arguments in a later section suggest that latite magma parental to the Eureka Valley Tuff would have been less enriched in LIL and incompatible elements than the Table Mountain Latite.

Comments on the RE curves of the Table Mountain Latite in the previous section apply to the Eureka Valley Tuff, because the abundances are essentially the same. The large negative Eu anomaly and low abundance of ferromagnesian elements characteristic of the tuffs reflect large amounts of high-level differentiation (Figures 16, 20, and 21).

The Tollhouse Flat Member is more silicic, higher in all LIL and incompatible elements (except Ba), and lower in ferromagnesian elements than the By-Day Member (Figures 17, 19, 21, and 22). This implies that the Tollhouse Flat Member is a more highly differentiated magma than the By-Day Member. The lower Ba content of the

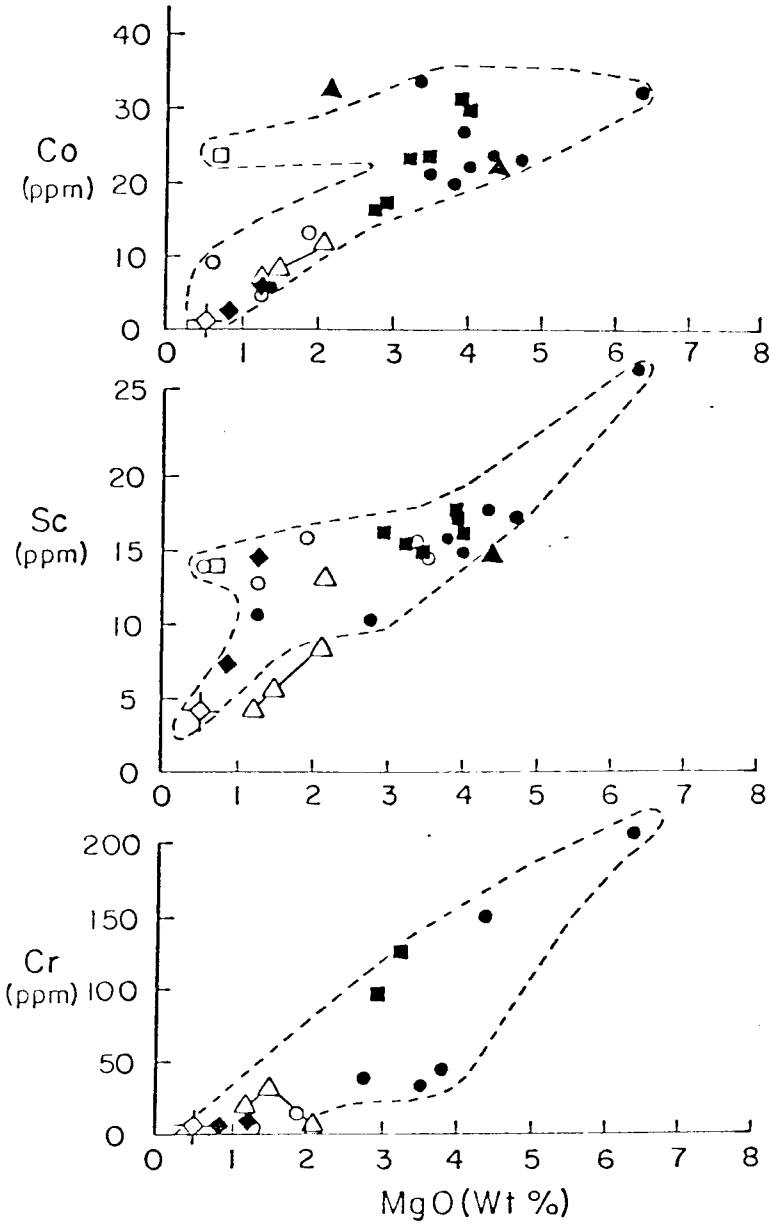

Figure 21. Variation of ferromagnesian elements with MgO. Symbols as before.

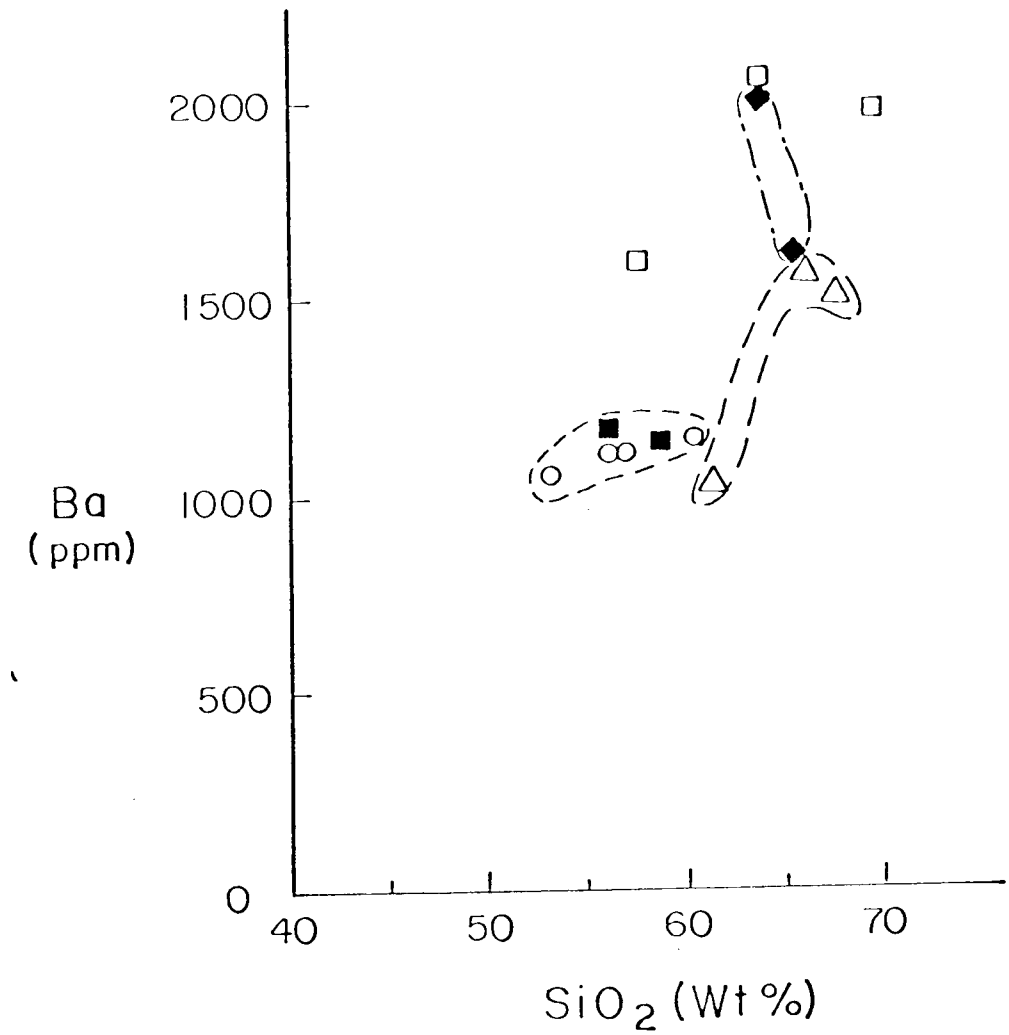

Figure 22. Ba versus SiO_2. Symbols as in Figure 13.

Tollhouse Flat Member (Figure 22) may be due to significant biotite separation, because Ba acts as an included element in biotite (Higuchi and Nagasawa, 1969). Because biotite is not present in the By-Day Member, no such depletion of Ba has affected it. Mass balance calculations of a later section indicate that separation of biotite from a magma similar but not identical to the By-Day Member could yield a daughter liquid similar to the Tollhouse Flat Member.

Fales Hot Springs Biotite Quartz Latite

The major element composition and mineralogy of the Fales Hot Springs Quartz Latite (FQL) is similar to the Tollhouse Flat Member of the Eureka Valley Tuff, although the FQL is somewhat lower in FeO, MgO, CaO and TiO_2 (Figures 16 and 17). Halsey (1953) even suggested that the outcrops at Fales Hot Springs might mark the vent area for tuffs of the Stanislaus Group.

The paucity of the LIL and, especially, incompatible elements in the FQL in comparison to the Eureka Valley Tuff makes relation between these units by fractional crystallization unlikely (Figures 13 and 19). The somewhat lower ferromagnesian element content (more evolved composition) of the FQL in comparison to the tuffs further precludes any simple relation between the two (Figure 21). Clearly, any magma parental to the FQL must have been less enriched in large-cation elements than magmas parental to the Eureka Valley

Tuff. These data confirm a general decrease of LIL and incompatible elements in the younger Stanislaus magmas.

The chondrite-normalized RE pattern of the FQL is similar to that of the Eureka Valley Tuff, although absolute abundances are lower than the tuffs (Figure 23). The large negative Eu anomaly probably reflects significant plagioclase fractionation at high levels in the crust. The steep negative slope of the RE pattern is essentially identical to the other Stanislaus rocks, probably reflecting similar processes of partial fusion from a common source.

Lavas and Tuffs of Poore Lake

No unaltered pumice of the tuffs of Poore Lake have been found for analysis, so they will not be discussed in this section. Mineralogically similar lithic fragments with only slight alteration at Poore Lake (samples ME-3, ME-4, and F-333, Appendix Tables I.1 and II.1) and one arcuate dike north of Poore Lake (sample F-336) provide the basis for a preliminary analysis of the composition of the Lavas of Poore Lake.

The presence of biotite as the only significant mafic silicate phase in both the lavas and tuffs of Poore Lake implies a highly evolved, silicic composition. This is confirmed by analyses of the lavas which have rather high alkalis and SiO_2 but low ferromagnesian elements (Figures 14, 16, and 21; Appendix Tables II.1 and II.2).

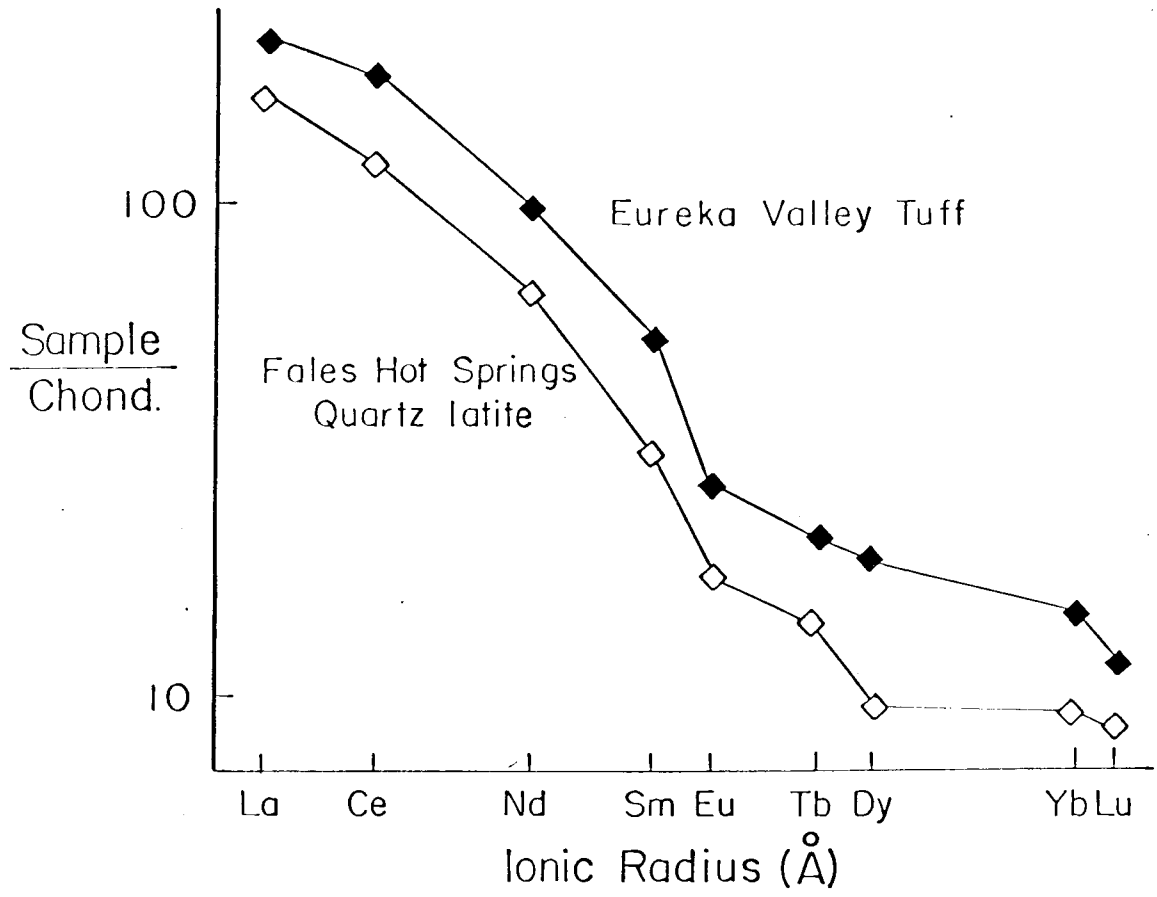

Figure 23. Chondrite-normalized REE curves for the Fales Hot Springs Quartz Latite and Eureka Valley Tuff.

The abundance of incompatible elements Th and Hf is anomalously low in the lavas (Figure 19). The significance of this is not readily apparent because the abundance of highly charged cations may be strongly affected by hydrothermal fluids (Holland, 1972), and all of the samples were exposed to slight alteration.

All of the Poore Lake lavas have Fe/Mg within the field of tholeiitic series on Figure 18, although they lie only a little way above the calc-alkaline series. More detailed treatment of the chemistry of these rocks is not warranted, because mapping of the field relationships is not complete; also, completely fresh samples have not been found for analysis.

Latites of Devils Gate

Some lavas of this group are similar to aluminous low-Ca-Mg latites of the upper part of the Table Mountain Latite (e.g., the Large-plagioclase Member). The low-Ca-Mg latites are characterized by high Fe/Mg (lying wholly in the tholeiitic field of Figure 18), high Al_2O_3 and alkalis (Figures 13-15) but relatively low SiO_2 even in lavas almost completely depleted in MgO (e.g., D-289, Appendix Table II. 1).

The Devils Gate rocks also resemble the Poore Lake lavas in many respects. They have similar alkali, MgO, and SiO_2 contents (Figures 13-16).

Lavas of Mahogany Ridge

The Lavas of Mahogany Ridge are the youngest, most LIL and incompatible-element-depleted latitic magmas of the Stanislaus Group (Figures 13, 19, and 20). The bulk of this magma series is low-K, low-Si latite but small-volume differentiates may be as siliceous as quartz latite (Figure 13). The differentiation series is typically calc-alkaline, showing a strong rise in SiO_2 with falling MgO (Figure 15) as Fe/Mg remains constant or rises slightly (Figure 18).

These lavas stand apart from the earlier Table Mountain Latite not only by their depletion in incompatible elements (Figure 19) but by much lower TiO_2 (Figure 17). They also show smaller negative Eu anomalies than earlier Stanislaus rocks (Figure 20). It will be shown later that both characteristics may be compatible with rather high oxygen fugacity and, thus, possible high P_{H_2O} which would favor low Eu^{+3} and crystallization of iron-titanium oxides (Osborn, 1959). High P_{H_2O} may also explain the unique presence of two pyroxenes in these rocks (Green and Ringwood, 1968; Ringwood, 1974) and the tendency for hydrous minerals to occur in intermediate to silicic members (Stern and others, 1975).

Petrologic mixing models will be presented which show that the major element data is consistent with derivation of the silicic, calc-alkalic series by fractionation of a low-pressure plagioclase + two

pyroxene + iron-titanium oxide assemblage from low-silica, low-K latite parents. Another mixing model will show that a divergent chemical trend toward aluminous low-Ca-Mg latite with high Fe/Mg may be produced from Mahogany Ridge parents by high pressure, low P_{H_2O} fractionation. The latter, more "tholeiitic" trend can evolve magmas similar to the Laties of Devils Gate. These two trends are comparable to rather similar variations within the earlier Stanislaus rocks (e.g., differentiation to quartz latites of the Eureka Valley Tuff and aluminous low-Ca-Mg latite of the Large-plagioclase Member of the Table Mountain Latite).

The Lavas of Mahogany Ridge are enriched in potassium (Figure 13) and incompatible elements (Figure 19) relative to either the Relief Peak or Rickey Peak lavas. The Mahogany Ridge differentiates also show more increase in Fe/Mg with rising silica than do the Rickey Peak lavas (Figure 18). The iron-rich and strongly subsilicic nature of the biotite-hornblende-dominated liquidus assemblage of the Rickey Peak rocks may account for the differences in Fe/Mg and SiO_2 of their differentiates relative to the latitic series.

Conclusions

The latitic magmas of the Stanislaus Group are characterized by distinctly higher Fe/Mg, potassium, and incompatible elements than the typically calc-alkaline lavas of Rickey Peak and Relief Peak

at similar silica and MgO content. Stanislaus rocks show two distinctly different differentiation trends: one leading to quartz latite and one toward aluminous low-Ca-Mg latite. The trend toward low-Ca-Mg latite is characterized by sharply falling MgO, FeO, and CaO; rising alumina, alkalis, and FeO/MgO, and nearly constant or slightly rising silica. The final product is a ferromagnesian-poor latite with only plagioclase as the dominant phenocryst because of the high alumina content. Variation toward quartz latite is best documented for the Lavas of Mahogany Ridge which have a series of differentiates showing sharply rising silica and alkalis at nearly constant alumina as MgO, FeO, and CaO fall. The Fe/Mg rises only moderately during differentiation, in contrast to the low-Ca-Mg latite differentiates.

The younger Stanislaus magmas are generally less enriched in alkalis, incompatible trace elements, and REE than older units. The younger calc-alkaline suite (the Lavas of Rickey Peak) are, likewise, less enriched in large-ion elements relative to the older series (Relief Peak Formation). It may well be that progressive depletion of the Stanislaus source and the calc-alkalic source of large-ion elements may account for this long term chemical change.

QUALITATIVE EVIDENCE FOR CRYSTAL FRACTIONATION

Introduction

Certain elements are uniquely included or excluded from various crystal phases during magmatic crystallization. This section will utilize petrogenically distinctive major and trace element abundances and ratios to detect chemical "fingerprints" imposed by crystal fractionation.

Plagioclase Fractionation

All phenocryst minerals in the magmas considered here exclude Sr and Al relative to liquid except for plagioclase (Figure 24; Arth, 1976). Plagioclase also strongly accepts Eu relative to other REE (Figure 24). Plagioclase separation should enrich the residual liquid in CaO relative to Sr unlike all other phenocryst phases, especially augite and hornblende, which should strongly raise Sr/CaO (Figure 24; Higuchi and Nagasawa, 1969; Arth, 1976). Plagioclase is also the only low-pressure phase capable of raising SiO_2/Al_2O_3 in residual liquids (Figure 24).

Figure 25 shows only slight increase of Sr and Sr/Ca with differentiation in mafic members of all series; this may indicate that either hornblende or augite is overcoming the plagioclase effect. In more evolved members (e.g., below 2.0 percent MgO) Sr falls with

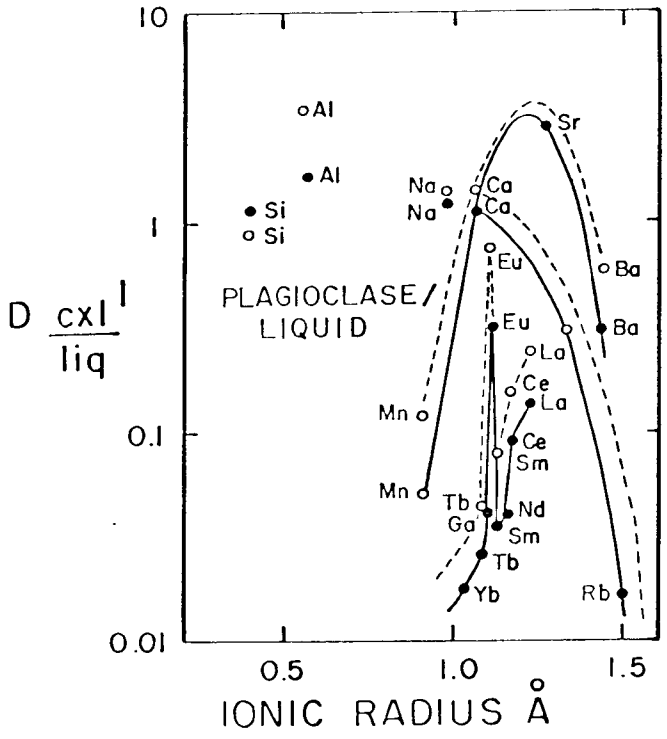

Figure 24. Distribution coefficients of plagioclase versus ionic radius for basalt (solid lines) and low-K, low-Si latite (open circles and dashed lines). Basaltic values from Higuchi and Nagasawa (1969).

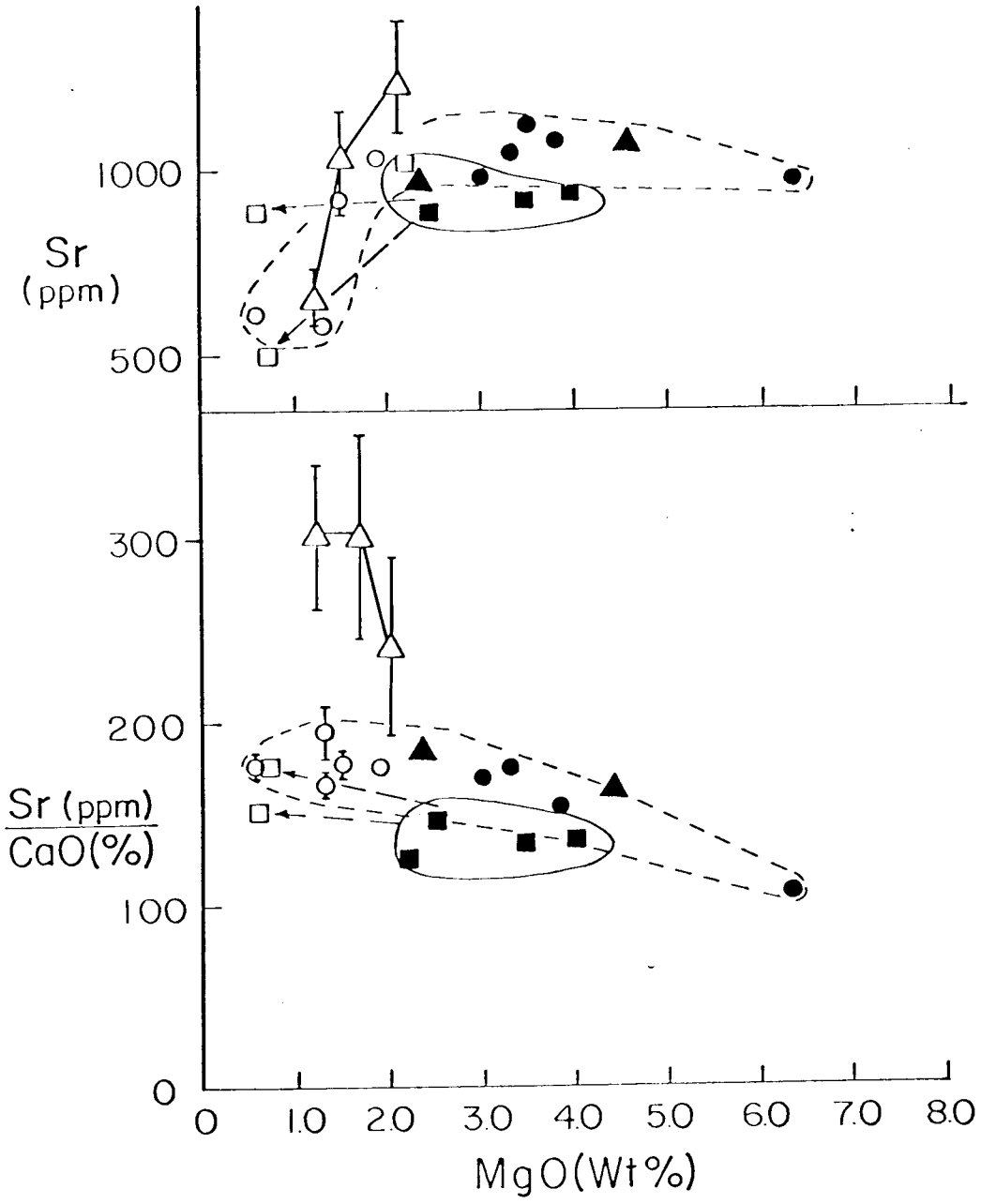

Figure 25. Plagioclase fractionation effects on Sr and Sr/CaO.

decreasing MgO, indicating predominance of plagioclase in the fractionating assemblages (Figure 25). Because the distribution coefficients of Sr and CaO are similar for plagioclase relative to melt, the change of Sr/CaO is more subtle than the change of Sr, but a leveling off or a slight decrease of this ratio with decreasing MgO is apparent in evolved samples (Figure 25). If the magma series were related by only augite or hornblende separation, both Sr and Sr/CaO would rise very steeply.

Sm/Eu should rise during fractionation if plagioclase in involved, because no other phenocryst can significantly affect this ratio. Figure 26 shows a very significant rise in Sm/Eu with increasing differentiation in all magma series. This is considered the best qualitative evidence for plagioclase fractionation. Sm/Eu was chosen, rather than some factor associated with the chondrite-normalized "Eu-anomaly", because the Eu anomalies associated with RE curves are a function of Tb/Eu as well as Sm/Eu. It will be shown later that augite may strongly raise Eu relative to Tb during fractionation in latites, thus tending to eliminate or reduce the condrite-normalized anomaly produced by plagioclase. The chondrite-normalized, RE-Eu anomalies are, thus, a function of the augite-plagioclase ratio of the fractionating assemblage in intermediate rocks. It should be noted that the Lavas of Mahogany Ridge have essentially no negative Eu anomaly on RE curves, yet show good negative correlation of Sm/Eu

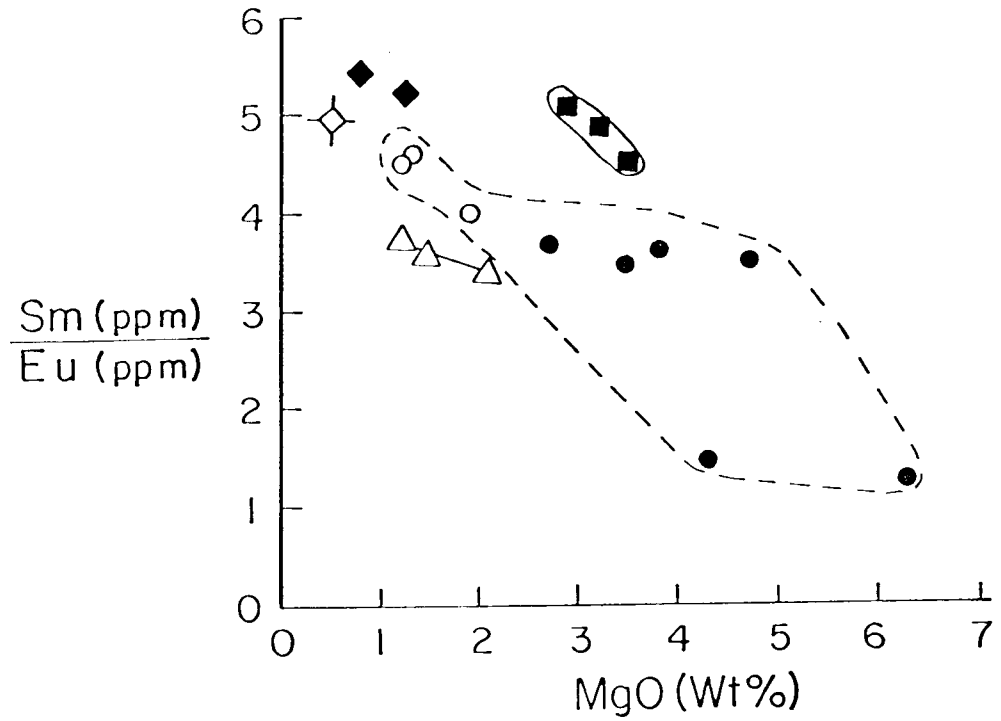

Figure 26. Effect of plagioclase fractionation on Sm/Eu. Symbols as before.

with MgO. This is probably because of the effect of augite fractionation.

SiO_2/Al_2O_3 is generally high in most fractionated, low-MgO members of each series (Figure 27). This is probably caused by dominance of feldspar crystallization from these felsic differentiates.

Augite Fractionation

The augite distribution coefficient for iron is greater than 1.0 in latitic magma (Figure 28). This is in marked contrast to the case for basaltic magma in which Fe acts as a slightly excluded element for augite (Figure 28). Because other ferromagnesian phases are generally at least as iron-rich as coexisting augite (Figures 8 and 30; Appendix III), no absolute iron enrichment is possible in latitic or andesitic magma, unlike basaltic magma. Fe/Mg of residual liquids will tend to rise during pyroxene fractionation from both (Figure 28). This relationship is demonstrated by universal depletion of FeO in successively more evolved (MgO-poor) samples throughout the latitic series (Figure 16). In contrast, FeO/MgO is highly variable, tending to rise sharply in trends toward highly differentiated aluminous, low-Ca-Mg latite and rise less sharply or fall in highly evolved quartz latites and dacites (Figure 19).

Variations in Fe and Fe/Mg in residual liquids may also be caused by orthopyroxene and olivine fractionation, thus such

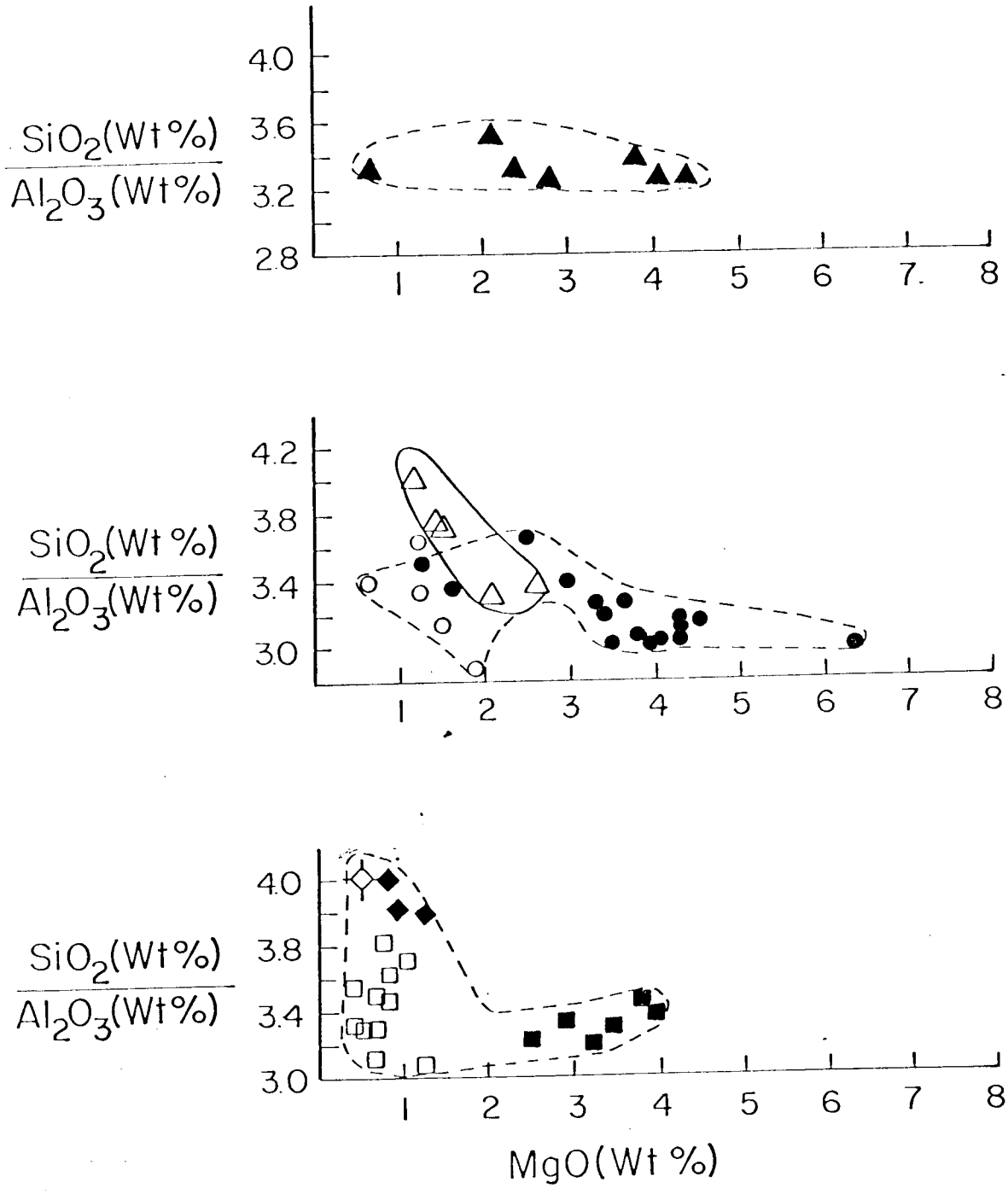

Figure 27. SiO_2/Al_2O_3 versus MgO. Symbols as before.

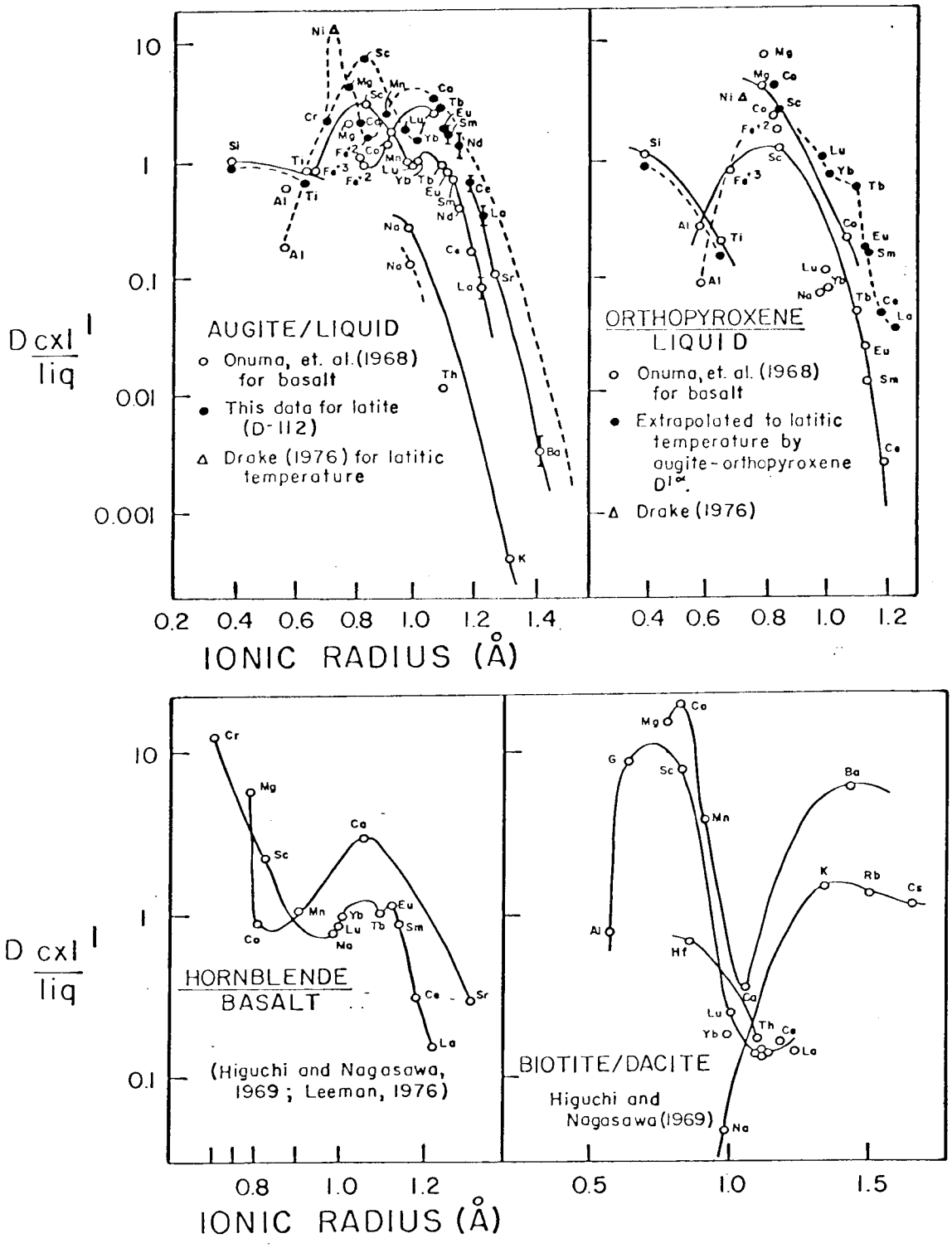

Figure 28. Plots of distribution coefficients against ionic radii. Ions with similar valence are plotted on contiguous lines.

variations are not unique to clinopyroxene involvement (Figures 28 and 29). Only augite and hornblende may raise Co/Sc by selectively including Sc relative to Co (Figures 28, 29, and 30). In members of the latitic series lacking hydrous assemblages, rising or constant Co/Sc during differentiation would be evidence that augite is a major phase in the fractionation history, because all other ferromagnesian phases lower Co/Sc of residual liquids.

The Large-plagioclase Member of the Table Mountain Latite has a high (1.7) Co/Sc ratio equal to or higher than much more mafic members of that series (sample 177-6, Figure 31). Likewise a biotite-bearing quartz latite member of the Lavas of Mahogany Ridge (sample F-206) has similar or higher Co/Sc compared to mafic members (e.g., sample D-240 with 6.35 percent MgO, Figure 31). Because hornblende is absent from the Table Mountain lavas and only very minor in one unit of the Mahogany Ridge rocks, it seems most probable that these two samples show evidence of dominant augite fractionation.

The higher Al_2O_3 of the Large-plagioclase Member compared to F-206 (Appendix Table II.1) may indicate much higher augite/plagioclase in the fractionating assemblages which yield aluminous low-Ca-Mg latite liquids relative to those which yield quartz latite residual liquid. If this is the case, then low-Ca-Mg latite may be a residual liquid evolved at high confining pressures where plagioclase

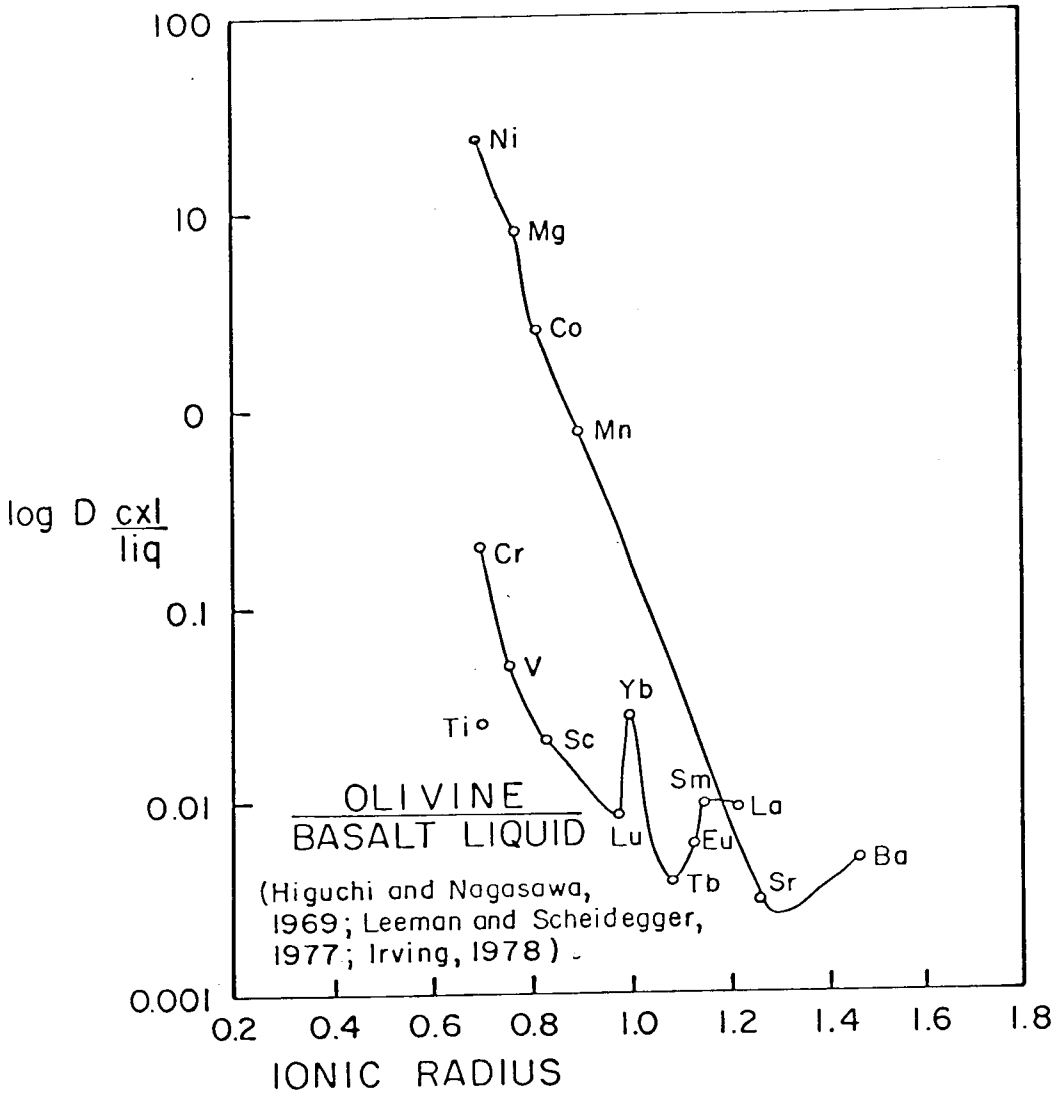

Figure 29. Olivine/basalt distribution coefficients versus ionic radius.

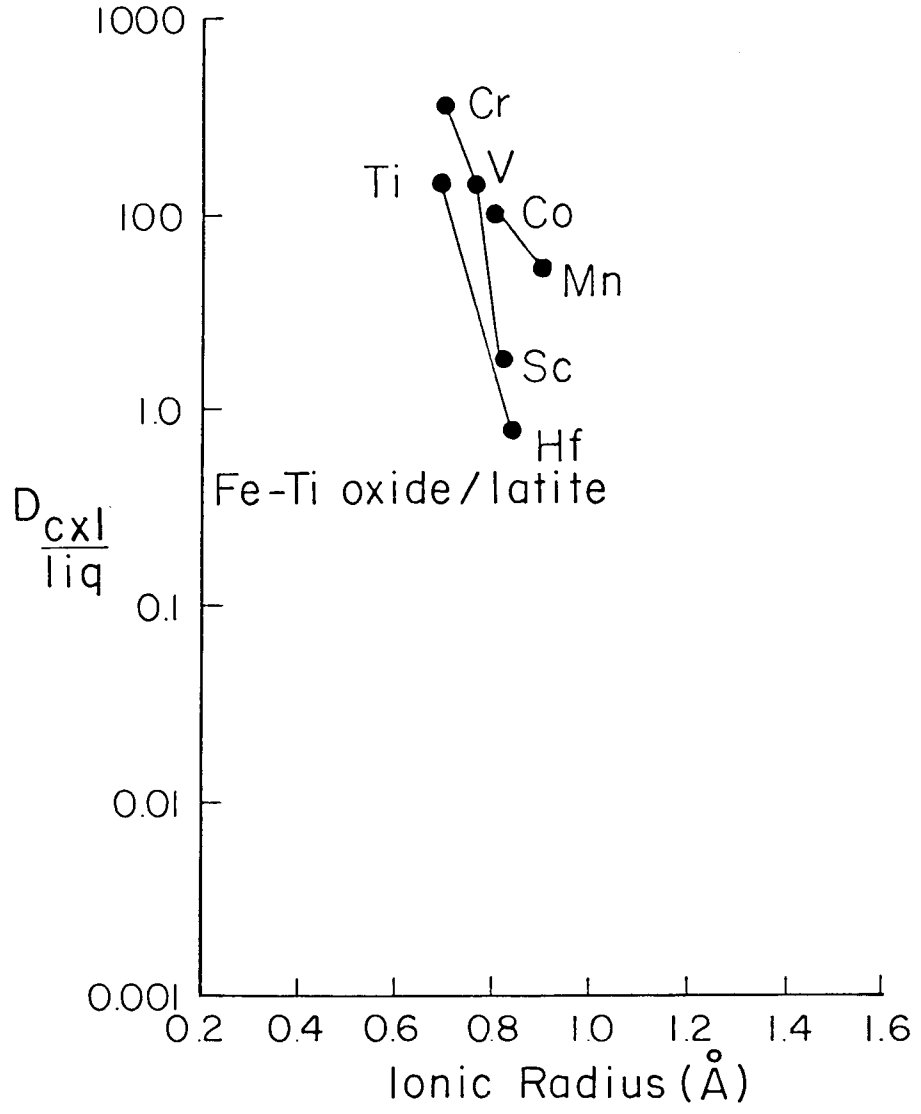

Figure 30. Iron-titanium oxide distribution coefficients versus ionic radius for low-K, low-silica latite.

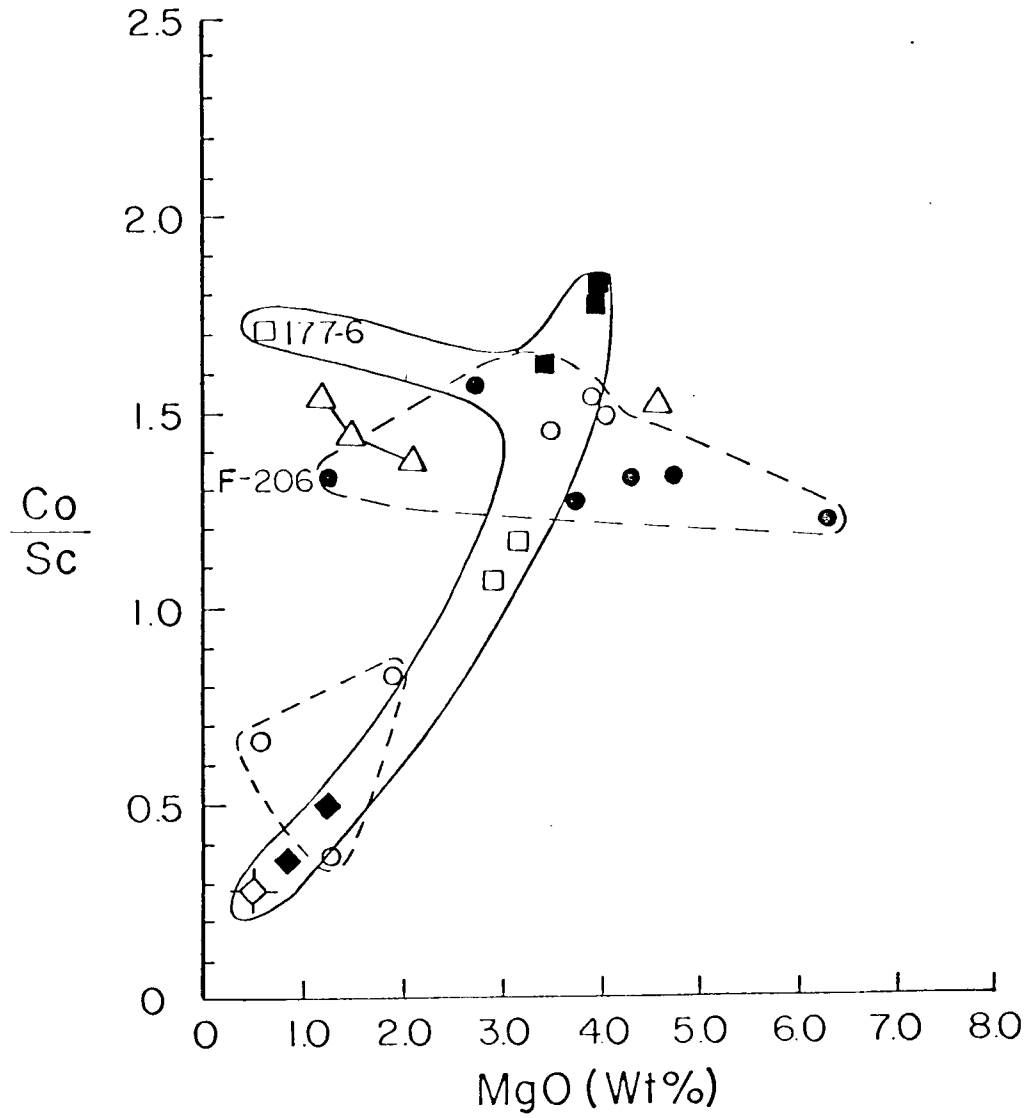

Figure 31. Co/Sc versus MgO. Symbols as in Figure 13.

is a near-solidus phase. The very high Co/Sc of the Large-plagioclase Member may mean that abundances of mafic phases fractionating from its parent magma were very subordinate to augite.

Green and Ringwood (1968) and Ringwood (1974) have suggested from experimental evidence that augite is favored over orthopyroxene in dry magmas. O'Hara (1967) and Yoder (1977) have noted that olivine is not a stable liquidus phase at high confining pressure and is generally less stable in dry relative to wet magmas. Osborn (1959) found crystallization of iron-titanium oxides is favored at high P_{H_2O} because of the high oxygen fugacity of hydrous magma. It is apparent that crystallization of augite-rich assemblages which are poor in hypersthene, olivine, plagioclase and Fe-Ti oxides will be favored in rather anhydrous magmas crystallizing at moderately high confining pressure. One might reasonably expect that magmas showing evidence of considerable plagioclase fractionation (e.g., negative Eu anomalies, high Sm/Eu and SiO_2/Al_2O_3 as in the Fales Hot Springs Quartz Latite and Eureka Valley Tuff) and moderately high H_2O (e.g., ash flows of the Eureka Valley Tuff) would have low Co/Sc and Al_2O_3. As may be seen from Figures 31 and 14, this is, in general, true for quartz latites.

The possibility of olivine and Fe-Ti oxide as important fractionating phases in parents to these quartz latites would lend a much more subsilicic character to the fractionating assemblage compared

to the anhydrous, augite-dominated case. The result should be much more silicic residual liquids, which is a characteristic feature of the quartz latites, compared to the low-Ca-Mg latites.

Dominant control by augite in fractionation should also raise Fe/Mg sharply (Figure 28) in daughter liquids, which is an important characteristic of the low-Ca-Mg latitic series (Figure 18). Any involvement of Fe-Ti oxides would, however, curtail the increase in Fe/Mg in residual liquids. Perhaps the lower Fe/Mg of the quartz latites (Figure 18) may be due to this factor, because all other anhydrous ferromagnesian phases raise Fe/Mg (Figure 28). This will be explored in the next section.

Iron-Titanium Oxide Fractionation

Fe-Ti oxides may significantly lower Co/Sc in residual liquids (Figure 30). The Latites of Devils Gate, the Eureka Valley Tuff and Fales Hot Springs Quartz Latite have the lowest Co/Sc of any units in the center (Figure 31). The low Co/Sc of the Tollhouse Flat Member of the Eureka Valley Tuff and Fales Hot Springs Quartz Latite might be explained, in part, by biotite fractionation, but no biotite occurs in the By-Day Member of the Eureka Valley Tuff or Latites of Devils Gate (Appendix Table I. 1). Likewise hypersthene separation could explain the low Co/Sc of the Devils Gate rocks (Figure 28), but no orthopyroxene occurs in the By-Day Tuff which has one of the lowest

Co/Sc values. Clearly, Fe-Ti oxide fractionation may account for some of the Co depletion in the By-Day Tuff, because fractionation of all other phenocrysts in the rock would either raise Co/Sc or leave it unchanged (Figures 28-30).

Fractionation of Fe-Ti oxides is also supported by the much lower Fe/Mg of the quartz latites compared to similarly-evolved low-Ca-Mg latites (Figure 18). This difference in Fe/Mg at similar, low MgO between these groups is difficult to explain without calling on differences in degree of Fe-Ti oxide involvement, as mentioned in the previous section.

The low-Ca-Mg latites of the Latites of Devils Gate do not have Fe/Mg as high as the low-Ca-Mg latites of the Table Mountain latite series such as the Large-plagioclase Member (Figure 18; Appendix Table I. 1). The low-Ca-Mg latites of Devils Gate lavas seem to represent an intermediate case between augite-dominated fractionation, leading to the aluminous low-Ca-Mg latites of the Table Mountain lavas, and Fe-Ti oxide, plagioclase-rich fractionation which leads to quartz latite.

Vanadium and halfnium may also be indicators of Fe-Ti oxide fractionation. Vanadium is very strongly partitioned into Fe-Ti oxides (Figure 30) compared to all other phases (Figures 28 and 29), although it is an included element in all ferromagnesian phases except olivine. Fe-Ti oxide is also the only phase besides biotite which

incorporates measurable Hf (Figures 28 and 30). Fe-Ti-oxide-dominated fractionation would cause V and V/Co to fall and Th/Hf to rise in residual liquids (Figure 30).

Biotite and hornblende may duplicate many aspects of Fe-Ti oxide transition metal partitioning. Because biotite apparently accepts Co and Mg in preference to the trivalent transition metals (e.g., Cr, V, Sc), biotite separation should raise V/Co (Figure 28). Hornblende, however, may cause V/Co to fall, if the crystal-liquid D for V (.74 Å) in hornblende lies between Sc (.83 Å) and Cr (.60 Å) (Figure 28). Because hydrous phases may duplicate some of the effects of Fe-Ti oxide fractionation, only the latitic series, which has few hydrous minerals, will be considered.

It is possible that apatite fractionation may also affect Th/Hf. Apatite incorporates significant Th (Irving, 1978) and Hf (Goldschmidt, 1954), but it is unknown how it affects Th/Hf. Fortunately, apatite fractionation was probably insignificant, because it is a very minor phase in most samples, generally less than 0.3 percent.

With the above considerations in mind, a test for Fe-Ti oxide fractionation may be made by considering variation of V/Co relative to MgO in various differentiation series. Figure 32 shows that V/Co in the latitic series is nearly constant in the Lavas of Mahogany Ridge but quite high in the low-Ca-Mg latites of Devils Gate. It is also high in the quartz latites of the Eureka Valley Tuff, but not notably high for

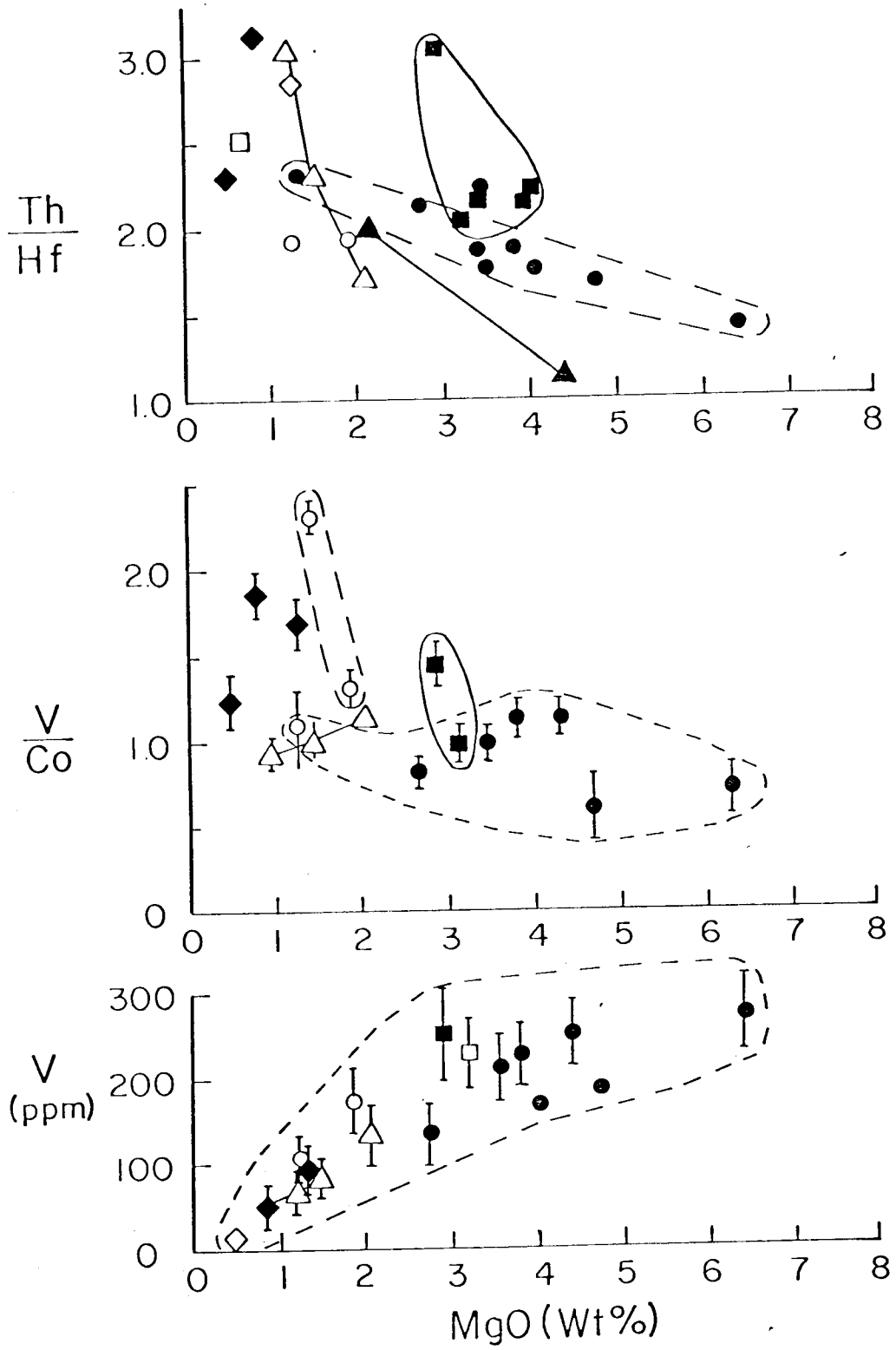

Figure 32. Variation of parameters sensitive to Fe-Ti oxide fractionation. Symbols as before.

the Fales Hot Springs Quartz Latite. The ratio decreases sharply with falling MgO in the hornblende-dominated lavas of Rickey Peak, owing to hydrous mineral effects. The constancy of V/Co in the Lavas of Mahogany Ridge is difficult to account for without calling on Fe-Ti oxide fractionation, because the other major ferromagnesian phenocrysts in this series (hypersthene, augite and olivine) would tend to raise V/Co (Figures 28 and 29). Likewise, the rather high V/Co of the By-Day tuff and the Latites of Devils Gate may reflect less involvement of Fe-Ti oxides.

Th/Hf variations lend support to the V/Co arguments in hydrous magmas lacking biotite. The Lavas of Rickey Peak and Relief Peak Formation have abundant hornblende and pyroxene phenocrysts and show sharp rise of Th/Hf with decreasing MgO in members lacking biotite. Because hornblende and pyroxene probably have little effect on this ratio, Fe-Ti oxides may account for the rise. It is interesting that the rise of Th/Hf with falling MgO is much steeper for the two biotite-bearing end members of the Lavas of Rickey Peak, compared to the biotite-free Relief Peak lavas. This may be from the sum effect of Fe-Ti oxide and biotite fractionation.

Th/Hf in the rather anhydrous latitic series shows variations between differentiation trends toward low-Ca-Mg latite and quartz latite which may be explained by differences in Fe-Ti oxide fractionation. The Th/Hf of the low-Ca-Mg latite of Devils Gate is relatively

low, corresponding to that of the voluminous intermediate members of the Lavas of Mahogany Ridge (Figure 32). There is also no apparent change of the ratio between the two samples of low-Ca-Mg latite even though there is a very significant difference in their MgO content (Figure 32). This may mean that there is little Fe-Ti oxide involvement in the genesis of these rocks. This is also suggested by the high Fe/Mg of these units (Figure 18). The Eureka Valley Tuff has the highest Th/Hf of the samples (Figure 32). This may mean that considerable Fe-Ti oxide has separated from parental magmas of the tuff. This is most convincing for the By-Day Member which lacks biotite but has Fe-Ti oxide phenocrysts. A low-Ca-Mg latite of the Large-plagioclase Member of the Table Mountain Latite has MgO lower than the Eureka Valley Tuff, yet possesses Th/Hf much lower than that of the tuff. This contrast in Th/Hf may reflect much less Fe-Ti oxide involvement in the evolution of low-Ca-Mg latite relative to quartz latite.

Rapid decline of V with decreasing MgO in highly evolved, latitic series or in hydrous series may signal the entrance of Fe-Ti oxides in the fractionating crystals. Total V tends to decrease slowly in mafic latitic rocks with falling MgO but quickly falls to essentially zero in quartz latites and dacites with MgO less than about 2 percent (Figure 32). In magmas with hydrous minerals this sharp decline may be due to combined hornblende and Fe-Ti oxide fractionation (e.g.,

the lavas of Rickey Peak, Figure 32). In latites the change in slope may be caused by increased crystallization of Fe-Ti oxides, perhaps owing to increasing P_{H_2O} in units lacking significant biotite or hornblende.

Biotite Fractionation

Ba is uniquely partitioned into biotite relative to liquid, unlike all other phases in this study. Ba should, then, fall when biotite becomes a significant part of the fractionating assemblage. The biotite-bearing Tollhouse Flat Member of the Eureka Valley tuff and the most biotite-rich dacite of the Lavas of Rickey Peak have anomalously low Ba compared to less evolved lavas from the same formations (Figure 33). This is considered the best evidence for biotite fractionation.

Separation of biotite also increases silica but sharply decreases Fe, Mg, and Fe/Mg, causing typical calc-alkaline trends in residual liquids. The low Fe/Mg and FeO of silicic members of the Lavas of Rickey Peak (Figures 16 and 18) may be partly from biotite fractionation.

Hornblende Fractionation

The distribution coefficients of hornblende are similar to those of augite owing to the similarity of their crystal structures.

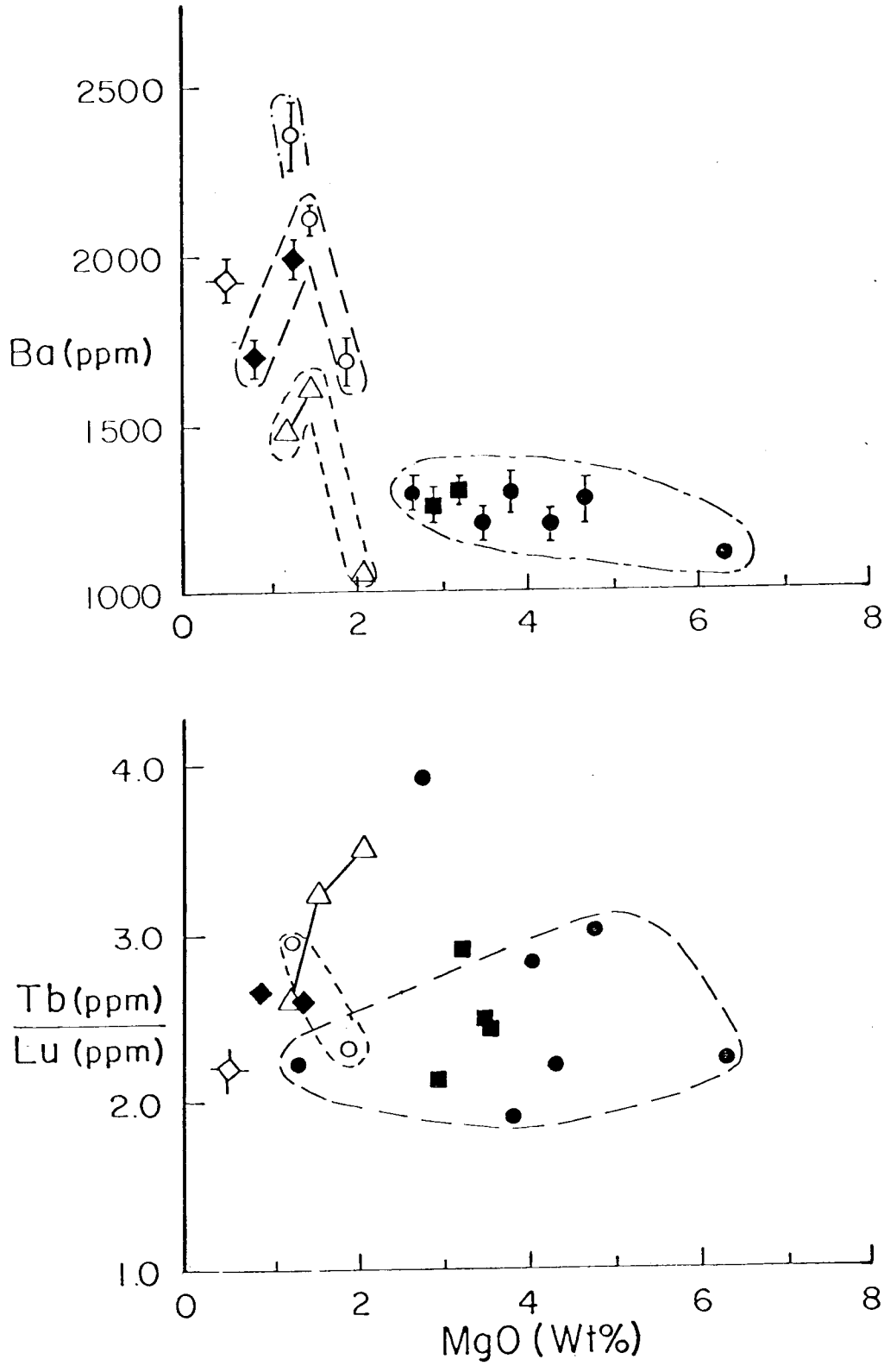

Figure 33. Variations from fractionation of hydrous minerals. Symbols as in Figure 13.

Hornblende, however, tends to be much more subsilicic and Fe-rich than augite, so that, like biotite, hornblende tends to produce calc-alkaline residual liquids that are high in SiO_2 with low Fe/Mg (Green and Ringwood, 1968). The combination of abundant biotite and hornblende in the Lavas of Rickey Peak and, to a lesser extent, the Relief Peak Formation has combined to produce magma series with the low Fe/Mg and high SiO_2 of the calc-alkaline trend (Figure 18).

Hornblende may strongly fractionate Tb relative to Lu. Arth and Barker's (1975) data show that hornblende can sharply increase the Tb/Lu of residual liquids in dacitic rocks, while Higuchi and Nagasawa's (1969) data predicts a fall in Tb/Lu. Unfortunately, at latitic-dacitic temperatures, orthopyroxene can also increase Tb/Lu, although not to the extent that amphibole may be able to (Figure 28). Augite tends to decrease Tb/Lu in residual liquids, so that it may curtail the effect of orthopyroxene and hornblende fractionation.

Because the hornblende-biotite andesites and dacites of the Lavas of Rickey Peak lack significant augite or hypersthene, they should provide an accurate test to see if Arth and Barker's (1975) or Higuchi and Nagasawa's (1968) data are more relevant to these liquids. Figure 33 shows that Tb/Lu decreases sharply in more evolved magmas of the Lavas of Rickey Peak. It seems that Higuchi and Nagasawa's data may be more relevant to these magmas, provided they indeed represent a liquid line of descent governed by

low-pressure crystallization. High pressure garnet-rich fractionation, or progressive partial melting of garnet-bearing assemblages raise Tb/Lu, so the data do not support high pressure processes (Irving, 1978). Low-pressure hornblende fractionation is, thus, the most probable explanation for variations of Tb/Lu in the Rickey Peak rocks.

The latitic series shows a highly random spread of Tb/Lu on the MgO variation diagram of Figure 33. This may be the result of conflicting effects of hypersthene and augite fractionation on this ratio such that slight changes in the crystallization ratio of clinopyroxene to orthopyroxene may cause increase or decrease of Tb/Lu (Figure 28).

One sample of the Lavas of Mahogany Ridge plots far outside of their compositional range on Figure 33. This sample is unique in being the only unit of that series with significant hornblende. It, in fact, plots within a possible extension of the compositional range of the Lavas of Rickey Peak which also have considerable hornblende. This is the main indication that this unit may be more closely related to the Lavas of Rickey Peak than to the Lavas of Mahogany Ridge. Figure 19 (sample LW-4) shows, however, that this unit is much too rich in incompatible elements (Th and Hf) to be one of the Lavas of Rickey Peak. For now the field evidence for close association with the Lavas of Mahogany Ridge and laboratory data showing incompatible

element content cause the correlation of this hornblende-bearing unit with the Lavas of Mahogany Ridge to be retained.

Conclusions

Data presented here show that essentially all of the common phenocrysts in both the latitic and calc-alkaline series could have been involved to some extent in high level fractional crystallization. The most important finding is that all of the major ferromagnesian minerals cause depletion of absolute Fe and increase in SiO_2 in residual liquids from basaltic andesite parent magmas. It was also noted that fractionation of biotite, hornblende and Fe-Ti oxides was the most effective means of lowering Fe/Mg and increasing SiO_2 in residual liquids, thus producing calc-alkalic differentiation.

Separation of pyroxenes was found to be less effective in increasing SiO_2 in differentiates and caused increase in Fe/Mg. In general, augite-dominated fractionation at moderate (10-15 Kb) pressures in relatively dry (low P_{O_2}) latite magmas probably leads to aluminous low-Ca-Mg latite. At shallower levels and higher water contents, plagioclase and Fe-Ti oxides may become significant phases leading to residual liquids with lower Al_2O_3, higher SiO_2, and low Fe/Mg, as in quartz latites.

It is probable that slight variations in level of fractionation and original water content may cause a spectrum of differentiation trends

with daughter liquids varying from rather "tholeiitic" low-Ca-Mg latite to more "calc-alkaline" quartz latites. At very high (saturated) water contents, amphibole, biotite, and Fe-Ti oxides will separate to produce extreme calc-alkalic differentiation typified by very low Fe/Mg and rapid increase of silica in residual magmas.

QUANTITATIVE TRACE AND MAJOR ELEMENT FRACTIONATION MODELS

Introduction

To quantify general conclusions reaching in qualitative consideration of chemical trends noted in the previous section, major element data for possible parent and daughter magmas were tested with the petrologic mixing program of Brian, Finger and Chayes (1969). This program is capable of obtaining "best fit" solutions for subtracting crystalline assemblages of constant composition from mafic parent magmas to obtain specified daughter compositions. The program is completely unconstrained, in that it simply find the best mixture of crystals + parent magma to obtain the daughter, by addition or subtraction of one or all of the crystal compositions. Any solution thus obtained is, then, relatively free of bias on the part of the programmer.

In general the program is increasingly less successful in relating parent daughter compositions as the two diverge in degree of differentiation. This is primarily due to the inability of the program to take into account progressive changes in the compositions of fractionating minerals exhibiting solid solution. While it is sometimes possible to select an "average" fractionating assemblage which approximates the total variation from solid solution, this is not a good

approximation to actual conditions. This is especially true for minerals with nearly ideal solid solution, such as olivine, which vary roughly according to Rayleigh fractionation laws (Hanson and Langmuir, 1978).

Modeling of oxides of low abundance such as MnO and TiO_2 was, in general, the least successful, because these elements probably vary in a manner not approximated by either an ideal major or trace (dispersed) element. As a consequence, no attempt was made to constrain the models with these oxides, although in some cases successful mixes were obtained for them.

Major element compositions for crystalline phases were taken from mineral separate analyses for augite, Fe-Ti oxide and plagioclase, whereas other phenocryst analyses (e.g., orthopyroxene, olivine, and biotite) were taken from the literature (Appendix III). No attempt to evaluate apatite fractionation could be made, because phosphorus contents were not available for most samples.

Tables 1 and 2 show major successful mixes, "successful" being defined as computed-daughter compositions matching real-daughter analysis to within two standard deviations of analytical error for all oxides except MnO and TiO_2, which were allowed much larger errors for reasons mentioned above. All successful parent-daughter pairs are plotted on the Fe/Mg Harker diagram of Figure 34 together with groundmass-whole-rock pairs.

Table 1a. Major element mixing models 1-4.

	Model 1				Model 2			
	Parent	Daughter	Calculated Daughter	Difference	Parent	Daughter	Calculated Daughter	Difference
Sample No:	TML-1	BD			BD	THF		
% crystals extracted:	-22% plag., -7.6% cpx, -4% opx, -2.4% mgt.				-3.4% biotite, -2.1% cpx			
SiO_2	57.9	63.6	64.2	0.4	63.6	65.7	63.4	2.3
TiO_2	1.07	0.93	1.14	0.21	0.93	0.67	0.84	0.17
Al_2O_3	17.3	16.8	16.8	0.0	16.8	16.6	16.8	0.2
MgO	2.8	1.3	1.3	0.0	1.3	0.83	0.84	0.01
FeO	6.1	3.9	3.9	0.0	3.9	2.8	2.8	0.0
MnO	0.10	0.09	0.03	0.06	0.09	0.09	0.08	0.01
CaO	5.9	2.5	2.5	0.0	2.5	2.0	2.0	0.0
Na_2O	3.6	4.3	4.1	0.2	4.3	4.7	4.3	0.4
K_2O	3.6	5.5	5.5	0.0	5.5	5.3	5.4	0.1
	Model 3				Model 4			
Sample No:	D-240	D-112-2			D-240	LW-37		
% crystals extracted:	-24.2% plag., -7.5% opx, -6.8% cpx, -3.2% ol, -0.7% mgt.				-23.3% plag., -6.0% cpx, -4.6% ol, -3.4% cpx, -1.0% mgt.			
SiO_2	51.9	56.0	56.2	0.2	51.9	55.6	4.0	1.6
TiO_2	1.00	0.97	1.42	0.45	1.00	0.95	0.95	0.00
Al_2O_3	17.4	18.3	18.4	0.1	17.4	17.2	16.7	0.5
MgO	6.2	4.0	4.0	0.0	6.2	4.2	4.2	0.0
FeO	7.6	6.9	6.9	0.0	7.6	6.3	6.4	0.1
MnO	0.13	0.09	0.06	0.03	0.13	0.10	0.11	0.01
CaO	8.5	7.4	7.4	0.0	8.5	7.2	7.2	0.0
Na_2O	3.4	4.3	4.1	0.2	3.4	3.5	3.7	0.2
K_2O	1.6	2.7	2.7	0.0	1.6	2.5	2.5	0.0

Table 1b. Major element mixing models 5 and 6.

	Model 5				Model 6			
Sample No:	Parent LW-37	Daughter D-12	Calculated Daughter	Difference	Parent 177-5	Daughter 177-6	Calculated Daughter	Difference
% crystals extracted:	-12.1% plag., -9.5% cpx, -6.6% opx				-15.1% plag., -13.9% cpx, -3.5% ol			
SiO_2	55.6	55.2	56.1	0.9	55.0	56.3	56.8	0.5
TiO_2	0.95	1.13	1.17	0.04	1.31	1.65	1.68	0.03
Al_2O_3	17.2	19.1	18.4	0.7	17.8	19.6	19.4	0.2
MgO	4.2	1.8	1.8	0.0	3.8	0.63	0.63	0.0
FeO	6.3	5.5	5.4	0.1	6.6	6.6	6.9	0.3
MnO	n				0.10	0.03	0.03	0.0
CaO	7.2	5.8	5.7	0.1	8.3	5.2	5.2	0.0
Na_2O	3.5	3.7	3.8	0.1	4.3	4.9	5.2	0.3
K_2O	2.5	3.6	3.5	0.1	2.9	4.1	4.1	0.0

Table 2a. Trace element fractionation models 1 and 2.

	Model 1				Model 2			
Sample No:	Parent ppm TML-1	Daughter ppm BD	Calculated Daughter ppm	Difference ppm	Parent ppm BD	Daughter ppm THF	Calculated Daughter ppm	Difference ppm
Cs	11.4(.8)*	13.8(.47)	18	4.2	13.8(1)	16.5(1.1)	14.6	1.9
Ba	1252(61)	2000(61)	1966	34	2000(30)	1703(83)	1694	9
La	64(1)	72.6(1.3)	96	23.6	72.4(1)	69.3(1.3)	75.7	6.4
Ce	125(3)	153(9.8)	182	29	153(4)	143(4)	159	16
Nd	59(5)	63(5)	79.9	16.6	63(5)	61(5)	64	3
Sm	9.7(.2)	10.25(.32)	12.3	2.05	10.3(.2)	8.95(.2)	10.33	1.38
Eu	1.90(.05)	1.96(.08)	1.66	0.30	1.96(.05)	1.66(.05)	1.97	0.31
Tb	1.05(.07)	1.02(.09)	1.23	0.21	1.02(.06)	0.98(.06)	1.01	0.03
Dy	5.4(.3)	6.1(.3)	--	--	6.1(.2)	4.83(.24)	--	--
Yb	2.64(.07)	3.27(.09)	4.39	1.12	3.27(.07)	2.81(.07)	3.31	0.50
Lu	0.36(.03)	0.40(.03)	0.55	0.15	0.40(.03)	0.37(.03)	0.40	0.03
Th	31(1)	36(1)	49	13	36(1)	42(1.27)	38	4
U	9.6(.9)	11.8(0.6)	15	3.2	12(1)	14.1(1.29)	12.5	1.6
Hf	9.92(.7)	12.48(.29)	15.2	2.52	12.5(1)	13.44(.96)	13.2	0.24
Ta	1.00(.03)	1.43(.04)	1.57	0.14	1.43(.04)	1.43(.04)	1.49	0.06
Co	17.3(.3)	5.32(.11)	3.61	1.71	5.3(.1)	2.71(.10)	1.8	0.91
Sc	16.1(.3)	10.45(.11)	6.62	3.83	10.5(.1)	7.5(.12)	5.3	2.2

*Numbers in parentheses are counting errors at one sigma. These are minimum errors.

Table 2b. Trace element fractionation models 3 and 4.

	Model 3				Model 4			
Sample No:	Parent ppm D-240	Daughter ppm D-112-2	Calculated Daughter ppm	Difference ppm	Parent ppm D-240	Daughter ppm LW-37	Calculated Daughter ppm	Difference ppm
Cs	0.9(.2)*	3.0(.3)	1.57	1.43	0.9(.2)	1.8(.2)	1.5	0.5
Ba	1108(52)	1185(76)	1657	472	1108(52)	1208(60)	1571	363
La	28.0(1)	34.0(.4)	44.6	10.6	28.0(1)	32.9(.74)	42.3	9.4
Ce	54.7(1.6)	69(1)	86	17	54.7(1.6)	69(1.9)	82	13
Nd	33.4(2.5)	--	--	--	33.4(2.5)	36.5(3.3)	50.4	13.9
Sm	5.9(.1)	6.84(.05)	8.83	1.99	5.9(.1)	6.13(.13)	8.51	2.38
Eu	1.67(.05)	1.83(.02)	2.11	0.28	1.67(.05)	1.60(.04)	2.05	0.45
Tb	0.71(.06)	0.59(.03)	1.02	0.43	0.71(.06)	0.71(.05)	1.0	0.29
Dy	3.4(.2)	--	--	--	3.4(.2)	3.57(.19)	--	--
Yb	1.69(.05)	1.7(.17)	2.42	0.72	1.69(.05)	1.66(.05)	2.43	0.77
Lu	0.23(.01)	0.21(.03)	0.32	0.11	0.23(.01)	0.23(.02)	0.33	0.10
Th	5.8(.3)	8.3(.2)	10.1	1.8	5.8(.3)	10.3(.4)	9.55	0.75
U	1.7(.2)	3.4(.5)	3.0	0.4	1.7(.2)	3.18(.29)	2.81	0.37
Hf	4.1(.3)	4.71(.14)	7.17	2.46	4.1(.3)	5.57(.41)	6.74	1.17
Ta	0.36(.01)	0.55(.06)	0.63	0.08	0.36(.01)	0.48(.01)	0.59	0.11
Co	31.7(.5)	22.18(.14)	23.7	1.52	31.7(.5)	23.66(.39)	27.9	4.24
Sc	26.0(.4)	14.91(.04)	19.2	4.29	26.0(.4)	17.7(.29)	21.7	4.0

*Numbers in parentheses are counting errors at one sigma. These are minimum errors.

Table 2c. Trace element fractionation models 5 and 6.

	Model 5				Model 6			
Sample No:	Parent ppm LW-37	Daughter ppm D-12	Calculated Daughter ppm	Difference ppm	Parent ppm 177-5	Daughter ppm 177-6	Calculated Daughter ppm	Difference ppm
Cs	1.8(.2)*	1.6(.2)	2.5	0.9	1.1(.1)	6.2(.21)	1.63	4.6
Ba	1208(60)	1686(82)	1537	149	--	--	--	--
La	32.9(.74)	46.9(.97)	42.3	4.6	--	--	--	--
Ce	69.0(1.9)	90.7(2.4)	88.0	2.7	117(2)	169(2)	157	12
Nd	36.5(3.3)	48.8(4.1)	--	--	--	--	--	--
Sm	6.13(.13)	8.3(.17)	7.14	1.16	--	--	--	--
Eu	1.60(.06)	2.08(.06)	1.69	0.39	2.20(.05)	2.89(.02)	2.39	0.50
Tb	0.71(.05)	0.89(.06)	0.72	0.17	0.78(.04)	1.13(.06)	1.18	0.38
Dy	3.57(.19)	4.27(.21)	--	--	--	--	--	--
Yb	1.66(.05)	2.06(.05)	1.75	0.31	--	--	--	--
Lu	0.23(.02)	0.28(.02)	0.24	0.04	--	--	--	--
Th	10.3(.4)	13.35(.44)	14.33	0.98	18.5(.8)	33(1)	27.4	5.6
U	3.18(.29)	4.25(.39)	4.42	0.17	--	--	--	--
Hf	5.57(.41)	7.05(.51)	7.75	0.70	8.6(.3)	13.2(.4)	12.7	0.5
Ta	0.48(.01)	0.63(.02)	0.66	0.03	1.17(.09)	1.8(.1)	1.7	0.1
Co	23.66(.39)	12.8(.25)	18.50	5.7	30.8(.4)	23.8(.3)	28.7	4.9
Sc	17.7(.29)	15.1(.25)	8.2	6.9	17.5(.1)	14.1(.09)	8.56	5.54

*Numbers in parentheses are counting errors at one sigma. These are minimum errors.

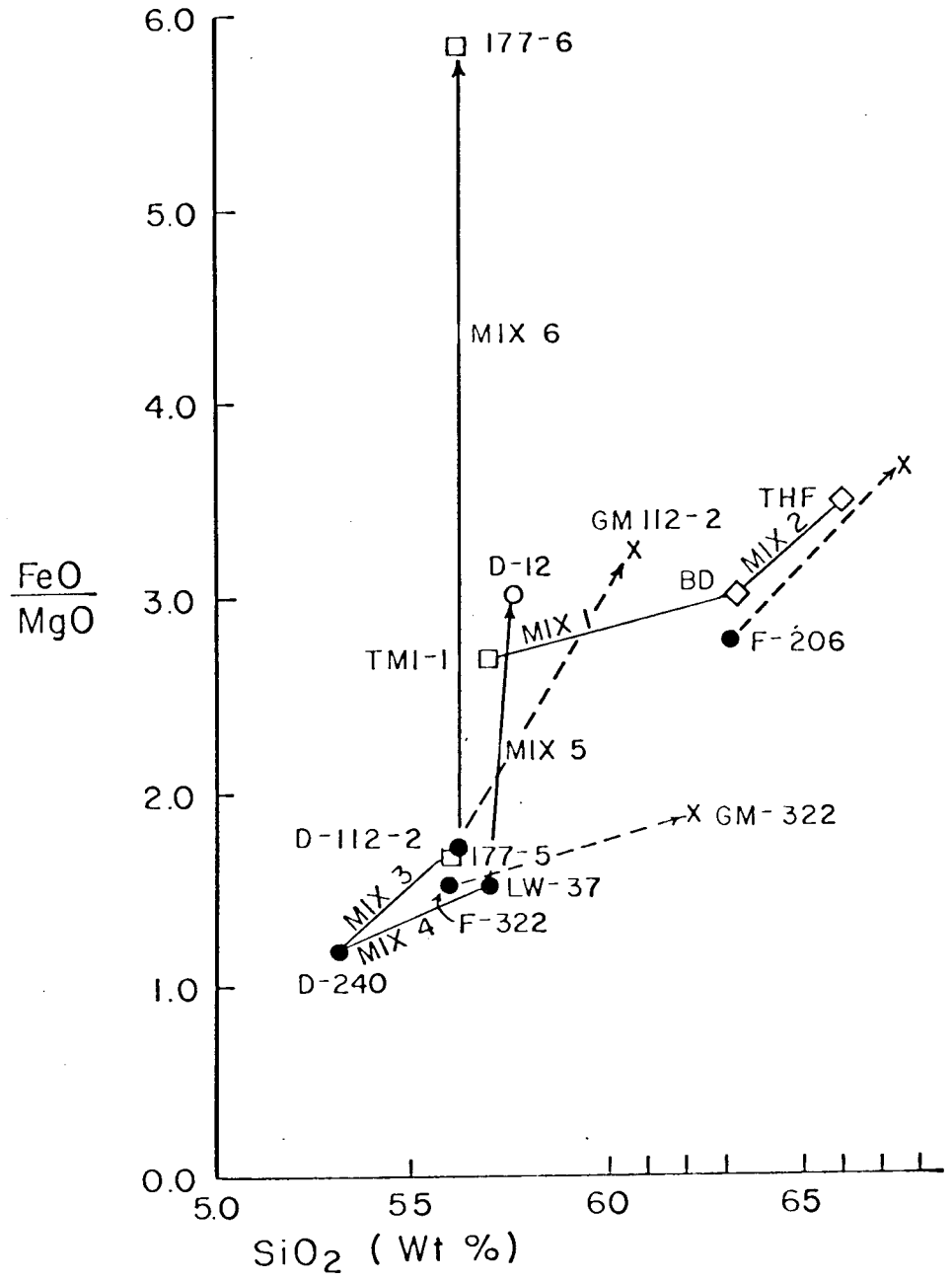

Figure 34. FeO/MgO versus SiO_2 for petrologic mixes and groundmass-whole rock pairs. GM = groundmass.

Major element models have been tested against trace element composition of each parent-daughter pair (Tables 2a, 2b, and 2c). Surface-equilibrium, Rayleigh fractionation was assumed in each case such that:

$$\frac{C_l}{C_o} = F^{\bar{D}-1}$$

where

C_l = concentration in the residual (daughter) liquid

C_o = concentration in the original (parent) liquid

F = fraction of residual liquid remaining

$\bar{D}$ = weighted average (bulk) crystal/liquid distribution coefficient for the entire fractionating crystalline assemblage.

Phenocryst/groundmass distribution coefficients (D's) for augite, plagioclase, and Fe-Ti oxides were determined for mafic low-K latite (F-322), low-K latite (D-112), and biotite-bearing quartz latite (F-206) from the Lavas of Mahogany Ridge (Appendix III). Details of the separatory procedure are summarized in Appendix III.

Distribution coefficients for biotite were taken from the literature (Appendix III). Orthopyroxene D's were extrapolated to latitic temperature-composition by normalizing augite-bronzite D's for basalt (Onuma and others, 1968) to augite/liquid D's of latites (Appendix III).

Model 1. Lower Member-Table Mountain Latite Parental to the By-Day Member-Eureka Valley Tuff

The major element mix which obtains the By-Day ash flow from a Table Mountain Latite parent requires subtraction of 36 percent crystals consisting of 22 percent plagioclase, 7.6 percent augite, 4 percent hypersthene, and 2.4 percent Fe-Ti oxides (Figure 34). This is probably a reasonable model because plagioclase and augite are the two dominant phenocryst phases in both parent and daughter, while hypersthene and Fe-Ti oxides are minor.

Consideration of trace element data (Table 2a) shows that this model is disallowed, because incompatible elements and REE are 20 to 30 percent too high in the projected daughter. D's for Co and Sc, isothermal with respect to the REE D's, produce daughter liquids with Co and Sc too low by 32 to 37 percent respectively (Table 2a). Choosing higher temperature D's for Co and Sc can produce a match between the model and actual By-Day liquid for one or the other element but not both at the same temperature, and this only aggravates the disparity in model REE. Because Co-Sc cannot be matched, this implies that the model is in error with respect to the ratio of ferromagnesian phases which affect this ratio (e.g., pyroxenes and Fe-Ti oxides).

In order to resolve the disparity in incompatible elements between the model and the actual By-Day data, the total percent of

subtracted crystals would have to be reduced from 36 percent to 17-19 percent. This is probably not within the limits of any model which could relate a mafic latite similar to TML-1 to a quartz latite as highly evolved as the By-Day Tuff. It is more reasonable to assume that the parent of the By-Day was depleted in incompatible elements by as much as 30 percent relative to the Table Mountain Latite.

Because the Table Mountain Latite has a negative Eu anomaly similar in magnitude to that of the By-Day, fractionation of the plagioclase-rich assemblage of Model 1 results in a Eu content too low in the model relative to the By-Day. It may be that the By-Day parent had a smaller Eu anomaly than the Table Mountain Latite. If the amount and proportion of plagioclase separating from the By-Day parent was similar to that of the model, then the By-Day parent may have had a higher oxygen fugacity (higher Eu^{+3}/Eu^{+2}) than the Table Mountain Latite. This might be caused by higher water content in the Eureka Valley Tuff parent (Osborn, 1969). However, if the By-Day magma evolved along a liquid line of descent appreciably different from that of the model, lack of a larger Eu anomaly in the tuff could reflect different ratios of pyroxenes to plagioclase in the actual crystalline fraction from those of the model (see the previous sections on plagioclase and pyroxene fractionation).

Model 2. By-Day Member Parental to the Tollhouse Flat Member of the Eureka Valley Tuff

Subtraction of 2.1 percent augite and 3.4 percent biotite produced a magma similar to the Tollhouse Flat tuff from the By-Day tuff (Figure 34, Table 1a). This mixing model is unique, because it requires no plagioclase separation. It may be that plagioclase does not settle significantly in quartz latite magma. Separation of significant biotite is in harmony with the low Ba content and presence of phenocrystic biotite in the Tollhouse Flat (THF) Member (Figure 33).

The trace element model (Table 2a) predicts a daughter 10 to 11 percent low in U, Th, and Cs and 3 to 19 percent (average of 11 percent) high in various REE. The Sc/Co ratio and absolute abundance of Ba, Hf, and Ta of the model match the THF within experimental error.

Absolute Sc and Co are 32 percent low in the model, but this could be due to the poorly known distribution coefficients for Sc and Co in biotite. The D's used here were taken directly from a dacite analyzed by Higuchi and Nagasawa (1969) and probably represent a magmatic temperature lower than that of the Eureka Valley Tuff. This is further suggested by comparing the D for Ba in biotite from Higuchi and Nagasawa's dacite (D = 9.7) to the successful value used in the model (D = 6.36 from values of Arth, 1976). The lower D of the model may indicate higher temperature in the quartz latite

relative to dacite. For this reason absolute Co and Sc are considered unreliable, whereas Co/Sc should be very sensitive to both the absolute amount and ratio of augite to biotite fractionation, because these phases partition Co and Sc quite differently (Figure 28). Match of Co/Sc of the By-Day and the model may indicate that the ratio of augite to biotite subtracted is reasonable.

It is more difficult to explain the 10 percent difference of Th and U between the model liquid and the THF (Table 2a). To achieve the higher U and Th of the THF, it would be necessary to subtract 15 to 16 percent crystals or nearly three times the amount of crystalline solid predicted by the model. It is difficult to believe that the major element model could be this much in error. This leads to the conclusion that although the model is reasonable for a parent magma closely similar to the By-Day Member, the actual parent magma of the THF must have been somewhat more enriched in incompatible elements than the By-Day Member.

The model REE may be high due to a combination of error in the projected D values and lack of consideration of possible apatite fractionation (apatite may strongly deplete the liquid in REE). The RE data neither confirm nor refute the model.

Model 3. Low-Silica Low-K Latite Parental to Latite of the Lavas of Mahogany Ridge

This model allows derivation of sample D-122-2 (two-pyroxene latite) from sample D-240 (two-pyroxene-olivine latite); both samples are members of the Lavas of Mahogany Ridge. The major element mix required subtraction of 24.2 percent plagioclase, 7.5 percent hypersthene, 6.8 percent augite, 3.2 percent olivine, and 0.7 percent magnetite from D-240 to yield D-122-2 (Figure 34; Table 1a). The amount and type of phases subtracted are reasonable for these rocks, because all phases are common phenocryst minerals and the relative proportion of phases is similar to proportions in the rocks (Appendix Table I.1).

Dominance of plagioclase and significant olivine fractionation suggest rather low-pressure fractionation (Green and Ringwood, 1967). As mentioned earlier, presence of two pyroxenes and Fe-Ti oxides in the fractionating assemblage may indicate substantial water content in the magmas.

The trace element model for this mix (Table 2b), however, shows that all LIL and incompatible elements except Cs and U are too high by 14 to 52 percent in the residual liquid of the model. In contrast, Cs and U are low by 48 and 12 percent, respectively. Co is only 6.8 percent high but Sc is 29 percent high using D's at a reasonable isotherm. Use of Sc and Co D's from mineral separates of

D-112-2. These D's seem unreasonable, because substantial fractionation must have occurred at temperatures higher than the temperature of the D-112-2 daughter liquid.

While the Co and Sc data may be considered somewhat equivocal, the RE and incompatible element content of the model cast considerably more doubt on the model. The low Cs and U may be explained by leaching of these relatively mobile elements from the D-240 parent, but the high model RE and Th contents are more difficult to explain. Even making the unreasonable assumption that the bulk (weighted average) D during fractionation approximated that of the D-112-2 phenocrysts, the model REE still remain much too high, while model Th is unaffected by this change in the assumed temperature. Perhaps apatite fractionation could cause daughter REE and Th(?) to be anomalously low (Arth, 1976).

The trace element data do not confirm this model. The data suggest that significant apatite and more ferromagnesian phases than used in the model may eliminate some of the discrepancies.

Model 4. Low-Silica Latite Parental to Latite of the Lavas of Mahogany Ridge

This mix closely resembles Model 3, requiring subtraction of 23.3 percent plagioclase, 6.0 percent augite, 4.6 percent olivine, 3.4 percent hypersthene and 1.0 percent Fe-Ti oxides from sample

D-240 to yield LW-37 (Table 1a; Figure 34). This model, however, allows more olivine and Fe-Ti oxide and less hypersthene to separate, causing greater SiO_2-enrichment but lower Fe/Mg in the residual liquid than in Model 3 (Figure 34). Such a difference in fractionation might be produced by slightly higher P_{H_2O} in the parent magma, which would favor earlier separation of olivine and Fe-Ti oxides than indicated for Model 3 (Osborn, 1969; Stern and Wyllie, 1976).

Cs, Th, and U are low, while all other trace elements, especially the REE, are too high in the model residual liquid (Table 2b). The low Th of the model and similarity of the U/Th of LW-37 and D-240 make it difficult to attribute the discrepancy in U, Th, and Cs to weathering, because Th is relatively insoluble in water relative to Cs and U (Rosholt and others, 1971). This suggests that either the fraction of remaining liquid (F) is too low or the actual parent magma of LW-37 had U, Th, and Cs higher than D-240. The discrepancies in RE content may again be from lack of consideration of apatite fractionation.

Model Co and Sc are too high in this mix, as in Model 3, and the problem may be eliminated by using Co and Sc D's of D-112-2 mineral separates. This is as unreasonable for this mix as it was for the previous case, because D-112-2 is as siliceous as the LW-37 daughter (Figure 34), indicating a similar temperature. It is clearly unwise to use distribution coefficients of a daughter liquid to approximate the

partitioning from more mafic liquids.

Again, the trace element data do not confirm this model. It must be pointed out, however, that the general pattern of ferromagnesian and RE elements of the model daughter closely resemble LW-37, indicating that the ratio of fractionating phases is reasonable, even if one rock is not directly related to the other.

Model 5. Latite (Lavas of Mahogany Ridge) Parental to Low-Ca-Mg Latite (Latites of Devils Gate)

Separation of 12.1 percent plagioclase, 9.5 percent augite and 6.6 percent hypersthene from a typical latite of the Lavas of Mahogany Ridge (LW-37) yields aluminous low-Ca-Mg latite similar to sample D-12 from the Latites of Devils Gate (Table 1b). The ratio of plagioclase to ferromagnesian phases in the fractionating assemblage of this mix (0.75) is much lower than the ratio in Models 3 and 4 (1.33 and 1.55, respectively). It is also noteworthy that no Fe-Ti oxide subtraction is necessary in this mix because Fe/Mg must climb steeply at nearly constant SiO_2, unlike the previous two models (Figure 34). The subordinate role of plagioclase fractionation is required to produce the high Al_2O_3 content of D-12 and may be achieved if the site of fractionation were at relatively high confining pressure where plagioclase would not be a liquidus phase (Green and Ringwood, 1968). Lack of Fe-Ti oxides may indicate low P_{O_2} and thus low water content

of the D-12 parent (Osborn, 1969). Because Fe-Ti oxides are common phenocrysts in the actual LW-37 sample, it is unlikely that LW-37 could have been the direct parent of D-12. However, a very similar magma with slightly lower water content than LW-37 may well have been the parent.

The trace element pattern of the model daughter is withn 3 to 20 percent for all REE and 5 to 9 percent for all incompatible elements except Cs, which is 56 percent too high in the model liquid, possibly owing to leaching of this highly mobile alkali ion from D-12. Many of the problems with the large-ion elements could probably be resolved by slight adjustments in average D's and amounts of subtracted phases. Consideration of serious Co and Sc discrepancies, however, make such adjustments pointless.

The model Co is 44.5 percent too high while Sc is 47.7 percent low. There is no way of adjusting both the Co and Sc distribution coefficients for the pyroxenes, such that both D's are isothermal, to produce the Co, Sc, and Co/Sc of D-12. The high Co/Sc of the model is chiefly caused by augite involvement (Figure 29). All other anhydrous ferromagnesian phases (olivine, Fe-Ti oxides, and orthopyroxene) lower Co/Sc (Figures 29-31). The model may, then, be in error in allowing too little orthopyroxene fractionation. Olivine and Fe-Ti oxide separation are precluded owing to the necessity of producing a low SiO_2 and high Fe/Mg of D-12.

Alternatively, the parent of D-12 may have not closely resembled the Lavas of Mahogany Ridge. If D-12 were evolved from a magma produced from or reequilibrated with an olivine-rich (mantle?) rock by smaller degrees of partial melting than that which produced LW-37, then the Co/Sc of the actual D-12 parent may have been much lower to begin with than that of LW-37. Equilibration of a small amount of melt with a large amount of olivine would produce low Co/Sc, because olivine strongly includes Co but excludes Sc even at latitic temperatures (Figure 29). While Co would not change appreciably with higher degrees of melting, because of the buffering action of the high crystal/liquid D of Co in olivine, Sc would be diluted, causing progressively lower Co/Sc as melting proceeded.

Low Co/Sc could also be produced by olivine fractionation from a picritic or olivine basaltic parent. This method would yield a daughter liquid highly depleted in Co, because Co is included in olivine (Figure 29). This might explain the relatively low Co of D-12, which is 44 percent lower than LW-37 (Table 2c). However, olivine fractionation cannot explain a similar Co/Sc discrepancy in the following model.

Model 6. Latite (Lower Member-Table Mountain Latite) Parental to Low-Ca-Mg Latite (Large-Plagioclase Member-Table Mountain Latite)

This mix has many of the attributes of Model 5. Model 6 allows latite (177-5) to produce aluminous low-Ca-Mg latite (177-6) by subtraction of 15.1 percent plagioclase, 13.9 percent augite, and 3.5 percent olivine (plagioclase/mafic phases = 0.87 versus 0.75 for the previous model; see Table 1b). The subordinate role of plagioclase is required to produce the high alumina content of 177-6. Lack of Fe-Ti oxides is necessary to account for the high Fe/Mg and low SiO_2 of 177-6 (Figure 34). Such a plagioclase-poor assemblage may be produced at moderate confining pressures, as explained earlier, or to ineffective fractionation of plagioclase relative to mafic phases. Large negative Eu anomalies in the Table Mountain Latite (Figure 20) suggest that plagioclase may effectively separate from those magmas under the correct conditions (e.g., low pressure), so the former hypothesis seems most likely. Lack of Fe-Ti oxides suggests low oxygen fugacity and, thus, low P_{H_2O} (Osborn, 1969).

Trace element modeling of this mix is limited by the meager data available for both samples. Within the limitations of the data it may, however, be seen (Table 2c) that RE and incompatible elements of the model are from 3.8 percent to 24.4 percent low (Cs is not considered owing to its extreme mobility during weathering). The

largest difference is in Eu, whereas the light RE element, Ce, is only 7 percent low relative to 177-6. The model Hf and Ta are within analytical error but model Th is 17 percent low.

The ferromagnesian elements Sc and Co offer more serious objections to the model than the LIL elements discussed above. The model Co is 20.6 percent high while Sc is 39.2 percent low. Adjusting the weighted average D for the model to a slightly higher (lower temperature) value requires using an isothermal Sc D which is so high that the model Sc is over 50 percent low. This Sc problem arose in Model 5 and may be from the same factors discussed there. In this case, however, increased olivine fractionation is incapable of explaining the relatively high Co of 177-6 which is only 22.7 percent lower than 177-5. If olivine had separated more extensively from a picritic or olivine basaltic parent of 177-6, compared to the parent of 177-5, then Co should be much more depleted in the 177-6 magma (Figure 29).

Implications of the Mixing Models

It is apparent that none of the major element mixing models convincingly pass trace element testing. This leads to the conclusion that either the distribution coefficients used in the trace element calculations are grossly in error, or that none of the analyzed samples are simply related to one another by subtraction of the model crystals. Because phenocryst/groundmass distribution coefficients from

samples similar to or identical with those of the model rocks were used, it seems that the distribution coefficients are probably not the main source of error. Even if the distribution coefficients were not accurate, this does not explain why some models (e.g., Models 5 and 6) failed even when large variations of the distribution coefficients were allowed. Some models (e.g., Models 1-4) failed, in part, owing to REE and incompatible element content which was too high in the model relative to actual daughter liquid. It is possible that apatite fractionation could have solved these problems by lowering model RE and incompatible element contents. Unfortunately, the degree of apatite fractionation could not be independently estimated because of lack of data on phosphorous contents. Some of these models (e.g., Models 1, 3, and 4) had problems with elements not included in apatite as well, so that even with apatite fractionation they would have been disallowed.

The most reasonable conclusion is that all of the Stanislaus magmas have probably had slightly different partial melting and crustal fractionation histories. Thus, all are probably the products of slightly or significantly different liquid lines of descent. It hardly seems likely that all or even most volcanic liquids in any volcanic center would follow identical paths to the surface from identically melted source rocks. It is also almost a certainty that the source area for the partial melts would undergo progressive changes in

composition with respect to major and, especially, trace constituents. When such systematic changes are coupled with probable heterogeneities in the source rocks, it is not surprising that no single lava at the surface can be related to another by these simple mixing calculations.

The most systematic failures were between older units and younger. Whenever such a mix was tested (e.g., Table Mountain Latite to the Eureka Valley Tuff; By-Day Tuff to the Tollhouse Flat Tuff, and Lavas of Mahogany Ridge to the Latites of Devils Gate), the U and Th contents, particularly, were much too low in the younger unit. Because these problems cannot be explained by apatite fractionation effects, it is very probable that there is a definite trend toward decreasing incompatible elements in younger units. This may well be evidence of progressive depletion of a common source in these elements. It is absolutely certain that the earliest unit (the Table Mountain Latite) is much richer in these large-ion elements than the youngest unit (Lavas of Mahogany Ridge), and all mixes between these two were disallowed by the high K_2O of the Table Mountain Latite.

PARTIAL MELTING MODELS

Introduction

To infer the mineralogy of possible source rocks, REE data have been modeled for equilibrium batch melting, using equation 15 of Shaw (1970). Trial calculations assuming disequilibrium (fractional) melting for REE gave results very similar to the equilibrium melting calculations. For this reason, and because equilibrium batch melting is considered petrologically more reasonable under mantle conditions, only equilibrium conditions have been assumed.

Distribution coefficients have been taken from average values of Arth (1976) for andesitic and basaltic rocks (Table 3). These coefficients are from higher temperature, more mafic magmas than most of the latites, but are probably representative of values to be expected in mafic parents of latites. It was found that relative differences in augite/liquid distribution coefficients among various REE were small between Arth's (1976) values and those determined for latites. Because the relative differences of distribution coefficients among REE are the most important factors determining the slope and shape of REE curves, use of these average values of Arth (1976) is probably warranted.

Table 3. Crystal/liquid distribution coefficients used in melting models.

Crystal Phase:	Olivine[1]	Orthopyroxene[1]	Clinopyroxene[1]	Garnet[2]
Melting Proportion:[3]	0.05	0.15	0.40	0.40
Element:	$D_{ol/l}$	$D_{opx/l}$	$D_{cpx/l}$	$D_{ga/l}$
La	0.007	0.02	0.10	0.01
Ce	0.007	0.024	0.15	0.021
Sm	0.007	0.054	0.50	0.217
Eu	0.007	0.054	0.051	0.320
Tb	0.009	0.120	0.65	0.720
Yb	0.014	0.34	0.62	4.03
Lu	0.016	0.42	0.56	5.60

[1] From average values of basaltic and andesitic rocks in Arth (1976); La and Tb values estimated by extrapolation.

[2] From 1275°C, 30 Kb data of Shimizu and Kushiro (1975); La, Tb, and Lu estimated by extrapolation. Values are somewhat lower than those of Arth (1976).

[3] Melting proportions taken from estimate of garnet peridotite eutectic by Murali and others (1977).

Transition Metal Constraints

In order to pick a reasonable source mineralogy for testing, it is necessary to consider transition metal abundances in the most mafic members of the Stanislaus Group. Transition trace metals (e.g., Co, Cr, Ni, and Sc) have very high crystal/liquid distribution coefficients in ferromagnesian silicate-magma systems (e.g., Figures 28 and 29). During batch melting or zone refining of a mafic or ultramafic source the content of these highly included transition metals will be relatively constant up to reasonably high (10-20 percent) degrees of melting (Arth, 1976). The melt abundance will be buffered by the refractory assemblage of mafic silicates such that the ratio of concentrations in liquid (C_l) to original source concentration (C_o) will remain relatively constant at about the reciprocal of the weighted average distribution coefficient of the source ($C_l/C_o = 1/\bar{D}$).

This attribute of highly included elements makes them relatively good indicators of the amount of mafic silicates, especially olivine and pyroxenes, in the source, provided crystal fractionation has not depleted the liquid in these elements during ascent. Because basalts are considered to be partial melts of ultramafic mantle sources, it is useful to compare the least-evolved Stanislaus lava with continental and oceanic basalts to see if their trace metal abundances are similar. Table 4 shows that least evolved "high-Cr" and "high-Mg" Columbia

Table 4. Comparison of the least-evolved lava of the Stanislaus Group (number 1) with least-evolved Columbia River Basalts (CRB) and MORB.

	1	2	3	4
Weight %				
SiO_2	53.1	50.14	54.09	49.61
Al_2O_3	17.8	15.47	14.33	16.01
FeO	7.7	11.20	11.42	10.99
MnO	0.13	0.20	0.20	0.18
MgO	6.4	6.65	4.90	7.84
CaO	8.7	10.62	8.72	11.12
Na_2O	3.4	2.94	2.84	2.76
K_2O	1.6	0.57	1.17	0.22
TiO_2	1.03	1.55	1.78	1.43
ppm				
Sc	26	42	33	60
Cr	208.5	180	36	300
Co	31.7	44	38	32
Ni	75	60	16	120
Th	5.8	0.6	3.5	0.15
La	28	8	22	2.7

1: Pyroxene-olivine high-K basalt (D-240)-Lavas of Mahogany Ridge.

2: High-Cr-type Picture Gorge (CRB)*.

3: High-Mg-type Grande Ronde (CRB)*.

* Taken from Osawa and Goles (1970); Wright and others (1973); Nathan and Fruchter (1974); and McDougall (1976).

4: Cann. J.R. (1971), Major element variations in ocean-floor baslats, Phil. Trans. Roy. Soc. London. Ser. A. 268, p. 495-505. Average mid-ocean ridge basalt (MORB).

River Group basalts have Cr and Ni contents similar to or lower than the most mafic Stansilaus rock, while Co and Sc are slightly lower in the latitic sample. The Stanislaus rock is, however, 30 to 50 percent lower than oceanic tholeiite in Sc, Cr, and Ni, although Co is subequal. More crystal fractionation together with somewhat smaller degrees of partial melting might account for the lower transition metal content of the Stanislaus sample compared to oceanic tholeiite, if both are from mantle sources.

In reviewing the origin of low-silica latite very similar to the D-240 sample, Noble and others (1975) concluded that these rocks could not be the product of melting of subducted oceanic tholeiite, because crystal/liquid distribution coefficients for Co, Ni, and Cr of eclogitic assemblages are so high that nearly complete melting of subducted tholeiite would be required to generate the high transition metal content of low-silica latite. Complete melting is not only petrologically unlikely, but also yields magmas very low in incompatible elements (note the low Th and La of oceanic tholeiite, Table 4). Low degrees of partial melting of ultramafic (mantle) assemblages is probably a much more efficient process for generating both the high incompatible and ferromagnesian element content of latites.

Strontium Isotopic Constraints

The initial Sr-87/Sr-86 of a low-K latite sample of the Lavas of Mahogany Ridge (LW-37, Appendix Table II. 1) is 0. 7057 (Hedge and Noble, 1971), while more highly evolved quartz latites of the Eureka Valley Tuff have initial ratios of 0. 7054 to 0. 7055 (Noble and others, 1976). The high Sr content of the low-K latites of Mahogany Ridge (+ 1, 000 ppm, Figure 25) cause it to be unlikely that the 0. 7057 value reflects contamination from old sialic crust, so it is probably representative of a radiogenic mafic source.

Noble and others (1976) concluded that these ratios are consistent with an ultramafic upper mantle source (possibly a mantle plume) for the latitic magmas. Indeed, these values are well within the range of adjacent continental basalts of the Great Basin (Hedge and Noble, 1971) and basalts of the Columbia River Group (McDougall, 1976).

Whereas these isotopic ratios could be the result of melting of Rb-depleted lower crustal (mafic) material, arguments of the previous section suggest that an ultramafic (mantle) source is more consistent with the transition metal content of latite. In any case, the isotopic data certainly do not rule out a mantle source for the Stanislaus Group, but neither does this data eliminate the possibility of wall-rock reactions of the mantle-derived magma with Mesozoic crustal rocks.

The high initial Sr-87/Sr-86 of latites compared to most oceanic rocks may be caused by melting of a source with Rb/Sr higher than that of the oceanic mantle. This would imply that the probable mantle source of latitic magma was enriched in Rb and other large-ion elements relative to oceanic mantle. This is completely consistent with the extremely high content of these elements in latite, as well as the high large-ion abundances of continental basalts (McDougall, 1976).

If, in fact, the source of the Stanislaus Group has undergone enrichment in REE in addition to Rb at some stage in its history, this process may have seriously changed the relative abundance of REE from a probably chondritic original pattern. The implications of this and later changes in the relative abundance of source REE will be explored in the next section.

Rare Earth Melting Models

Relative abundances of REE in partial melts are very sensitive to proportions of minerals in the residuum which contain the highest concentrations of REE (e.g., garnet, clinopyroxene, and amphibole). The relative abundances are not, however, particularly sensitive to the eutectic (or "eutectic-like") melting proportions used in batch melting calculations, nor are they sensitive to the abundance of minerals which strongly exclude REE (e.g., olivine and orthopyroxene). Constant melting proportions (values from Murali and others,

1977) and a constant weight ratio of olivine to orthopyroxene were thus used in all models. As already noted in Figures 20 and 23, chondrite-normalized RE curves for all rocks of the Little Walker center are distinguished by great enrichment in light REE relative to heavy REE and high Tb/Lu ratios. The light REE act as moderately excluded elements relative to the heavy REE in high-pressure assemblages considered here (Table 3), thus La/Sm is chiefly a function of degree (percent) of partial melting. High La/Sm is correlative with small percentage partial melts, where excluded elements like La are most highly concentrated.

Only garnet can significantly raise Tb/Lu in melts when it is in the residuum. Thus, the high Tb/Lu of the Little Walker rocks requires garnet in the source residuum at segregation, provided mantle (?) assemblages had roughly chondritic initial REE abundances. If the source of the magmas had other than chondritic REE content, then this model is in error to the extent that the source was not chondritic.

Figure 35 shows chondrite-normalized REE curves of various melt fractions produced from garnet pyrolite with a chondritic initial abundance. As noted above, La/Sm is a sensitive function of percent melting, whereas Tb/Lu is high and relatively constant until high degrees of melting. This is because both Tb and Lu are strongly

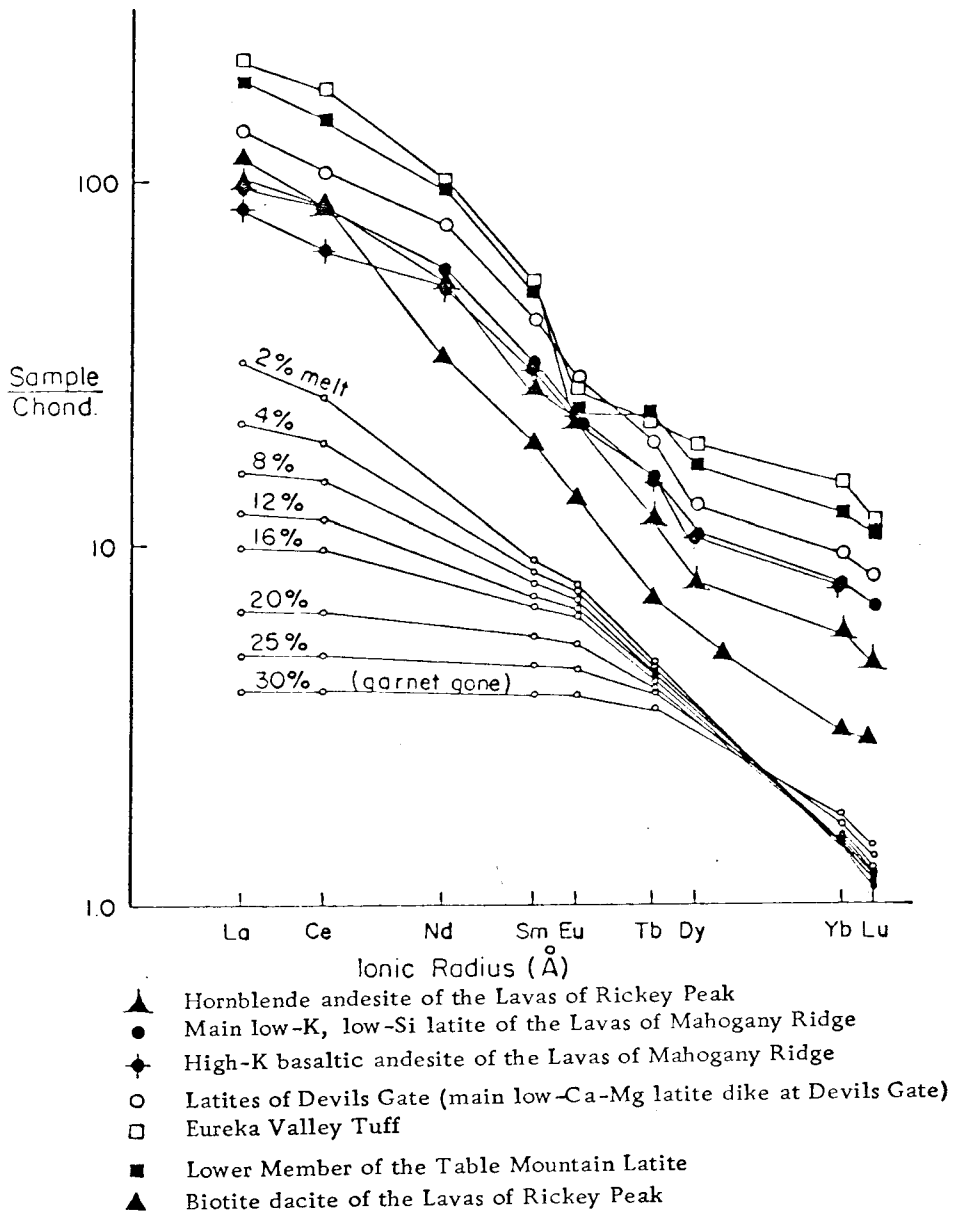

Figure 35. Partial melting models for garnet pyrolite (Ringwood, 1974).

included in garnet, thus effectively buffering their abundance in the melt.

Heavy REE of partial melts are chiefly constrained by garnet and clinopyroxene in this model, owing to the high content of heavy REE in these phases relative to other phases (Table 3), thus Tb/Lu of partial melts is chiefly a function of the garnet/clinopyroxene ratio of the residuum. Tb/Lu may be increased by later, low-temperature orthopyroxene fractionation at high levels in the crust (Figure 28), but Figure 33 shows no trend of increasing Tb/Lu with decreasing MgO in the two-pyroxene latites of Mahogany Ridge. This is probably caused by the opposing effect of high level augite fractionation (Figure 28).

It is apparent that garnet pyrolite produces liquids with Tb/Lu much higher and absolute REE much lower than values of the Little Walker magmas (Figure 35). It follows that a viable source must have a lower garnet-clinopyroxene ratio and higher absolute REE abundance than chondritic pyrolite.

The most completely analyzed units in the center are the Lavas of Mahogany Ridge which have Tb/Lu ranging from 1.89 to 2.4 (averaging 2.15) and La/Sm from 2.74 to 3.21 (averaging 3.03). It was decided that these units would be used as targets for a "best fit" model, because their chemical composition is well known. Solution of a number of simultaneous equations and numerous trial melting calculations revealed that source assemblages with clinopyroxene (cpx) to

garnet (ga) ratios of 4.0 to 5.5 yield liquids with the required Tb/Lu at 2 to 10 percent melting. The La/Sm values of these mantle melts are also within the allowable range at 6 to 10 percent melting but were low at greater than 10 percent and high at less than 6 percent melting. Because high level augite and, to a lesser extent, orthopyroxene fractionation may increase La/Sm (Figure 28), melting percentages somewhat higher than 6 percent are probably allowable. Slight positive Eu anomalies in the model are eliminated during high level plagioclase fractionation (Figure 24).

Variation of absolute eclogite component at constant ga/cpx showed that eclogite-depleted assemblages yielded liquids with slightly lower La/Sm and Tb/Lu. Depleted models also showed a much greater change of La/Sm during progressive melting than eclogite-rich assemblages, so that only a very limited range of melting would yield target La/Sm values at a given ga/cpx. Also, eclogite-depleted models were incapable of yielding large volumes of melt, owing to the low basaltic (eclogitic) component. Because La/Sm is not notably variable in Stanislaus rocks (Figures 20 and 35), and it is known that their source yielded voluminous magmas during several melting episodes, an eclogite-depleted source is not favored.

The source which best fits the data, then, must be characterized by ga/cpx much lower than pyrolite and be relatively enriched in eclogite. A reasonable source which matches the relative REE

abundances of the average Mahogany Ridge magmas very well contains 10 percent garnet, 42 percent clinopyroxene, 37 percent olivine, and 11 percent orthopyroxene. Such a source generates mafic magma with the relative abundances of REE similar to the Lavas of Mahogany Ridge at about 6 percent melting (Figure 36).

With relative proportions of garnet and clinopyroxene in the source established, absolute eclogite abundance was varied to see what effect this would have on the melts. Increasing the percent of eclogite component at constant ga/cpx allowed generation of liquids with the same REE pattern at slightly higher degrees of melting, but the correct La/Sm could be produced at only 10 percent melting, even from 100 percent eclogite models. Melting of 100 percent eclogite produced much less absolute REE enrichment in the melt relative to melting of garnet peridotite, because of the higher average RE distribution coefficient of the residuum. Thus the garnet peridotite of Figure 35 produced a liquid 12.0 times the chondritic La and 1.25 times chondritic Lu while eclogite yields a liquid only 7.2 times chondritic La with Lu unchanged from chondrite at 6 percent melting. The high absolute abundance of light REE in the latites would favor melting of the peridotite rather than eclogite composition, as does the high ferromagnesian element content of mafic samples (see previous section on transition metals).

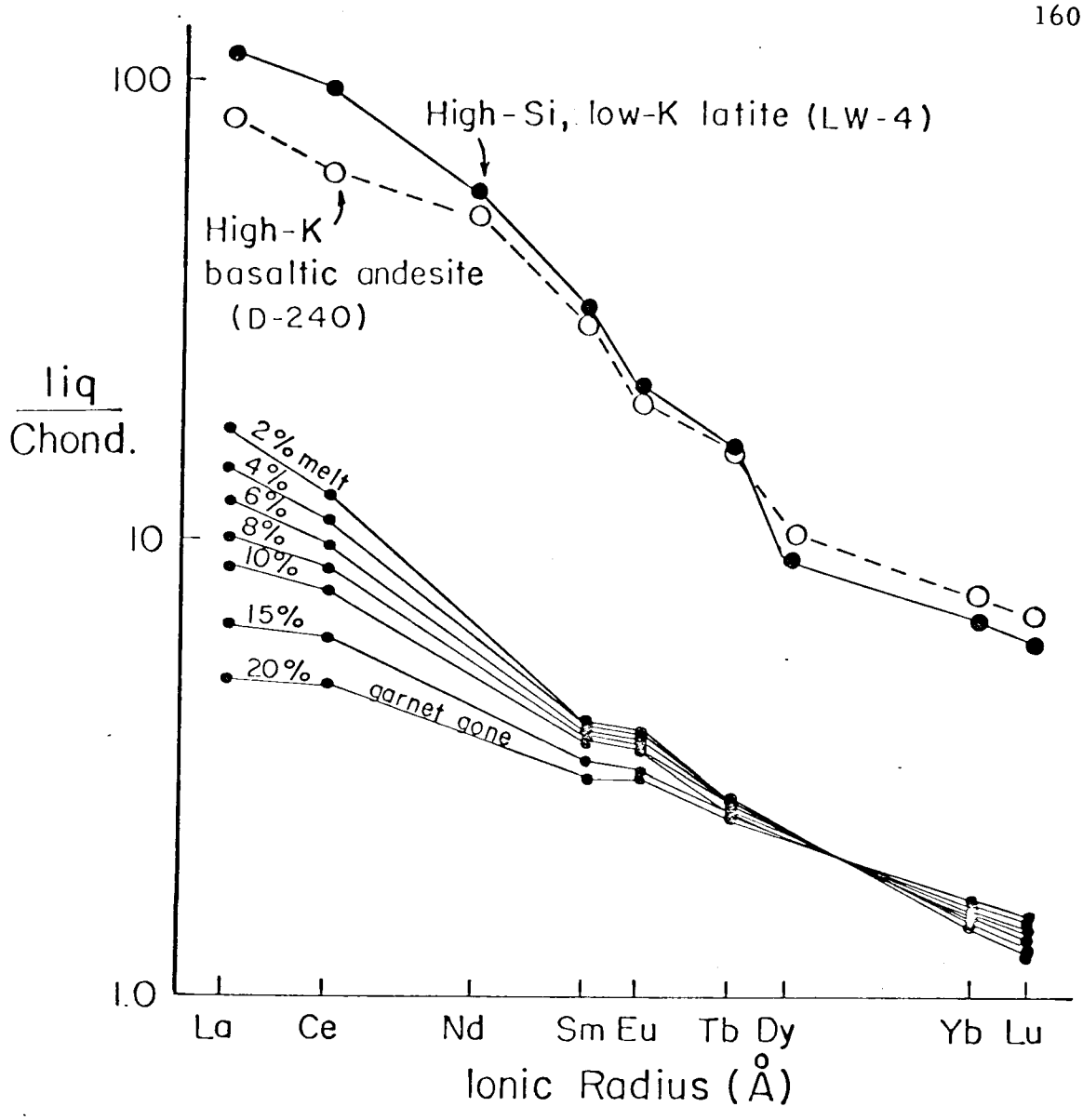

Figure 36. Partial melting models for melting of best match garnet peridotite assemblage (42% clinopyroxene, 37% olivine, 11% orthopyroxene, and 10% garnet). Model is calculated to match the Lavas of Mahogany Ridge within the range shown.

Even zone refining of an eclogitic source could not enrich Lu in the liquid to the target (6 to 7 times chondrite) value, because Lu is not appreciably partitioned into the liquid from eclogite. Extensive zone refining of a clinopyroxene-orthopyroxene-olivine (harzburgite) source would, however, lead to extreme enrichment of all REE without changing the original pattern, whereas zone refining of garnet-bearing peridotite would appreciably raise La/Sm and Tb/Lu as well as absolute REE. The degree that zone refining has occurred in garnet-bearing material during rise of the magmas is a critical control on La/Sm and Tb/Lu in the liquids and, thus, on the amount of garnet inferred for the source. In postulating more zone refining of a garnet-bearing source, less garnet need be present during melting and larger original percentages of melting may be allowed. Clearly, the low value of the distribution coefficient of La in all peridotite or eclogite phases relative to Sm will cause La to be extremely enriched during zone melting such that very low initial La/Sm (high percent partial melting) would be required to finally produce a magma with the target La/Sm.

Fractional crystallization could not account for the high absolute REE content of the Lavas of Mahogany Ridge relative to the model of Figure 36. Even if the REE were completely excluded from all fractionating phases, 83 to 93 percent crystallization would be required to attain latitic RE values. Such highly fractionated liquids would be

completely depleted in most ferromagnesian elements, especially Cr and Ni, whereas low-SiO_2, high-K andesite of the Lavas of Mahogany Ridge has high transition metal content equivalent to many continental basalts (Table 3).

If the latitic rocks were generated from a source with REE content several times that of chondrites, then this would eliminate the problem of enriching the initial liquid in large-ion elements. Ringwood (1975) has predicted that the upper mantle can become enriched by hydrous acid melts distilled from descending oceanic lithospheric slabs at convergent plate boundaries. Eruption of the Stanislaus Group was preceded by voluminous calc-alkalic volcanism (the Relief Peak Formation) probably associated with subduction (Noble, 1972). If eruption of the Relief Peak andesites was accompanied by enrichment of the upper mantle in large-ion lithophile elements from this distillation process, then any latitic parents of the Stanislaus magmas might have reacted with or been melted from this contaminated mantle to produce melts with highly enriched REE content. Perhaps the most important point to be emphasized here is that not only absolute but relative abundances of REE would be drastically changed from chondritic values by such contamination. Small percentage partial melts removed from a descending lithospheric slab would almost certainly be highly enriched in light REE relative to heavy REE, if the slab were in the eclogite or even amphibolite facies,

and would imprint this pattern on the overlying mantle. If this has occurred, the partial melting models considered here will tell very little about the mineralogy of the actual source of the latites.

If the latitic source had a non-chondritic REE content characterized by high La/Sm and Tb/Lu, for example, if contaminating melts were from eclogitic oceanic crust, then the amount of garnet predicted by the model of Figure 36 is much too large. This garnet content was completely constrained by Tb/Lu, so correspondingly less garnet is required as the original Tb/Lu of the source is assumed to be higher than chondrite. Because it was concluded above that zone refining in even a very garnet-poor upper mantle would also raise Tb/Lu, thus requiring a smaller ga/cpx ratio than the original model, it is probable that the model ga/cpx of Figure 36 is an upper limit, whether zone refining or contamination or both have operated to enrich absolute REE. Likewise, the distribution coefficients chosen for Tb, Yb and Lu in garnet-liquid were much lower than average values of Arth (1976) used by most writers. Because using higher garnet D's for these elements would further reduce the projected model ga/cpx ratio, ga/cpx predicted here is, indeed, an uppermost limit.

It seems unlikely that garnet was absent from the source assemblage, because an aluminous phase is necessary to account for the high Al_2O_3 content of the Stanislaus Group. If, however, the

source had high original Tb/Lu, then a spinel peridotitic source cannot be ruled out, because spinel would also be a source of Al_2O_3 and would not significantly fractionate the heavy REE from one other (Irving, 1978).

If partial reequilibration of the rising magma with a source having low Tb/Lu occurred, then an originally high Tb/Lu may have been partially reduced. It is difficult to evaluate the likelihood of this or other multistage processes which may have occurred, because they are not amenable to quantitative proof or disproof.

Source of the Lavas of Rickey Peak

The calc-alkaline rocks of the Lavas of Rickey Peak differ sharply from the latitic series in both chemical and mineralogical composition. Figures 20 and 35 show that the Lavas of Rickey Peak have La/Sm and Tb/Lu greater than that of latites. Although the Lavas of Rickey Peak (LRP) have generally higher MgO than latites at similar SiO_2, reflecting their more calc-alkaline character (Figure 15), they have much lower Co, Cr, and Sc than latite at similar MgO (Figure 21). The LRP are also much less enriched in all large-ion elements than any Stanislaus unit (Figures 13, 19, and 22). Whereas anhydrous mafic silicates dominate the Stanislaus rocks, hornblende and biotite are liquidus minerals of the Lavas of Rickey Peak.

These unique characteristics of the LRP suggest a source aseemblage capable of producing magmas with lower large-ion elements and ferromagnesian trace elements than latites but higher initial water content (Stern and Wyllie, 1974) and higher relative fractionation of REE. Such a source would necessarily be less mafic, more hydrous than latitic sources, and characterized by garnet involvement in some stage of its history, owing to the high Tb/Lu of the LRP.

It may be that mafic rocks richer in mica eclogite or garnet amphibolite components than the latite source would be logical sources of these calc-alkalic rocks. Their association with a large continental volcanic arc of similar rocks along the western United States during Mio-Pliocene time certainly argues for generation during active subduction (Noble, 1972) where mica eclogites and garnet amphibolites may be involved in melting (Jakes and White, 1970). Perhaps a lower crustal source may have been melted to produce the LRP, because the transition element contents do not demand an ultramafic source. Even a garnet-free amphibolite might be a viable source, if the original REE pattern were quite highly fractionated to high La/Sm and Tb/Lu by various contamination processes outlined in the previous section.

In any case very significant high level fractionation has probably affected all samples. This is suggested not only by their low

ferromagnesian element contents and phenocryst-rich petrography, but by the high water content inferred from their mineralogy. It is difficult to imagine a magma nearly saturated with water reaching the surface without very significant crystallization-differentiation. Involvement of large amounts of hornblende during differentiation would probably lower Tb/Lu, as shown in the section on hornblende fractionation. It appears that, regardless of other uncertainties, the assumption of significant garnet involvement at some stage is definitely warranted, because parent magmas of the LRP must have had even higher Tb/Lu than the already high values of the daughter liquids sampled (Figure 33). Hornblende also raises La/Sm very efficiently in residual liquids (Figure 28), so that erroneously low degrees of melting will be predicted by partial melting calculations on fractionated liquids like the samples available here. From these considerations, it is not considered fruitful to pursue detailed calculation of melting models for such highly fractionated rocks.

The lack of enrichment of large-ion elements compared to latites might be caused by generation from either a source more depleted in these elements, lesser degrees of zone refining (shallower depths), greater degrees of partial melting, or presence of a residual phase or phases which contained significant amounts of large-ion elements. These possibilities are not distinguishable with the data available.

Conclusions

An ultramafic (mantle) source for latitic magma is required by the high transition metal content of mafic Stanislaus samples and is consistent with the Sr isotopic data. Initial strontium isotopic ratios and high content of large-ion elements of Stanislaus rocks suggest that this mantle source had high Rb/Sr and large-ion elements compared to oceanic mantle. This either implies that the mantle under the Little Walker center 10 m.y. ago was undepleted from a primitive (chondritic) content of large-ion elements or that it may have been enriched in these elements above primitive levels, because suboceanic mantle appears to be depleted in these elements relative to chondrites (Gast, 1968). If progressive (early) or recent (Relief Peak-aged) enrichment of large-ion elements, including REE, has occurred, then it is likely that the relative REE pattern of the source has also been changed from chondritic. If garnet was in the residuum of the contaminating liquids in either case, this enrichment of the mantle would have caused rise of the La/Sm and Tb/Lu above chondritic values. Such variations of the relative REE pattern from chondrites place severe constraints on the amount of garnet allowed in the residuum of latites at segregation, as well as the amount of possible deep level garnet fractionation.

Partial melting models assuming a chondritic source predict a mantle garnet/clinopyroxene of about 0.24, much lower than that of pyrolite (1.14). Any process such as enrichment of the source by liquids from the lower mantle (garnet-bearing) or subducted basalt (eclogite facies), or enrichment of the partial melts by zone refining of garnet-bearing assemblages would tend to increase the La/Sm and Tb/Lu of the source or, in the latter case, the magma, causing the projected model source assemblage to assume even lower ga/cpx. Even contaminated spinel peridotite may have been the source, if contaminants possessed high Tb/Lu.

It is clear that the high absolute REE content of latites cannot be obtained by simple melting of a chondritic mantle, combined with crystal fractionation of the partial melts. At least 83 percent crystallization of a parent magma would be required to produce latitic RE levels from the model melt, but the high transition metal content of these rocks (Table 4) suggests much less fractionation. These arguments require that the latite source be non-chondritic or that significant zone refining acted to increase absolute REE. This further implies that the ga/cpx ratio inferred for the RE model may be an upper limit, because zone refining of the source would raise Tb/Lu if garnet were involved.

The high alumina of the Stanislaus Group (16 to 20 percent) requires that an aluminous phase such as spinel or garnet was

present, and the large volume of latitic magma found at the Little Walker center requires a substantial percentage of that aluminous phase in the source. If a garnet-bearing source is postulated, this requires that the source have high absolute garnet, whereas previous arguments imply that the ga/cpx be no higher than about 0.24. Clearly, to have high absolute garnet and low ga/cpx, the source would have to be very rich in clinopyroxene, suggesting an assemblage similar to the "best fit" REE model of Figure 36 which has over 50 percent clinopyroxene-rich eclogitic component. As one assumes a source ga/cpx lower than 0.24, the absolute amount of eclogitic component relative to harzburgite component in the source must increase to yield sufficient magma. If the source is to retain an ultramafic character, as required by the Ni and Cr data (Table 4), the amount of eclogite cannot be much greater than the model values.

If spinel was the aluminous phase in a highly contaminated mantle, these arguments do not apply, except insofar as clinopyroxene must be a significant phase with spinel to generate sufficient liquid. It is interesting that this writer's attempts to mathematically mix major element compositions of naturally-occurring high pressure spinels and other peridotite minerals to produce roughly basaltic or andesitic melts met with universal failure. It may be that spinel peridotite is not a reasonable parent for mafic lavas.

Perhaps partial reequilibration of the latitic magmas with spinel peridotite or other upper mantle with low Tb/Lu may have lowered magmatic Tb/Lu from a formerly high value (e.g., the pyrolite model of Figure 35). If this is the case, then all of the magmas have reequilibrated to a similar degree, because Tb/Lu is not highly variable in the latites (Figures 20 and 35).

It is obvious from these arguments that the trace element evidence does not specify a unique model for generation of the latitic magma. Perhaps a better understanding of high pressure distribution of trace elements, especially highly included transition metals, may eventually help to better constrain these models. It is certain that the mafic latites were produced from an ultramafic source bearing some aluminous phase such as garnet or spinel, and that garnet was probably involved at some stage in their evolution.

It was concluded from consideration of the high Tb/Lu and low transition metal contents of the Lavas of Rickey Peak compared to latites at similar MgO content, that these rocks may have been partially melted from a less ultramafic source with higher garnet involvement than that of latites. Uncertainties arising from evidence of very significant degrees of amphibole fractionation precluded detailed modeling of these rocks, but it was found that garnet amphibolite-rich or mica eclogite-rich assemblages, probably with high garnet/(clinopyroxene or amphibole) ratios were compatible with

the data. Such sources might be present in subducted oceanic crust or overlying mantle. Even garnet-free amphibolite (lower crust?) was not precluded as a possible source provided it has a very high initial Tb/Lu.

PETROGENETIC SUMMARY

Potassic volcanism began in the study area about 10 m.y. ago with outpouring of voluminous, mafic latite lavas (Lower Member of the Table Mountain Latite) from vents at Sonora Pass and, possibly, the Little Walker center. Progressively smaller-volume, more highly differentiated lavas continued to erupt wholly from the Little Walker center (upper parts of the Table Mountain Latite) until two voluminous quartz latite ash-flow sheets (the Eureka Valley Tuff) caused a large caldera to form.

Initial intracaldera volcanism was dominated by ash flows (Upper Member of the Eureka Valley Tuff and Tuffs of Poore Lake), but these were much cooler, poorly welded deposits compared to the early, highly welded ash flow sheets. The intracaldera tuffs are interbedded with fluvial and lacustrine deposits suggestive of repeated eruption into a caldera lake. Latitic volcanism came to a close with eruption of numerous small, highly differentiated dikes along the caldera margin (Latites of Devils Gate) and, finally, moderately large-scale extrusion of viscous, phenocryst-rich, lavas of two-pyroxene, low-K latite to high-K andesite along arcuate and ring fractures within the caldera. These ring fractures may have been the result of small-scale resurgent doming of the cauldron subsidence block.

The early latitic magmas (Table Mountain Latite) crystallized chiefly augite and plagioclase with minor olivine and evolved numerous highly aluminous low-Ca-Mg latitic magmas with a trachytic character (high K_2O and Fe/Mg, but low SiO_2). Petrologic mixing models suggest that such differentiates may evolve from latite at moderately high pressure where pyroxene is dominant over plagioclase in the fractionating assemblage.

Voluminous quartz latite ash flows (the Eureka Valley Tuff) extruded in the middle stages of the eruptive cycle seem to be the product of lower-pressure, plagioclase-rich fractionation from latitic parents depleted in incompatible elements relative to the Table Mountain Latite. Succeeding latitic activity was progressively less potassic and lower in other incompatible elements until, by the time of eruption of the Lavas of Mahogany Ridge, two-pyroxene low-K latites and high-K basaltic andesites were the dominant magmas. Silicic differentiates of these low-K latitic magmas contain early-crystallizing Fe-Ti oxides, hornblende and/or biotite with two pyroxenes and have only slightly higher Fe/Mg than mafic low-K latite.

The petrochemical character of the magmas thus changed from truly latitic to more typically calc-alkaline through time. Younger magmas seem also to have been slightly more water-rich than earlier magmas, because hornblende is a stable phenocryst in them, but very rare in earlier eruptions. Higher water content may have caused

early crystallization of Fe-Ti oxides (Osborn, 1969) which, with sub-silicic pyroxenes and hornblende, caused typically calc-alkaline series differentiates with low Fe/Mg and high SiO_2 at relatively high oxygen fugacity ($10^{-8.5}$, Appendix III). Magmatic temperatures were, however, relatively high (1178°C to 1154°C, Appendix III) in mafic members in spite of significant H_2O. This high temperature, together with persistence of two liquidus pyroxenes in biotite-bearing members, suggest that the Mahogany Ridge magma was still undersaturated in H_2O.

Consideration of trace element batch melting models and major element composition required that the latitic source be ultramafic (mantle) and rich in clinopyroxene plus some aluminous phase such as garnet or spinel. Simplest single-stage melting models required a much lower garnet/clinopyroxene ratio (0.24) in the source than typical pyrolite compositions (garnet/cpx = 1.17). Without calling on considerable zone refining, no models could generate the high absolute REE content of latites from a mantle with condritic REE. Metasomatic processes which might raise primitive mantle well above (at least three or four times) chondritic abundances would probably increase Tb/Lu above that of chondrites, if garnet was involved, which was considered very likely. Such changes would require model source rocks with even lower projected garnet/clinopyroxene than the single stage model. Partial reequilibration of magmas with

spinel-bearing assemblages with low Tb/Lu could, however, lower Tb/Lu of latitic melts and mask the imprint of a very garnet-rich source. From these considerations, it is apparent that REE evidence for source mineral assemblages is highly equivocal, except in so far as garnet must have been involved at some stage in evolution of the source. High absolute content of ferromagnesian minerals in mafic latitic rocks, however, precluded any but ultramafic (mantle) sources, so olivine and pyroxenes were probably important constituents as well.

Fractional crystallization was investigated with binary variation diagrams for major and trace elements as well as quantitative modeling. After establishing that all magmatic series in the center show specific progressive changes in major and trace element content consistent with fractional crystallization of all phenocryst phases, detailed least-squares mixing calculations were performed on petrologically significant parent-daughter pairs. Trace element (Rayleigh) modeling of the major element mixing models showed that it is unlikely that any of the latitic Magmas can be simply related to one another by crystal fractionation from shared parent magmas. This could be the result of a continuously evolving source which produced unique partial melts that followed equally unique liquid lines of descent.

It seems, at first sight, anomalous that large, highly welded ash-flow sheets are absent from hornblende-rich andesites of the Relief Peak Formation and younger lavas of Rickey Peak which enclose the Stanislaus Group. According to known experimental data (e.g., Stern and others, 1975), liquidus hornblende occurs only in magmas nearly saturated with water. Such liquids might seem logical producers of voluminous ash flows, yet is is this writer's observation that hornblende andesitic series differentiates rarely produce major rhyolitic "flood" ash-flow eruptions.

Welded ash-flow sheets of the Eureka Valley Tuff lack hydrous minerals (the By-Day Member) or have coexisting biotite and pyroxene (Tollhouse Flat Member). These ash-flow sheets are completely welded with only very thin upper and lower glassy zones in most areas, indicating very high eruptive temperature. Fumarolic alteration, vapor phase crystallization, and devitrification are, however, absent. All of these factors argue for low total water content in the quartz latites. Anhydrous phenocryst assemblages and lack of fumarolic alteration also typify most other major ash flow centers (e.g., the Black Mountain center and other rhyolitic ash flow centers of the southern Great Basin, Figure 1). If H_2O is not the major volatile agent in these large-scale ash-flow eruptions, then CO_2 is the most likely choice from consideration of the most common constituents of volcanic gases (Macdonald, 1972) and abundance of CO_2 in

carbonatites. Mysen (1977) has shown that H_2O is much more soluble than CO_2 in magmas, so that magma with high H_2O/CO_2 will have a much larger component of gas in solution than magma with low H_2O/CO_2. It follows that relatively anhydrous, CO_2-rich melts will exert greater total volatile pressure on surrounding rocks than magmas with equal total volatiles but high H_2O/CO_2. It is gradual build up of tremendous volatile pressures that favors catastrophic failure of roof rocks with rapid evolution of magma-gas emulsions from shallow magma reservoirs.

CO_2-rich, anhydrous magmas would also tend to be erupted at much higher temperature, because anhydrous melting occurs at much higher temperatures than under hydrous conditions. Ash flows from such magmas would then tend to weld to a much greater degree than cooler, hydrous ash flows. In fact, calc-alkaline volcanic centers, such as the High Cascades of Oregon and Washington are thought to evolve from melting of hydrous peridotite assemblages (McBirney, 1969) and characteristically have only small, poorly welded ash flows compared to the huge rhyolitic ash-flow sheets of the Great Basin. These Great Basin ash flows are thought by Noble and Hedge (1974) to be differentiation products of relatively anhydrous continental basalt.

In the Little Walker center cool, poorly welded ash flows of the Upper Member of the Eureka Valley Tuff and Tuffs of Poore Lake are characterized by biotite without pyroxenes as is the Fales Hot Springs

Quartz Latite. Decrease in the volume and welding of ash flows after eruption of the welded ash flow sheets and extrusion of quartz latite lavas at Fales Hot Springs are apparently correlated with high H_2O/CO_2. Likewise, all ash flow activity ceased upon eruption of the hydrous two-pyroxene to hornblende-bearing Lavas of Mahogany Ridge.

Variation in original H_2O/CO_2 at the site of melting may account for the change from highly alkaline to calc-alkaline volcanism at the Little Walker volcanic center. Mysen and Boettcher (1975) and Eggler (1974, 1975) have shown that melts change from alkali-rich basaltic to andesitic as mantle sources with increasingly high H_2O/CO_2 are tapped. This may, in part, explain why the early CO_2-rich, one-pyroxene latitic magmas are so much more alkaline than the later hydrous two-pyroxene, high-K andesite to low-K latite Lavas of Mahogany Ridge. Likewise, the hornblende-biotite acid andesites and dacites of Rickey Peak, which closely followed the last latitic activity, are the least alkaline, most hydrous magma series in the area.

Progressive increase in H_2O/CO_2 of the magmas may be inconsistent with partial melting from a common source. Mysen (1977) concluded that H_2O/CO_2 would fall to very low values in source rocks undergoing sequential melting owing to much higher solubility of H_2O relative to CO_2 in partial melts at high pressure. One would then

expect that continuous melting of a single source would produce lowest H_2O/CO_2 in the youngest extrusions, yet the Lavas of Mahogany Ridge seem to have higher H_2O/CO_2 than all older units. This anomaly, coupled with the fact that small volumes of low-K, two-pyroxene lavas erupted in the upper part of the Table Mountain Latite and within the Eureka Valley Tuff, suggest that two mantle sources with very different H_2O/CO_2 may have been active during the Stanislaus eruptions. Noble (1972) and Snyder, and others (1976) noted the existence of a late Cenozoic calc-alkaline volcanic arc along the Sierran axis, inferred to be associated with an active subduction zone. This subduction produced a vast blanket of hornblende andesite mudflows and autobreccias across the northern and central Sierras (Relief Peak, Disaster Peak, and Mehrten Formations). These eruptions completely overlap volcanism at the Little Walker center (Slemmons, 1966; Figure 3). Because experimental evidence favors production of hydrous andesitic magma from melting of hydrous mantle peridotite (Mysen and Boettcher, 1975; Mysen, 1977) during degassing of subducted oceanic lithosphere (McBirney, 1969), this hydrous mantle may have been present during the Stanislaus eruptions as a viable second source.

A possible model for evolution of the Little Walker volcanic center could involve rise of a relatively anhydrous, CO_2-rich mantle diapir through subducted and fragmented oceanic lithosphere into

hydrous upper mantle still producing orogenic andesitic magmas. Spontaneous melting of the diapir would proceed as confining pressure fell during rise, causing liquid zones to rise and progressively deplete the diapir of its large-ion (incompatible) element component. These liquid zones erupted at the surface as the early latitic series (Table Mountain Latite and Eureka Valley Tuff) after undergoing variable amounts of high pressure fractionation toward aluminous low-Ca-Mg latite (the Large-plagioclase Member) and lower pressure differentiation toward quartz latite (the Eureka Valley Tuff). Rising geotherms accompanying this activity precipitated increased melting of mixed sources at the interface between the diapir and overlying hydrous upper mantle until such mixed sources dominated activity at the time of eruption of the Lavas of Mahogany Ridge. At that time, much of the eclogitic component of the diapir was exhausted and latitic volcanism ceased. Continued high heat flow from on-going subduction and, perhaps, the diapir caused hornblende-andesitic volcanism to continue unabated from sources within the overlying hydrous upper mantle and possibly the lower crust. Both the latitic and calc-alkalic series magmas may have undergone variable amounts of interaction with crustal material as they rose. This would have been more effective in the latitic series, because the latites were probably much hotter than the hydrous calc-alkaline series.

MINERAL RESOURCES

Gold and Silver

Subvolcanic monzodiorite stocks located in the Mount Emma area (Figure 2) are thought to be cogenetic with the late volcanic dome-forming stage represented by the Lavas of Mahogany Ridge. These high level intrusions are associated with wide-spread epithermal alteration of highly permeable autobreccias and ash-flow tuffs from Mount Emma to Poore Lake. Only minor deuteric alteration, affects the intrusives, however. Highly iron-oxide-stained, sericitized and silicified zones next to these stocks along ridge crests have numerous coxcomb quartz veins, locally excavated by prospectors (Plate 1). Adjacent, deeply entrenched valleys have chiefly propylitic alteration with fresh disseminated pyrite. It is possible that at least some of the heavy alteration on the ridge crests may be the product of supergene processes.

Several grab sample traverses of the most intensely altered gossans were made near Mount Emma (Figure 37). Sixteen of these samples were assayed for gold and silver by the Freeport Exploration Company (Table 5). Only one sample had measurable Au and Ag (Sample F-7-128 with 0.5 ppm Au and 18 ppm Ag). The alteration was apparently not associated with economic mineralization, but the quartz veins of sample F-7-128 certainly carry Au and Ag above

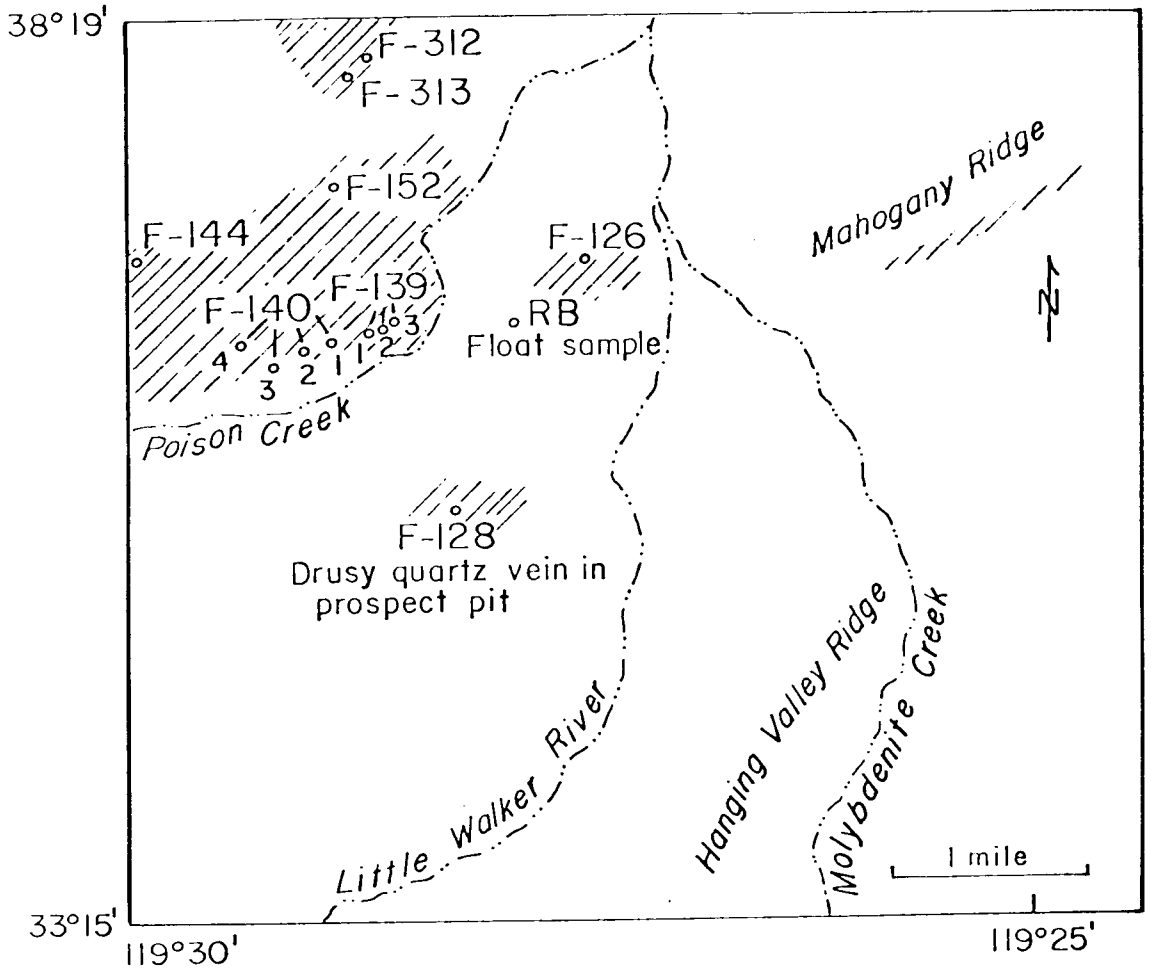

Figure 37. Location map of Au-Ag assay samples.

Table 5. Assays by atomic absorption by Hunter Mining Laboratory, Inc., Sparks, Nevada.

Sample No.	Au (ppm)	Ag (ppm)
F-7-126	-0.1*	-1
F-7-128	0.5	18
F-139-1	-0.1	-1
F-139-2	-0.1	-1
F-139-3	-0.1	-1
F-140-1	-0.1	-1
F-140-2	-0.1	-1
F-140-3	-0.1	-1
F-140-4	-0.1	-1
F-140-5	-0.1	-1
F-144	-0.1	-1
F-147	-0.1	-1
F-152	-0.1	-1
F-312	-0.1	-1
F-313	-0.1	-1
RB	-0.1	-1

*Minus sign indicates less than the amount listed.

background concentrations. Further exploration of the highly altered areas is probably warranted to better evaluate the extent of mineralization.

There may be a genetic relation between hydrothermal ore formation and hydrous calc-alkaline magmas with low CO_2/H_2O. Because the monzodiorite plugs at and near Mount Emma are cogenetic with the Lavas of Mahogany Ridge, petrogenetic arguments applied to the low-K latites of Mahogany Ridge apply equally well to the potentially mineralized plugs. The low-K latites were probably more hydrous and more closely related to the normal calc-alkaline andesite series (e.g., the Relief Peak Formation and Lavas of Rickey Peak) of the area than the early, highly potassic Table Mountain Latites and Eureka Valley Tuff. It was also concluded that the low-K latites may have come from a different source than the early latites. Hydrous magmas have a tendency to crystallize rapidly as they rise to levels where P_{H_2O} in the magma becomes equal to P_{total} because of loss of heat and rise of the melting temperature as water "boils" from the magma. This may explain the tendency for the low-K latitic series to have more phenocrysts than any other formation in the area and their occurrence as subvolcanic intrusions. The effusive eruptions of the low-K latites were attributed to their low total volatile content and low CO_2/H_2O. It was concluded that the early latite series had high CO_2/H_2O and tended to erupt completely to the surface as

widespread, phenocryst-poor flows (e.g., the Table Mountain Latite) or as pyroclastic deposits (e.g., the Eureka Valley Tuff). The change from alkali-rich magmas with high CO_2/H_2O in the early latite series to low-K latites with low CO_2/H_2O seems to be a fundamental control on the tendency for hydrothermal ore deposition to occur. The late, hydrous calc-alkaline rocks tend to form plutonic bodies and exsolve a hydrothermal fluid upon crystallization. The exsolved fluid would efficiently transport incompatible ore metals and geothermal heat to permeable, water-saturated intracaldera tuffs. Such a hydrothermal system would be ideal for disseminated ore deposition as large volumes of intracaldera groundwater became involved in thermal convection.

The critical conclusions to be drawn from the above model are that the caldera-forming magmas were not associated with mineralization, while the later, petrogentically distinct, low-K latites were directly associated with weak mineralization. The formation of a caldera seems to be important for providing permeable, water-saturated host rocks for the ore and favorable fracture systems but is not critical to formation of the ore deposit. There seems to be no direct link between ash-flow volcanism and hydrothermal mineralization. Only after all ash-flow activity has ceased, are hydrous, calc-alkaline magmas with only weak or nonexistent genetic relation to the ash-flow-forming magmas able to take advantage of the favorable

ore-forming environment of the caldera.

An extreme example of the above model is provided by the Goldfield District, where early ring fracturing and ash-flow activity was followed 8 m.y. later by localization of ore-forming rhyodacite plug domes around the ring fracture system (Ashley, 1974). It is improbable that the dacites had any direct genetic relation to the early ash-flow activity. The dacites at Goldfield seem instead to be part of a wider pulse of calc-alkaline magmatism which affected much of the western Great Basin and northern Sierras in the interval 22 m.y. to about 5 m.y. (Byers and others, 1968; Noble, 1972; Ashley, 1974; Silberman and McKee, 1974). This episode of calc-alkalic activity is associated with voluminous eruption of hydrous, biotite-hornblende-bearing high-K andesites and dacites as well as numerous epithermal gold-silver deposits. The only districts in this western Great Basin province which are associated with calderas are the Goldfield and Silver Peak areas (Robinson, 1972; Ashley, 1972). The Bodie-Aurora, Tonopah, and Comstock Lode districts do not have calderas, but were among the most important gold-silver producers in the United States when at full production; all of these mines are in biotite or hornblende-bearing calc-alkalic lavas of this 22 to 5 m.y. episode (Chesterman, 1968; Bonham and Garside, 1974; Bonham and Papke, 1969). It appears that ash flows and calderas are only very incidently related to epithermal mineralization, while hydrous, calc-alkaline magmas are

essential to the evolution of an ore-bearing fluid.

Copper

Plutonic equivalents of low-K latite magmas of the Lavas of Mahogany Ridge may have formed "porphyry copper" mineralization at depth. Recent data of Mason and McDonald (1978) and Mason (1978) have shown that many calc-alkaline batholiths have early potassic suites which are followed by later plutonic suites with lower potassium, higher water content and important copper mineralization. The magmas of the Little Walker volcanic center are also characterized by an early potassic series and a later low-K series. The low-K series is the only phase of activity associated with hydrothermal mineralization and appears to be the most hydrous eruptive unit. It is suggested that plutonic equivalents of the low-K series may have produced significant copper mineralization under mesothermal conditions. The depth of this mineralization would probably be too great to allow economic extraction even if ore-grade material were present.

Uranium

The high U (12 to 14 ppm or 0.37-0.45 oz./ton) in widespread quartz latites of the Eureka Valley Tuff make these deposits potential low grade ores of U, provided some economically feasible surface extraction method such as in-place leaching becomes available in the

future. High grade secondary concentrations of uranium may also be formed by oxidation and leaching of U in the form of soluble uranyl ion. Reprecipitation of this soluble uranium in reducing environments high in organic debris can form very rich ores.

The probability of formation of high grade secondary concentrations of U is a function of the leachability of the U from primary igneous rocks and availability of buried organic debris in aquifers. Constancy of the U/Th ratio in most Stanislaus rocks at about 3.1 (Figure 38) regardless of the degree of hydration is probably good evidence that uranium is not readily leached from these volcanic rocks, because U is far more soluble than Th. Measurements of stream uranium from a stream having only Eureka Valley Tuff as its provenance at Burcham Flat (Plate 1) indicate that the stream is not notably enriched in U compared to adjacent streams (unpublished data, Lawrence Livermore Laboratory). This further confirms that the uraniferous Stanislaus rocks are probably not good sources of soluble uranium and may apply to all volcanic rocks where uranium is locked in a compact glassy or devitrified matrix. Phaneritic rocks may, in fact, be better U source rocks, because U is probably present in easily leached sites along grain boundaries of silicate crystals.

Even if rocks in the area were good sources of soluble U, it is doubtful that aquifers filled with organic debris are available. No

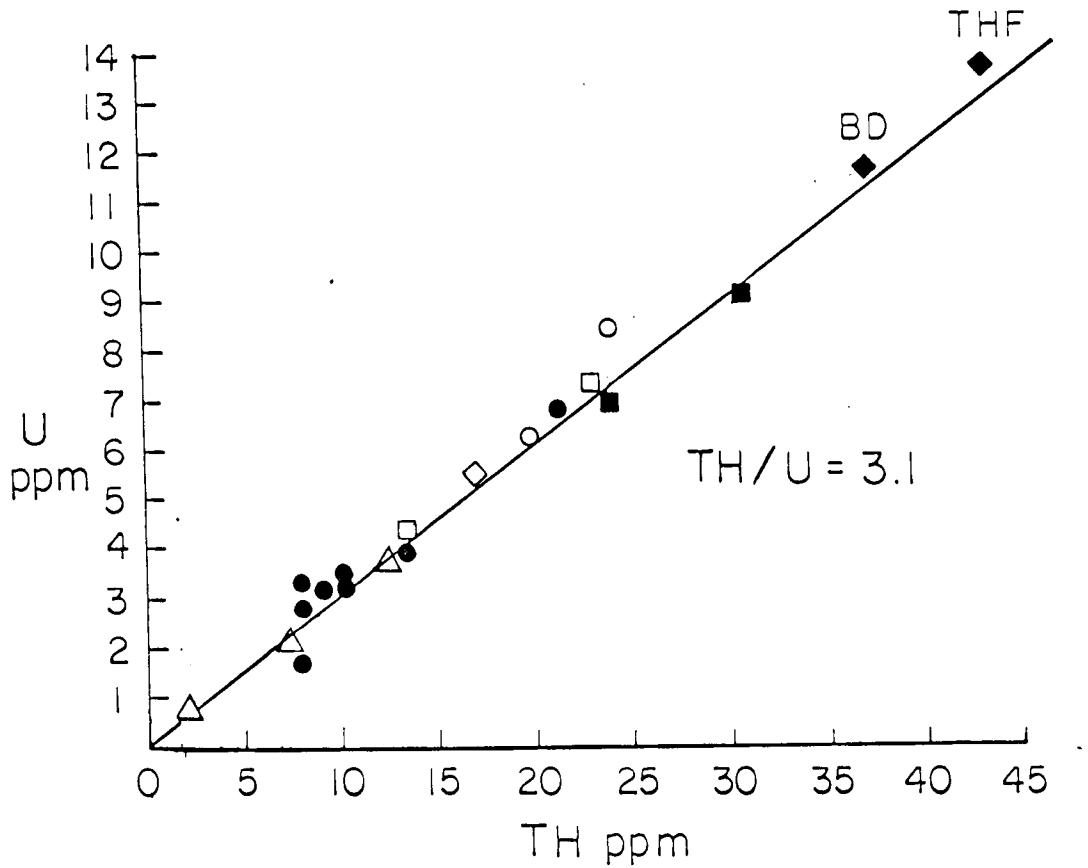

Figure 38. Constancy of Th/U in all volcanic rocks at the Little Walker center. Symbols as in Figure 13.

such accumulations are known to the writer in the vicinity of the Little Walker center.

A small hydrothermal uranium prospect of unknown potential has been rumored to exist (M. Enos, personal communication, 1977) at the north end of the contiguous range of mountains north of Mount Emma (Plate 1). A rough four-wheel-drive road cut into the slopes southeast of the Marine Cold Weather Station near Pickle Meadow is the only evidence thus far found of this prospect. Additional sampling and geiger counter exploration may be warranted in this area (Plate 1).

SELECTED REFERENCES

Allegre, C.J., Treuil, M., Minster, J.F., Minster, B., and Albarede, 1977, Systematic use of trace element in igneous processes, I. Fractional crystallization processes in volcanic suites: Contrib. Mineral. Petrol., v. 61, p. 57-75.

Al-Rawi, Y.T., 1969, Cenozoic history of the northern part of Mono Basin, California and Nevada: Ph.D. dissertation, Univ. California, Berkeley, 163 p.

Arth, J.G., 1976, Behavior of trace elements during magmatic processes - a summary of theoretical models and their applications: Jour. Research, U.S. Geol. Survey, v. 4, no. 1, p. 41-47.

_____, and Barker, F., 1976, Rare-earth partitioning between hornblende and dacitic liquid and implications for the genesis of trodhjemitic-tonalitic magmas: Geology, v. 4, no. 9, p. 534-536.

Ashley, R.P., 1974, Road log and trip guide, Goldfield District: Nevada Bur. Mines and Geol. Rept. 19, p. 14-21.

Atwater, T., 1970, Implications of plate tectonics for the Cenozoic tectonics of western North America: Geol. Society America Bull., v. 81, p. 3513-3536.

Berggren, W.A., 1972, A Cenozoic time-scale--some implications for regional geology and paleobiogeography: Lethaia, v. 5, no. 2, p. 195-215.

Bonham, H.F., and Garside, L.J., 1974, Tonopah Ming District and vicinity: Nev. Bur. Mines Report 19, p. 42-48.

_____, and Papke, K.G., 1970, Geology and mineral deposits of Washoe and Storey Counties, Nevada: Nev. Bur. Mines Bull. 70, 140 p.

Bowman, H.R., Asaro, F., and Perlman, I., 1973, On the uniformity of composition in obsidians and evidence for magmatic mixing: Jour. Geol., v. 81, p. 312-327.

Brem, G.F., 1975, Petrogenesis of latites, Little Walker center, Mono County, California: Geol. Soc. America Abs. with Programs, v. 7, no. 7, p. 1008.

Bryan, W.B., 1972, Morphology of quench crystals in submarine basalts: Jour. of Geophys. Res., v. 77, no. 29, p. 5812-5819.

_____, Finger, L.W., and Chayes, F., 1969, Estimating proportions in petrographic mixing equations by least-squares approximation: Science, v. 163, p. 926-927.

Byers, F.M., Jr., Orkild, P.P., Carr, W.J., and Quinlivan, W.D., 1968, Timber Mountain Tuff, southern Nevada, and its relation to cauldron subsidence: Geol. Soc. America Mem. 110, p. 87-97.

Cann, J.R., 1971, Major element variations in ocean-floor basalts: Phil. Trans. Roy. Soc. London, Ser. A. 268, p. 495-505.

Carmichael, I.S.E., 1967, The mineralogy and petrology of the volcanic rocks from the Leucite Hills, Wyoming: Contr. Mineral. and Petrol., v. 15, p. 24-66.

Chappell, B.W., Compston, W., Arriens, P.A., and Vernon, M.J., 1969, Rubidium and strontium determinations by X-ray fluorescence spectrometry and isotope dilution below the part per million level: Geochim. et Cosmochim. Acta, v. 33, p. 1002-1006.

Chesterman, C.W., 1968, Volcanic geology of the Bodie Hills, Mono. County, California: Geol. Soc. America Mem. 116, p. 45-68.

Christiansen, R.L., and Lipman, D.W., 1972, Cenozoic volcanism and plate-tectonic evolution of the western United States. II Late Cenozoic: Phil. Trans. R. Soc. London A., v. 271, p. 249-284.

Clark, M.M., 1967, Pleistocene glaciation of the drainage of the West Walker River, Sierra Nevada, California, Ph.D. Thesis: Stanford Univ., 170 p.

Cornwall, H.R., 1972, Geology and mineral deposits of southern Nye County, Nevada: Nevada Bur. Mines and Geol. Bull. 77, 49 p.

Dalrymple, G.B., 1963, Potassium-argon dates of some Cenozoic volcanic rocks of the Sierra Nevada, California: Geol. Soc. America Bull., v. 74, no. 4, p. 379-390.

_____, 1964, Cenozoic chronology of the Sierra Nevada, California: California Univ. Pub. Geol. Sci., v. 47, 41 p.

Deer, W.A., Howie, R.A., and Zussman, J., 1963, Rock-forming minerals, volume 2, chain silicates: John Wiley and Sons, Inc. 379 p.

_____, Howie, R.A., and Zussman, J., 1971, An introduction to the rock-forming minerals: John Wiley and Sons, Inc. 528 p.

Doell, R.R., Dalrymple, G.B., Smith, R.L., and Bailey, R.A., 1968, Paleomagnetism, potassium-argon ages, and geology of rhyolites and associated rocks of the Valles Caldera, New Mexico: in Coats, R.R., Hag, R.C., and Anderson, C.A., eds., Studies in volcanology: Geol. Soc. America Mem. 116, p. 275-329.

Drake, M.J., 1975, The oxidation state of europium as an indicator of oxygen fugacity: Geochim. et Cosmochim. Acta, v. 39, p. 55-64.

_____, 1976, Evolution of major mineral compositions and trace element abundances during fractional crystallization of a model lunar composition: Geochim. et Cosmochim. Acta, v. 40, p. 401-411.

_____, and Holloway, J.R., 1977, Partitioning of Sm between plagioclase, clinopyroxene, amphibole, and hydrous silicate liquid at high pressures (abstract), in Papers presented to the International Conference on Experimental Trace Element Geochemistry, p. 21-23.

_____, 1978, "Henry's Law" behavior of Sm in a natural plagioclase/melt system: importance of experimental procedure: Geochim. et Cosmochim. Acta, v. 42, p. 679-683.

Drake, M.J., and Weill, D.F., 1975, The partition of Sr, Ba, Ca, Y, Eu^{+2}, Eu^{+3} and other REE between plagioclase feldspar and magmatic silicate liquid: an experimental study: Geochim. et Cosmochim. Acta, v. 39, p. 689-712.

Elston, W.E., 1976, Tectonic significance of mid-Tertiary volcanism in the Basin and Range province: A critical review with special reference to New Mexico, in Elston, W.E., and Northrop, S.A., eds., Cenozoic volcanism in southwestern New Mexico: New Mexico Geol. Soc. Special Publication no. 5, 151 p.

Engel, A.E.J., Engel, C.G., and Havens, R.G., 1965, Chemical characteristics of oceanic basalts and the upper mantle: Geol. Society America Bull., v. 76, p. 719-734.

Gilbert, C.M., Christiansen, M.N., Al-Rawi, Y.T., and Lajoie, K.R., 1968, Structural and volcanic history of Mono Basin, California-Nevada, in Coats, R.R., Hag, R.C., and Anderson, C.A., eds., Studies in volcanology: Geol. Soc. America Mem. 116, p. 275-329.

Gill, J.B., 1974, Role of underthrust oceanic crust in the genesis of a Fijian calc-alkaline suite: Contr. Mineral. Petrol., v. 43, p. 29-45.

Goldschmidt, V.M., 1958, Geochemistry: Clarendon Press, Oxford, 730 p.

Green, T.H., and Ringwood, A.E., 1967, The genesis of basaltic magmas: Contr. Mineral. and Petrol., v. 15, p. 103-190.

_____, 1968, Genesis of the calc-alkaline rock suite: Contrib. Mineral. Petrology, v. 18, p. 105-162.

Guest, D.E., 1977, Preliminary petrogenetic study of absarokites, shoshonites, and associated flows, Absaroka Mountains, Wyoming, M.S. thesis: University of Oregon, Eugene, 94 p.

Halsey, J.G., 1953, Geology of parts of the Bridgeport, California, and Wellington quadrangles, Ph.D. dissert.: Univ. Calif., Berkeley, Calif., 506 p.

Hamilton, W., 1964, Geology and petrogenesis of the Island Park Caldera of rhyolite and basalt, eastern Idaho: U.S. Geol. Survey Prof. Paper 504-C, 37 p.

Hanson, G.N., and Langmuir, C.H., 1978, Modelling of major elements in mantle-melt systems using trace element approaches: Geochim et Cosmochim. Acta, v. 42, p. 725-741.

Harris, P.G., 1957, Zone refining and the origin of potassic basalts: Geochim. et Cosmochim. Acta, v. 12, p. 195-208.

Harrison, W., 1977, An experimental study of the partitioning of samarium between garnet and liquid at high pressures (abstract), in Papers presented to the International Conference on Experimental Trace Element Geochemistry, p. 41-42.

Haskin, L.A., and Korotev, R.L., 1977, Test of a model for trace element partition during closed-system solidification of a silicate liquid: Geochim. et Cosmochim. Acta, v. 41, p. 921-939.

Hebert, A.J., and Street, K., Jr., 1974, Nondispersive soft X-ray fluorescence spectrometer for quantitative analysis of the major elements in rocks and minerals: Anal. Chem., v. 46, no. 2, p. 203-207.

Hedge, C.E., and Noble, D.C., 1971, Upper Cenozoic basalts with high Sr-87/Sr-86 and Sr/Rb ratios, southern Great Basin, western United States: Geol. Society America Bull., v. 82, p. 3503-3510.

Higuchi, H., and Nagasawa, H., 1969, Partition of trace elements between rock forming minerals and host volcanic rocks: Earth and Planetary Sci. Letters, v. 7, p. 281-287.

Holland, H.D., 1972, Granites, solutions, and base metal deposits: Econ. Geol., v. 67, p. 281-301.

Irving, A.J., 1978, A review of experimental studies of crystal/liquid trace element partitioning: Geochim. et Cosmochim. Acta, v. 42, p. 743-770.

Jakes, P., and White, A.J.R., 1970, K/Rb ratios of rocks from island arcs: Geochim. et Cosmochim. Acta, v. 34, p. 849-856.

Johnson, R.F., 1951, Geology of the Masonic Mining District, Mono County, California: Unpub. M.A. thesis, Univ. California, Berkeley.

Joplin, G.A., 1965, The problem of potash-rich basaltic rocks: Mineral. Mag., v. 34, p. 266-275.

_____, 1968, The shoshonite association: a review: J. Geol. Soc. Austral., v. 15, pt. 2, p. 275-294.

_____, Kiss, E., Ware, N.G., and Widdowson, J.R., 1972, Some chemical data on members of the shoshonite association: Mineral. Mag., v. 38, p. 936-945.

Kushiro, I., 1972, Effect of water on the composition of magmas formed at high pressures: J. Petrol., v. 13, no. 2, p. 311-334.

Leeman, W.P., and Lindstrom, D.J., 1978, Partitioning of Ni^{+2} between basaltic and synthetic melts and olivines - an experimental approach: Geochim. et Cosmochim. Acta, v. 42, p. 801-816.

_____, and Scheidegger, K.F., 1977, Olivine/liquid coefficients and a test for crystal-liquid equilibrium: Earth Planetary Sci. Letters, v. 35, p. 247-257.

Lipman, P.W., Christiansen, R.L., and O'Conner, J.T., 1966, A compositionally zoned ash-flow sheet in southern Nevada: U.S. Geol. Survey Prof. Paper 524-F, p. F1-F47.

_____, Fisher, F.S., Mehnert, H.H., Naeser, C.W., Luedke, R.G., and Steven, T.A., 1976, Multiple ages of mid-Tertiary mineralization and alteration in the western San Juan Mountains, Colorado: Econ. Geol., v. 71, p. 571-588.

Lofgren, G., 1971, Spherulitic textures in glassy and crystalline rocks: J. Geophys. Res., v. 76, no. 23, p. 5635-5648.

Macdonald, G.A., 1972, Volcanoes: Prentice-Hall, Inc., 510 p.

Mason, D.R., 1978, Compositional variations in ferromagnesian minerals from porphyry copper-generating and barren intrusions of the Western Highlands, Papua New Guinea: Econ. Geol., v. 73, p. 878-890.

_____, and McDonald, J.A., 1978, Intrusive rocks and porphyry copper occurrences of the Papua New Guinea-Soloman Islands Region: A reconnaissance study: Econ. Geol., v. 73, p. 857-877.

McBirney, A.R., 1969, Compositional variations in Cenozoic calc-alkaline suites of Central America, in McBirney, A.R., ed., Proceedings of the Andesite Conference; 193 p.: Ore. Dept. Geology and Mineral Indus. Bull. 65, p. 185-189.

McDougall, I., 1976, Geochemistry and origin of basalt of the Columbia River Group, Oregon and Washington: Geol. Society America Bull., v. 87, p. 777-792.

Miyashiro, A., 1974, Volcanic rock series in island arcs and active continental margins: Am. Jour. Sci., v. 274, p. 321-355.

Murali, A.V., Leeman, W.P., Ma, M.-S., and Schmitt, R.A., 1979, Evaluation of fractionation and hybridization models for Kilauea eruptions and probable mantle source of Kilauea and Mauna Loa tholeiitic basalts, Hawaii - a trace element study: Jour. Petrol., submitted for publication.

Mysen, B.O., 1977, Solubility of volatiles in silicate melts under the pressure and temperature conditions of partial melting in the upper mantle: Ore. Dept. Geol. and Mineral Indus. Bull. 96, p. 1-14.

_____, 1978, Limits of solution of trace elements in minerals according to Henry's Law: Review of experimental data: Geochim. et Cosmochim. Acta, v. 42, p. 871-885.

_____, and Boettcher, A.L., 1975, Melting of a hydrous mantle: II. Geochemistry of crystals and liquids formed by anatexis of mantle peridotite at high pressures and high temperatures as a function of controlled activities of water, hydrogen, and carbon dioxide: Jour. Petrol., v. 16, pt. 3, p. 549-593.

Nagasawa, H., 1970, Rare earth concentration in zircon and apatite and their host dacites and granites: Earth and Planetary Sci. Letters, v. 5, p. 47-51.

_____, and Schnetzler, C.C., 1971, Partitioning of rare earth, alkali, and alkaline earth elements between phenocrysts and acidic igneous magma: Geochim. et Cosmochim. Acta, v. 35, p. 953 968.

Nagasawa, H., Schrieber, H.D., and Blanchard, D.P., 1976, Partition coefficients of REE and Sc in perovskite, melilite, and spinel and their implications for Allende inclusions. (abstract), in Lunar Science VII: The Lunar Science Institute, Houston, p. 588-590.

Nathan, S., and Fruchter, J.S., 1974, Geochemical and paleomagnetic stratigraphy of the Picture Gorge and Yakima basalts (Columbia River Group) in central Oregon: Geol. Soc. America Bull., v. 85, p. 63-76.

Nicholls, J., and Carmichael, I.S.E., 1969, A commentary on the absarokite-shoshonite-banakite series of Wyoming, U.S.A.: Schweiz Mineralogische und Petrographische Mitteilunger, v. 49/1, p. 47-64.

Nicholls, I.A., and Ringwood, A.E., 1972, Production of silica-saturated tholeiitic magmas in island arcs: Earth and Planetary Sci. Letters, v. 17, p. 243-246.

Noble, D.C., 1968, Kane Springs Wash volcanic center, Lincoln County, Nevada: Geol. Soc. America Mem. 110, p. 109-116.

_____, 1972, Some observations on the Cenozoic volcano-tectonic evolution of the western United States: Earth and Planetary Sci. Letters, v. 17, p. 142-150.

_____, Bowman, H.R., Hebert, A.J., Silberman, J.L., Heropoulos, C.E., Fabbi, B.P., and Hedge, C.E., 1975, Chemical and isotopic constraints on the origin of low-silica latite and andesite from the Andes of central Peru: Geology, v. 3, no. 9, p. 501-504.

_____, and Christiansen, R.L., 1974, Black Mountain volcanic center: Nev. Bur. Mines Report 19, p. 27-34.

_____, Dickinson, W.R., and Clark, M.M., 1969, Collapse caldera in the Little Walker area, Mono County, California: Geol. Soc. America Spec. Paper 121, p. 536-537.

_____, and Hedge, C.E., 1969, Sr^{87}/Sr^{86} variations within individual ash-flow sheets: U.S. Geol. Survey Prof. Paper 650-C, p. 133-139.

_____, and McKee, E.H., 1972, Description and K-Ar ages of volcanic units of the Caliente volcanic field, Lincoln County, Nevada, and Washington County, Utah: Isochron/West, no. 5, p. 17-24.

_____, Korringa, M.K., Church, S.E., Bowman, H.R., Silberman, M.L., Heropoulos, C.E., 1976, Elemental and isotopic geochemistry of nonhydrated quartz latite glasses from the Eureka Valley Tuff, east-central California: Geol. Soc. America Bull., v. 87, p. 754-762.

Noble, D.C., McKee, E.H., and Walker, G.W., 1974, Pantellerite from the Hart Mountain area, southeastern Oregon - interpretation of radiometric, chemical, and isotope data: Jour. Research U.S. Geol. Survey, v. 2, no. 1, p. 25-29.

_____, Sargent, K.A., Mehnert, H.H., Ekren, E.B., and Byers, F.M., Jr., 1968, Silent Canyon volcanic center, Nye County, Nevada: Geol. Soc. America Mem. 110, p. 65-75.

_____, Slemmons, D.B., Korringa, M.K., Dickinson, W.R., Al-Rawi, Y., and McKee, E.H., 1974, Eureka Valley Tuff, east-central California and adjacent Nevada: Geology, v. 2, p. 139-142.

O'Hara, M.J., 1965, Primary magmas and the origin of basalts: Scottish Jour. Geol., v. 1, p. 19-40.

Onuma, N., Higuchi, H., Wakita, H., and Nagasawa, H., 1968, Trace element partition between two pyroxenes and the host lava: Earth and Planetary Sci. Letters, v. 17, p. 142-150.

Osawa, M., and Goles, G.G., 1970, Trace element abundances in Columbia River Basalts, in Gilmour, E.H., and Stradling, D., eds., Proceedings of the Second Columbia River Basalt Symposium: Cheney, Eastern Washington State College, p. 173-175.

Osborn, E.F., 1969, Experimental aspects of calc-alkaline differentiation, in McBirney, A.R., ed., Proceedings of the andesite conference: Ore. Dept. Geology and Mineral Industries Bull. 65, p. 33-42.

Peck, L.C., 1964, Systematic analysis of silicates: U.S. Geol. Surv. Bull. 1170, 89 p.

Peterson, D.W., 1970, Ash-flow deposits - their character, origin, and significance: Jour. Geol. Ed., v. 18, no. 2, p. 66-76.

Philpotts, J.A., and Schnetzler, C.C., 1970, Phenocryst-matrix partition coefficients for K, Rb, Sr, Ba, with applications to anorthosite and basalt genesis: Geochim. et Cosmochim. Acta, v. 34, p. 307-322.

Priest, G.R., in press, Latites, quartz latites, in Fairbridge, R., and Green, J., eds., Volcanoes and volcanology: Dowden, Hutchinson and Ross, Inc., Publishers, 5 p.

_____, Bowman, H.R., Hebert, A.J., Silberman, M.L., Street, K., Jr., and Noble, D.C., 1974, Eruptive history and geochemistry of the Little Walker Volcanic center, east-central California: a progress report: Geol. Soc. America Abs. with Programs, v. 6, p. 237.

_____, Noble, D.C., Bowman, H.R., Hebert, A.J., and Wollenberg, H.A., 1975, Eruptive and geochemical evolution of the Little Walker Volcanic Center: Calif. Geology, v. 28, no. 5, p. 106.

Ransome, F.L., 1898, Some lava flows of the western slope of the Sierra Nevada, California: U.S. Geol. Survey Bull., v. 89, 74 p.

Ringwood, A.E., 1975, Composition and petrology of the earth's mantle: McGraw-Hill Book Co., 618 p.

Robinson, P.T., 1972, Petrology of the potassic Silver Peak volcanic center, western Nevada: Geol. Soc. America Bull., v. 83, p. 1693-1708.

Rosholt, J.N., Prijana, and Noble, D.C., 1971, Mobility of uranium and thorium in glassy and crystallized silicic volcanic rocks: Econ. Geology, v. 66, p. 1061-1069.

Ross, C.S., and Smith, R.L., 1961, Ash-flow tuffs: their origin, geologic relations, and identification: U.S. Geol. Survey Prof. Paper 366, 81 p.

Schnetzler, C.C., and Philpotts, J.A., 1970, Partition coefficients of rare earth elements and barium between igneous matrix materials and rock forming mineral phenocrysts - II: Geochim. et Cosmochim. Acta, v. 34, p. 331-340.

Shaw, D.M., 1970, Trace element fractionation during anatexis: Geochim. et Cosmochim. Acta, v. 34, p. 237-243.

Shimizu, N., and Kushiro, I., 1975, The partitioning of rare earth elements between garnet and liquid at high pressures: preliminary experiments: Geophys. Res. Lett., v. 2, p. 413-416.

Silberman, M. L., 1974, unpublished K-Ar data, U.S. Geological Survey.

_____, Chesterman, C. W., Kleinhample, F. J., and Gray, C. H., Jr., 1972, K-Ar ages of volcanic rocks and gold-bearing quartz-adularia veins in the Bodie Mining District, Mono County, California: Econ. Geol. v. 67, p. 597-604.

_____, and McKee, E. H., 1974, Ages of tertiary volcanic rocks and hydrothermal precious-metal deposits in central and western Nevada: Nev. Bur. Mines Report 19, p. 67-72.

Slemmons, D. B., 1953, Geology of the Sonora Pass region, Ph. D. dissertation: Univ. Calif., Berkeley, 201 p.

_____, 1966, Cenozoic volcanism of the central Sierra Nevada, California, in Bailey, E. H., ed., Geology of northern California: California Div. Mines and Geology Bull. 190, p. 199-208.

Smith, R. L., and Bailey, R. A., 1968, Resurgent cauldrons: Geol. Society America Mem. 116, p. 613-662.

Snavely, P. D., Jr., MacLeod, N. S., and Wagner, H. C., 1973, Miocene tholeiitic basalts of coastal Oregon and Washington and their relations to coeval basalt of the Columbia Plateau: Geol. Soc. America Bull., v. 84, p. 387-424.

Snyder, W. S., Dickinson, W. R., and Silberman, M. L., 1976, Tectonic implications of space-time patterns of Cenozoic volcanism in the western United States: Earth and Planetary Sci. Letters, v. 32, p. 91-106.

Stern, C. R., Huang, Wuu-Liang, and Wyllie, P. J., 1975, Basalt-andesite-rhyolite-H_2O: crystallization intervals with excess H_2O and H_2O-undersaturated liquidus surfaces to 35 kilobars, with implications for magma genesis: Earth and Planetary Sci. Letters, v. 28, p. 189-196.

Stirton, R.A., and Goeriz, H.F., 1942, Fossil vertebrates from superjacent deposits near Knights Ferry, California: California Univ., Dept. Geol. Sci. Bull., v. 26, no. 5, p. 447-472.

Taylor, S.R., Kaye, M., White, A.J.R., Duncan, A.R., and Ewart, A., 1969, Genetic significance of Co, Cr, Ni, Sc, and V content of andesites: Geochim. et Cosmochim. Acta, v. 33, p. 275-286.

Templeton, D.H., and Dauben, C.H., 1954, Lattice parameters of some rare earth compounds and a set of crystal radii: Jour. Amer. Chem. Soc., v. 76, p. 5237.

Wright, J.V., and Walker, G.P.L., 1977, The ignimbrite source problem: Significance of a co-ignimbrite lag-fall deposit: Geology, v. 5, p. 727-732.

Wright, T.L., Grolier, J.J., and Swanson, D.A., 1973, Chemical variation related to the stratigraphy of the Columbia River basalt: Geol. Soc. America Bull., v. 84, p. 371-386.

Yoder, Jr., H.S., 1977, Generation of basaltic magma: Natl. Acad. Sci., Printing and Publishing Office, 265 p.

_____, and Tilley, C.E., 1962, Origin of basalt magmas: an experimental study of natural and synthetic rock systems: Jour. Petrology, v. 3, p. 342-532.

APPENDICES

APPENDIX I: MAJOR ELEMENT ANALYSES

After careful examination of over 200 thin sections from the Little Walker area, at least one sample from each major unit was chosen for major element analysis. Samples were pulverized in a tungsten-carbide shatter box after being reduced to coarse sand by a steel pulverizer. Representative splits were then analyzed by standard X-ray fluorescence techniques (Peck, 1964) supplemented by atomic absorption methods and instrumental neutron activation analysis (Na_2O only). Table I. 1 lists all analyses recalculated to 100 percent with percentages of major phenocrystic phases.

Depending upon degree of hydration and amount of carbonate, all whole rock powders lost from 0. 5 percent to 6 percent volatiles upon fushion during the X-ray fluorescence procedure. This volatile loss was detected even in samples baked for 1/2 hour at 600°C and then weighed for analysis. If water is the main volatile it is locked in thermally stable minerals. It seems likely that CO_2 locked in carbonates or glass (?) accounts for much of the volatile loss above 600°C. This weight loss in samples did not, however, always occur in specimens known to contain either hydrous minerals or carbonate. Original totals before recalculation are included for reference.

Table I. 1. Footnotes.

[1] These are average counting errors at one sigma. Percentage errors are larger for samples impoverished in the oxide of interest; a range of error is indicated where there is a large range in absolute abundance of oxide.

[2] n. d. = not determined.

[3] Abundant secondary calcite.

[4] Rock names: bas. and. = basaltic andesite; ol. bas. = olivine basalt; hi-K and. = high-K andesite; hi-K dac. = high-K dacite; lo-Si, lo-K lat. = low-silica, low-K latite; low-K lat. = low-K latite; hi-K b. a. = high-K basaltic andesite; qtz. lat. = quartz latite; monzodi = monzodiorite.

[5] Hydrated pumice of the Tollhouse Flat Member.

[6] Non-hydrated pumice of the Tollhouse Flat Member.

[7] Lava intercalated in the Eureka Valley Tuff.

[8] Fales Hot Spring Quartz Latite; RHV = perlitic lavas of Sawmill Creek; D-77 = highly crystallized lavas of Bush Mt.

[*] No thin section or hand sample available, but biotite and plagioclase phenocrysts were present.

[9] Hornblende-biotite-bearing high-silica latites at Mahogany Ridge.

[10] Biotite-bearing quartz latite near New Range.

Table I. 1. Major element analyses.

	Formation:	Basalts, Basaltic Andesites					Relief Peak Formation								
	Member:														
	Sample No:	D-106	F-120	F-167	F-172	F-272	RP-3	RP-5	177-1	D-275	F-32	F-69-2	F-160	F-212	F-248
	Wt. % Error														
SiO_2	±1%[1]	54.7	52.4	52.6	56.1	54.8	56.5	58.6	54.8	60.8	60.8	61.3	57.9	63.0	62.4
Al_2O_3	±2%	16.9	15.1	15.2	16.3	16.5	17.3	18.1	19.8	17.3	19.1	17.3	17.8	18.9	18.3
FeO	±2%	7.7	8.5	8.0	8.2	7.2	6.8	5.9	5.5	5.7	5.7	5.1	6.4	4.4	4.6
MgO	±3-7%	4.6	10.1	10.8	3.7	6.9	4.4	2.8	1.7	2.2	0.31	2.3	4.1	0.66	0.59
CaO	±2%	7.2	8.4	7.7	8.3	8.6	6.3	6.4	10.5	5.3	5.3	5.2	5.8	5.0	3.1
Na_2O	±2-5%	3.8	3.2	3.6	3.6	4.1	4.1	4.7	3.9	4.0	4.9	4.7	4.6	4.6	4.7
K_2O	±2%	2.8	1.1	1.0	2.0	1.5	2.9	2.6	2.2	3.4	2.8	2.9	2.5	2.4	5.1
MnO	±5-20%	0.14	0.16	0.14	0.27	n.d.[2]	0.12	n.d.	0.19	0.09	0.09	0.08	n.d.	0.02	n.d.
TiO_2	±3-5%	1.44	0.90	0.82	1.12	0.58	1.07	0.90	1.08	0.92	0.87	0.77	0.87	0.70	1.25
P_2O_5	±3-6%	0.77	0.23	0.23	0.28	n.d.	0.55	n.d.	0.34	0.31	0.32	0.26	n.d.	0.37	n.d.
Recalculated Total		100.0	100.0	100.0	100.0	100.0	100.0	100.0	100.0	100.0	100.0	100.0	100.0	100.0	100.0
Original Total		97.3	95.8	94.9	96.4	99.1	97.0	97.3	91.0[3]	96.9	97.3	97.7	97.6	95.8	97.8
Vol % plagioclase		0.5						3.5	15	35	35	30	6	0.5	9
Vol % clinopyroxene		0.5	0.9	2.7	10.4	5	3	3.0		3	4	1			
Vol % orthopyroxene										2		2			
Vol % olivine			19.3	16.6	9.0	6									
Vol % hornblende							10	7.0	1	2		0.5	10	1	6
Vol % biotite		0.5													
Vol % xenocrystic quartz					5.6										
Rock Name[4]		bas. and.	ol. bas.	ol. bas.	ol. b. a.	bas. and.	hi-K b. a.	hi-K and.	bas. and.	hi-K and.	hi-K and.	hi-K and.	hi-K and.	hi-K and.	latite

Table I. 1. Continued.

	Formation:	Relief Peak		Table Mountain Latite											
	Member:			Lower Member						Large-plagioclase Member				2px Member	
	Sample No:	F-337	F-338	TML-1	TML-5	177-2	177-3	177-4	177-5	177-6	TML-6	D-148	F-330	F-259	F329
	Wt. % Error														
SiO_2	±1%	60.3	60.9	58.9	56.0	56.4	56.7	56.0	56.0	56.3	61.8	61.6	62.2	57.9	58.9
Al_2O_3	±2%	17.8	18.5	17.6	18.1	18.2	18.7	17.6	17.2	19.6	18.8	18.5	19.9	18.1	17.8
FeO	±2%	4.6	4.8	6.2	6.7	6.4	6.5	6.6	6.7	6.6	4.6	4.7	3.1	5.7	6.2
MgO	±3-7%	3.8	2.4	2.9	3.2	3.4	2.4	3.9	3.9	0.63	0.79	0.42	0.65	3.3	3.0
CaO	±2%	6.3	5.3	6.0	7.2	6.4	5.2	6.3	7.8	5.2	3.4	3.2	3.3	6.3	5.9
Na_2O	±2-5%	4.0	4.4	3.7	4.1	4.5	4.6	4.2	3.6	4.9	4.6	4.9	4.6	4.3	4.3
K_2O	±2%	2.5	3.2	3.6	3.3	3.4	3.6	3.4	2.8	4.1	4.9	5.4	5.2	3.3	3.1
MnO	±5-20%	n. d.	n. d.	0.10	0.13	n. d.	0.10	0.10	0.13	0.03	n. d.	0.065	n. d.	n. d.	n. d.
TiO_2	±3-5%	0.77	0.66	1.09	1.30	1.30	1.34	1.34	1.34	1.65	1.18	1.28	1.23	0.98	0.96
P_2O_5	±3-6%	n. d.	n. d.	n. d.	n. d.	n. d.	0.72	0.67	0.70	1.00	n. d.	n. d.	n. d.	n. d.	n. d.
Recalculated Total		100.0	100.0	100.0	100.0	100.0	100.0	100.0	100.0	100.0	100.0	100.0	100.0	100.0	100.0
Original Total		97.9	98.6	98.3	97.1	96.3	95.9	96.9	95.1	96.8	97.8	98.3	98.1	97.7	99.0
Vol % plagioclase		17	42	15	15	15.4	15	11	27.5	26.6	6	5	5	20	19.7
Vol % clinopyroxene		5	1	1/2	2	1.7	2	1.5	2.3					3	10.8
Vol % orthopyroxene		2	2											6	4.7
Vol % olivine				1	5	4.6	4	3	7.7	3.1					
Vol % hornblende		6	2												
Vol % biotite															
Vol % xenocrystic quartz															
Rock Name		hi-K and.	hi-K and.	latite	lo-Si lat.	lo-Si lat.	lo-Si lat.	lo-Si lat.	lo-Si lo-Klat.	lo-Si lat.	latite	latite	latite	lo-K lat.	lo-K lat.

Table I. 1. Continued.

	Formation:	Table Mountain Latite												
	Member:	Upper Member					Tentative TML-NE Caldera Margin					Upper Member (?)		
	Sample No:	D-180	F-316	177-7	177-8	F-293	F-10	F-69-1	C-82-1	C-82-2	F-212	F-41	F-319	F-320
	Wt. % Error													
SiO_2	±1%	58.7	62.8	56.4	62.3	61.1	56.3	60.6	58.8	56.3	55.2	61.2	63.6	62.0
Al_2O_3	±2%	20.3	19.0	18.1	17.3	18.2	17.0	17.9	18.4	17.7	17.3	17.5	18.1	18.0
FeO	±2%	5.0	4.3	6.1	5.0	7.2	6.1	4.8	6.2	6.5	6.7	5.1	4.1	5.3
MgO	±3-7%	1.3	0.52	2.3	0.76	0.4	2.9	0.94	1.2	3.3	4.3	1.0	0.70	0.84
CaO	±2%	5.8	5.7	8.18	2.8	2.7	5.2	4.5	4.8	7.3	6.1	4.4	2.5	3.1
Na_2O	±2-5%	4.1	4.2	4.1	4.9	6.1	8.9	4.8	4.6	4.3	4.8	4.3	4.9	4.5
K_2O	±2%	3.2	3.0	3.0	5.1	5.2	2.4	4.8	3.3	2.6	3.3	5.2	5.0	5.1
MnO	±5-20%	0.07	n. d.	0.18	0.05	n. d.	0.08	0.05	0.07	0.07	0.13	n. d.	n. d.	n. d.
TiO_2	±3-5%	1.01	0.64	1.23	1.21	1.26	1.29	1.15	1.42	1.32	1.39	1.31	1.09	1.15
P_2O_5	±3-6%	0.43	n. d.	0.49	0.49	n. d.	0.31	0.44	0.74	0.68	0.81	n. d.	n. d.	n. d.
Recalculated Total		100.0	100.0	100.0	100.0	100.0	100.0	100.0	100.0	100.0	100.0	100.0	100.0	100.0
Original Total		98.5	97.0	96.4	96.6	99.8	98.9	96.4	94.9	96.1	96.0	98.1	98.1	97.7
Vol % plagioclase		28	3	15	3	2	15	7	0.5	27	7	1	2	0.5
Vol % clinopyroxene		0.5	1	3	1	0.5	7	0.5		5	1		0.5	0.5
Vol % orthopyroxene			0.5	5	0.5		0.5						0.5	
Vol % olivine						0.5	4	0.5		4	7			
Vol % hornblende														
Vol % biotite														
Vol % xenocrystic quartz														
Rock Name		lo-K lat.	lo-K lat.	lo-K lat.	latite	latite	lo-K lo-Si lat.	latite	lo-K lat.	lo-K lo-Si lat.	lo-K lo-Si lat.	latite	latite	latite

Table I. 1. Continued.

	Formation:	Eureka Valley Tuff (EVT)				FQL[8]		EVT	Lavas of Poore Lake					Lat. of Devils Gate	
	Member:	Tollhouse Flat[7]		Tmel	By-Day			Upper							
	Sample No:	F-70[5]	THF[6]	F-317	BD	RHV	D-77	F-351	ME-3	ME-4	F-333	F-336	F-166	D-1	D-12
	Wt. % Error														
SiO_2	±1%	64.5	66.4	58.9	64.0	69.6	69.6	65.4	61.7	61.7	64.8	63.0	62.9	63.6	57.6
Al_2O_3	±2%	18.0	16.8	20.3	16.9	16.8	17.3	17.2	18.6	19.3	17.7	18.3	17.9	17.4	19.9
FeO	±2%	3.3	2.9	4.8	4.0	1.9	1.6	3.8	5.1	3.7	3.3	4.5	4.5	4.1	5.8
MgO	±3-7%	0.98	0.83	1.4	1.3	0.50	0.20	0.9	1.5	0.68	0.92	1.3	1.4	1.2	1.9
CaO	±2%	2.7	2.0	5.6	2.5	1.4	1.2	2.6	4.1	3.8	3.0	3.4	5.1	3.0	6.1
Na_2O	±2-5%	4.9	4.8	4.4	4.3	3.3	5.5	5.2	4.1	5.1	6.0	5.24	4.3	4.4	3.8
K_2O	±2%	4.9	5.4	3.6	5.6	6.1	4.3	4.1	3.5	4.4	3.6	3.8	3.5	5.1	3.8
MnO	±5-20%	n. d.	0.09	n. d.	0.09	0.10	n. d.	n. d.	0.10	0.6	n. d.	n. d.	n. d.	0.112	0.66
TiO_2	±3-5%	0.70	0.67	0.99	0.95	0.43	0.25	0.83	0.86	0.82	0.66	0.54	0.46	1.09	1.18
P_2O_5	±3-6%	n. d.	0.19	n. d.	0.31	n. d.	n. d.	n. d.	0.38	0.31	n. d.	n. d.	n. d.	n. d.	n. d.
Recalculated Total		100.0	100.0	100.0	100.0	100.0	100.0	100.0	100.0	100.0	100.0	100.0	100.0	100.0	100.0
Original Total		97.1	98.8	97.4	98.8	95.7	98.8	98.5	97.5	97.2	98.4	98.4	95.5	95.5	95.9
Vol % plagioclase		12	12	25	3	2	8	4	*	*	12	28.8	8	4.1	25.3
Vol % clinopyroxene		0.5	0.5	2	0.5			0.5						0.6	1.5
Vol % orthopyroxene				0.5										1.5	0.9
Vol % olivine															
Vol % hornblende		0.5	0.5					0.5				0.1			
Vol % biotite		2	2			1	2	1	*	*	3	8.0	3		
Vol % xenocrystic quartz															
Rock Name		qtz. lat.	qtz. lat.	lo-K lat.	qtz. lat.	qtz. lat.	qtz. lat.	qtz. lat.	lo-K lat.	latite	lo-K lat.	latite	lo-K lat.	qtz. lat.	latite

Table I. 1. Continued.

	Formation:	Latites of Devils Gate			Lavas of Mahogany Ridge										
	Member:				Main Two-Pyroxene Low-K Latite Series										
	Sample No:	N-41	D-74	D-289	LW-37	D-44	D-71	D-91	D-112	D-112-2	D-240	F-99	F-265-2	F-297	F-300
	Wt. % Error														
SiO_2	±1%	61.3	61.0	61.2	57.0	56.4	59.5	57.9	56.3	56.1	53.1	55.2	56.3	56.1	62.0
Al_2O_3	±2%	19.3	18.1	18.1	12.6	18.3	17.5	17.7	18.6	18.3	17.8	16.8	18.5	17.7	18.5
FeO	±2%	3.8	4.9	4.9	6.5	6.7	5.9	6.5	6.8	6.9	7.7	7.5	6.4	6.9	4.3
MgO	±3-7%	1.5	1.2	0.58	4.3	3.8	3.0	3.4	3.5	4.0	6.4	3.6	4.1	4.5	1.6
CaO	±2%	5.3	4.5	4.2	7.4	7.4	5.7	6.2	7.6	7.4	8.7	7.9	7.1	7.2	4.0
Na_2O	±2-5%	3.8	4.5	4.0	3.6	3.5	3.6	3.9	3.3	4.3	3.8	4.9	4.2	4.0	4.3
K_2O	±2%	4.2	4.6	4.6	2.6	2.7	3.4	2.8	2.9	2.7	1.6	2.5	2.6	2.6	4.3
MnO	±5-20%	0.067	0.111	0.08	0.101	0.114	0.11	0.10	0.12	n.d.	0.13	0.15	n.d.	n.d.	n.d.
TiO_2	±3-5%	0.86	1.11	1.20	0.98	1.05	0.90	1.03	0.97	0.97	1.03	1.15	0.94	0.97	1.02
P_2O_5	±3-6%	n.d.	n.d.	0.48	n.d.	n.d.	0.43	0.44	n.d.	n.d.	n.d.	0.39	n.d.	n.d.	n.d.
Recalculated Total		100.0	100.0	100.0	100.0	100.0	100.0	100.0	100.0	100.0	100.0	100.0	100.0	100.0	100.0
Original Total		98.8	98.9	95.4	97.6	98.3	96.2	97.7	97.9	97.5	97.7	97.8	97.1	97.6	98.2
Vol % plagioclase		15	10	9	35.3	14	30	26	38.5	29.9	10	15	25	25	8
Vol % clinopyroxene		0.5			3.4	10	4	2	6.3	3.8	15	4	7	6	1
Vol % orthopyroxene		0.5			1.1	5.4	4	1	2.0	2.3	0.5	2	6	3	1
Vol % olivine						0.5		0.5	0.5	1.3	10				
Vol % hornblende												0.5			
Vol % biotite															
Vol % xenocrystic quartz															
Rock Name		latite	latite	latite	lo-K lat.	lo-K lo-Si lat.	lo-K lat.	lo-K lat.	lo-K lo-Si lat.	lo-K lo-Si lat.	hi-K b. a.	lo-K lo-Si lat.	lo-K lo-Si lat.	lo-K lo-Si lat.	latite

Table I. 1. Continued.

	Formation:	Lavas of Mahogany Ridge									Lavas of Rickey Peak				
	Member:	Main Two-px		Intrusives-Mt. Emma			Tmlh[9]		Tmlq[10]	Upper					
	Sample No:	F-322	F-324	F-331	F-165	F-127	LW-4	F-109	F-206	F-266	D-4	D-129	D-175	D-210	D-218
	Wt. % Error														
SiO_2	±1%	56.2	55.0	58.2	57.4	58.8	60.2	62.0	63.4	56.9	67.9	61.4	66.0	61.2	65.2
Al_2O_3	±2%	17.6	17.8	18.2	17.2	17.4	17.9	17.0	18.1	18.2	16.9	18.2	17.6	18.5	17.5
FeO	±2%	7.1	7.6	6.1	6.6	6.0	5.5	4.3	3.7	6.3	2.5	4.7	2.8	5.0	3.5
MgO	±3-7%	4.7	4.4	3.4	4.3	3.9	2.7	2.5	1.3	4.35	1.2	2.7	1.5	2.1	1.5
CaO	±2%	7.3	7.8	6.1	6.7	5.5	5.7	5.8	3.3	6.4	2.6	5.6	3.5	6.2	4.1
Na_2O	±2-5%	3.5	3.7	4.1	3.8	4.6	4.1	4.1	4.4	4.4	4.2	3.8	4.5	4.2	4.5
K_2O	±2%	2.5	2.7	3.1	2.3	2.5	2.9	3.1	4.9	2.7	4.3	2.8	3.6	2.1	3.0
MnO	±5-20%	n.d.	n.d.	n.d.	0.13	0.06	0.115	0.11	0.15	n.d.	0.04	0.03	0.055	0.1	0.056
TiO_2	±3-5%	0.97	1.01	0.87	1.01	0.97	0.84	0.85	0.95	1.01	0.46	0.82	0.48	0.68	0.563
P_2O_5	±3-6%	n.d.	n.d.	n.d.	0.46	0.39	n.d.	0.32	n.d.	n.d.	n.d.	n.d.	n.d.	n.d.	n.d.
Recalculated Total		100.0	100.0	100.0	100.0	100.0	100.0	100.0	100.0	100.0	100.0	100.0	100.0	100.0	100.0
Original Total		98.4	97.5	98.0	96.8	94.9	99.6	96.6	97.6	98.8	100.0	97.5	100.9	98.7	100.4
Vol % plagioclase		31.8	20	25	20	73	10	10	12.5	0.5	19	10	13	21	20
Vol % clinopyroxene		7.7	3	2	5	13	4	4	0.9	0.5	0.5	0.5			
Vol % orthopyroxene		0.7	5	5	2		0.5	0.5	0.7						
Vol % olivine		2.1	2							1					
Vol % hornblende							5	5			2	8	4	7	5
Vol % biotite						8	2	2	0.9		3		3		1
Vol % xenocrystic quartz						3									
Vol % K-feldspar						3									
Rock Name		lo-K lo-Si lat.	lo-K lo-Si lat.	lo-K lat.	hi-K and.	mon-zodi	lo-K lat.	lo-K lat.	qtz. lat.	lo-K lo-Si lat.	dacite	and.	dacite	and.	dacite

APPENDIX II: TRACE ELEMENT ANALYSES

Samples chosen for trace element analysis were carefully selected to be free of secondary alteration effects, if this was possible. Where a series of samples from one formation were to be analyzed, samples were chosen so that the complete range of chemical variation could be represented. All analyses are listed in Table II. 1.

Trace elements, except Sr and Rb, were determined by standard instrumental neutron activation analysis (Bowman, et at., 1973; Murali, et al., 1977). All samples were pulverized in an alumina pulverizer after careful washing in deionized water. About 200 milligrams of each was then placed in laboratory-grade polyvials and irradiated. It was found that about six hours of irradiation at one megawatt in the rotating rack of a standard TRIGA reactor produced optimum activities for long-lived nuclides. Short-lived nuclide activities were optimized by irradiation in the core at about 60 KW for one minute.

Rb and Sr were determined from pressed powder pellets by standard X-ray fluorescence techniques (Chappell, B. W., et al., 1969). Duplicates showed less than 2 percent variation for both elements.

Table II.1. Footnotes.

[1]Basaltic andesite of Plate 1.

[2]Values in parentheses are the counting errors at one sigma. These are minimum errors. Sample inhomogeneity, minor contaminants, inequality of counting geometry, minor sample losses in transfers, and other random errors probably raise the minimum error at least 1% for all samples.

[3]Sample from western Sierras.

[4]Tollhouse Flat Member.

[5]By-Day Member.

[6]Fales Hot Springs Quartz Latite.

[7]Biotite-bearing, pyroxene monzodiorite at Mount Emma.

[8]Biotite-hornblende-bearing high-silica latites of Mahogany Ridge.

[9]Biotite-bearing, two-pyroxene quartz latite.

Table II. 1. Whole rock trace element analyses.

Formation:	Tb[1]	Relief Peak			Table Mountain Latite					
Member:					Lower Member					
Sample No:	D-106	RP-3	177-1	D-275	TML-1[3]	TML-5	177-2	177-3	177-4	177-5
Cs	-	1.30(.08)	-	3.4(.2)	11.4(.8)	2.0(.2)	2.2(.4)	-	6.3(.3)	1.1(.1)
Rb	57(3.6)[2]	66(3.4)	39(3.2)	86(3.7)	199(8)	133(5)	128(4.4)	155(4.7)	140(4.5)	-
Sr	1169(8.8)	1012(7.7)	619(5.8)	958(7.5)	722(187)	1014(232)	838(7.1)	765(6.6)	845(7.1)	-
Ba	-	-	-	-	1252(61)	1299(61)	1530(66)	-	-	-
La	-	-	-	-	64(1)	66(2)	60.4(.7)	-	-	-
Ce	-	44(1)	-	60(1)	125(3)	141(4)	117(2)	-	108(2)	117(2)
Nd	-	-	-	-	60(5)	68(5)	59(10)	-	-	-
Sm	-	-	-	-	9.7(.2)	10.2(.2)	9.37(.05)	-	-	-
Eu	-	1.80(.01)	-	1.59(.01)	1.90(.05)	2.06(.06)	2.07(.02)	-	2.2(.02)	2.20(.05)
Tb	-	0.54(.03)	-	0.48(.03)	1.05(.07)	1.32(.08)	0.81(.03)	-	0.73(.03)	0.78(.04)
Dy	-	-	-	-	5.4(.3)	4.7(.2)	-	-	-	-
Yb	-	-	-	-	2.64(.07)	2.30(.06)	2.27(.16)	-	-	-
Lu	-	-	-	-	0.36(.03)	0.33(.02)	0.33(.03)	-	-	-
Th	-	4.7(.4)	-	10.2(.5)	31(1)	23.9(.8)	21.0(.2)	-	21.8(.9)	18.5(.8)
U	-	-	-	-	9.6(.9)	7.4(.7)	7.3(.5)	-	-	-
Hf	-	4.3(.2)	-	5.1(.3)	9.9(.7)	11.4(.8)	9.7(.2)	-	9.5(.4)	8.6(.3)
Ta	-	0.42(.06)	-	1.07(.07)	1.00(.03)	1.07(.03)	1.2(.1)	-	1.2(.1)	1.17(.09)
Co	-	22.3(.3)	-	32.4(.5)	17.3(.3)	23.7(.4)	23.7(.15)	-	29.8(.4)	30.8(.4)
Ni	-	-	-	-	41(14)	66(15)	-	-	-	-
Sc	-	14.69(.09)	-	13.01(.08)	16.1(.3)	15.4(.3)	14.95(.04)	-	16.3(.1)	17.5(.1)
V	200(6)	-	-	183(8)	252(44)	232(40)	-	-	-	-
Cr	-	-	-	-	87(4)	127(5)	97(2)	-	-	-
Zn	-	-	-	-	88(13)	115(16)	-	-	-	-
Mn	999(10)	-	-	664(10)	700(22)	839(26)	-	-	-	-
Sb	-	-	-	-	1.3(.1)	1.0(.1)	-	-	-	-

Table II.1. Continued

Formation:	Table Mountain Latite					Eureka Valley Tuff		Tmf[6]
Member:	Large-Plagioclase		Upper Member			Tmet[4]	Tmeb[5]	
Sample No:	177-6	D-148	D-180	177-7	177-8	THF	BD	RHV
Cs	6.2(.2)	-	-	-	-	16.5(1.1)	13.8(1)	95.(.7)
Rb	182(5.1)	259(6.3)	82(3.6)	69(3.6)	261(6.3)	225(6)	202(6)	193(6)
Sr	781(6.8)	551(5.4)	1030(7.8)	1008(7.9)	499(5.2)	384(5)	-	458(148)
Ba	-	-	-	-	-	1703(83)	2000(90)	1940(93)
La	-	-	-	-	-	69(1)	72.4(1)	56(1)
Ce	169(2)	-	-	-	-	143(4)	153(4)	102(3)
Nd	-	-	-	-	-	61(5)	63(5)	42(4)
Sm	-	-	-	-	-	9.0(.2)	10.3(.2)	6.3(.1)
Eu	2.89(.02)	-	-	-	-	1.66(.05)	1.96(.05)	1.26(.04)
Tb	1.95(.04)	-	-	-	-	0.98(.06)	1.02(.06)	0.66(.04)
Dy	-	-	-	-	-	4.8(.2)	6.1(.2)	3.2(.2)
Yb	-	-	-	-	-	2.81(.07)	3.27(.07)	2.08(.05)
Lu	-	-	-	-	-	0.37(.03)	0.40(.03)	0.30(.02)
Th	33(1)	-	-	-	-	42(1)	36(1)	23.1(.7)
U	-	-	-	-	-	14(1)	12(1)	7.6(.7)
Hf	13.2(.4)	-	-	-	-	13(1)	12.5(1)	9.9(.7)
Ta	7.8(.1)	-	-	-	-	1.41(.04)	1.43(.04)	0.82(.02)
Co	23.8(.3)	-	-	-	-	2.7(.1)	5.3(.1)	1.24(.07)
Ni	-	-	-	-	-	10(10)	9(9)	5(8)
Sc	14.0(.1)	-	-	-	-	7.5(.1)	10.5(.1)	4.26(.07)
V	-	-	102(4)	-	-	51(19)	90(25)	16(15)
Cr	-	-	-	-	-	3.5(.13)	1.5(1.0)	3.6(1.1)
Zn	-	-	-	-	-	86(12)	85(12)	71(10)
Mn	-	-	476(8)	-	-	632(20)	-	683(22)
Sb	-	-	-	-	-	2.7(.2)	-	1.3(.1)

Table II.1. Continued.

Formation:	Lavas of Poore Lake				Latites of Devils Gate				
Member:									
Sample No:	ME-3	ME-4	F-336	F-166	D-1	D-12	N-41	D-74	D-289
Cs	16.5(1.1)	-	5.3(.6)	1.5(.1)	8.4(.6)	1.6(.2)	-	-	2.74(.13)
Rb	110(4)	125(4)	-	-	148(4.4)	82(3.6)	119(4)	125(4)	119(4)
Sr	860(7)	790(7)	-	-	588(5.5)	1076(8.1)	936(7)	757(6)	741(6)
Ba	-	-	2031(61)	-	2104(101)	1686(82)	-	-	-
La	-	-	46.5(.5)	-	58(1)	47(1)	-	-	-
Ce	-	-	85(2)	76(1.4)	116(3)	91(2)	-	-	44(1)
Nd	-	-	29(8)	-	53(4.5)	49(1)	-	-	-
Sm	-	-	6.61(.04)	-	9.2(.2)	8.3(.2)	-	-	-
Eu	-	-	1.65(.02)	1.72(.01)	2.02(.06)	2.08(.06)	-	-	2.4(.02)
Tb	-	-	0.55(.02)	0.46(.02)	1.00(.06)	0.89(.06)	-	-	0.77(.04)
Dy	-	-	-	-	4.8(.3)	4.3(.2)	-	-	-
Yb	-	-	2.0(.15)	-	2.50(.06)	2.06(.05)	-	-	-
Lu	-	-	0.29(.03)	-	0.34(.02)	0.28(.02)	-	-	-
Th	-	-	16.7(.2)	13.1(.6)	19.8(.6)	13.4(.4)	-	-	16.8(.4)
U	-	-	6.7(.5)	-	6.4(.6)	4.3(.4)	-	-	-
Hf	-	-	7.2(.1)	5.7(.2)	10.2(.7)	7.0(.5)	-	-	7.3(.3)
Ta	-	-	0.84(.07)	0.69(.06)	0.89(.03)	0.63(.02)	-	-	0.92(.06)
Co	-	-	6.98(.07)	13.0(.2)	4.5(.1)	12.8(.2)	-	-	9.35(.16)
Ni	-	-	-	-	8(12)	0.7(13)	-	-	-
Sc	-	-	6.93(.02)	9.29(.06)	12.7(.2)	15.1(.25)	-	-	13.97(.09)
V	-	-	-	-	104(30)	170(35)	-	-	137(7)
Cr	-	-	-	-	3.5(1.5)	12(.17)	-	-	-
Zn	-	-	-	-	97(14)	100(15)	-	-	-
Mn	-	-	-	-	791(25)	516(17)	-	-	441(7)
Sb	-	-	-	-	0.9(.1)	0.8(.1)	-	-	-

Table II-1. Continued.

Formation:	Lavas of Mahogany Ridge							
Member:	Main Two-Pyroxene, Low-K Latite Series							
Sample No:	LW-37	D-44	D-71	D-91	D-112	D-112-2	D-240	F-322
Cs	1.8(.2)	3.7(.3)	-	-	3.4(.3)	3.0(.3)	0.9(.2)	2.5(.2)
Rb	57(3)	76(3.7)	93(4)	80(3.7)	70(4)	-	35(3)	-
Sr	1070(8)	1144(8.6)	963(8)	1087(8.3)	1219(9)	-	921(8)	-
Ba	208(59)	1295(60)	-	-	1223(57)	1185(76)	1108(52)	1293(63)
La	32.9(.7)	35(1)	-	-	36(1)	34.0(.4)	28(1)	32.2(.4)
Ce	69(2)	74(2)	-	66(1.4)	74(2)	69(1)	54.7(1.6)	63.9(.9)
Nd	37(3)	39(3)	-	-	36(3)	-	33.4(2.5)	-
Sm	6.1(.1)	6.54(.14)	-	-	6.4(.1)	6.84(.05)	5.9(.1)	6.24(.05)
Eu	1.60(.04)	1.81(.05)	-	2.33(.02)	1.82(.05)	1.83(.02)	1.67(.05)	1.75(.02)
Tb	0.71(.05)	0.68(.05)	-	0.74(.04)	0.70(.05)	0.59(.03)	0.71(.06)	0.57(.03)
Dy	3.6(.2)	3.3(.2)	-	-	3.2(.2)	-	3.4(.2)	-
Yb	1.66(.05)	1.60(.05)	-	-	1.55(.04)	1.7(.2)	1.69(.05)	1.7(.1)
Lu	0.23(.02)	0.26(.02)	-	-	0.21(.01)	0.21(.03)	0.23(.01)	0.19(.02)
Th	10.3(.4)	10.1(.4)	-	11.4(.5)	9.3(.4)	8.3(.2)	5.8(.3)	8.0(.2)
U	3.2(.3)	3.1(.3)	-	-	3.0(.3)	3.4(.5)	1.7(.2)	2.96(.5)
Hf	5.6(.4)	5.4(.4)	-	5.1(.3)	5.2(.4)	4.71(.14)	4.1(.3)	4.3(.1)
Ta	0.49(.01)	0.47(.01)	-	0.99(.08)	0.49(.01)	0.55(.06)	0.36(.01)	0.50(.05)
Co	23.7(.4)	19.9(.3)	-	33.7(.5)	21.3(.4)	22.18(.14)	31.7(.5)	22.9(.15)
Ni	63(15)	32(14)	-	-	24(14)	33(15)	65(18)	-
Sc	17.7(.3)	15.8(.3)	-	15.7(.1)	14.7(.2)	14.91(.04)	26.0(.4)	17.22(.04)
V	252(44)	255(44)	195(7)	214(8)	212(40)	162(5)	270(47)	183(6)
Cr	150(6)	44(3)	-	-	34(2)	31(1.5)	208(8)	59(2.6)
Zn	97(14)	87(13)	-	-	90(13)	-	113(17)	-
Mn	719(22)	772(24)	825(9)	705(8)	818(25)	727(5)	983(30)	1076(7)
Sb	0.4(.1)	0.4(.1)	-	-	0.3(.1)	-	0.3(.1)	-

Table II. 1. Continued.

Formation:	Lavas of Mahogany Ridge			Lavas of Rickey Peak		
Member:	Tmli[7]	Tmlh[8]	Tmlq[9]			
Sample No:	F-127	LW-4	F-206	D-4	D-175	D-210
Cs	6.4(.3)	3.2(.3)	9.7(.8)	5.9(.4)	2.2(.2)	0.8(.1)
Rb	98(4)	93(4)	-	157(5)	69(4)	43(3)
Sr	1036(8)	1349(293)	-	1500(166)	1068(217)	1472(291)
Ba	-	1295(61)	2008(99)	1500(70)	1624(75)	1063(5)
La	-	39(1.3)	59.6(.7)	39(1)	36(1)	34(1)
Ce	76(1.5)	80(2)	116(1.3)	70(2)	68(2)	72(2)
Nd	-	37(3)	44(9)	27(2)	28(2)	34(2.5)
Sm	-	6.0(.1)	9.46(.06)	3.77(.08)	3.98(.08)	5.4(.1)
Eu	2.20(.02)	1.58(.04)	2.06(.02)	1.00(.03)	1.10(.03)	1.59(.04)
Tb	0.69(.04)	0.78(.05)	0.82(.02)	0.34(.03)	0.39(.03)	0.56(.04)
Dy	-	2.85(.15)	-	1.7(.1)	1.74(.12)	2.6(.15)
Yb	-	1.51(.04)	2.9(.2)	0.92(.03)	0.97(.03)	1.28(.04)
Lu	-	0.20(.01)	0.37(.03)	0.13(.01)	0.12(.01)	0.16(.01)
Th	14.3(1.1)	18.1(.5)	21.9(.2)	16.5(.6)	11.3(.4)	8.0(.3)
U	-	3.9(.4)	8.7(.6)	5.0(.5)	3.6(.3)	2.2(.2)
Hf	6.2(.3)	6.1(.5)	9.6(.14)	5.4(.4)	5.1(.4)	4.7(.3)
Ta	0.75(.06)	0.49(.01)	1.3(.1)	0.76(.02)	0.64(.02)	0.39(.01)
Co	26.7(.4)	16.6(.3)	5.84(.07)	6.58(.14)	8.0(.16)	11.4(.2)
Ni	-	47(12)	-	15(8)	9.1(8.8)	14(11)
Sc	17.3(.1)	10.6(.2)	10.14(.03)	4.29(.07)	5.57(.09)	8.3(.14)
V	-	137(27)	63(5)	60(19)	78(21)	131(29)
Cr	-	39(2)	12.6(1.5)	15.7(1.4)	30(2)	9(2)
Zn	-	96(14)	-	58.5(8.1)	78(1)	92(13)
Mn	-	714(22)	1164(8)	287(9)	476(15)	660(20)
Sb	-	0.3(.1)	-	0.5(.1)	0.4(.1)	(.1)(.1)

APPENDIX III: MINERAL SEPARATE DATA

Analytical Procedure

Three samples representative of the full range of composition of the Lavas of Mahogany Ridge were carefully selected to be free of weathering effects. Exact mineral-groundmass proportions were determined by counting 2000 to 4000 points across rock thin sections of each sample (Table III. 1).

Major element compositions of whole rock powders were determined by X-ray fluorescence procedures similar to Peck (1964), supplemented by atomic absorption methods. Trace elements and limited major elements were determined by techniques of Bowman and others (1973) and Murali and others (1977) for both whole rocks and mineral separates, utilizing instrumental neutron activation analysis (INAA). INAA is not a precise technique for determination of certain major elements (e.g., K_2O, MgO), while others (SiO_2 and P_2O_5) could not be determined. Because only INAA could be used for the small quantity of sample available from mineral separates, the major element analyses are, in part, estimated and rather imprecise for these samples.

Mineral separations were accomplished by sieving out the 100 to 120 mesh fraction of crushed whole rocks. Fe-Ti oxides and highly magnetic groundmass were removed with a hand magnet covered

Table III. 1. Point count data.

Sample:		F-322	±*	D-112	±	F-206	±
Total No. of points:		2045		2075		4066	
Groundmass	(vol. %)	57	2	62	2	84	1
	(wt. %)	53	2	59	2	78	1
Plagioclase	(vol. %)	32	2	30	2	12	1
	(wt. %)	32	2	30	2	15.7	1.3
Augite	(vol. %)	8	1	3.8	0.8	0.9	0.2
	(wt. %)	9.6	1	3.6	1.0	1.4	0.3
Orthopyroxene	(vol. %)	0.7	0.2	2.3	0.5	0.69	0.15
	(wt. %)	0.9	0.2	3.0	0.7	1.17	0.25
Olivine	(vol. %)	2.1	0.5	1.3	0.3	--	--
	(wt. %)	2.7	0.6	1.7	0.4	--	--
Fe-Ti Oxides	(vol. %)	0.9	0.2	0.8	0.2	1.0	0.2
	(wt. %)	1.6	0.4	1.4	0.4	2.34	0.5
Apatite	(vol. %)	0.1	0.05	0.3	0.1	0.15	0.04
	(wt. %)	0.1	0.05	0.3	0.1	--	--
Biotite	(vol. %)					0.9	0.2
	(wt. %)					1.35	0.3

*Counting error at one sigma.

with clean paper. The remainder of the sample was then passed through the Franz Isodynamic Separator to obtain a relatively pure plagioclase separate (final separate achieved at 1.25 amperes, 15° forward slope, 20° side slope). This plagioclase separate was then passed through 1, 1, 2, 2-tetrabromoethane (specific gravity = 2.96 at 20°C) to separate unwanted nonmagnetic heavy minerals.

If the volume of the magnetic portion from the Franz separation was small enough, it was passed through heavy liquid (G = 2.96) to separate heavy minerals from groundmass-rich grains. Heavy minerals were then put through the Franz until a split was isolated which passed undeflected at 0.6 amperes, 20° side slope, and 15° forward slope. This portion was generally about 98 percent or more pure clinopyroxene.

If the magnetic portion from the first Franz separation was too large to put directly through heavy liquid, then it was reduced by running it through the Franz at various settings of less than 0.6 amperes and 20° side slope, taking the least magnetic fraction to put through heavy liquid. Heavy minerals from this separation were then passed through the Franz, and the clinopyroxene separate (undeflected at 0.6 amperes, 20° side slope) was saved.

If the whole rock was relatively Fe-rich (7.0 percent or more FeO) the original split obtained with the hand magnet also contained most pure groundmass grains, but if the whole rock was relatively

Fe-poor (3.7 percent or less FeO) then groundmass grains were 90 percent of the highly magnetic portion having a specific gravity less than 2.96 saved during the clinopyroxene separation.

In the Fe-rich samples groundmass picked up with the hand magnet was separated from Fe-Ti oxides by passing the paper-covered hand magnet about one inch above thinly spread grains, saving the oxides which clung to the magnet. The less magnetic fraction was then passed through heavy liquid (G = 2.96) to obtain a light-weight split of 70 to 80 percent pure groundmass.

Both low-Fe and high-Fe groundmass separates were then passed through the Franz and Fe-Ti oxide-groundmass composite grains deflected at 0.05 to 0.10 amperes, 25° side slope were discarded. The remainder of the sample was then passed through the Franz at an amperage which deflected about 90 percent of the sample at 20° side slope. The undeflected grains were then discarded, being groundmass-plagioclase composites.

After each heavy liquid separation, important fractions were washed at least 30 times with acetone, 15 times with deionized water, and baked in crucibles at 50°C above the boiling point of the heavy liquid (about 200°C) for at least 12 hours. Only after baking was it possible to pass the sample through the Franz without clinging.

Each Franz separation was performed as many times as necessary to achieve maximum purity. Purity was improved at low forward

slope (12-15°) and very slow feed rates.

Final separation of Fe-Ti oxides from the most magnetic (hand magnet) fraction was accomplished by passing a metal probe, magnetized by the hand magnet, through the sample and saving only those grains which clung tenaceously to the probe. These grains were then washed at least 30 times with acetone and 15 times with deionized water.

Contamination introduced during the separatory procedure was measured by running a split from a reagent grade silica powder through the same process. Both contaminated and uncontaminated powders were then analyzed via INAA for contaiminants. Contamination levels for various elements are listed in Table III. 2. It is obvious that the separatory procedure produced no significant contamination.

In general some glass clung to Fe-Ti oxides and Fe-Ti oxide phenocrysts persisted in the groundmass along with other microphenocrysts, chiefly plagioclase. The opacity of groundmass particles prevented hand separation of these contaminants, so contaminant minerals were mathematically mixed out of the groundmass analyses using a least squares petrologic mixing program (Bryan, Finger, and Chayes, 1969) to find a best match to the ideal major element composition estimated from mass balance calculations constrained by the point count data (Table III. 3).

Table III. 2. Contamination levels from measurements of pure SiO_2 powder.

Sample Unit	Si ppm ±	Si-D ppm ±	Difference
Cs	0.0002*	0.007(9.001)	**
Ba	9(20)	31(40)	22 ± 28
La	.01*	.03*	**
Ce	.16*	.31*	**
Nd	3.1*	7.5*	**
Sm	.01*	.02*	**
Eu	.04(.06)	.2(.15)	.16 ± .15
Tb	.14*	.016*	**
Dy	.4*	.4*	**
Yb	.08*	.18*	**
Lu	.010*	.022	.01 ± .02
Th	.03*	.056	**
U	.06(.10)	.1(.2)	.04 ± .08
Hf	.02*	.02*	**
Ta	.02*	.02*	**
Co	.61(.01)	1.24(.01)	.63(.01)
Sc	.01(.01)	.02(.02)	.01 ± .01
V	.9(.8)	1.2(1.1)	.3 ± .3
Cr	.11*	.36*	**
Mn (%)	.52(.15)	1.7(.3)	1.2(.3)
Al_2O_3	.51(.01)	.55(.01)	.04(.01)
FeO	.03(.02)	.04(.06)	.01(.06)
MgO	--	--	--
CaO	--	--	--
Na_2O	.010(.001)	.069(.003)	.060(.003)
TiO_2	--	--	--

Si-D = Powder put through mineral separation procedure.
Si = Powder not put through mineral separation procedure.

*Below this amount at three sigma.

**Difference between three-sigma estimates are not considered meaningful.

Table III. 3. Corrected groundmass compositions.

Sample		Measured F-322(σ)[1]	Corrected F-322	Measured D-112-2(σ)	Corrected D-112-2	Measured F-206(σ)	Corrected F-206
% Plag.			16		8		10
% Fe-Ti Oxide			3.1		4.6		2
% Augite			4.2				
% Olivine			1.6				
Ideal SiO_2			62		61		68
SiO_2			62		60		69
Ideal Al_2O_3			14.7		15.6		17.04
Al_2O_3	%	16.2(.2)	14.8	16.4(.2)	16.1	17.8(.2)	17.04
Ideal FeO	%		7.19		6.65		1.30
FeO	%	8.83(.07)	6.90	9.63(.07)	6.63	2.72(.03)	1.30
Ideal CaO	%		3.03		4.49		0.92
CaO	%	5.2(.4)	3.05	4.95(.4)	4.55	2.2(.3)	1.09
Ideal Na_2O	%		3.07		3.11		4.28
Na_2O		3.20(.02)	3.24	3.2(.2)	3.22	4.18(.03)	4.2
Ideal K_2O			4.70		4.3		6
K_2O		--	4.70	--	4.3	--	6
Ideal MnO	%		0.1		0.035		0.15
MnO	%	0.136(.006)	0.1	0.117(.006)	0.09	0.090(.005)	0.08
Ideal TiO_2	%		1.2		1.23		0.70
TiO_2	%	1.5(.1)	1.4	1.9(.1)	1.40	0.60(.08)	0.34

Table III.3. Continued.

Sample		Measured F-322(σ)	Corrected F-322	Measured D-112-2(σ)	Corrected D-112-2	Measured F-206(σ)	Corrected F-206
Cs	ppm	3.8(.3)	4.86(.4)	4.2(.4)	4.7(.5)	12(1)	13.9(1)
Ba	ppm	1499(45)	1916(58)	1593(85)	1782(95)	2359(60)	2680(68)
La	ppm	44.8(.5)	54.5(.6)	41.8(.5)	45.7(.5)	62.6(.7)	69(.8)
Ce	ppm	94.6(1.0)	116(1.3)	85.3(.9)	94(1)	128.3(1.3)	142.4(1.5)
Nd	ppm	57(9)	70(12)	41(10)	47(11)	57(9)	65(10)
Sm	ppm	8.33(.04)	9.93(.05)	8.68(.04)	8.59(.06)	11.04(.04)	11.0(.06)
Eu	ppm	2.08(.02)	2.27(.05)	1.92(.02)	2.01(.02)	2.13(.03)	2.17(.03)
Tb	ppm	0.80(.03)	0.94(.04)	0.67(.03)	0.74(.03)	0.88(.02)	0.99(.03)
Dy	ppm	22(2)	27(3)	18(2)	20(2)	35(2)	40(2)
Yb	ppm	2.3(.1)	2.8(.13)	1.7(.1)	1.9(.1)	3.4(.2)	3.9(.2)
Lu	ppm	0.31(.02)	0.38(.03)	0.24(.03)	0.27(.03)	0.44(.03)	0.50(.03)
Th	ppm	13.1(.2)	16.7(.3)	11.85(.16)	13.3(.18)	27.3(.3)	31(.3)
U	ppm	4.2(.3)	5.2(.4)	4.6(.4)	5.15(.45)	9.8(.5)	11.1(.6)
Hf	ppm	6.90(.13)	8.8(.2)	6.54(.13)	7.26(.15)	11.46(.15)	12.9(.17)
Ta	ppm	0.85(.07)	1.09(.09)	0.84(.07)	0.94(.08)	1.5(.1)	1.7(.1)
Co	ppm	28.56(.2)	27.5(.2)	28.9(.16)	20.9(.2)	4.03(.07)	1.77(.05)
Sc	ppm	15.79(.04)	14.02(.04)	12.12(.03)	12.33(.03)	9.34(.03)	9.68(.03)
V	ppm	288(6.5)	--	373(8)	272(8)	34(5)	--
Cr	ppm	52(7.7)	--	81(1.8)	--	--	--

[1] Counting error at one sigma.

Only the most accurately known major oxides were used to constrain the mixing models. Uncertainties in these calculations are large, owing to the necessity of estimating the compositions of possible hypersthene and olivine contaminants and probable non-uniqueness of the mixes. These uncertainties are also very difficult to quantify due to the large number of unknown variances involved, but errors equal to 25 percent of the difference between "ideal" and measured values may be well within the uncertainty of the data.

The chief groundmass contaminants were plagioclase and iron-titanium oxides. These phases contain only minor amounts of large-ion elements, so that their effect is to dilute groundmass concentrations of these elements. The high (4529 to 2564 ppm) V and Cr (1324 to 1009 ppm) content of Fe-Ti oxides caused very large correction factors to be applied to groundmass Cr and V, resulting in unstable calculations for the very low Cr and V of groundmass. Ni suffered from similar problems, but was of such low precision (high gamma ray spectral interference) that it was not reported. Owing to these problems no distribution coefficients have been reported for Cr, V, and Ni.

Fe-Ti oxides contain an order of magnitude less Co and Sc relative to Cr and V, so that groundmass corrections for these elements were much smaller. This allowed calculation of reasonable distribution coefficients for these elements.

Minor sieving by glass inclusions was noted in plagioclase separates, and some glass (groundmass) clung to all final Fe-Ti oxide separates. The amount of glass was estimated by the Th content of the separates, since Th should be essentially incompatible with all major crystal phases, but quite high in glass. Using the corrected glass analyses above, mass balance calculations were used to calculate out glass contamination completely constrained by Th. Corrections were minor for plagioclase but rather large in Fe-Ti oxides (Tables III. 4 and III. 5). Anomalously high REE in Fe-Ti-oxides can not be accounted for by silicate-contamination, and since REE must be very low in these oxides (Nagasawa and others, 1976), perhaps RE-rich apatite or perovskite is the contaminant. Clinopyroxenes were essentially free of contaminants and required no mass balance corrections. Clinopyroxene analyses are reported in Table III. 6.

In general major element contents of phases reported here agree well with microprobe data for phenocrysts in other shoshonitic (latitic) rocks (Table III. 7). Augites are slightly less aluminous and more MgO-rich than those of Guest (1977), while Fe-Ti oxides are more titaniferous than Joplin's (1972) compositions.

Olivine, hypersthene, and biotite analyses were taken from the literature for use in petrologic mixing calculations (Table III. 7). Biotites from the lavas of Poore Lake have about 8. 1 percent K_2O (unpublished data of Silberman, 1974) which is close to the K_2O of the

Table III.4. Fe-Ti oxide analyses.

Sample		Measured F-322(σ)[1]	Corrected F-322	Measured D-112(σ)	Corrected D-112	Measured F-206(σ)	Corrected F-206
% cpx			(10.83)				21.24
% groundmass			8.38		9.05		12.26
SiO_2	%	--		--		--	
Al_2O_3	%	5.4(.2)	4.54(.2)	2.44(.02)	1.08(.04)	4.46(.08)	2.7(.1)
FeO	%	67.8(.5)	73.4(.6)	71.5(.5)	78.0(.6)	67.0(.5)	76.2(.6)
MgO	%	4(2)	4(2)	3(1.8)	3(1.8)	2.7(1.6)	3.0(1.8)
CaO	%	--	--	--	--	--	--
Na_2O	%	0.28(.02)	0.01(.02)	0.20(.02)	-0.1	0.41(.05)	-0.1(.05)
K_2O	%	--	--	--	--	--	--
MnO	%	--	--	--	--	--	--
TiO_2	%	9.4(.4)	10.1(.4)	13.4(.6)	14.6	12.2(.4)	13.9(.5)
Cs	ppm	--	--	--	--	--	--
Ba	ppm	--	--	--	--	--	--
La	ppm	5.9(.2)	--	5.2(.3)	--	26.2(.7)	20.2(.7)
Ce	ppm	18.8(.4)	--	27.7(.7)	--	70(2)	60(2)
Nd	ppm	--	--	--	-	--	--
Sm	ppm	1.2(.1)	--	1.5(.1)	--	7.1(.1)	6.6(.1)

Table III. 4. Continued.

Sample		Measured F-322(σ)	Corrected F-322	Measured D-112(σ)	Corrected D-112	Measured F-206(σ)	Corrected F-206
Eu	ppm	0.36(.04)	--	0.25(.03)	--	0.9(.05)	0.7
Tb	ppm	--	--	--	--	0.7(.2)	0.6(.2)
Dy	ppm	--	--	--	--	13(6)	9(6)
Yb	ppm	--	--	--	--	--	--
Lu	ppm	--	--	--	--	0.4(.2)	0.4(.2)
Th	ppm	1.4(.5)	--	1.2(.6)	--	3.8(.5)	--
U	ppm	--	--	--	--	--	--
Hf	ppm	2.5(.3)	1.9(.3)	1.6(.3)	1.0(.3)	4.6(.4)	3.4(.4)
Ta	ppm	0.6(.1)	--	0.26(.13)	--	1.4(.2)	--
Co	ppm	179.9(.9)	196(1)	203(1)	223(1)	110(.7)	125(.8)
Ni	ppm	235(76)	256(83)	299(81)	329(89)	141(115)	161(131)
Sc	ppm	28.3(.1)	30.9(.5)	21.7(.1)	23.9(.5)	36.2(.1)	41.2(.5)
V	ppm	4529(85)	4942(93)	2564(44)	2819(48)	2230(24)	2542(27)
Cr	ppm	1324(11)	1445(12)	1009(11)	1109(12)	110(8)	125(9)

[1]Counting error at one sigma.

Table III. 5. Plagioclase analyses.

Sample		Measured F-322(σ)[1]	Corrected F-322	Measured D-112(σ)	Corrected D-112	Measured F-206(σ)	Corrected F-206
% Groundmass			5.43		4.52		4.61
SiO_2	%	--		--		--	
Al_2O_3	%	29.3(.2)	30.1(.2)	29.5(.3)	30.1	28.0(.3)	28.5(.3)
FeO	%	1.0(.01)	0.66(.01)	0.81(.01)	0.53(.01)	0.71(.06)	0.68(.06)
MgO	%	0.3(.5)	0.09(.5)	0.2(.5)	0.05(.5)	--	--
CaO	%	12.0(.8)	12.5(.8)	12.2(.9)	12.6(.9)	11.3(.9)	11.8(.9)
Na_2O	%	4.69(.02)	4.77(.02)	4.76(.03)	4.83(.03)	5.1(.04)	5.1(.04)
K_2O	%	--	--	--	--	--	--
TiO_2	%	0.3(.1)	0.2(.1)	0.1(.1)	0.04(.1)	0.25(.1)	0.25(.11)
MnO	ppm	86(1)	33(1)	89(5)	50(5)	99(1)	65(1)
Cs	ppm	0.24(.03)	--	0.21(.03)	--	0.57(.06)	--
Ba	ppm	943(46)	741(49)	997(63)	903(48)	1260(50)	1191(50)
La	ppm	10.4(.2)	7.9(.2)	12.0(.2)	10.4(.2)	18.4(.3)	16(.3)
Ce	ppm	15.9(.4)	14.7(.4)	17.1(.4)	13.5(.4)	29.2(.5)	23.7(.5)
Nd	ppm	--	--	--	--	--	--
Sm	ppm	0.98(.02)	0.47(.02)	1.00(.02)	0.64(.02)	1.63(.02)	1.18(.02)
Eu	ppm	1.34(.01)	1.29(.01)	1.50(.02)	1.54(.02)	2.19(.02)	2.19(.02)

Table III. 5. Continued.

Sample		Measured F-322(σ)	Corrected F-322	Measured D-112(σ)	Corrected D-112	Measured F-206(σ)	Corrected F-206
Tb	ppm	0.056(.006)	0.005(.006)	0.061(.007)	0.03(.01)	0.119(.008)	0.077(.008)
Dy	ppm	0.4(.8)	--	2.7(.9)	1.9(.6)	1(1)	-0.9(1)
Yb	ppm	--	--	--	--	--	--
Lu	ppm	0.03(.02)	0.01(.02)	0.02(.02)	0.008(.02)	0.024(.009)	0.011(.009)
Th	ppm	0.91(.06)	--	0.60(.06)	--	1.43(.06)	--
U	ppm	0.3(.4)	--	--	--	--	--
Hf	ppm	0.47(.04)	--	0.28(.04)	--	0.59(.04)	--
Ta	ppm	--	--	--	--	0.08(.02)	--
Co	ppm	2.2(.5)	0.97(.5)	2.4(.5)	1.3(.5)	1.23(.03)	1.2(.03)
Sc	ppm	0.805(.007)	-0.046(.007)	0.458(.005)	-0.1(.005)	0.72(.04)	0.3(.04)
V	ppm	12(6)	--	7(13)	-2.4(13)	13(8)	13(8)
Cr	ppm	--	--	--	--	--	--

[1]Counting error at one sigma.

Table III. 6. Augite analyses.

Sample		F-322	D-112	F-206
SiO_2	%	--	--	--
Al_2O_3	%	3.24(.02)*	2.99(.02)	3.69(.03)
FeO	%	8.20(.07)	8.96(.08)	7.93(.08)
MgO	%	14.1(.4)	14.3(.5)	14.3(.7)
CaO	%	22.3(1.5)	22.8(.13)	21.8(1.4)
Na_2O	%	0.41(.01)	0.4(.01)	0.54(.01)
K_2O	%	--	--	--
MnO	%	0.48(.01)	0.50(.01)	0.40(.01)
TiO_2	%	0.86	0.58(.04)	0.55(.15)
Cs	ppm	0.32(.15)	--	--
Ba	ppm	--	--	--
La	ppm	11.3(.1)	14.1(.2)	30.7(.3)
Ce	ppm	36.6(1.2)	44.4(1.2)	89.4(2.4)
Nd	ppm	--	54(10)	100(17)
Sm	ppm	9.65(.05)	11.6(.06)	24.8(.1)
Eu	ppm	2.21(.04)	2.6(.05)	4.50(.08)
Tb	ppm	1.3(.1)	1.7(.1)	2.8(.2)
Dy	ppm	23(23)	10(17)	13.4(1.3)
Yb	ppm	2.7(.15)	3.2(.15)	5.5(.2)
Lu	ppm	0.29(.03)	0.45(.04)	0.61(.06)
Th	ppm	--	--	--
U	ppm	0.7(.4)	0.24(.4)	0.6(.5)
Hf	ppm	2.3(.2)	3.0(.3)	3.7(.4)
Ta	ppm	--	--	--
Co	ppm	4.4(.3)	44.9(.3)	24.8(.2)
Ni	ppm	87(50)	99(59)	50(88)
Sc	ppm	100.9(.1)	108(.01)	159.6(.3)
V	ppm	233(3)	224(3)	158(4)
Cr	ppm	344(5.6)	79(4)	16(8)

*Values in parentheses are counting errors at one sigma.

Table III. 7. Major element analyses of silicates (literature values).

Mineral Sample No.	Plag. Y7	Plag. 1B	Cpx Y7	Cpx 7	Olv T7	Olv 2	Mgtt T7	Biot
Reference	1	2	1	2	1	2	1	3
SiO_2	49.0	53.2	47.9	49.8	38.4	37.0	0.15	37.2
Al_2O_3	32.2	29.4	4.7	3.5	0.08	--	5.31	14.6
FeO	0.68	0.83	7.8	9.3	19.9	25.8	76.2	30.2
MgO	0.06	0.04	13.4	16.0	40.6	35.8	4.0	4.2
CaO	15.9	11.5	22.8	20.0	0.26	0.22	0.01	0.17
Na_2O	2.18	4.2	0.4	0.3	0.02	--	--	0.15
K_2O	0.35	0.6	0.03	--	0.01	--	--	8.25
TiO_2	--	--	0.91	0.69	--	--	8.13	3.1
MnO	--	--	0.16	0.46	0.35	0.91	0.37	--
CrO_2	--	--	--	--	--	--	0.61	--
Va_2O_5	--	--	--	--	--	--	0.34	--

1. Guest (1977) in shoshonite.
2. Joplin and others (1972) in shoshonite.
3. Deer and others (1971) in granite.

biotite chosen from the literature (8.25 percent K_2O, Table III.7). The hypersthene was chosen to coincide with average estimates of hypersthene compositions in the Lavas of Mahogany Ridge from optical measurements. The olivine listed in Table III.7 comes from a latite (shoshonite) very similar in all respects to Stanislaus latites.

Distribution Coefficient Calculations

Distribution coefficients (D's) were calculated using the equations of Haskin and Korotev (1977). These calculations utilize the whole rock, groundmass, and phenocryst trace element contents, together with an estimate of the total weight fraction of residual liquid (groundmass) from the point count data, to correct the distribution coefficients for surface-equilibrium, closed-system crystallization effects (i.e., internal fractional crystallization from zoned crystals). Final calculated D's for all trace elements are tabulated in Tables III.8 and III.9 with estimated D's for unanalyzed minerals.

Large correction factors were required to eliminate the effects of contaminants in groundmass separates (see the previous section). Because errors in the correction factors of as much as 25 percent were possible, it is appropriate to examine the propagation of this error in the distribution coefficient calculations. Distribution coefficients for highly included elements such as cobalt in clinopyroxene were found to be the most sensitive to errors in the groundmass data.

Table III. 8. Crystal/liquid distribution coefficients for plagioclase and augite.

Phase/Liquid Sample	Plag/L F-322	Plag/L F-112-2	Plag/L F-206	Cpx/L F-322	Cpx/L D-112-2	Cpx/L F-322
Cs	--	--	--	--	--	--
Ba	0.48(.02)*	0.63(.03)	0.48(.02)	--	--	--
La	0.19(.01)	0.26(.01)	0.25(.01)	0.27(.01)	0.35(.01)	0.48(.02)
Ce	0.17(.01)	0.17(.01)	0.19(.01)	0.43(.02)	0.55(.02)	0.70(.04)
Nd	--	--	--	--	1.3(.1)	2.0(.15)
Sm	0.06(.005)	0.08(.005)	0.116(.006)	1.24(.06)	1.49(.07)	2.14(.1)
Eu	0.65(.03)	0.80(.04)	1.04(.05)	1.12(.06)	1.34(.07)	2.13(.1)
Tb	0.007(.01)	0.04(.03)	0.09(.01)	1.80(.09)	2.5(.1)	3.1(.2)
Dy	--	--	--	--	--	--
Yb	--	--	--	1.22(.06)	1.48(.07)	1.7(.1)
Lu	0.04(.03)	0.004(.01)	0.008(.01)	1.13(.1)	1.9(.2)	1.5(.2)
Th	--	--	--	--	--	--
U	--	--	--	--	--	--
Hf	--	--	--	--	--	--
Ta	--	--	--	--	--	--
Co	0.04(.01)	0.06(.01)	0.34(.02)	1.66(.08)	2.1(.1)	7(1)
Sc	--	--	0.030(.002)	6.4(.3)	7.8(.4)	16(1)
V	--	--	--	--	1.1(0.1)	2.2(.2)
Cr	--	--	--	--	2(.5)	--

*Minimum error at one sigma. Errors from corrections are probably at least 4 percent.

Table III. 9. Distribution coefficients for Fe-Ti oxide, orthopyroxene, olivine, biotite.

Phase/Liquid:	Fe-ox/L	Fe-ox/L	Fe-ox/L	Opx/L	Opx/L	Opx/L	Olv/L	Olv/L	Biot.
Sample:	F-322	D-112-2	F-206	Normalized[7] F-332	Normalized D-112-2	Normalized F-206	Normalized F-322	Normalized D-112-2	Dacite
References				1, 2, 3	1, 2, 3,	1, 2, 3,	4, 5	4, 5	4, 6
Cs	--	--	--	--	--	--	--	--	--
Ba	--	--	--	--	--	--	--	--	--
La	--	--	--	0. 02-0. 04	0. 02-0. 05	0. 03-0. 06	0. 009	0. 009	0. 03
Ce	--	--	--	0. 03	0. 04	0. 04	0. 009	0. 009	0. 037
Nd	--	--	--	0. 07	0. 09	0. 12	0. 01	0. 01	0. 044
Sm	--	--	--	0. 13	0. 16	0. 225	0. 01	0. 01	0. 058
Eu	--	--	--	0. 13	0. 15	0. 25	0. 01	0. 01	0. 145
Tb	--	--	--	0. 3-0. 4	0. 3-0. 56	0. 46-0. 7	0. 01	0. 01	--
Dy	--	--	--	0. 34	0. 41	0. 59	0. 014	0. 014	0. 097
Yb	--	--	--	0. 6-0. 8	0. 7-1. 0	0. 8-1. 4	0. 023	0. 023	0. 179
Lu	--	--	--	0. 6-0. 9	1. 0-1. 2	0. 8-1. 7	0. 026	0. 026	0. 185
Th	--	--	--	--	--	--	--	--	--
U	--	--	--	--	--	--	--	--	--
Hf	0. 33(. 02)	0. 80(. 03)	0. 32(. 02)	--	--	--	--	--	--
Ta	--	--	--	--	--	--	--	--	--
Co	7. 9(. 4)	10. 3(. 5)	36(2)	3. 1-3. 5	3. 9-4. 4	13-15	4. 2	4. 7	28. 5
Sc	2. 0(. 1)	1. 7(. 1)	4. 2(. 2)	2. 5-2. 7	3. 0-3. 3	6. 2-6. 8	0. 7	-/0	11. 3
V	--	14(. 7)	36(2)	--	--	--	--	--	--
Cr	--	36(4)	--	--	--	--	--	--	13

1. Allegre and others, 1977.
2. Onuma and others, 1968.
3. Schnetzler and Phillpotts, 1970.
4. Arth, 1976.
5. Leeman and Scheidegger, 1977.
6. Higuchi and Nagasawa, 1969.
7. Normalized to the temperature-composition of the sample listed.

Assuming a 25 percent error in the groundmass data of sample F-206, less than 5 percent error was introduced for D's of all elements except Co, which gained a 19 percent error in its D value. Cobalt distribution coefficients for the other two whole-rock samples (F-322 and D-112-2) are smaller than F-206, because those magmas crystallized at much higher temperature than F-206. The D's for F-322 and D-112-2 should therefore have much less than 5 percent error for most elements and less than 19 percent error for Co in augite.

Only Ba and the light REE were abundant enough in plagioclase to yield reasonably accurate D's. Figure III. 1 shows a plot of REE D's for plagioclase against ionic radius with some similar plots from the literature. It is apparent that heavy REE (Tb and Lu) D's are very low and show wide variance in the low-K latitic samples. This is probably because the absolute abundance of these elements is quite low in plagioclase relative to groundmass glass contaminants (note the literature D's, Figure III. 1). This causes mass balance subtraction of groundmass contamination to yield absolute heavy REE contents for plagioclase that so closely approach zero that any slight error in the calculations yields drastic changes in calculated D's. Owing to the instability of these calculations, plagioclase D's for heavy REE reported here are not considered reliable. Light REE and Ba D's for plagioclase, are considered much more reliable, because absolute abundance of these elements in plagioclase approaches that

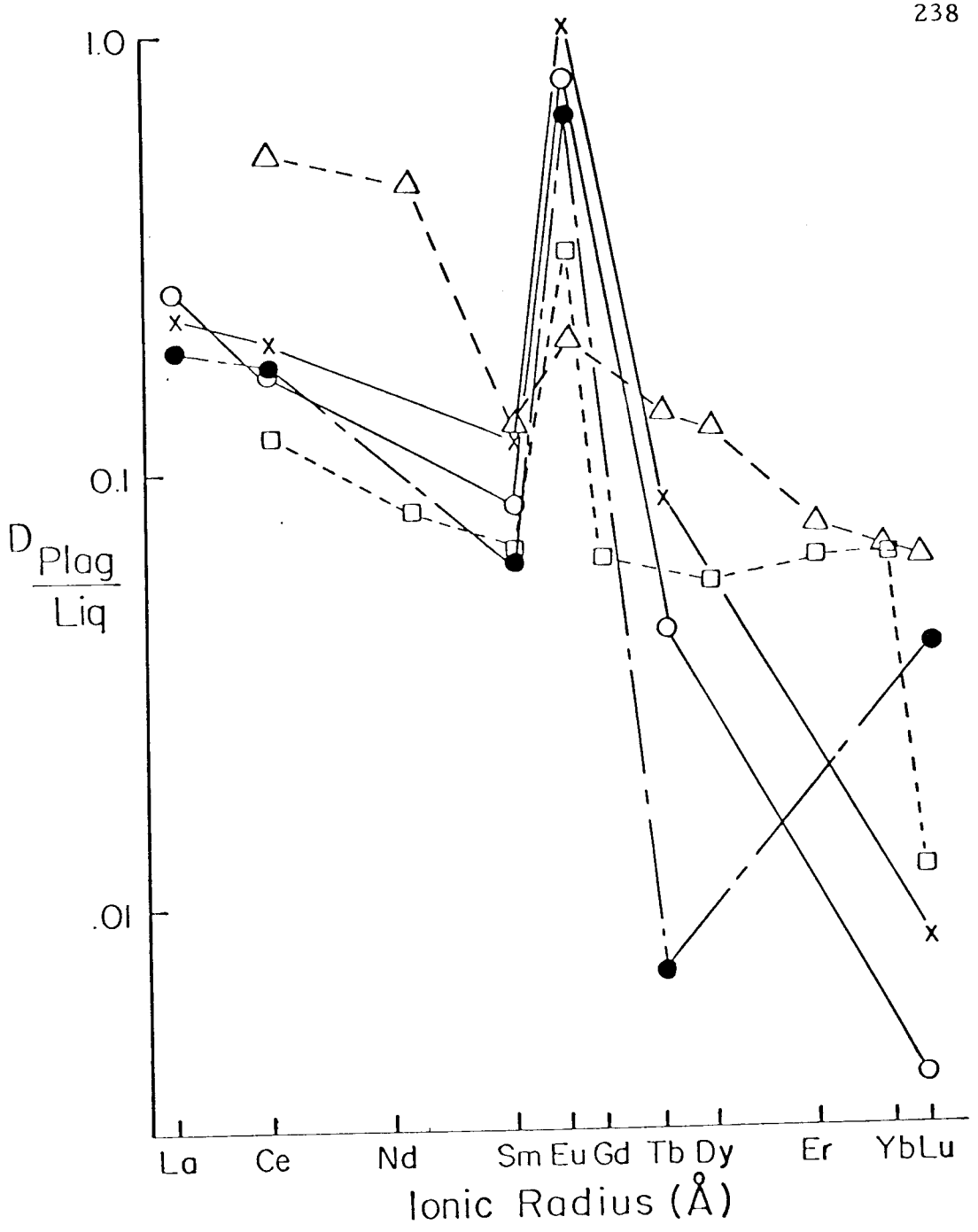

Figure III. 1. REE distribution coefficients of plagioclase.

of groundmass. This yields mathematically stable corrected D's which do not closely approach zero.

The variation of light REE D's resembles that of the literature D's (Figure III. 1), but Eu is much more highly included than adjacent REE than is the case for the literature Eu anomalies. This may be due to high Eu^{+2} in latites compared to the literature examples. An estimate of xoygen fugacity and Eu^{+2}/Eu^{+3} will be attempted in a later section, utilizing this data and the well known dependence of Eu^{+2}/Eu^{+3} on oxygen fugacity (Drake and Weill, 1975). If there is a correlation between oxygen fugacity and water content of magmas (Osborn, 1969), then the Lavas of Mahogany Ridge must be rather anhydrous compared to many calc-alkaline rocks. This is also suggested by the paucity of hydrous minerals in the entire latitic series and tendency toward differentiates with high Fe/Mg (pages 173-174).

Distribution coefficients for orthopyroxene, olivine and biotite were estimated from experimental data and natural phenocryst/groundmass partition coefficients. Coefficients for orthopyroxene were estimated from augite/orthopyroxene D's of Schnetzler and Philpotts (1970), Onuma and others (1968) and Allegre and others (1977) by normalizing to augite/liquid D's of latite (Table III. 8). This has the effect of changing the literature D's to latitic (low-T) values. A calculation of this sort assumes that there will be little change of a crystal-crystal distribution coefficient with temperature-liquid

composition changes. This is probably valid for crystalline phases like coexisting pyroxenes which have very similar crystal-chemical properties. Figure III. 2 shows REE distribution coefficients for augite and various orthpyroxene estimates plotted against ionic radius. Uncorrected augite and hypersthene D's from andesitic rocks are included for comparison. Olivine distribution coefficients for large-ion elements were taken from values for basaltic and andesitic rocks of Arth (1976), while Sc D's were estimated from augite/olivine D's of Allegre and others (1977). Co D's were estimated using the Arrhenius equation of Leeman and Scheidegger (1977) and augite-Co-estimated temperatures discussed in the next sections. Biotite D's were taken from data of Arth (1976) for dacites. These are the least likely to correspond to latitic D's of all distribution coefficients used here, because they are not constrained to latitic temperature and composition.

Only transition metal and Hf D's could be reported for Fe-Ti oxides, because of low abundance of other elements in these minerals, coupled with extreme instability of mass balance corrections for large-ion elements from groundmass contaminants. Values reported here (Table III. 8) vary smoothly with ionic radius and charge of the element involved (Figure 30). Elements with ionic radius of about 0.7 Å and low charge (+2) are most highly included. Larger, more

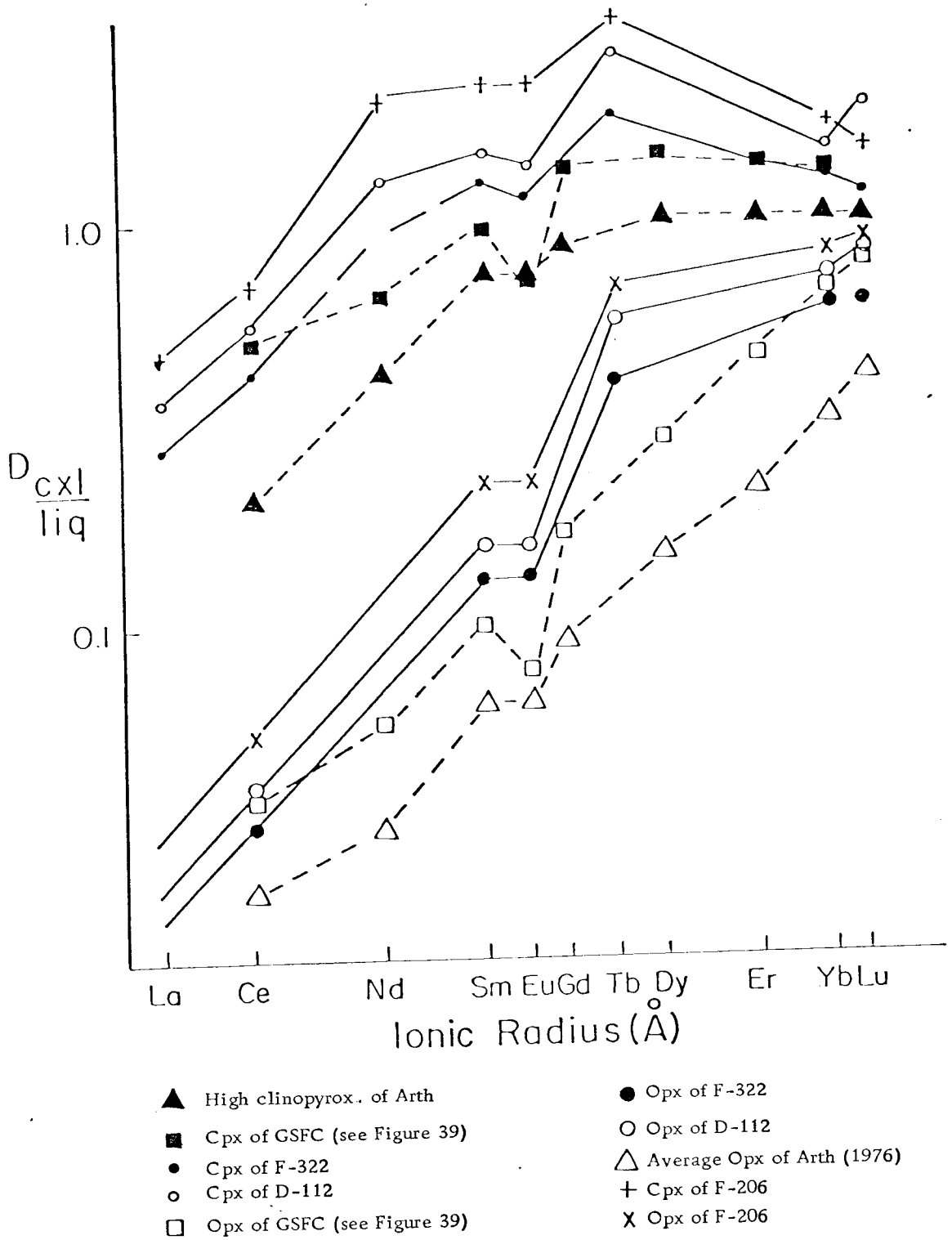

Figure III. 2. REE distribution coefficients of pyroxenes.

highly charged transition metals are less compatible with Fe-Ti oxides (Figure 30).

Trace Element Geothermometry

Crystal/liquid distribution coefficients generally rise uniformly with falling temperature (Irving, 1978). This is normally attributed to the temperature dependence of equilibrium constants for exchange reactions governing crystal-liquid distribution of trace elements (Leeman and Lindstrom, 1978). For example, a reaction such as:

$$X_{A_{liq}} + (Y_{SiO_2})_{liq} \quad A(SiO_2)_{y\ cxl}$$

$A(SiO_2)$ = some nesosilicate crystal formula, would be described by the equilibrium constant

$$K_{eq.} = \frac{A[SiO_2]_{y\ cxl}}{[A]^x_{liq}[SiO_2]^y_{liq}}$$

Such an equilibrium constant will vary with temperature according to the relation:

$$\ln K_{eq.} = \frac{-\Delta G^o}{RT} = \frac{-\Delta H^o}{RT} + \frac{S^o}{} = \frac{A}{T} + B$$

at constant pressure.

Because the distribution coefficient (D) for "A" in this reaction is just the concentration of A in the crystal divided by the concentration of A in the liquid, it follows that D is proportional to $K_{eq.}$ and thus should vary inversely with temperature for exothermic incorporation of a trace element into a lattice position from melt. Furthermore, a plot of the log of D verses the reciprocal of absolute temperature (an Arrhenius plot) should yield a straight line with a positive slope for exothermic reactions, provided ΔG^{o} and ΔS^{o} do not vary greatly within the temperature interval of interest. Irving (1978) summarized numerous experimental data for a variety of trace element D's which yield such straight line Arrhenius plots. Theoretically, a measured D could be used with such experimental data to estimate magmatic temperature. It is difficult, however, to separate compositional and temperature effects when generating experimental data, because one melt composition will seldom crystallize specific crystals over the entire temperature range of interest. Irving (1978) has noted changes in partitioning of elements related to Mg/Fe, alkali content, alkali/aluminum, phosphorous, and, most importantly, Si/O of melts.

Other complications arise when trace elements have multiple valences. Elements like Eu and Cr which have several stable ionic valences have D's strongly dependent on oxygen fugacity (Irving, 1978). Irving also summarized evidence for reduction of crystal liquid D's

with increasing volatile content (H_2O, Cl_2 and others) of melts. Drake and Holloway (1977), however, found that distribution coefficients for Sm in both clinopyroxene-melt and amphibole-melt systems rise with increasing P_{H_2O}.

One of the most troublesome observations of Irving (1978) and other workers is the apparent rise of crystal-liquid D's with increasing Si/O. This effect is very serious, since it is parallel to the temperature effect in normal calc-alkaline and many "tholeiitic" differentiation series. It is still unknown to what extent rise of D's for these differentiation series noted by Arth (1976) is a function of temperature relative to composition.

A basic requirement of all theoretical considerations of trace element partitioning is the assumption that the element of interest is truly "dilute" or "dispersed", such that it approximately follows Henry's Law in mixing behavior over the concentration interval of natural rocks. Such deviations would take the form of variation of D's as a function of trace element concentration, rather than factors such as temperature summarized above. Deviations from Henry's Law behavior have been described by Mysen (1978) for very dilute solutions, but no such variations were found by Drake and Holloway (1978) for a very great range of Sm concentration (1 ppm to 5 percent) in plagioclase-melt systems. Because the data of Drake and Holloway (1978) were conducted at low pressure under anhydrous conditions,

they probably apply more directly to the high level phenocryst/matrix distribution coefficients measured here than do Mysen's (1978) 20 Kbar (P_{H_2O}) data. In addition, none of the distribution coefficients considered here involve elements present at extreme (less than 1 ppm) dilution where possible crystal defect substitution effects may become important (Harrison, 1977). This applies even to REE such as Lu (commonly less than 1 ppm), because Harrison (1977) has demonstrated that partitioning of any REE depends on total REE concentration, which is at least 130 ppm in all samples of the Lavas of Mahogany Ridge.

Temperature Estimates-Lavas of Mahogany Ridge

Various temperature estimates for three samples of the Lavas of Mahogany Ridge are summarized in Table III. 10. Temperatures were estimated from Arrhenius equations of Drake (1976) and Drake and Weill (1975) for clinopyroxene/liquid and plagioclase/liquid systems. All sets of estimates except those for La show a series of decreasing temperatures from F-322 (the most MgO-rich low-K latite sample) to F-206, a biotite-pyroxene bearing quartz latite with very low MgO, FeO, and CaO, but high SiO_2. Only temperature estimates for Co in clinopyroxene-liquid systems are considered to be relatively free of experimental error, because plagioclase data is

Table III. 10. Temperature estimates.

Arrhenius Equation	Reference	Phase	°C T_{F-322}	°C T_{D-112}	°C T_{F-206}
$\ln D^{Co} = \frac{18310}{T} - 12.1$	1	Cpx	1179 (9)	1154 (8)	1029 (8)
$\ln D^{Lu} = \frac{3200}{T} - 5.40$	2	plagioclase	1211 (800)	--	--
$\ln D^{Ba} = \frac{11800}{T} - 8.85$	2	plagioclase	1182 (72)	1163 (71)	1136 (71)
$\ln D^{Ba/Ca} = \frac{4100}{T} - 4.43$	2	plagioclase	1161 (72)	1107 (70)	643 (70)
$\ln D^{La} = \frac{7000}{T} - 6.40$	2	plagioclase	1201 (23)	1111 (21)	1124 (22)
$\ln D^{Ce} = \frac{4600}{T} - 5.21$	2	plagioclase	1057 (27)	1074 (27)	1023 (26)
$\ln D^{Sm} = \frac{2340}{T} - 4.13$	2	plagioclase	1491 (80)	1149 (80)	911 (80)
$\ln D^{Ca} = \frac{5820}{T} - 3.32$	2	plagioclase	1128 (72)	1074 (70)	791 (70)

1. Drake (1976).
2. Drake and Weill (1975).

subject to large uncertainties, owing to the need for mass balance corrections for glass inclusions.

Nevertheless, La, Ba, Ca, and Ba/Ca plagioclase geothermometers yield temperature estimates closely similar to those of the clinopyroxene-Co temperature for the most mafic latite sample, F-322 (Table III. 10). This is partly because La, Ba, Ca and Ba/Ca are, in general, less affected by the plagioclase mass balance corrections than other listed elements. Sample F-322 also corresponds most closely to the basaltic liquids used to generate the Arrhenius equations for plagioclase and clinopyroxene, so this would minimize compositional effects relative to the literature data for basalts.

Arrhenius plots of the D's, using Co-estimated temperatures show that elements similar to Co in their crystal-chemical properties plot on straight lines, while other elements deviate from straight line behavior (Figure III. 3). Figure III. 3 shows all D's for compatible elements Co, Sc, V, and Ca for augite, plagioclase and Fe-Ti oxides on an Arrhenius plot normalized to the augite-Co temperature estimates. All of these elements have similar crystal-chemical properties and their D's plot on straight lines at the Co-estimated temperatures. Ba, Ba/Ca, and REE D's for augite and plagioclase, however, do not form straight-line Arrhenius plots at the Co-estimated temperatures (Figures III. 3 and III. 4). This is no doubt a result of the very different crystal-chemical properties of these elements relative

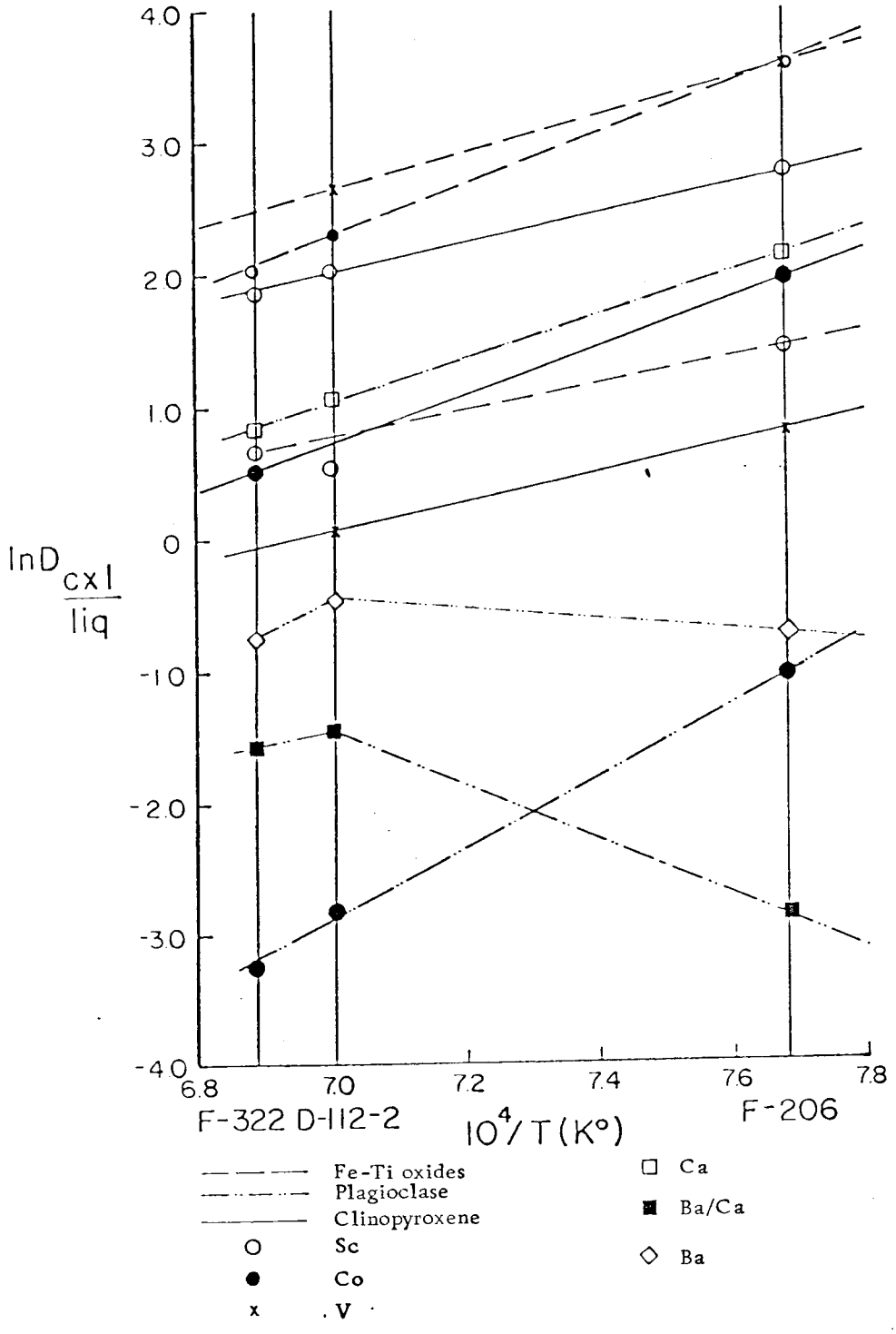

Figure III. 3. Arrhenius plot of Co, Sc, V, Ca, Ba and Ba/Ca for Fe-Ti oxides, clinopyroxene, and plagioclase.

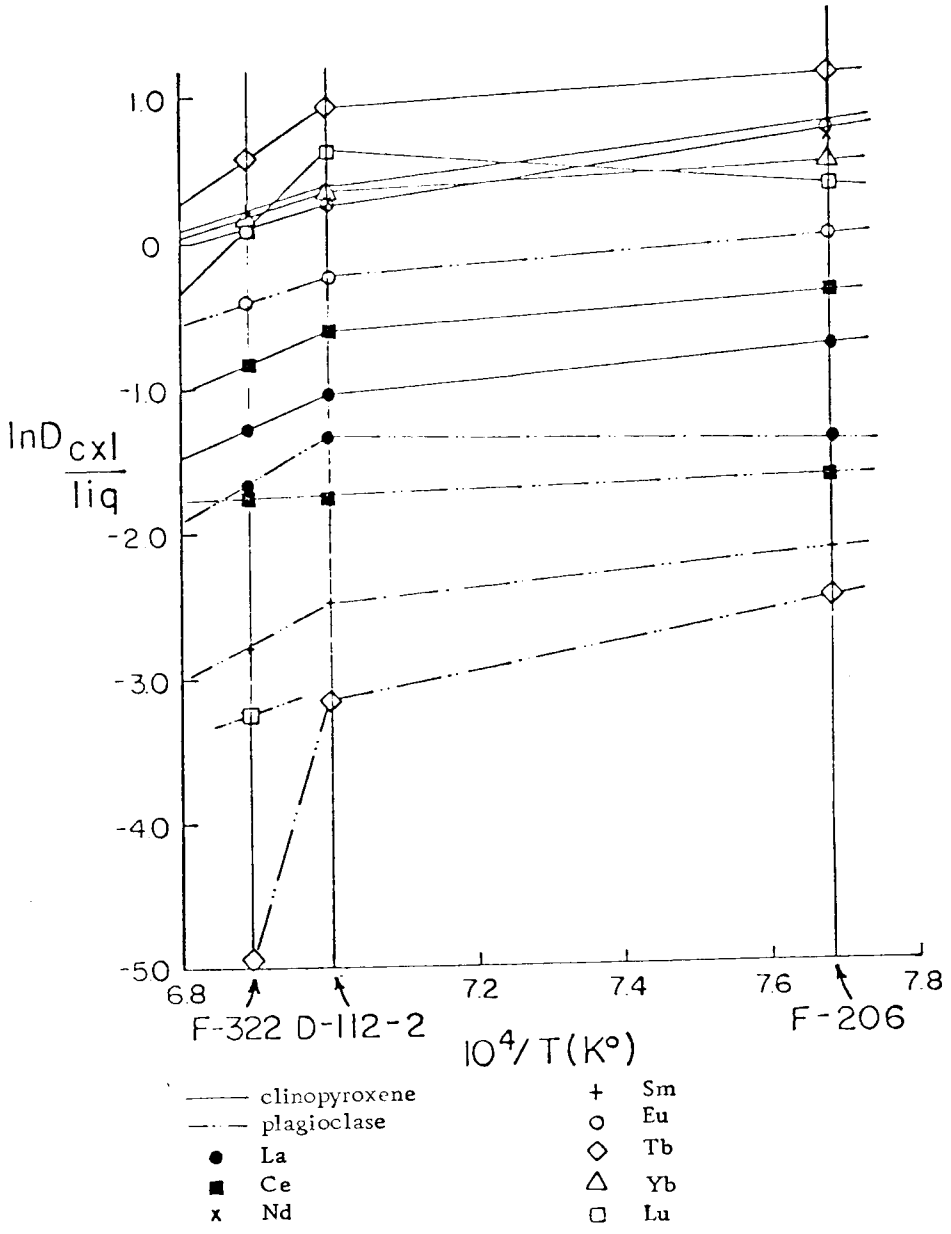

Figure III. 4. Arrhenius plot for mineral separates normalized to temperatures of the Co-clinopyroxene geothermometer.

to Co. Such differences cause serious deviation of the D's for these elements from the pattern of variation of more compatible elements in the siliceous sample, F-206. Sample F-206 has anomalously low D's for REE and Ba compared to the variation predicted by the geothermometer for the two mafic samples (F-322 and D-112).

It may be that rise of D's for the compatible elements with rising Si/O is higher than the increase for incompatible element D's. Alternatively, the incompatible elements may be nearly saturated in crystals of the F-206 sample relative to the incompatible element-depleted samples, F-322 and D-112, causing anomalously low crystal/liquid D's in F-206. Arguments of Drake and Holloway (1978) outlined in the previous section make it unlikely that the incompatible elements are saturated in the F-206 crystals, or (i.e., deviate from Henry's Law). It seems more likely that D's of ferromagnesian elements and Ca rise more sharply at high SiO_2 than those of REE and Ba.

Phenocrystic biotite pseudomorphic after hornblende in the F-206 sample suggests that this sample had a higher H_2O content than the two mafic samples. Presence of quantities of phenocrystic pyroxene equal to the volume of hydrous minerals in F-206, however, probably requires that F-206 was far from saturated in H_2O. Drake and Holloway (1977) have suggested that high H_2O activity may increase Sm D's for clinopyroxene and amphibole, but Sm D's of plagioclase were not affected by H_2O in their experiment. Irving

(1978), however, believes high water contents can decrease D's. Whatever the effect of water, it is possible that it affects REE and Ba partitioning differently from that of ferromagnesian elements and Ca. If this is the case,then this may also account for the variations of Figure III.4.

Regardless of the exact reasons for deviation of the biotite quartz latite data, it is apparent that simple Arrhenius equations generated for basaltic and andesitic liquids do not readily apply to highly siliceous liquids. However, concordance of temperature estimates for plagioclase La, Ba and Ca geothermometers with the Co-clinopyroxene temperature for the most mafic sample, implies that compositional disparity between this sample and the liquids used to calibrate the geothermometers was not large enough to cause dispersion of the La and Ba data from the Ca and Co data, as observed for F-206. Consequently, the F-322 temperature of 1179°C is probably accurate within the ±40°C spread of the data. D-112 differs only slightly in composition from F-322, so that its Co-estimated temperature is probably reasonable if somewhat less accurate.

Oxygen Fugacity Estimates

Drake (1975) has determined equations which allow estimation of oxygen fugacity from REE distribution in plagioclase, if temperature and Sr distribution are known. Temperature estimates for F-322

and D-112 from the previous section allow estimate of Sr distribution between plagioclase and liquid from the Arrhenius equation of Drake and Weill (1975):

$$\ln D_{Sr}^{P/L} = 9,050/T(°K) - 5.24$$

$$D_{Sr}^{F-322} = 2.70$$

$$D_{Sr}^{D-112} = 3.01$$

Taking this data together with an estimate of the D for Eu^{+2} ($D_3^{P/L}$) obtained by extrapolating the REE-distribution coefficient plot of Figure III. 2 beneath the positive Eu anomaly, and the concentrations of Eu in plagioclase (Eu_p) and coexisting liquid (Eu_L) prior to closed system fractional crystallization (estimated from whole rock Eu and corrected actual $D_{Eu}^{Plag./Liq.}$ the Eu^{+2} and Eu^{+3} of the liquid may be estimated by:

$$Eu^{+3} = \frac{Eu_p - (D_{Sr}^{P})(Eu_L)}{D_3^{P/L} - D_{Sr}^{P/L}}$$

where Eu_L = whole rock Eu content

$$Eu^{+2} = Eu_L - Eu^{+3}$$

Because this gives Eu^{+2}/Eu^{+3} of the liquid, oxygen fugacity may be estimated from:

$$\log f_{O_2} = 4.55(\pm 0.17)\left(\log \frac{Eu^{+2}}{Eu^{+3}}\right) - 10.89(\pm 0.19)$$

$$f_{O_2}(F\text{-}322) = 10^{-8.48\pm 1.5}$$

$$f_{O_2}(D\text{-}112) = 10^{-8.68\pm 1.5}$$

The probable error of ±1.5 log units is the estimated deviation observed by Drake (1975) from measurements of natural whole rocks and mineral separates. The fugacities are comparable to Drake's (1975) estimates of oxygen fugacity for the lower Mazama dacite ash flow ($\log f_{O_2} = -8.3$) and other pyroclastic dacites of the Cascades and Japan (-6.3 to -11.4), as well as measurements for a variety of andesites and basalts (-3.9 to -10.6 for andesites, and -6.9 to -7.3 for basalts).